Faculty of Engineering and Computing
Department of Civil Engineering

Investigation of Soil Failure Mechanisms during Spudcan Foundation Installation

Muhammad Shazzad Hossain

This thesis is presented for the Degree of
Master of Engineering (Civil Engineering)
of
Curtin University of Technology

April 2004

DECLARATION

This thesis contains no material which has been accepted for the award of any other degree or diploma in any university.

To the best of my knowledge and belief this thesis contains no material previously published by any other person except where due acknowledgment has been made.

Signature: …….

Date: ……April 2004……...

ABSTRACT

Mobile jack-up rigs are widely used in offshore oil and gas exploration and increasingly in temporary production and maintenance work. There is a steadily increasing demand for their use in deeper water and harsher environments. A typical modern jack-up has three independent legs, each equipped with a footing known as 'spudcan'. This thesis is concerned with the performance of spudcan foundation subjected to vertical loading correspondent to preloading during its installation into uniform clay.

The chief aim of this study is to investigate the bearing behaviour with the corresponding soil failure mechanisms during spudcan penetration. Centrifuge model test and Finite Element (FE) analysis are carried out extensively. In centrifuge modelling, a half-spudcan model and a full spudcan model are used. In the half-spudcan model test, a novel system for revealing soil failure mechanisms and measuring soil deformation has been adopted, in which the half-spudcan model is placed against a transparent window and a subsequent Particle Image Velocimetry (PIV) analysis is performed. The full-spudcan model test is conducted to measure the load-penetration response. In numerical simulation, both small strain and large deformation analyses are carried out with smooth and rough soil-spudcan interfaces considered.

At the initial stage of penetration, it is observed that a cavity is formed above the spudcan as it is penetrating into a uniform clay. Meanwhile, soil flows towards the surface and thus soil heave forms close to the spudcan shoulders. With further penetration, the soil underneath the spudcan starts to flow back into the cavity on the exposed top of the spudcan. This backflow causes the spudcan to be embedded while the initially formed cavity remains open. Eventually, the spudcan becomes fully embedded and the soil flow mechanism reaches a fully localised failure mechanism with deep embedment. The lateral extent of visible distortion due to soil flow is confined well within 1.5~1.6 D (D: spudcan diameter).

From both centrifuge and numerical investigations, it is found that in uniform clay, it is inevitable to form a cavity above the spudcan foundation. Thus, the stable cavity depth and soil back flow mechanisms are studied. It is clear that the back flow is caused by a *Flow Failure*, where it is due to the downward penetration of the spudcan. This is contrary to the *Wall Failure* that is the mechanism recommended by the current offshore design guidelines to estimate the stable cavity depth. In wall failure, the soil back flow is due to the cavity wall too high to stand. The stable cavity depth is estimated up to 4 times higher by the wall failure mechanism than the one by the flow failure. This explains that the wall failure is never observed in model test. Therefore, a new design chart with design formula is developed for design engineers in the stable cavity depth calculation.

The spudcan bearing response is strongly correspondent with the variation of soil failure mechanisms during penetration. At the initial stage of the penetration, the spudcan bearing capacity increases with penetration, which is due to the increase of overburden pressure from cavity formation. At the second stage of the penetration, soil back flow embeds the spudcan, and the spudcan bearing capacity is increasing as the soil flow mechanism transits from its shallow failure mechanism to its deep failure mechanism. At the final stage of the penetration, the spudcan bearing capacity reaches its ultimate value, where the deep/localised failure mechanism remains. A rough spudcan shows 14 % higher bearing capacity than a smooth spudcan. And a flat-plate shows 8 % higher capacity than a spudcan with a same surface roughness. The ultimate bearing capacity factor N_c = 10.5 in uniform soil is recommended as a conservative value when the deep failure mechanism is reached. A correspondent N_c = 10.1 in NC clay is suggested for a deeply embedded spudcan.

Keywords: Jack-up Rig, Spudcan Foundation, Preloading, Uniform Clay, Soil Flow Mechanisms, Cavity Stability, Bearing Capacity.

"*Nobody believes in theoretical calculations,*
except the one who did it.
Everybody believes in experimental results,
except the one who did it."
……Albert Einstein

ACKNOWLEDGEMENTS

First and foremost I wish to acknowledge the supervision provided by Dr. Yuxia Hu. Dr. Hu has always been generous with her time and has constantly been on hand to provide guidance and inspiration when needed. Thanks to pick me up from my country and through me into this Research Ocean. I would also like to express my gratitude and appreciation to Prof. Mark Randolph for his stimulating supervision, wonderful insight and constructive advice. Sincere thanks are extended to Dr. Hamid Nikraz for his friendly inspiration, pastoral care and for serving as co-supervisor.

Experiments could not have been performed without the support of the Centre for Offshore Foundation Systems (COFS), UWA, especially the drum centrifuge technician Mr. Bart Thompson. Mr. Thompson taught me enthusiastically and with long endurance on how to perform a test in a drum centrifuge. Like to show a path to a blind man, he did it so frankly since I did not known about centrifuge before coming here. Special thanks are also due to Mr. Clem Ryan for his cordial suggestions during testing.

The research presented here is supported by the Australian Research Council through the Large ARC discovery scheme (A00105806). In addition, I was supported by the same source to go to Hawaii, a paradise of this world, to present one of my papers. These supports are gratefully acknowledged.

Dr. Dave White, of Cambridge University, and Mrs. Zarnaz Mehryer, of Curtin University, helped me to perform PIV analysis and FE analysis respectively. I am grateful to them all.

Finally, Mrs. Diane Garth, of Curtin University of Technology, and Mrs. Monica Mackman, of UWA, helped me cordially with patience and good humour. I become astonished to see that they show their smiling face all the time. Thank you, Ladies; I am indebted to you forever.

Finally, I am grateful to Dr. Maureen Massam, Lecturer, Student Learning Support Unit, to go through this dissertation enthusiastically. Thanks are also due to the IT support staff in the Faculty of Engineering and Computing.

PUBLICATIONS ARISING FROM THE RESEARCH

Journal Papers

Hossain, M.S., Hu, Y., Randolph, M.F., and White, D.J. (2004). "Limiting cavity depth for spudcan foundations penetrating clay." Submitted to *Géotechnique* for review.

Hossain, M.S., Hu, Y., Randolph, M.F., and White, D.J. (2004). "A novel technique for capturing soil failure mechanisms in centrifuge tests." Submitted to *Int. J. of Physical Modelling in Geotechnics* for review.

Hossain, M.S., Hu, Y., Randolph, M.F., and White, D.J. (2004). "Soil failure mechanisms associated with spudcan foundations on clay." Submitted to *Australian Geomechanics* for review.

Refereed Conference Papers

Hossain, M.S., Hu, Y., and Randolph, M.F. (2003). "Spudcan foundation penetration into uniform clay." *Proceedings of The 13th International Offshore and Polar Engineering Conference*, ISOPE, May, Honolulu, Hawaii, USA, pp. 647-652, CD-ROM.

Hossain, M.S., and Hu, Y. (2004). "Investigation of the response of spudcan foundation in uniform clay-water effect." *The 9th Australia New Zealand Conference on Geomechanics*, February, Auckland, New Zealand, Vol. 1, pp. 102-108.

Hossain, M.S., Hu, Y., and Randolph, M.F. (2004). "Bearing behaviour of spudcan foundation on uniform clay during deep penetration." *Proceedings of The 23rd International Conference on Offshore Mechanics and Arctic Engineering*, OMAE, June, Vancouver, Canada.

Hossain, M.S., Mehryar, Z., Hu, Y., and Randolph, M.F. (2004). "Deep penetration of spudcan foundation into NC clay." *Proceedings of The 23rd International Conference on Offshore Mechanics and Arctic Engineering*, OMAE, June, Vancouver, Canada.

Hossain, M.S., Hu, Y., Randolph, M.F., and White, D.J. (2005). "Cavity stability and bearing capacity of spudcan foundations on clay." Abstract submitted to OTC.

CONTENTS

CHAPTER 2: LITERATURE REVIEW

CHAPTER 3: PHYSICAL AND NUMERICAL MODELLING

CHAPTER 5: RESULTS AND DISCUSSION: EXPERIMENTAL AND NUMERICAL ANALYSIS

NOTATION

G	Depth above water surface to the hull bottom
W	Water depth
z	Soil depth
d_t	Penetration depth of footing tip
L′	Jack-up leg length below hull-bottom
L	Jack-up leg length
q_u	Ultimate bearing capacity
s_u	Undrained shear strength
N_c	Vertical bearing capacity factor
γ	Saturated unit weight of soil
d	Penetration depth of footing shoulder
R	Footing radius
R_{equiv}	Radius of equivalent conical footing
A	footing area at largest section, $= \frac{\pi D^2}{4}$
D	Spudcan/footing diameter
H	Depth of open cavity above the penetrating spudcan
β	Spudcan cone angle
V	Embedded spudcan volume
F_V	Ultimate vertical load
V_{Lo}	Maximum preload
F_o	Vertical load applied by the infill soil, $= \gamma$ (d-H)
σ'_{vp}	Vertical effective preconsolidation pressure
σ'_v	Vertical effective stress
N_s	Stability number, $= \frac{\gamma H}{s_u}$
H	Horizontal load (Section 3.2.1, 3.4.1, 4.2.3)
V	Vertical load
M	Moment load
N	Multiplication factor with earth gravity for centrifuge gravity

h	Depth
σ_v	Vertical stress
ρ	Mass density
g	Earth's gravity
T_v	Dimensionless time factor
c_v	Coefficient of consolidation
t	Time
H	Distance related to drainage path length (Section 3.3.3)
ω	Angular rotational speed
R_e	Effective centrifuge radius
R_t	Centrifuge radius to the top of the model
h_i	Depth where the vertical stress in model and in prototype are identical
l	Any length
e^*_i	Strain error estimator
Ωi	Area of element i in two-dimensional analysis
ε^h	Strains from the FE solutions
ε^*	Strains recovered by SPR
h	Element size (in Numerical Analysis)
e^*_{imax}	Maximum estimated strain error
ν	Poison's ratio
ϕ	Friction angle
ψ	Dilation angle
E	Young's Modulus
δ	Displacement increment
k	Gradient of s_u
s_{uo}	s_u at ground surface
θ, ϕ, φ	Euler angles of rotation
α	Aspect ratio (Section 3.5.4)
α	Adhesion factor
N_{ctb}	Vertical bearing capacity factor for T-bar
v	Penetration rate
T	Time
I_p	Plasticity index

G_s	Specific gravity
M	Critical state frictional constant (Table 4.2)
e_{cs}	Voids ratio at p′ = 1 kPa on critical state line
λ	Slope of normal consolidation line
κ	Slope of swelling line
Λ	Parameter
r	Spacing ratio
H_F	Depth of *Flow Failure*
H_W	Depth of *Wall Failure*
$H_{deep\ failure}$	Depth of deep (local) failure
γ_w	Unit weight of water
f	empirical constant
N_{sD}	Stability number for soil backflow, $=\frac{\gamma D}{s_u}$
a, b	Regression coefficients

SUBSCRIPTS

p	Prototype
m	Model
v	Vertical

ABBREVIATIONS

FE	Finite element
PIV	Particle image velocimetry
NC	Normally consolidated
OC	Overconsolidated
RITSS	Remeshing and interpolation technique with small strain
SPR	Superconvergent patch recovery
CCD	Charge coupled device
CPT	Cone penetration test
USB	Universal serial bus
PAL	Phase alternating line
LL	Liquid limit
PL	Plastic limit
E	Event
T	Test
FS	Full-Spudcan
HS	Half-Spudcan
TB	T-Bar
CD	Compact Disk
OCR	Overconsolidation ratio

CHAPTER 1

INTRODUCTION

1.1 Jack-up Units

1.1.1 General

Most of the world's offshore oil/gas drilling in water depths up to 120 m is performed from self-elevating mobile units, commonly known as jack-ups. Typical units consist of a buoyant triangular platform resting on three independent truss-work legs, with the weight of the deck and equipment more or less equally distributed. A rack and pinion system is used to jack the legs up and down through the deck.

1.1.2 Types

Mobile jack-up rigs can be divided into three broad categories according to their foundation type: (i) mat-supported, (ii) individual footings (spudcans) supported and more recently (iii) skirted gravity base supported.

Mat-supported jack-up platforms (one or several mats) have been designed with a particular view to set up the platform in soft soil areas with a low bearing capacity. These platforms are in service in various seas throughout the world such as Gulf of Mexico, Pacific coast of Latin America, Indonesia, West African Coast. Mats are usually A-shaped and connected to the platform by tubular or lattice-work legs (shown in Figure 1.1). The overall usual dimensions are 50 to 60 m long (Figure 1.3(a)) with an area of 1,000 to 2500 m^2 and 2 to 3 m thick, resulting in weights about 80 to 100 MN. Since mat supported rigs have a large foundation bearing area and impose relatively low bearing pressures on the seabed, a limited penetration is

resulted. However, mat-supported rigs require that the seabed be fairly level and their stability is sensitive to factors such as subsoil variability, lateral sliding resistance and seabed instability.

Rigs supported on individual footings are more numerous and much more widely used. A typical example of such unit is shown in Figure 1.2 and the key structural and foundation data are summarised in Table 1.1. About 440 jack-up rigs are in operation around the world, and these are used in more than half of the total offshore oil and gas extraction projects. Most of these platforms (about 60%) are supported by 3 or 4 independent legs with individual footings called "spudcan" (Poulos, 1988). The majority of spudcans are effectively circular in plan, typically with a shallow conical underside profile and a sharp protruding spigot (Figure 1.3(b)) to facilitate initial location and to provide extra horizontal stability (Martin, 1994; SNAME, 1997). Spudcan diameters in excess of 20 m have become quite common in post-1980 designs. A rack and pinion system is used to jack the legs up and down through the deck.

Very recently, the ACE self-installing steel gravity platform has been developed that changed the way of platform installation. Hang Tuah platform (Figure 1.4) is providing gas compression facilities for the West Natuna Sea Gas Development, offshore Indonesia. It is the first ACE platform, working from 2001. Figure 1.5 shows the annular inverted U-section skirted base adopted in the ACE platform design. This is more efficient in terms of bearing capacity to weight ratio, compared with a mat-supported jack-up foundation. This is because the skirts are deep enough to reach higher strength soils. The gravity base foundation inherent in the ACE concept is inherently adaptable to a wide range of seabed soil conditions. This is because loads are widely distributed so that the average stress levels are significantly lower than those from piled deep foundations, or even suction bucket foundations. The skirted foundations are designed for installation at a number of sites comprising various soils. A plate of 1 m deep and 80 mm thick is employed at the base of each 6 m deep skirt. The ACE platform has an uninterrupted deck that can easily be laid out with process equipment because the base and legs are merely hung from the deck via the strand jacking system and the transportation forces induced in the legs are transmitted to the annular skirt. Figure 1.6 displays the self-install jacking system in

the ACE platform design. More details can be found in Jackson and Pennington (2002).

This research is focused only on the performance of the spudcan foundation that is utilised in the jack-up rigs with individual legs.

1.1.3 Jack-up Installation Procedure

During installation, jack-ups are towed to the site with the hull floating on water and the legs elevated out of water (Figure 1.7). The typical installation procedure is shown in Figure 1.8. On site, the legs are jacked down and the rigs are positioned with the footing resting on the seabed. Before commencing operation, the hull is raised about 1.5 m out of the water and then the foundations are preloaded to the designed load by pumping seawater into ballast tanks in the hull (called 'proof test'). The preload causes the spudcans to penetrate into the seabed until the load on the spudcan is equilibrated by the resistance of underlying soil. In soft seabed conditions, the spudcan may need to penetrate up to 2-3 diameters to reach equilibrium (Endley *et al*., 1981). The purpose of preloading is to provide a safety margin against the environmental loads that the rig might experience during operation, usually based on a design storm of with 50-year return period. It is usual practice to preload (jack-up mass + sea water) the foundation to twice the working vertical load (Jack-up mass) since in a design storm, overturning moments caused by the wave and wind forces may increase the vertical load on the spudcan foundations (additional environmental and live load) by as much as 20-50% of the gravity load (McClelland *et al*., 1981; Baglioni *et al*., 1982; Kee and Ims, 1984). After preloading and when all conditions are deemed satisfactory, the preload is removed by dumping the ballast and the hull is jacked up to the desired operating height above the sea level. Figure 1.9 shows such a jack-up unit playing its role at North Sea.

1.1.4 Roles of Jack-up Units in Petroleum Industries

"The natural energy resources of the Earth (for example fossil fuels and renewables) are often located offshore, and most likely in remote harsh environments. Structures

are required to be placed in these environments so that the resources may be extracted. These structures are often subjected to very extreme loads from a variety of sources including hurricanes, tornadoes, large winds, large waves, high currents and perhaps ice flow. The ever increasing social need to extract these vital energy resources, in these harsh environments, has led to the development of large structures, which are often located in deep water." (Byrne, 2000). Mobile jack-up rigs are extensively playing a successful role around the world. Jack-up rigs are getting larger, expanding their geographical areas of operation, staying on location throughout the year in harsher environments, being used in temporary production, installing new flexible tripod platforms and maintenance work.

1.1.5 History (after Cassidy, 1999)

The earliest reference to a jack-up platform is in the description of a United States patent application by Samuel Lewis in 1869 (Veldman and Lagers, 1997). It was not until 85 years later in 1954 that Delong McDermott No. 1 became the first unit to utilise the jack-up principle for offshore drilling. Delong McDermott No. 1 was a conversion of one of the successful 'Delong Docks': a pontoon with a number of tubular legs which could be moved up and down through cut-outs in the pontoon. The Delong Docks, which were mostly used as mobile wharves for industrial purposes during the 1940s, could be towed into location with their legs drawn up. Once in position their legs could be lowered and the pontoon elevated off the water using the same principle as the modern jack-up. Interestingly, Delong Docks were used in World War II as mobile docks by the United States Army after the invasion of Normandy and before the major harbours of Western Europe were liberated (Veldman and Lagers, 1997).

Like many of the early jack-ups to follow, Delong McDermott No. 1 resembled a standard drilling barge with attached legs and jacks, which were often many in number. In 1956 R. G. LeTourneau, a former entrepreneur in earthmoving equipment (Ackland, 1949), revolutionised the design of jack-ups by reducing the number of legs to three (Stiff *et al.*, 1997). Another innovative design change was the electrically driven rack and pinion jacking system, which allowed for continuous

motion in any jacking operation. This replaced 'gripper' jacks where slippage often occurred on the smooth leg surface (Veldman and Lagers, 1997). Both revolutionary features are common on today's rigs. Zepata's "Scorpian", used in water depths up to 25 m in the Gulf of Mexico, was the first of many operated by the company Marathon LeTourneau. They dominated early jack-up design during the 1960s and 1970s with rigs of increasing size.

Since their first employment, jack-ups have continued to be used in deeper waters (Carlsen *et al*., 1986). Other companies, including Bethlehem, Friede and Goldman, Marine Structures Consultants and Mitsui have contributed to the rise in water depth capacity (Veldman and Lagers, 1997). This development is continuing with some of the largest units being used in about 120m of water in the relatively harsh North Sea environment (Hambly and Nicholson, 1991; Veldman and Lagers, 1997). Furthermore, jack-ups are now operating for extended periods at one location, often in the role of a production unit (Bennett and Sharples, 1987). An example of the long-term use of jack-ups is in the Siri marginal field development in the Danish sector of the North Sea. A purpose built jack-up is being used in 60 m water depths as a production platform with an expected life of ten years (Baerheim *et al*., 1997). A further example is the Shearwater development, where jack-up drilling is planned to continue for two and a half years at 90 m water depth in the Northern North Sea (Offshore Technology, 1999).

1.1.6 Mobility Nature of Jack-up Unit

Unlike a fixed platform or gravity structure, a jack-up unit is mobile in nature (Table 1.2). Because drilling locations change so do many of the loadings that the jack-up rig must resist. Each location will present a different combination of loads. In addition, the offshore soils around the world exhibit a wide range of strength and classification properties. Therefore, jack-up units are continually being reassessed for different sites and the tendency for their use in increasingly harsh environments has led to this inescapable necessity.

1.2 Fundamental Considerations

1.2.1 Spudcans vs Conventional Shallow Foundations (after SNAME, 1997)

- Spudcans are relatively smooth (steel) and (semi) conical whereas the other conventional footings are usually rough (concrete) and flat;
- Spudcan foundations rest on soil which, during installation, has been subjected to large strains, whereas conventional foundations are placed on soil which has not failed. Also for conventional foundations the soil may have been improved due to the "pre-design" foundation loads. This can lead to an increased soil strength by consolidation;
- Spudcans are an order of magnitude larger than most conventional foundations;
- Spudcans are subjected to large horizontal and moment force, due to environmental loading, as well as vertical loads. By comparison, conventional shallow foundations onshore are dominated usually by purely static vertical loading;
- Spudcans are often embedded to a significant depth below the seabed, typically by up to two diameters on soft clays, whereas by up to half a diameter for conventional foundations;
- Spudcans that support jack-up rigs are mobile in nature, i.e. they are continually being reassessed for different sites, whereas conventional shallow foundations are custom designed for a specific site.

1.2.2 Definition of Foundation Loadings

During initial preloading, and in a calm weather, the footings of a jack-up are essentially subjected to purely vertical loading. During drilling operation and a storm, however, the spudcans must also resist overturning moments, horizontal loads and changes in vertical load arising from environmental action on the structures. Therefore, it is appropriate to provide definitions of these different loading types.

These definitions apply to the response of the soil and not to the response of any structural component (after Byrne, 2000).

Monotonic loading: A monotonic load is a force or displacement path applied in a constant direction. It may be applied over a sufficiently long time period so that there are no dynamic or transient effects (usually referred to as a static load) or it may be applied so that there are time dependent effects (occasionally referred to as a transient load).

Transient loading: A transient load is one where there is a time dependent response associated with the loading. Transient loading is relevant where the soil is saturated with a pore fluid, as the soil response will depend on the timescale of the loading, compared to the rate of fluid flow within the soil matrix. Transient effects may also be evident for loading of dry soils, particularly in the case of foundations subjected to blast forces (rocket launch pads for example). Transient loading may also be referred to as dynamic loading.

Cyclic loading: Cyclic loads are those which involve reversals of load about a mean level and are repetitive in nature. The nature of the amplitudes is such that they correspond to a specified probability distribution, and hence amplitude power spectrum. Examples of cyclic loads would be a constant amplitude sine wave, or a random amplitude loading path with periods (in this case) corresponding to the relevant time-scale for loading of offshore structures. Cyclic loading may also include repeated loading where exactly the same load or displacement path is applied to the foundation in a repetitive fashion. Cyclic loads may or may not be transient depending on the period (short or long) and the nature of the soil (saturated or dry).

1.2.3 Why Undrained and Total Stress Analysis (after Byrne, 2000)?

The response of shallow foundations on clay during typical loading conditions is often described as undrained. This is because the time over which the load increment is applied is very short when compared to the typical fluid drainage times within the

clay macro-structure. The clay sample under load cannot undergo any volumetric change because of insufficient movement of water due to the very low permeability of the clay. Eventually, at the beginning of loading, the entire load increment is taken by the pore water fluid. As drainage, hence volume change, occurs, the load is transferred from the pore water to the soil skeleton. This process is referred to as consolidation. As it is not possible to determine the amount of stress being carried by the soil skeleton (effective stress) during spudcan installation it is usual to carry out a total stress analysis of the soil-foundation interaction. Over the depth of interest it is typical to assume an undrained shear strength profile, usually determined via numerous site-specific laboratory and field experiments, in which zero volume change occurs. By making these assumptions, it is then possible to take advantage of analytical and numerical techniques such as limit equilibrium and finite element analyses to determine the foundation stability.

1.2.4 Foundation Failure Modes

Review of the mobile jack-up rig accident record indicates that foundation failures or mishaps can be attributed to the following causes (after McClelland *et al*., 1981; Young *et al*., 1984; Rapoport and Young, 1987):

- Footing punch through during preload because of a soil profile that includes a strong layer overlying a weaker layer.
- Excessive storm penetration because the maximum footing preload did not exceed the maximum storm loads, since the preload was primarily vertical loading and storm loads were combinations of vertical, horizontal and moment loading.
- Footing instability induced by scour that undermined the footing and resulted in reduced bearing area.
- Seafloor instability triggered by mass movements of the seafloor sediments that produce destructive lateral forces on the rig.
- Inability to extract footings when the pullout resistance on the footing exceeds the available uplift force.

Details about the failures and probable remedies are explained in Kee and Ims (1984).

1.2.5 Site Investigation

McClelland *et al*. (1981) indicated that every failure mode could be predicted when soil data were available from site specific borings. Adequate geotechnical data can eliminate the risk of punch through and substantially reduce the risk of other foundation problems. The expansion of jack-up rig operations and the diversification of usage increase the need for sufficient site specific geotechnical data to evaluate the behaviour of the seabed as an adequate and safe foundation medium.

The majority of potential jack-up locations are assessed on the results of geophysical survey and geotechnical investigation. A high resolution geophysical survey identifies potentially hazardous geological features and helps to create an understanding of areal soil conditions surrounding the drilling site. Geophysical data are generally obtained with a side scan sonar and 1-3 different vertical profiling systems. In order to develop reasonable predictions of foundation performance of a mobile jack-up rig, site specific data showing the stratigraphy, classification, and engineering properties of the foundation soils are required. These data are obtained by geotechnical investigations i.e. one or more boreholes, with associated undisturbed sampling and laboratory testing, with an adjacent static cone penetration test (CPT), which provides a continuous profile of the soil resistance and would reflect strength variations which might be missed in the borehole. Investigations are normally carried out to a depth of 30 m below mudline but if significant spudcan penetrations are predicted, then the borehole is continued until a depth of one spudcan diameter below the final estimated penetration is reached (Reardon, 1986). Figure 1.10 shows typical profiles followed by geotechnical investigations. Recently, shallow seismic surveying techniques are widely used to investigate the jack-up sites. More details are explained in Semple and Johnston (1979), deRuiter and Richards (1983) and Reardon (1986).

Where soil data are not available of a specific location but in the area close to that location and the weather conditions are predictable and where the remoteness of the drilling location poses difficulties in obtaining a site investigation, a soil boring could be performed from the rig after initial jack-up but before the application of the

preload. This is done to check that there is no danger of failure during or after preloading.

1.2.6 Jack-up Analysis Modelling (after Cassidy, 1999)

Before a jack-up can operate at a given site, an assessment of its capacity to withstand a design storm, usually for a 50-year return period, must be performed. In the past, with jack-ups used in relatively shallow and calm waters, it has been possible to use overly simplistic and conservative jack-up analysis techniques for this assessment. However, as jack-ups have moved into deeper water and harsher environments, there has been an increased need to understand soil behaviour underneath and around the spudcans. The publication of the 'Guidelines for the Site Specific Assessment of Mobile Jack-Up Units' (SNAME, 1994) was an attempt by the offshore industry to standardise the total jack-up assessment procedures.

The foundations of independent-leg jack-up platforms approximate large inverted cones known as 'spudcans'. Roughly circular in plan, they typically have a shallow conical underside with a sharp protruding spigot, as shown in Figure 1.3. For the larger units operating in the North Sea spudcan diameters in excess of 20 m have become common.

During a storm, environmental wind and wave forces impose additional horizontal and moment loads onto the foundations of the jack-up, as well as alter the vertical load. During installation and in a perfectly calm sea, however, a vertical loading is the only dominant loading on the spudcans. Although most practical applications involve combination of vertical (V), moment (M) and horizontal (H) loadings, an understanding of soil behaviour under purely vertical loading is a key aspect of many offshore foundation designs.

1.3 The Need for Further Research

Mobile offshore drilling platforms face far greater risks (almost an order of magnitude in terms of rate of accidents), by the very nature of their function, than do most engineering structures (fixed platforms) in the same marine environments (McClelland *et al*., 1981; National Research Council, 1981; Rapoport and Young, 1987). Of all the types of mobile offshore platforms, jack-up experienced the worst accident rate (McClelland *et al*., 1981; Rapoport and Young, 1987). The literature dealing with the mishaps of jack-up units are quite extensive (Le Tirant, 1979; McClelland *et al*., 1981; National Research Council, 1981; Young *et al*., 1984; Leijten and Efthymiou, 1989; Sharples *et al*., 1989; Boon *et al*., 1997). As they concerned, the recorded accidents were presented in a table or in a graph. The largest single cause of accidents was shown to be soils related, and this was identified as the risk area with the highest potential for improvement. The most catastrophic type of failure was spudcan 'punch-through', usually occurs in layered soil deposits, while mishaps in uniform clay were also quite often (Young *et al*., 1984). The resulting damage to the rig can range from minor structural damage to the leg and its jacking mechanism to complete loss of the rig (≈ economy of about US$90 million and lives per annum). Sharples (1989) stated that around 80% of these occurrences resulted in serious damage. Moreover, the failure rate for jack-ups is increasing as the jack-up unit designers and operators are continually striving to extend the operating areas of units, especially in marginal fields. Under these circumstances, the mechanisms of soil failure underneath and around the spudcans during deep penetration need to be revealed to predict *in situ* jack-up behaviour prior to installation in an attempt to reduce the number of accidents. An understanding of soil failure mechanisms underpins successful prediction of bearing capacity, and hence accurate determination of spudcan penetration.

So far some techniques of revealing 'true' soil failure mechanisms associated with footing penetration have been developed in laboratory floor testing and in centrifuge testing but only to visualise the post-test mechanism (discussed in Chapter 2, Section 2.3). Consequently, soil failure mechanisms and continuous soil flow during spudcan penetration under *in situ* stress field have never been reported. It is therefore crucial

to develop a technique in visualising soil flow and failure mechanisms in centrifuge testing to mimic the prototype dimensions of footing and soil stress conditions *in situ*. The visual evidence from centrifuge testing, together with the results from numerical study will allow for a complete assessment of spudcan response during deep penetration.

1.4 Aims of Current Research

Currently, most of the world's offshore drilling is performed from jack-up platforms. Jack-up rigs are getting larger, expanding their geographical areas of operations, staying in location throughout the year in harsher environments, being used more in tandem with fixed structures and installing new flexible platforms and evolving into semi permanent production platforms (Hambly and Nicholson, 1991; Hampson and Power, 1992; Henriques and Petrobras, 1995; Veldman and Lagers, 1997). Although these units were originally designed for shallow waters, there is a growing demand for their use in deeper water (Figure 1.11, Carlsen *et al*., 1986; Bennett and Sharples, 1987). The number of jack-up units used as a production platform has increased after 1990 (Figure 1.11, Veldman and Lagers, 1997). In order to comply with all these increasing and extending roles, and to avoid excessive conservatism in design, it is now imperative to envisage seabed behaviour, prior to installation particularly during deep penetration. The main aims of this research are:

(i) to reveal the mechanisms of distortion of soil underneath and around spudcan foundations with deep penetration during installation,

(ii) to study the formation of any cavity above the spudcan foundation and its influence on the bearing capacity of the spudcan,

(iii) to investigate the bearing capacity of spudcan foundations during penetration in different soils.

In this study, physical testing and finite element analysis are performed. Centrifuge modelling technique is used to perform all of these experimental investigations. In this investigation, overconsolidated (OC) clay beds are mainly considered, with a few normally consolidated (NC) clay bed tests.

A new technique for the optical measurement of deformation based on particle image velocimetry (PIV) and photogrammetry (White, 2002; White *et al*., 2003) is used to obtain planar soil deformation measurements, subsequently analysing the images captured at discrete time intervals during centrifuge testing.

In a numerical investigation, the AFENA finite element package (Carter and Balaam, 1990) is used. Jack-up rigs are mobile and the offshore soils around the world exhibit a wide range of strength and classification properties. FE analysis is a key tool to reassess seabed behaviour for different sites by changing engineering parameters.

Although only single layer soil profiles are investigated in this study, it is the basis for a further PhD study in layered soils, which can provide more insight into the punch-though failure. This is because punch-through failure is the main cause of the sudden drop of jack-up legs on site.

1.5 Dissertation Structure

Chapter 2 includes a review of literature relevant to the behaviour of jack-up footings subjected to purely vertical loading on cohesive soil. The basic theories of quantifying vertical bearing capacity, during preloading or installation are discussed in detail. This thesis is based mainly on revealing soil failure mechanisms during footing penetration and additionally on soil characteristics and bearing capacity. Worldwide recent experimental works in the relevant area, are presented. Publications, devoted to depicting soil failure mechanisms from numerical analysis, have also been discussed. The relevant design recommendations of Offshore Design Guidelines (SNAME, 1997) are reported.

Chapter 3 describes in detail the techniques used in this research. The discussion is divided into three parts. The first part highlights physical centrifuge modelling technique, the development of scaling laws, and the probable effects of centrifuge scaling. The second part is devoted to the numerical modelling concept (AFENA). The third part focuses on the new technique for the measurement of small

deformation in geotechnical physical modelling. This technique is based on digital imaging technology, Particle Image Velocimetry (PIV) and close range photogrammetry. The operation of this technique is described in brief.

Chapter 4 forms four parts. Firstly, it outlines the design, construction and operation of a testing apparatus. The arrangements for load and displacement instrumentation, data acquisition and computerised control of the apparatus are summarised. Secondly, this chapter is concerned with the soil used for the physical modelling program. Clay sample preparation technique is described. Thirdly, this chapter briefly discusses how to capture good quality images successfully using digital camera during testing. Finally, test strategies and test procedures, which have been followed, are described. The way of performing tesst with water on top of the specimen at enhanced gravity has also been reported.

Chapter 5 contains a detailed description of the results of centrifuge tests performed using the apparatus, strategies and procedures described in Chapter 4. This Chapter is also devoted to an in-depth analysis of experimental results. It discusses the results from pre-embedded and continuous penetration FE analyses, which have been performed using FE package AFENA. The results, which are presented in this Chapter, are grouped into two parts. The first part discusses all the results of centrifuge tests which ultimately failed to reach the successful goal but were the foundation for improvement. In the second part, the results from successful centrifuge tests and FE analyses are described together as a comparative story, so that some significant conclusions can easily be drawn in the following Chapter.

Chapter 6 summarises the key conclusions from this work, and makes suggestions for future research.

Table 1.1 Reference design jack-up in 120 m water depth in North Sea (after Hambly and Nicholson, 1991)

Leg spacing (fwd-aft)	60 m
Leg height	145 m
Penetration	5 m
Air gap	20 m
Weight (including legs)	200 MN
Mass of hull + tops of legs	17 MN
Diameter of spudcan	22 m
Preload	133 MN
EI of single leg	7.5×10^6 MNm^2
EA of single leg	150×10^3 MN

Table 1.2 Dimensional characteristics of jack-up rigs (after Gemeinhardt and Focht, 1970)

Rig Name	Minimum Water depth (m)	Number of Footings	Approximate Footing Load (MN)	Number of Location
Mr. Louie	37	12	10	7
Offshore No. 52	31	14	4.5	11
Offshore No. 54	38	8	8.8	19
Julie Ann	42.5	3	19	28
Vinegaroon	32	3	17	12
Mr. Cap	27.5	3	16	14
Scorpion	24.5	3	16	13
Penrod No. 52	91.5	3	31.6	2
Penrod No. 55	46	3	25.3	2
Ocean Master I	91.5	3	43.3	3

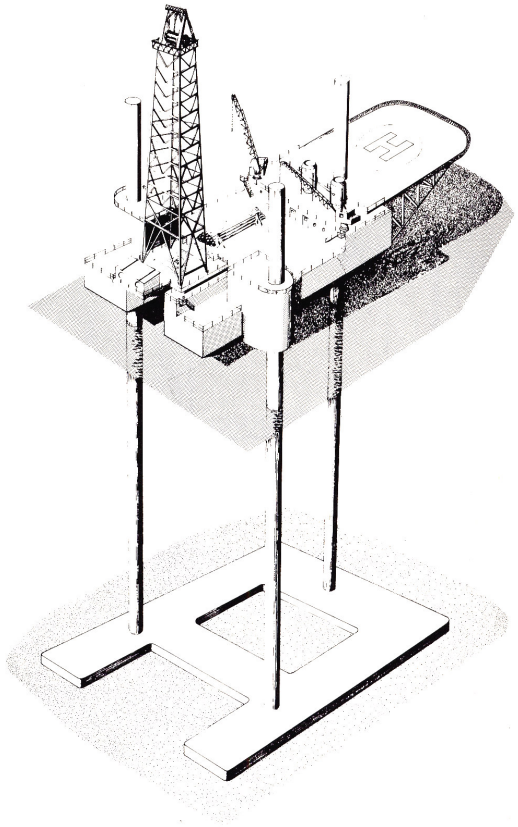

Figure 1.1 A-Mat supported jack-up platform (after Le Tirant, 1979)

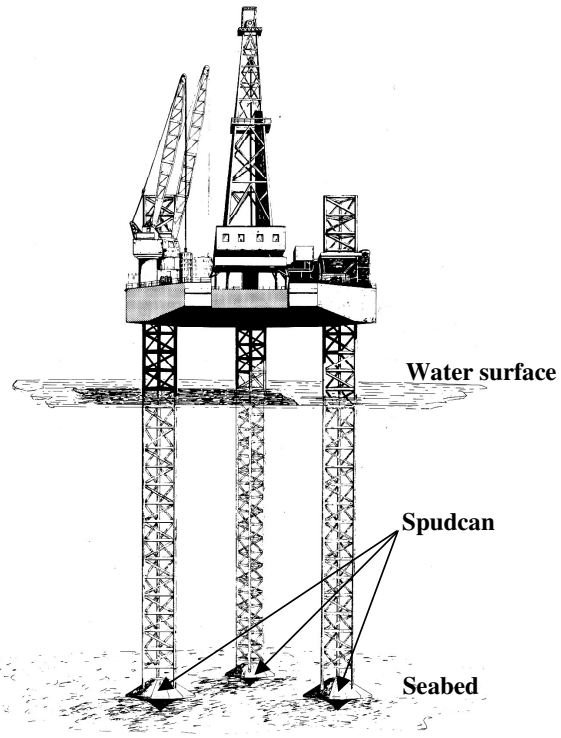

Figure 1.2 Typical tripod jack-up platform mounted on spudcans (after Le Tirant, 1979)

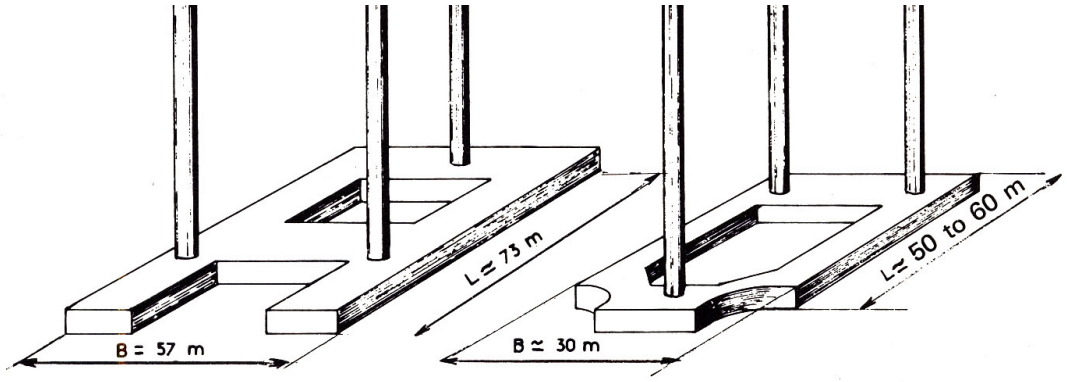

(a) A-mat footings (after Le Tirant, 1979)

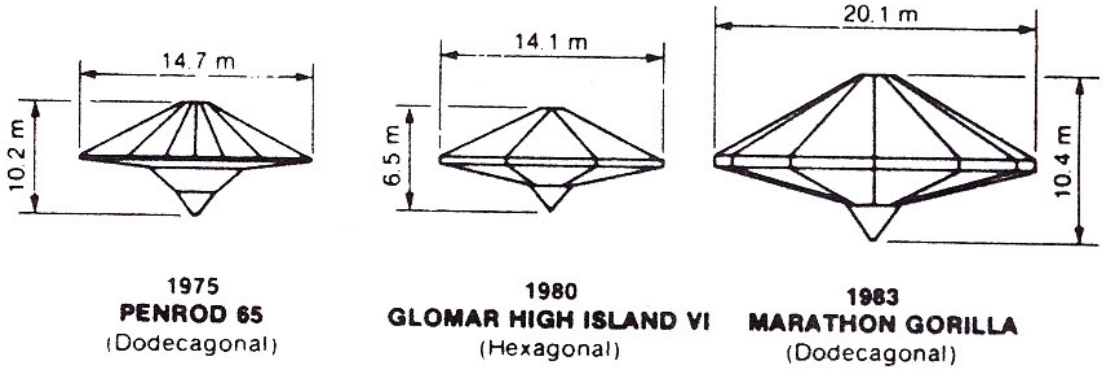

(b) Spudcan footings (after Young *et al*., 1984)

Figure 1.3 Typical footing of jack-up rig

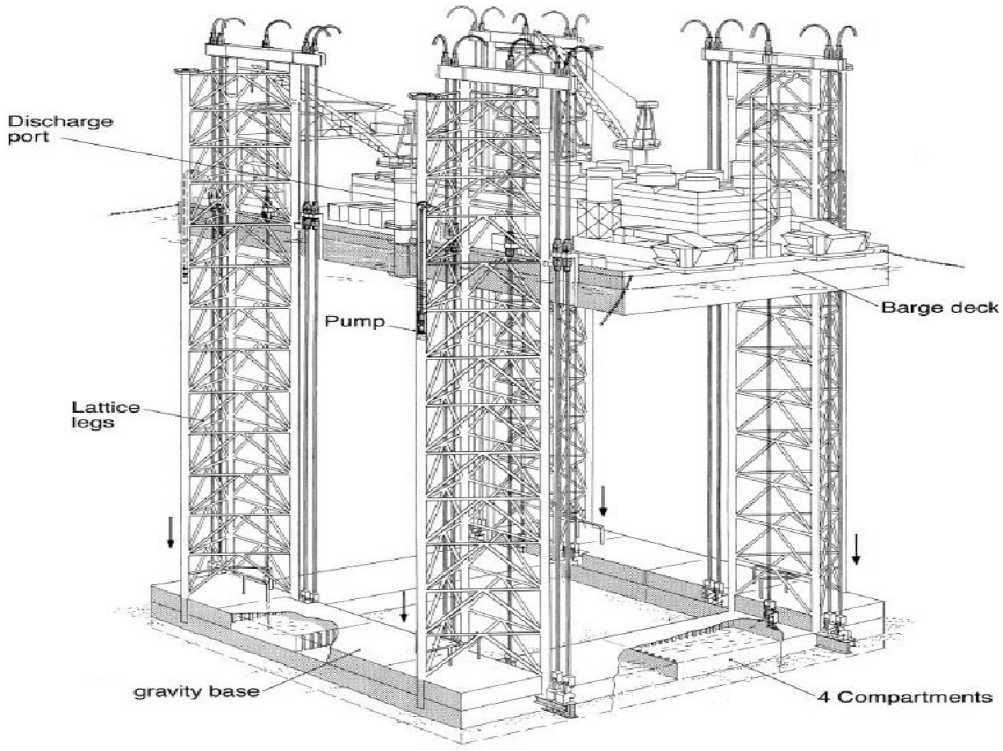

Figure 1.4 ACE Self-Installing gravity platform (after Jackson and Pennington, 2002)

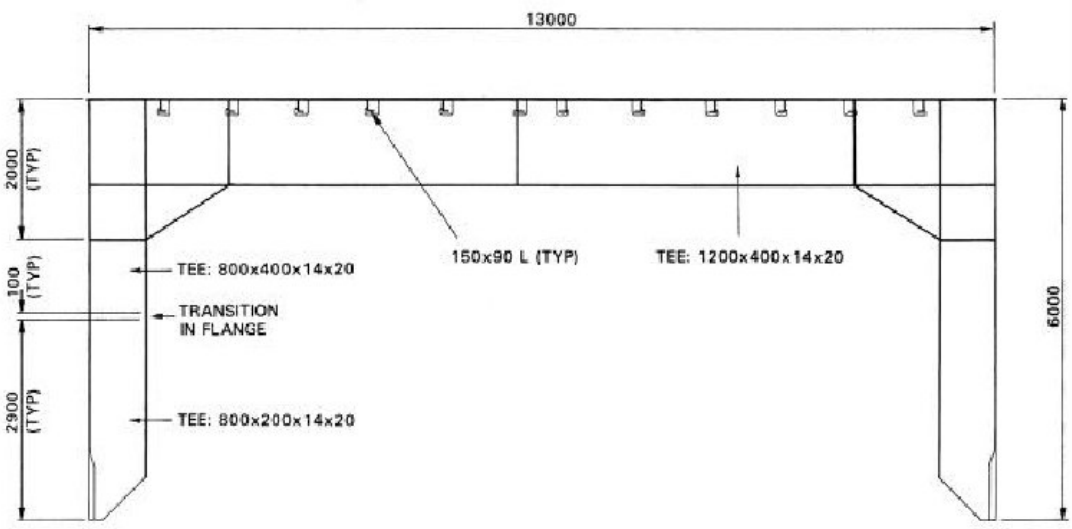

Figure 1.5 Typical Skirt section (after Jackson and Pennington, 2002)

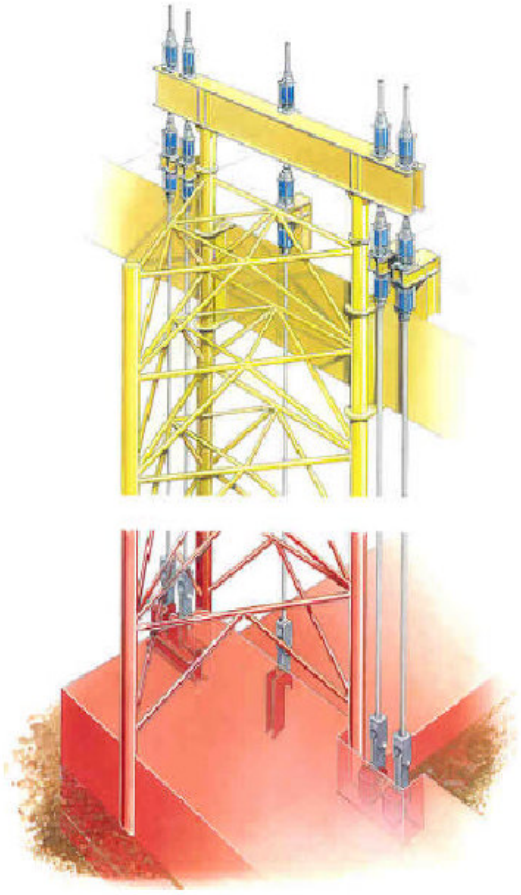

Figure 1.6 Jacking configuration (after Jackson and Pennington, 2002)

Figure 1.7 Jack-up is towed towards operation site after construction (after Veldman and Lagers, 1997)

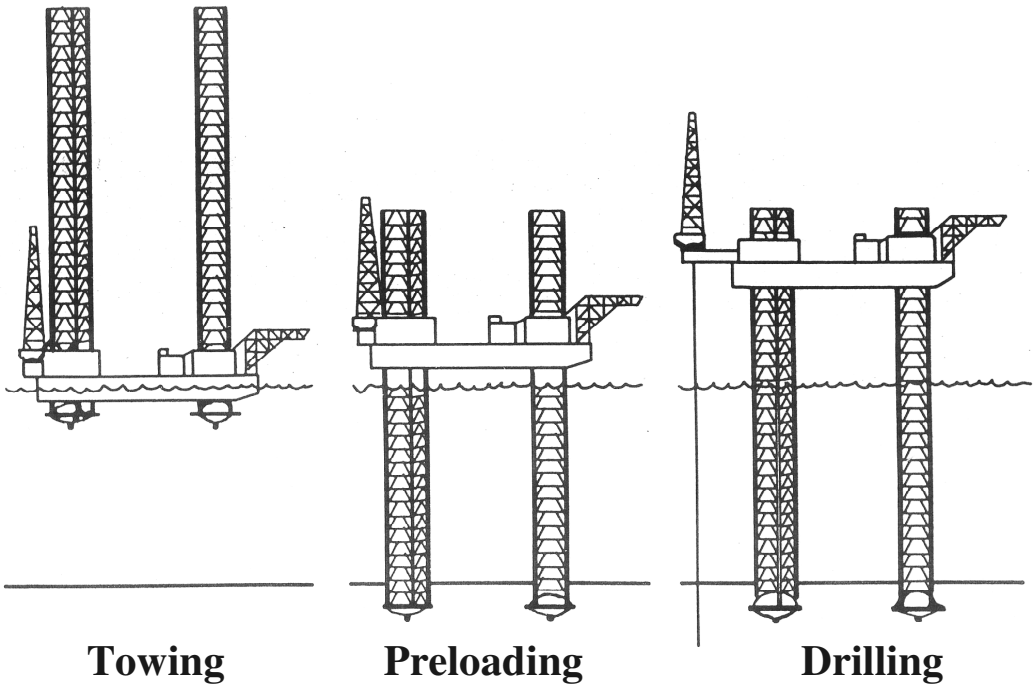

Figure 1.8 Jack-up installation procedures (after Young *et al*., 1984)

Figure 1.9 A completed Platform after installation in the North Sea (after Offshore Technology, 1999)

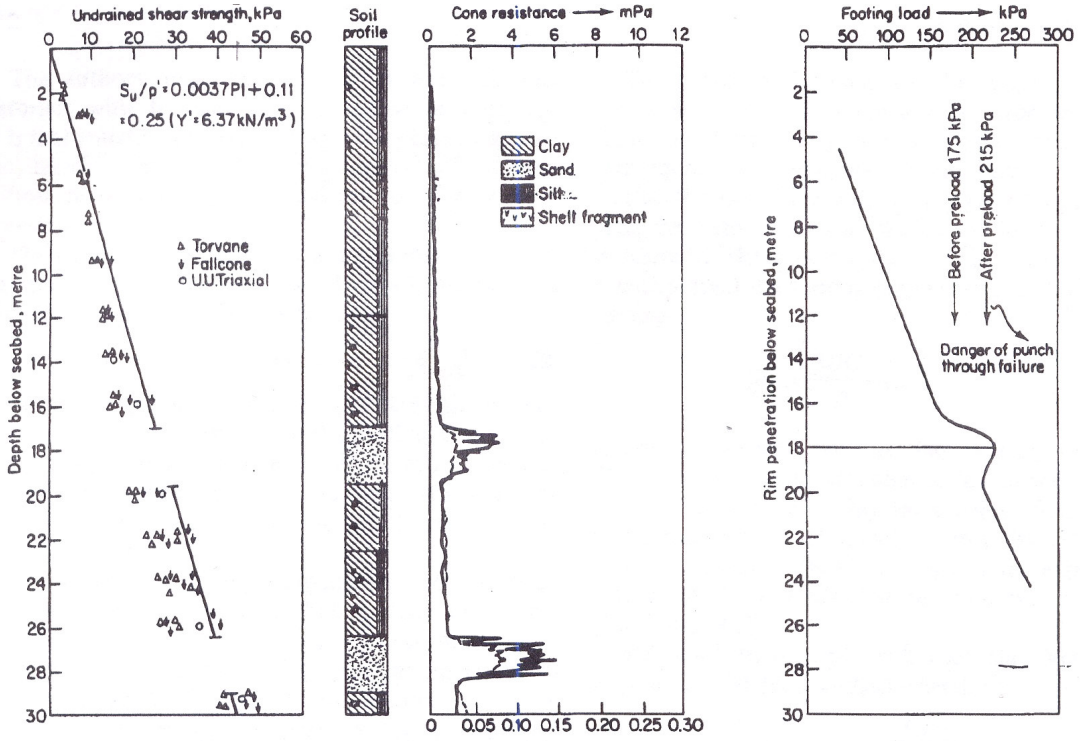

Figure 1.10 Typical profiles: (a) typical undrained shear strength-depth profile; (b) cone penetration tests results; (c) footing (D = 14 m) load-penetration below seabed (after Kee and Ims, 1984)

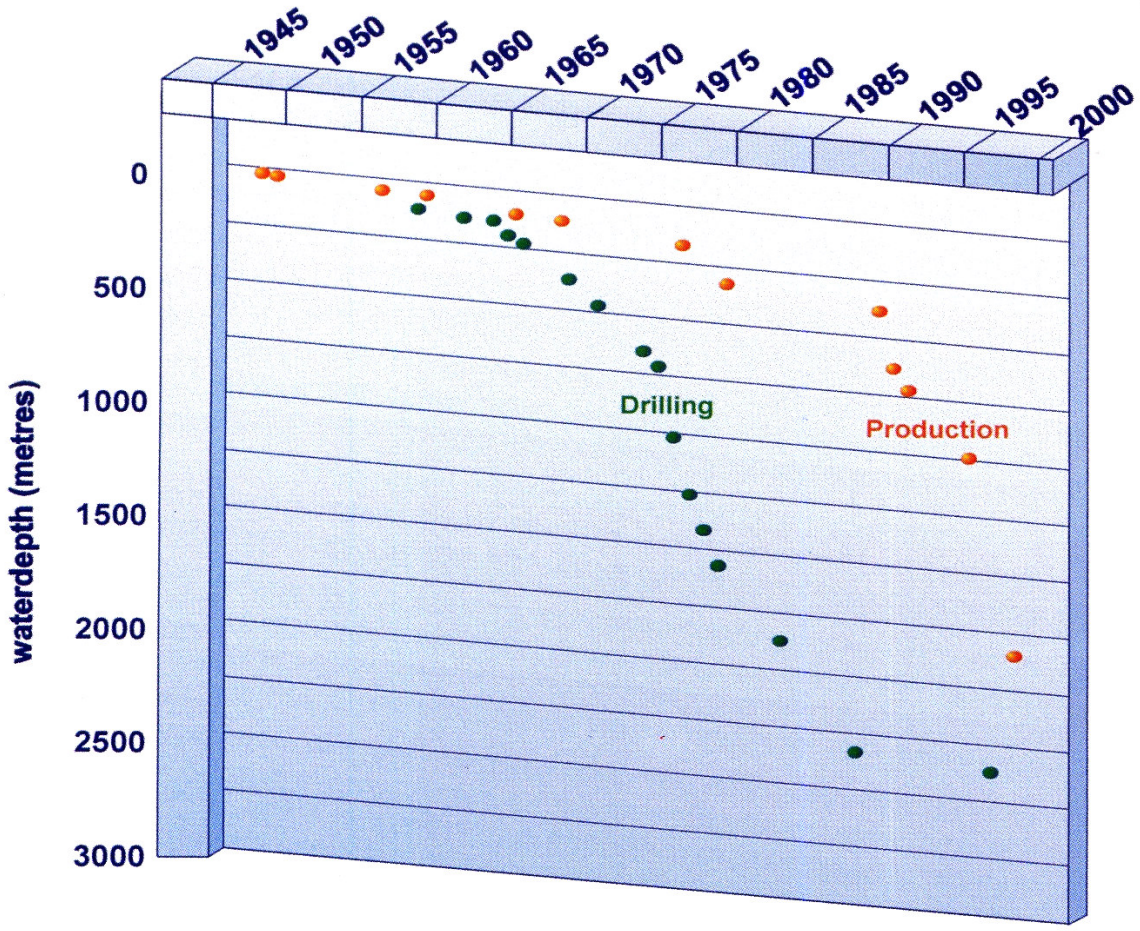

Figure 1.11 Exploration drilling and production go deep water (after Veldman and Lagers, 1997)

CHAPTER 2

LITERATURE REVIEW

2.1 General

This chapter incorporates a survey of literature relevant to the prediction of jack-up unit footing performance, with particular reference to clay. The basic theories of quantifying vertical bearing capacity, during preloading or installation, are discussed in detail. This thesis is based mainly on revealing soil failure mechanisms during footing penetration and additionally on soil characteristics and bearing capacity. Recent experimental work in the relevant areas are presented. Publications, devoted to numerical analysis, have also been discussed. The relevant recommendations of Offshore Design Guidelines (SNAME, 1997) are reported.

2.2 Bearing Capacity of Spudcan Footings

There are two principal concerns in the assessment of whether a jack-up unit may be safely used at a particular site:

(i) prediction of footing penetration during preloading (vertical load only),

(ii) assessment of footing stability under design storm conditions (combined vertical, horizontal and moment loading).

With some basic considerations these two aspects of bearing capacity analysis are discussed below. However, this research concentrates only on vertical undrained loading, with particular emphasis on the undrained loading of uniform clayey soils.

2.2.1 Vertical Loading

A reasonably accurate prediction of footing penetration under preloading is essential before any jack-up installation. This is because the combination of the depth above water surface to the hull bottom (G), water depth (W), and estimated footing penetration (d_t), as shown in Figure 2.1, must not exceed the available leg length (L′), which is the proportion of total leg length (L) that can safely extend below the hull bottom. Since G and W are fixed for a specific location and L′ is a constant for a constructed rig, the unknown factor needed for advance determination of suitability for the location is the probable footing penetration, d_t. Thus the penetration behaviour with bearing capacity and the penetration depth of the foundation need to be understood thoroughly.

For shallow footings on clays the general bearing capacity equation is:

$$q_u = s_u N_c + \gamma d \qquad (2.1)$$

where s_u is the soil undrained shear strength, γ is the soil unit weight, N_c is the footing bearing capacity factor and d is the penetration depth of spudcan shoulder (Figure 2.2). Note that for a partially penetrated spudcan $R = R_{equiv}$, A is the plan area of the footing in contact with the soil (πR^2_{equiv}), and d = 0. This equation and the broader one from which it was derived were originally proposed by Terzaghi (1943) and have been critically reviewed by a number of authors (Meyerhof, 1951; Skempton, 1951; Brinch Hansen, 1961; Vesic, 1975) on the basis of empirical and theoretical studies. Modifications of the Terzaghi equation have been made almost entirely in regard to the dimensionless coefficients and by addition of the different factors (depth, inclination, and shape factor) rather than in the form of the general equation.

2.2.1.1 Undrained shear strength, s_u

Young *et al*. (1984) mentioned that accurate predictions of footing penetration are more dependent on the selection of undrained shear strength value than on the chosen

analytical technique. Gemeinhardt and Focht (1970) suggested that a representative s_u be taken as the average strength over one diameter below the widest embedded cross-section of the footing (Figure 2.2). Current practice is, however, to take a s_u averaged over a depth of one radius below the widest embedded cross-section, proposed by Young *et al*. (1984) (Figure 2.2). This method is applicable if the shear strength values up to one diameter below the spudcan do not vary more than 50% from the average value (after Skempton, 1951). If significant s_u variations occur, the bearing capacity should be computed using a method for layered soil conditions to take into account the soil non-homogeneity (SNAME, 1997).

2.2.1.2 Overburden pressure, γd

When computing bearing capacity, the embedment conditions of the footing are significant. During footing penetration, a large volume of soil is displaced and the assumptions made regarding the "backfill" process influence the prediction of bearing capacity and corresponding leg penetration. The surcharge component of bearing capacity, γd (where γ needs to be substituted by γ' for soil under water, where water fills up the cavity above the foundation) in Equation 2.1 should be included where the cavity above the footing remains open (H = d, Figure 2.3) which could be the case in very firm clay (Gemeinhardt and Focht, 1970; Endley *et al*., 1981). Whereas, if the cavity above the footing is fully backfilled (H = 0, Figure 2.3), which could be the case in NC clay (Endley *et al*., 1981; Kee and Ims, 1984; Le Tirant and Pérol, 1993), the contribution of γd will be eliminated. However, if soil is intermediate between soft and stiff, the cavity above the spudcan may remain open partially. If so, this contribution will be reduced by the amount $\gamma(d-H)$ (Figure 2.3). Thus, Equation 2.1 can be generalised as:

$$q_u = s_u N_c + \gamma d - \gamma(d - H) \qquad (2.2)$$

Note that the effective unit weight γ' needs to be chosen for soil under water, where water fills up the cavity above the foundation. Endley *et al*. (1981) stated that better predictions of bearing capacity and hence footing penetration could be obtained by

assuming that the hole above the footing is backfilled completely. This provides a design towards the safer side, but more conservative.

In calculating γd, Gemeinhardt and Focht (1970) defined d as the penetration depth of footing tip. However, the common practice is to consider d as the depth below soil surface to the widest part of the footing (Endley *et al*., 1981; Young *et al*., 1984; SNAME, 1997), with γ defined as the average unit weight of the soil above the footing shoulder (Gemeinhardt and Focht, 1970).

2.2.1.3 Non-dimensional bearing capacity factor, N_c

"In the jack-up industry only a few methods are used to estimate N_c for computing spudcan penetration into homogeneous cohesive soils, notably the empirical bearing capacity equation of Skempton (1951) and the semi-empirical formulae of Brinch Hansen (1970) and Vesic (1975). In the application of all these techniques the spudcan is tacitly modelled as a flat circular footing." (Martin, 1994). The empirical correlation proposed by Skempton (1951) has been widely used to predict jack-up footing operations into clay ever since Gemeinhardt and Focht (1970) first proposed its use in this context. Skempton's equation is

$$N_c = 6\left(1 + 0.2\frac{\mathrm{d}}{\mathrm{D}}\right) \leq 9 \tag{2.3}$$

where the various quantities are as defined in Figure 2.3. The semi-empirical bearing capacity formulae of Brinch Hansen (1970) and Vesic (1975) are also well known. Brinch Hansen (1970) gives

$$N_c = (\pi + 2)\left(1.2 + 0.4\frac{\mathrm{d}}{\mathrm{D}}\right), \qquad \frac{\mathrm{d}}{\mathrm{D}} \leq 1 \tag{2.4}$$

$$N_c = (\pi + 2)\left(1.2 + 0.4\tan^{-1}\frac{\mathrm{d}}{\mathrm{D}}\right), \qquad \frac{\mathrm{d}}{\mathrm{D}} > 1 \tag{2.5}$$

and Vesic's (1975) method gives

$$N_c = (\pi + 2)\left(1 + \frac{1}{\pi + 2}\right)\left(1.2 + 0.4\frac{d}{D}\right), \qquad \frac{d}{D} \le 1 \tag{2.6}$$

$$N_c = (\pi + 2)\left(1 + \frac{1}{\pi + 2}\right)\left(1.2 + 0.4\tan^{-1}\frac{d}{D}\right), \qquad \frac{d}{D} > 1 \tag{2.7}$$

Figure 2.4 shows these values as a function of footing embedment. Complete backfilling (so that q_u/s_u is simply the familiar bearing capacity factor N_c) and uniform profile of s_u with depth have been assumed. Figure 2.4 also includes the solution obtained by Meyerhof (1951) using approximate slip-line fields. These bearing capacity factors do not vary by more than a maximum of about 18%, and consequently from experience Young *et al*. (1984) stated that the accuracy of each method is about the same. The API (1993) guidelines recommend Vesic's formula for predicting spudcan penetration under preload, although in Europe the Brinch Hansen method seems to be more popular (Reardon, 1986).

2.2.1.4 Other relevant research

At locations where there is a significant increase of s_u with depth, the approximate "critical strength zone" method illustrated in Figure 2.2 allows any of the above bearing capacity methods to be used for predicting spudcan penetration. A number of researchers such as Davis and Booker (1973), Houlsby and Wroth (1983), Salencon and Martar (1982) have, however, undertaken rigorous investigations of bearing capacity on soils where the undrained strength increases linearly with depth. These methods give bearing capacities less than those resulting from the use of Skempton's (1951) and Vesic's (1975) relationships. Empirical correction factors for the Skempton (1951) and the Davis and Booker (1973) methods are recommended by Endley *et al*. (1981).

All of the bearing capacity theories discussed so far assume a flat footing base and take no account of the spudcan roughness factor and the depth of spudcan embedment of the uppermost part of the bearing area below the soil surface. Meyerhof (1961) conducted vertical loading tests on rough cones in uniform clay. He found that all footings with cone angles $90° \le \beta \le 180°$ had very similar bearing

capacities, whereas sharper cones showed a rapid increase in bearing capacity factor, N_c with decreasing β. Houlsby and Wroth (1983) made a rigorous lower bound analysis of conical footing bearing capacity in a cohesive soil, and their results for rough cones were in close agreement with Meyerhof's observations. Recent experimental work by Santa Maria (1988) also confirmed Meyerhof's finding that, provided $90° \leq \beta \leq 180°$, the vertical bearing capacity of a surface conical footing on clay is not significantly different from that of a flat based footing having the same radius.

Gemeinhardt and Focht (1970) showed that the aforementioned theories, developed based on onshore soil mechanics and foundation engineering procedures, can be applicable to quantify offshore foundation behaviour reasonably. More recently Houlsby & Martin (2003) presented alternative bearing capacity factors of conical-based circular foundations from lower bound analysis. Values of the dimensionless bearing capacity factor N_c were presented in a tabulated form as a function of the cone angle, cone roughness, depth of embedment and the rate of increase of strength with depth of the clay. In all these analyses soil was assumed weightless with a rigid-plastic response and it was assumed that the space above the footing was occupied by a rigid, smooth-sided shaft. Therefore, these results should be used with caution for spudcan foundation design. The results can overestimate the vertical capacity of a spudcan where the soil is free to flow round into the cavity above the foundation, which will occur for high values of $\gamma H/s_u$. Conversely, these results can underestimate the vertical capacity of a fully-embedded spudcan since the modelling of a smooth-sided shaft above the spudcan prevents the shear strength of the backfill soil being mobilised.

SNAME (1997) suggested using the following equation to calculate ultimate vertical bearing capacity,

$$F_V = (s_u N_c + \gamma' d)A \tag{2.8}$$

and maximum preload,

$$V_{Lo} = F_V - F'_o A + \gamma' V \quad (2.9)$$

of a spudcan in clay, where, A is the spudcan effective bearing area and V is the embedded spudcan volume. In Equation 2.9, the last two terms are to take into account the effect of backflow (F'_o A) considering the spudcan buoyancy or the weight of the soil replaced by the spudcan (γ' V). Where, F'_o is the overburden pressure at penetration depth d due to backfill (γ' (d-H), Figure 2.3).

$$F'_o = \gamma' (d - H) \quad (2.9.1)$$

Note that these two terms (– F'_o A + γ' V) should always be considered together (SNAME, 1997).

2.2.1.5 Current experimental works

Santa Maria (1988), Santa Maria and Houlsby (1988)

A model testing program for both monotonic and cyclic loading is described. Four different shapes of footing (flat plate, 120° cone, 60° cone and spudcan) were adopted. Clay samples were prepared by consolidating a kaolin slurry under a maximum pressure of 200 kPa, followed by maintaining a 15 mm thick water layer on the clay surface. A miniature site investigation was always carried out, using shear vane, on the clay sample after the completion of each test. Soil undrained shear strength presented as uniform with s_u = 10 kPa. The results of vertical central loading tests, using a spudcan model of 50 mm diameter with a 130° enveloping angle, have been presented. However, all tests were performed at unit gravity.

Craig and Chua (1990)

A critical review was presented which drew together the results from model tests and computations on the mechanisms by which the spudcan foundation of an independent leg offshore jack-up structure can penetrate deeply into the seabed through both uniform and stratified deposits. A spudcan of 140 mm model diameter was used. Various beds of uniform clay with different undrained strength were prepared by consolidation. The characteristic undrained strengths (s_u) were deduced from an

accumulated database of information relating moisture content of this material and a triaxial compression test of 50 min duration. In order to obtain data closer to the field situation some tests were also carried out in softer clay beds with the clay surface submerged by a 70 mm water layer. All vertical penetration tests were conducted, at a constant rate 7 mm/sec, at 100 g. The cavity above the spudcan remained open up to d/D ≈ 0.90. Since the soil strength was predicted by soil moisture content and penetrometer measurements, and soil was assumed as uniform in the whole layer, the effect of presence of free water on soil strength was overlooked.

Houlsby and Martin (1992)

Theoretical and experimental investigations of the behaviour of spudcan foundations of jack-up units under vertical and combined loadings are described. A spudcan model of 100 mm diameter with a basic cone angle of 154° and a sharper 76° conical tip was considered. Speswhite kaolin slurry was consolidated (σ'_{vp} = 200 kPa) followed by a 15 mm water layer cover which was maintained to prepare heavily overconsolidated soft clay deposit. Well matched results, of undrained shear strength and vertical bearing capacity, have been presented from theoretical prediction (Wroth and Houlsby, 1985) and experiments. However, the experiments were conducted at unit gravity and therefore the contributions of overburden pressure and soil backflow have not been considered.

Martin (1994), Martin and Houlsby (2000)

These studies described a series of laboratory tests conducted at unit gravity. The footing was made of dural with diameter of 125 mm. The footing shape designed for the experiments was based on the representative spudcan profile adopted for the joint industry study of jack-up foundation fixity (Noble Denton Associates, 1987). The tests were performed on a heavily overconsolidated sample of kaolin (σ'_{vp} = 200 kPa). A 15 mm water layer covered the clay samples after consolidation and during testing. The following power law expression was a modified version of Ladd *et al*. (1977) and Wood (1990), to describe the variation of s_u with depth:

$$\frac{s_u}{\sigma'_v} = 0.25 OCR^{0.75} \qquad (2.10)$$

Shear strengths were calculated by using this expression and were measured by post-test miniature shear vane test and showed good agreement with the above expression. Footing loading-reloading tests were performed with a constant velocity of 0.33 mm/sec and up to 1.6 diameters. Note, however, that because of the 1 g nature of the laboratory tests, although flow failure occurred after d/D = 1, backfill soil above the model spudcan did not have a significant influence on the vertical load measured during the test.

Dean et al. (1998)

This paper reported centrifuge tests data of model three-leg jack-ups on kaolin clay. The tests modelled one prototype jack-up with 6.5 m diameter 13° conical spudcans, one with 6.5 m diameter flat-based spudcans, and one with 13.0 m diameter flat-based spudcans. Speswhite kaolin clay bed was prepared by preconsolidation ($\sigma'_{vp} \approx$ 600 kPa) and the final depth was about twice the footing diameter which was considered sufficient for the investigation of the soil-structure interaction behaviour. Water was introduced at lower gravity through the sand layer surrounding the clay. Eventually, 1-5 mm of water cover was maintained during testing. Undrained shear strengths were measured by a hand-driven miniature vane after completion of footing tests at 1 g and the results are shown in Figure 2.5. With these similar specimens, slightly different strengths were presented at identical gravity (128 g). In addition, different strengths were presented, although with different samples, at different gravity (128 g and 256 g). The bearing responses during preloading and reloading, at 128 g and 256 g, have shown good agreement (Figure 2.6), which indicates the absence of footing size effect. The prototype times required in preloading were longer than typical preloading times at field scale. A little drainage of the clay was expected to occur during the model preloading. However, a typical field preloading event on clay would be almost fully undrained.

Vlahos et al. (2001)

This paper reported the results from a series of 1 g experiments conducted using a scaled three-legged jack-up unit model (1:250), equipped with spudcan footings, on soft clay. A spudcan of 72 mm diameter was used. Heavily overconsolidated clay was prepared by consolidating kaolin slurry up to a final pressure of 110 kPa and followed by maintaining a 5 mm water coverage during swelling and testing. Soil

characterisation tests were undertaken using a T-bar penetrometer, both before and after completion of footing penetration tests. The strength profiles indicate a clear variation of 5-10% between pre-test and post-test results (Figure 2.7). The jack-up unit was installed at a constant rate of 1.5 mm/sec and the corresponding load-penetration responses have been illustrated. Additional contribution of overburden pressure to the vertical load capacity has been neglected due to insignificant soil weight at 1 g and no soil backflow observed up to d/D = 1.

Stewart and Randolph (1991), Stewart (1992) and Watson (1999)

Stewart (1992) stated that the undrained shear strength of a clay was not a constant that depended upon its water content, stress history and current effective stress. Shear strength may be measured by a variety of methods both in the field and in the laboratory, and the results of each test on identical samples are likely to be different.

In an attempt to clarify the variability of strength test results, a series of tests was performed, using different site investigation devices such as cone penetrometer; T-bar, on kaolin clay of different stress history, from normally consolidated to heavily overconsolidated. Centrifuge tests were undertaken, at different gravity, before and after model testing to determine any change in strength over the test period. Vane shear tests were also performed immediately after stopping the centrifuge. In addition, some laboratory floor tests (1 g) were also undertaken prior to centrifuge spinning. Interesting summary/conclusions of this valuable work are stated below:

- At 1 g, a lower soil strength resulted than the predicted strength based on the effective stress and overconsolidation ratio (Stewart, 1992) due to considerable swelling (and hence softening) of the sample, where several hours elapsed between releasing the preconsolidation pressure and conducting the soil tests.
- The measured vane strengths (post-test at 1 g) were marginally lower than the other results, which might be attributed to softening of the clay during swingdown (Figure 2.8).
- Laboratory tests (1 g) provide higher strength than centrifuge tests where soil was still in swelling although it might be reconsolidating under self-weight.

- In normally consolidated clay, a 10-15% strength increase occurred between the tests conducted before and after model tests, which was associated with secondary consolidation and with the dissipation of excess pore pressure generated during changes in g-level.
- In contrast to NC clay samples, the preconsolidated sample reduced its strength over the test period, which could be attributed to gradual swelling of the sample after removal of the high overburden pressure (Figure 2.9).
- Figure 2.10 shows the effect of increasing aspect ratio on T-bar resistance. As can be seen, there is a trend of reduced s_u with increased bar length. This may be largely attributed to the relative proximity of each test to previous test sites, rather than to the influence of end effects (which in NC soil were shown to be negligible). In addition, the reduction in deduced s_u might be associated with a reduction in the area correction with increasing T-bar length.
- 20 mm separation between T-bar tests is sufficient to minimise the effect of previous tests.
- Only small differences in strength result between penetration rates of 0.3 and 3 mm/s (Figure 2.11).
- The strength of laboratory clay would be expected to be slightly lower than normally found in field deposits, since the influence of long term chemical effects and secondary compression (which will lead to higher strengths –Bjerrum, 1972) are not present.

James and Tanaka (1984) and James and Shi (1988)

These researchers used a centrifuge to assess spudcan behaviour on beds of dry sand. The spudcan models represented a maximum prototype diameter of 7.2 m, with limited penetration. These tests had no application to a deep penetration, but it is of interest to note that for identically prepared beds of sand the use of accelerations of 30 g with a 100 mm diameter footing yielded dimensionless bearing capacity factors reduced by a factor of 3 when compared with results from a test at unit gravity. This was equivalent to a change in mobilized angle of friction of around 6°, emphasizing the loss of dilation in sand at field stress levels when compared with conventional 1 g models.

2.2.2 Combined Loading

In perfectly calm weather and during preloading, vertical self-weight is the only load on the spudcans. During a storm and drilling operations, however, additional cyclic, horizontal and moment loading of the jack-up, can alter the vertical load.

Cyclic loading has the effect of reducing soil strength and possibly causing washout beneath the edges of the footing. Horizontal loads and moments have the effect of reducing the bearing capacity of a foundation (Kee and Ims, 1984; Reardon, 1986; SNAME, 1997). For conservative assessment of the effects of cyclic loading on clay foundation the following vertical bearing capacity factors may be applied to the capacities calculated from static soil properties (Andersen, 1988), recommended by SNAME (1997).

Leeward leg vertical bearing capacity reduction factor = 1.0
Windward leg vertical bearing capacity reduction factor = 0.8

Details about combined loading are not discussed here but can be found elsewhere as the research in this thesis focuses on vertical loading.

2.2.3 Other Influential Factors

The following factors may affect bearing capacity predictions (after Gemeinhardt and Focht, 1970 or Endley *et al*., 1981 or Young *et al*., 1984):

*Anisotropy of natural soils***:** The aforementioned techniques are based on the assumption of isotropic and perfectly plastic behaviour. The undrained shear strength of natural cohesive soils is, however, anisotropic (Davis and Christian, 1971). Based on Lo and Milligan (1967) it can be concluded that the conventional values of s_u (assuming the soil is isotropic) may overestimate actual bearing capacity. For that, Davis and Christian (1971) have suggested that instead of using s_u, a value of 0.85 s_u should be used for calculating bearing capacity.

Yielding of soils: During footing penetration the foundation soil distorted underneath and around the footing. When the footing comes to rest, it is conceivable that some of the soil below the footing (within the pressure bulb) has yielded. Generally, for stiffer soils the strength after yielding will be less than the peak value, whereas for softer soils the strength after yielding may be equal to the peak strength. Therefore, it may be more appropriate to use a residual shear strength instead of s_u as determined by conventional tests.

Remolding of soils: After flow failure, during penetration, the footing pushes up the underneath soil, which is completely remolded due to plastic failure, to the cavity formed above the footing. It is likely that after the footing has stopped, not all of the failed and remolded soil has been pushed out. Some of this soil may remain below the footing. The shear strength in the remolded zone will probably be in the order of half the shear strength determined by testing. This will again reduce the average s_u in the zone of interest.

Leg inclination: Meyerhof (1953) has demonstrated that either a slight inclination of the footing, a small eccentricity of the load, or a small inclination of the load decreases footing bearing capacity slightly. Thus, footing penetration for a given load should be slightly greater for an inclined position than for a vertical position.

Interrupted preloading (after SNAME, 1997): It is noted that in some clays, following remoulding during spudcan penetration, the strength may increase over a time period. For certain clays the strength may be regained in a matter of hours. In such cases, a crust of stronger material may develop underneath the spudcan and this crust may then be underlain by weaker clay. In this condition a potential punch-through situation could occur during subsequent reloading. Several actual failures have been attributed to this type of soil behaviour (Young *et al*., 1984). For soils where this type of strength hardening (thixotropy) is possible, caution should be exercised as interruptions during the preloading operations could lead to severe consequences.

2.3 Soil Failure Mechanisms

The behaviour of a jack-up is affected by the interaction between the structure and foundation soils. The governing parameters are soil conditions, foundation geometry, structural stiffness and loading conditions. In general the emphasis is on ensuring any footing displacements that occur do not create damaging internal stresses within the structure. It is for this reason the structure is preloaded.

The failure of a shallow foundation footing in terms of vertical capacity is only clearly defined in the case of general shear failure, which results in the appearance of sliplines at ground surface (Vesic, 1975). The two other general modes of failure are local and punching shear failures (Figure 2.12). The latter two failure modes in which the point of failure is less clearly defined would be more likely to occur on a material as compressible as kaolin clay. In order to account for these uncertainties designers utilise safety factors on footing bearing capacities, to minimise movement of the footing. The API recommends a safety factor of 2 be used in relation to vertical bearing capacity.

Some researchers have extensively studied soil failure mechanisms during foundation penetration. Major works are listed below-

Terzaghi (1943) and Meyerhof (1951)

Basic soil failure mechanisms, based on which bearing capacity theories were developed, were assumed by Terzaghi (1943) and Meyerhof (1951). Terzaghi considered only shallow foundation but Meyerhof considered foundation at any depth. However, both of them presented soil flow mechanisms for flat-based strip footing independent of soil type (in general).

Craig and Chua (1990, 1991)

Visual evidence was depicted by Craig and Chua (1990, 1991) to show the complexity of soil flow with a view to improving the techniques for quantifying bearing capacity in a profile of known characteristics. Dry spaghetti markers were inserted vertically into the clay bed across the strongbox centreline; these markers

absorbed sufficient moisture from the clay to become continuous non-reinforcing flexible indicators of gross deformations without measurably changing the clay strength. After completion of tests involving penetration or penetration/extraction of the foundation, the sample was bisected along the center to reveal the failure mechanisms. Figure 2.13 (a) and (b) show the photographs of soil distortion below and around the spudcan footing in clay (s_u = 29 kPa) at penetrations around d/D = 0.75 and d/D = 1.6 respectively. At the shallow penetration, d/D = 0.75 (Craig and Chua,1990), the cavity formed in the clay bed remained open and the lateral visible distortion due to soil flow was confined well within three radial distances. At the deep penetration, d/D= 1.6 (Craig and Chua, 1991), however, it was observed that the wedge of clay was forced down with the footing and the clay flowed plastically around the footing from below to above the footing. To a limited extent, it was expected that soil had collapsed into the near surface cavity from the mudline. However, these illustrations display only the ultimate soil failure mechanisms and the vertically inserted spaghetti might not have remained always perfectly vertical. In the case of layered soil (sand-clay), dished plug i.e. non-vertical punching shear was envisaged at 1 g whereas at elevated gravity a completely different mechanisms, that of vertical punching was observed. Albeit layered soil analysis is beyond the scope of this thesis, the observed remarkable change of failure mechanisms at enhanced g-level could be a valuable guideline for soil flow analysis.

Martin and Randolph (2001)

There is also some research on circular plate foundation which might be considered as a simplified spudcan foundation. Martin & Randolph (2001) reported upper and lower bound analyses for surface and buried flat plate circular foundation, showing the predicted soil collapse mechanisms. The study considered the effects of degree of strength non-homogeneity, shape and relative roughness of the footing, but did not extend to continuous penetration and the cavity effect.

Hu and Randolph (1999), Hu et al. (2001) and Mehryar et al. (2002)

Soil flow mechanisms during foundation continuous penetration were presented by Hu and Randolph (1999), and Hu *et al*. (2001). In their research, the foundation was idealized as a flat circular plate and soil conditions were idealised as normally consolidated (NC) clay, with the strength increasing proportionally with depth. Soil

flow mechanisms showed that the soil initially flowed towards the top as shallow failure, but it became fully localized at d/D ≈ 2 as deep failure. The zone of lateral distortion around the plate edge was about 0.6 R (smooth) to 0.7 R (rough). From continuous penetration and pre-embedded analyses, Mehryar *et al*. (2002) displayed soil flow mechanisms during spudcan penetration. Smooth spudcan-soil interface was assumed in their analyses on NC clay. The soil flow became localized (deep failure mechanism) and was obtained at d/D ≈ 1.27. These papers also presented soil flow mechanisms from upper bound analysis for shallow and deep embedment. In upper bound analysis, a clear distinction between the shear plane with smooth interface and that with rough interface can be seen. The lateral distortion zone around the plate edge was about 1 R, which was longer than that from FE analysis.

White et al. (2001[1]), White et al. (2001[2]), White (2002), White et al. (2003)

These investigators provided a new dimension for non-contact deformation measurement of soil deformation in physical models and element tests. This system combines digital photography, close-range photogrammetry and image analysis by Particle Image Velocimetry (PIV). This allows soil displacements to be detected to a precision of 1/15000th of the field of view. This improved performance is achieved concurrently with an order-of-magnitude increase in the number of measurement points that can be established within the observed soil.

2.4 Stability Number

During vertical penetration of a spudcan foundation into homogeneous soil, a cavity could form above the spudcan during initial penetration. Soil might flow back into the cavity due to (i) plastically flow around the spudcan edge, or (ii) collapse of upstanding soil into the hole, or (iii) both. Whatever the mechanism of backflow above the penetrating spudcan, its effect will be to reduce the net vertical bearing capacity or increase the penetration depth. In the jack-up industry, stability numbers presented by Britto and Kusakabe (1983) and Meyerhof (1972) are commonly used to predict the depth of upholding cavity where soil backflow occurs. Figure 2.13 provides the estimation chart to assess the stability of an axi-symmetric excavated

cavity. The current offshore design guidelines (SNAME, 1997) recommends of use the stability numbers of Meyerhof (1972) for uniform clay and those of Britto and Kusakabe (1983) for normally consolidated clay for conservative evaluation of the cavity stability. The evaluation of the cavity stability is given by the stability numbers (N_s), as a function of the depth and the diameter of the cavity. Thus the stability number is defined as:

$$N_s = \frac{\gamma H}{s_u} \tag{2.11}$$

in which γ is the soil unit weight (γ is substituted by γ' for foundation submerged under water), H is the excavation depth (Figure 2.14) and s_u is the uniform undrained shear strength. In non-homogeneous soil, the average undrained shear strength over the depth of the cavity would be considered. However, all above mentioned stability factors are for wall failure of axisymmetric circular excavations in clay (Britto and Kusakabe, 1983) and of slurry supported axisymmetric, rectangular, and square excavations (Meyerhof, 1972). There is no consideration of the foundation penetration effect on the sustainable depth of the cavity formed above the foundation. In reality, the surrounding soil of the upstanding cavity is pushed by a penetrating foundation. Thus the infill soil above the spudcan comes from a soil flow from spudcan base to spudcan top, rather than from a soil collapse from the cavity wall.

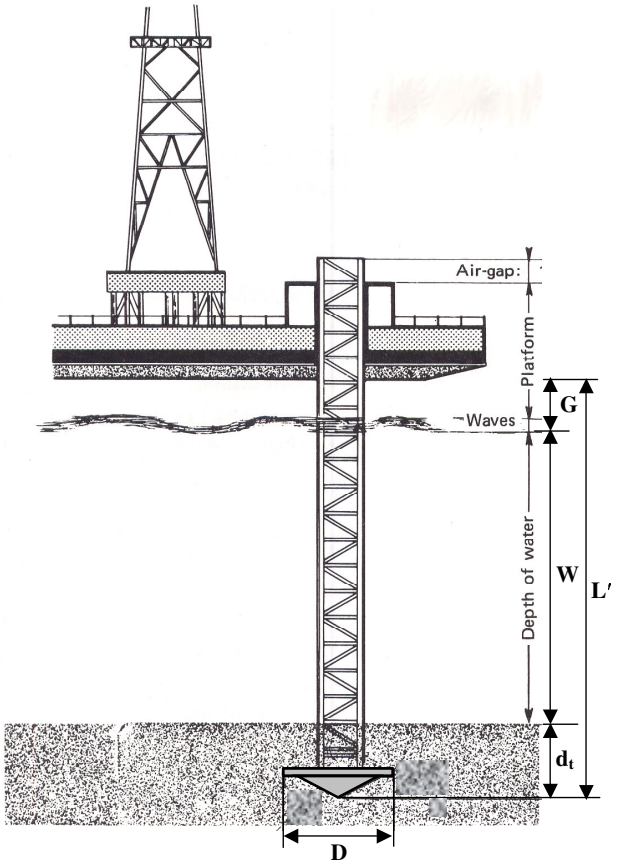

Figure 2.1 Jack-up platform installation conditions (after Le Tirant, 1979)

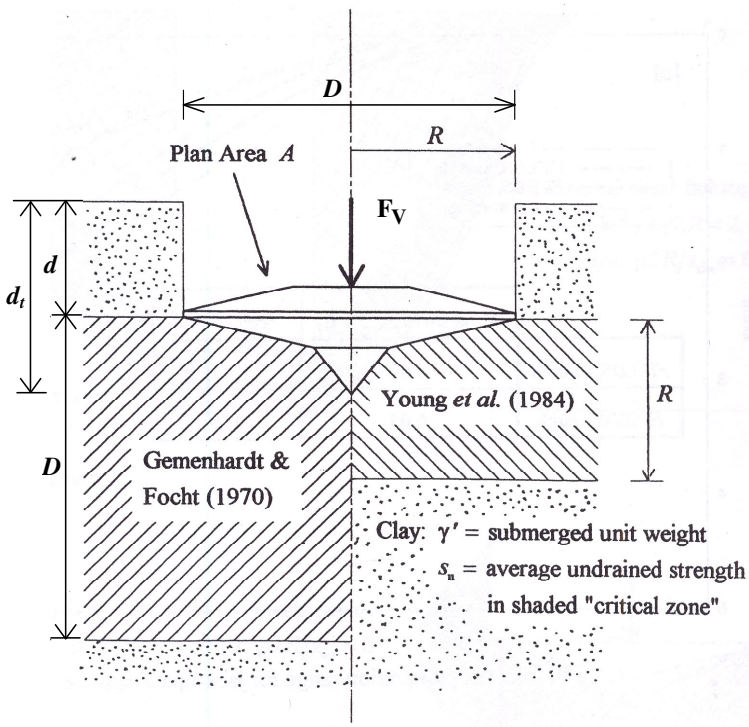

Figure 2.2 Vertical bearing capacity: terminology (after Martin, 1994)

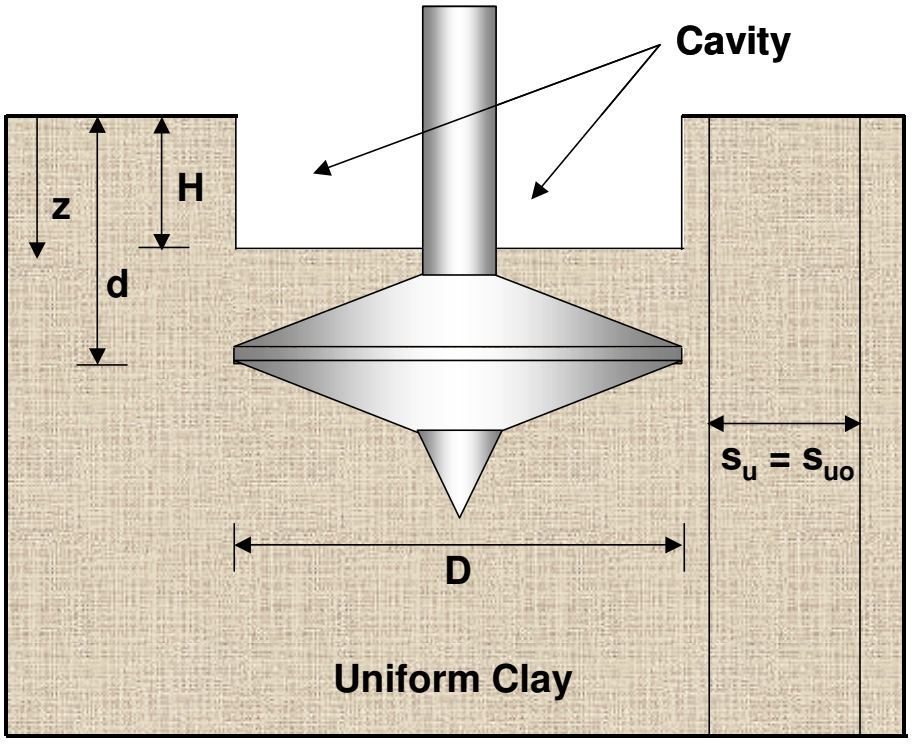

Figure 2.3 Significance of backflow on bearing capacity prediction

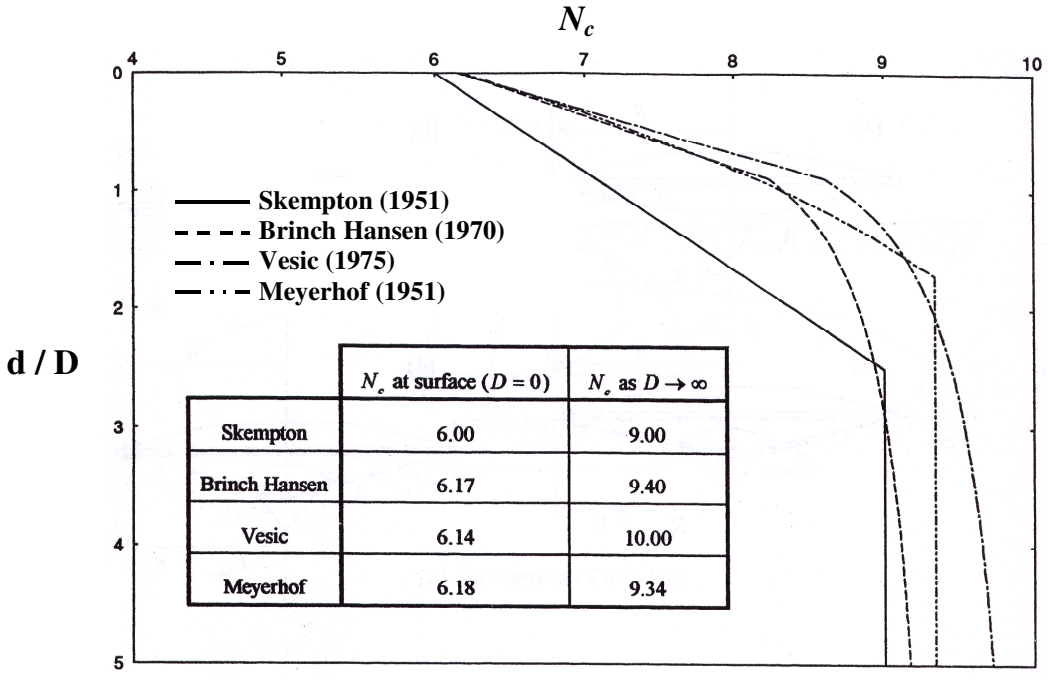

	N_c at surface ($D = 0$)	N_c as $D \to \infty$
Skempton	6.00	9.00
Brinch Hansen	6.17	9.40
Vesic	6.14	10.00
Meyerhof	6.18	9.34

Figure 2.4 Variation of vertical bearing capacity factor for circular footing, N_c with embedment (from theory, after Martin, 1994)

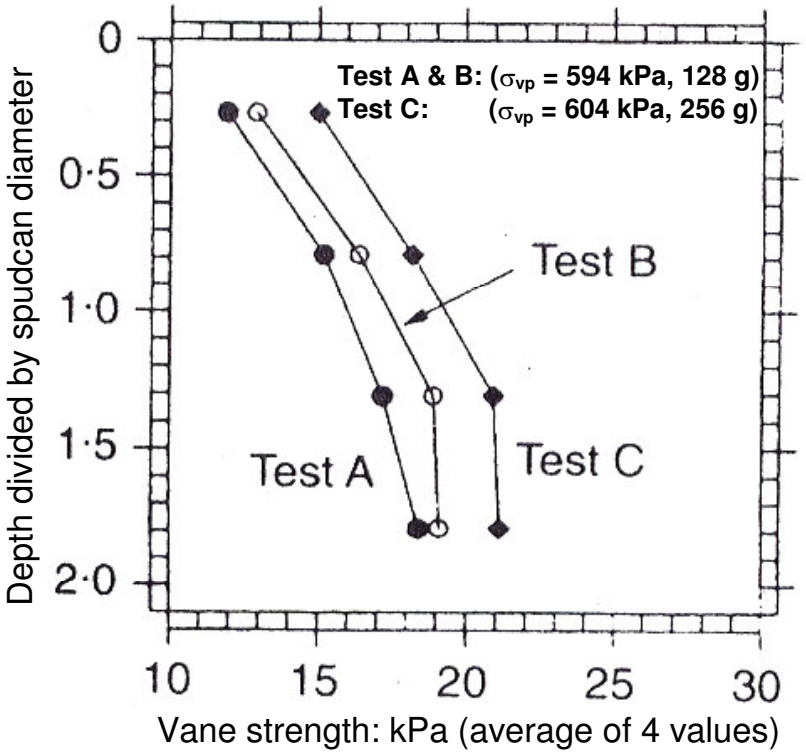

Figure 2.5 Post-test 1 g Vane strength (after Dean *et al*., 1998)

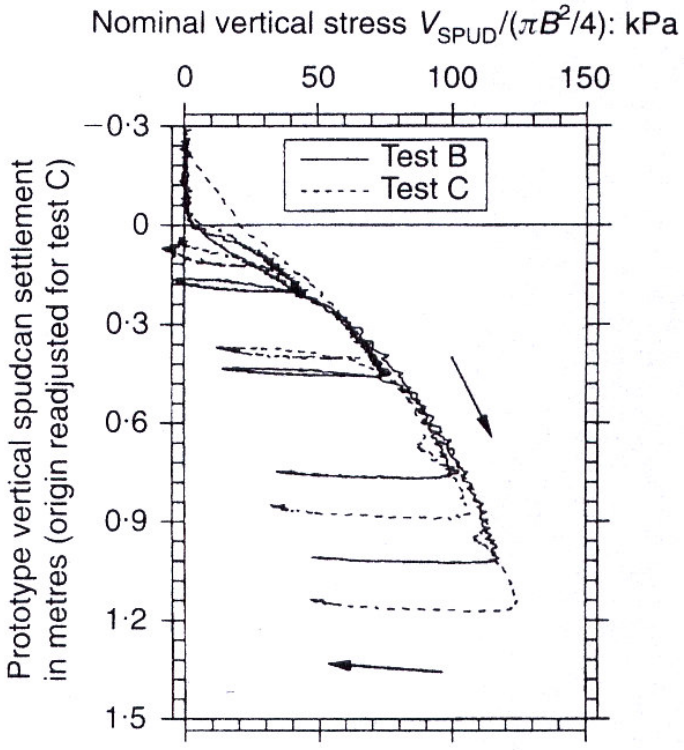

Figure 2.6 Effect of footing diameter (or gravity level) of load-penetration response (after Dean *et al*., 1998)

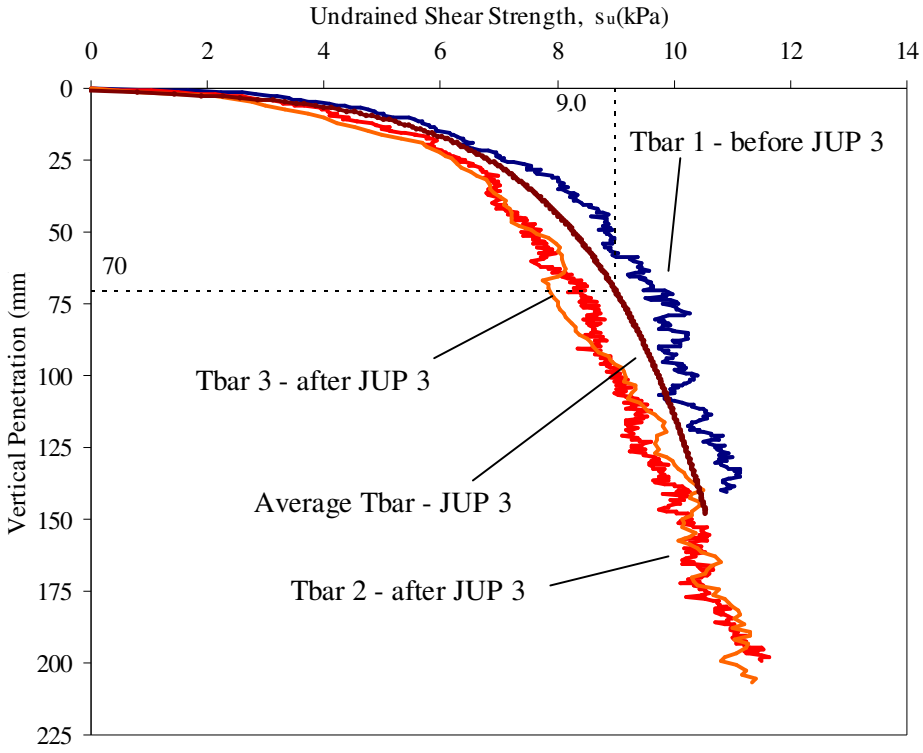

Figure 2.7 Soil strength profile from T-bar tests (after Vlahos *et al.*, 2001)

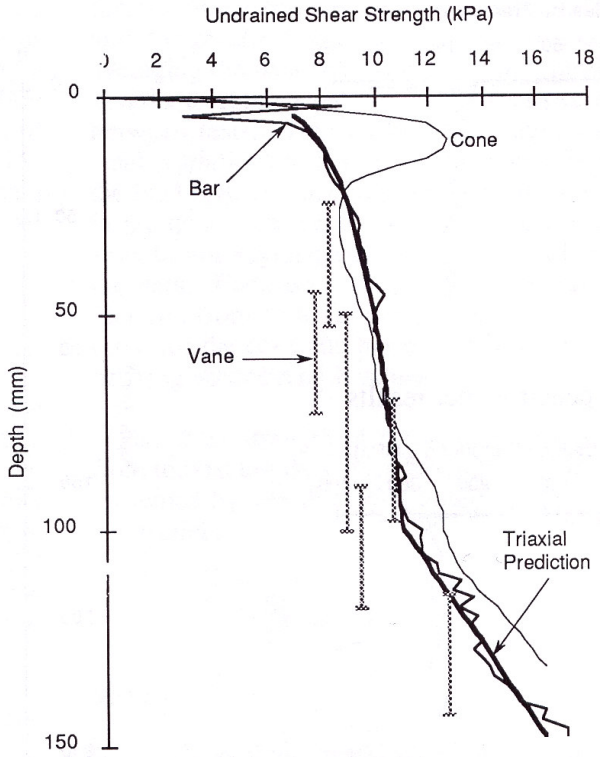

Figure 2.8 Comparison of in-flight T-bar and post-test shear vane test results (after Stewart and Randolph, 1991)

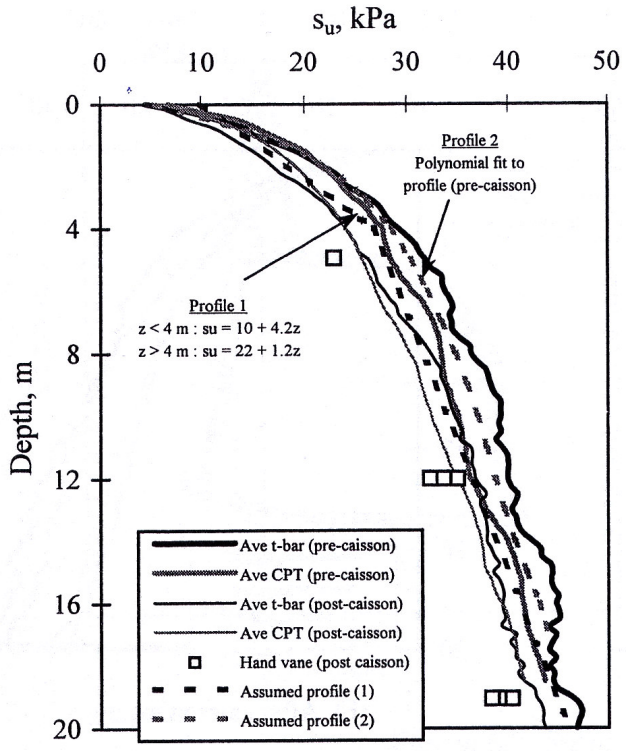

Figure 2.9 Comparison of in-flight T-bar, before and after footing tests, test results (after Watson, 1999)

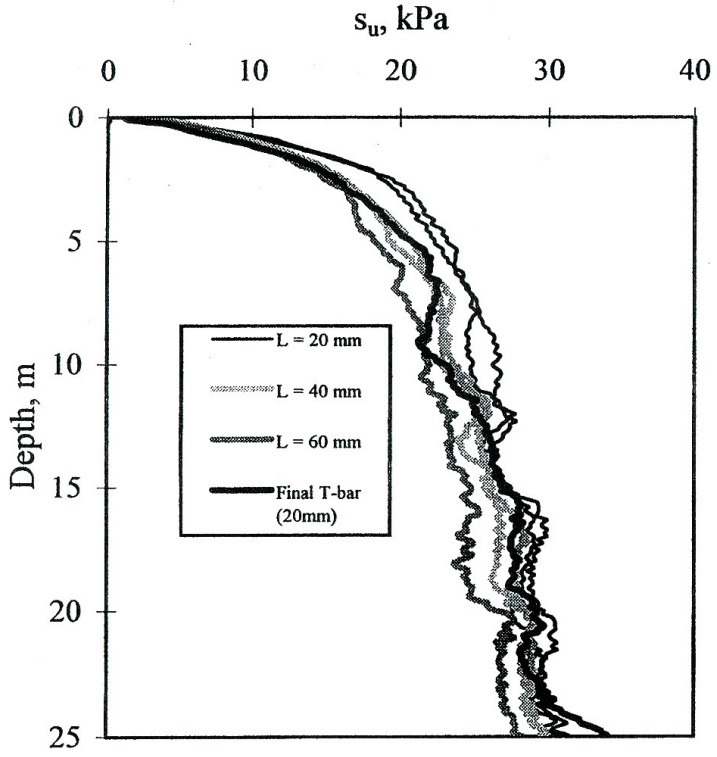

Figure 2.10 Effect of T-bar size (length) on measured undrained clay strength (after Watson, 1999)

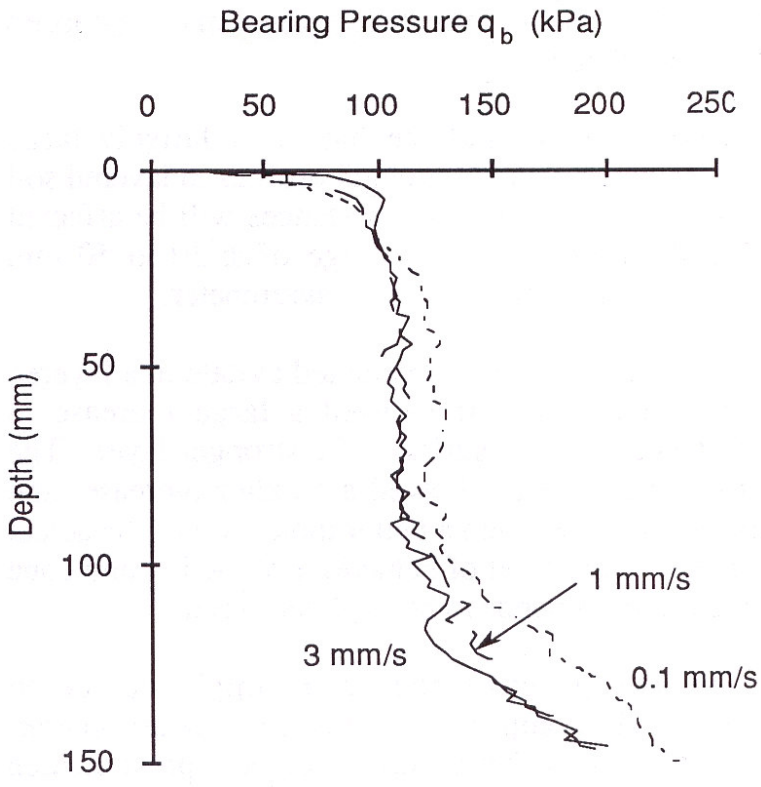

Figure 2.11 Effect of T-bar penetration rate on measured undrained clay strength (after Stewart and Randolph, 1991)

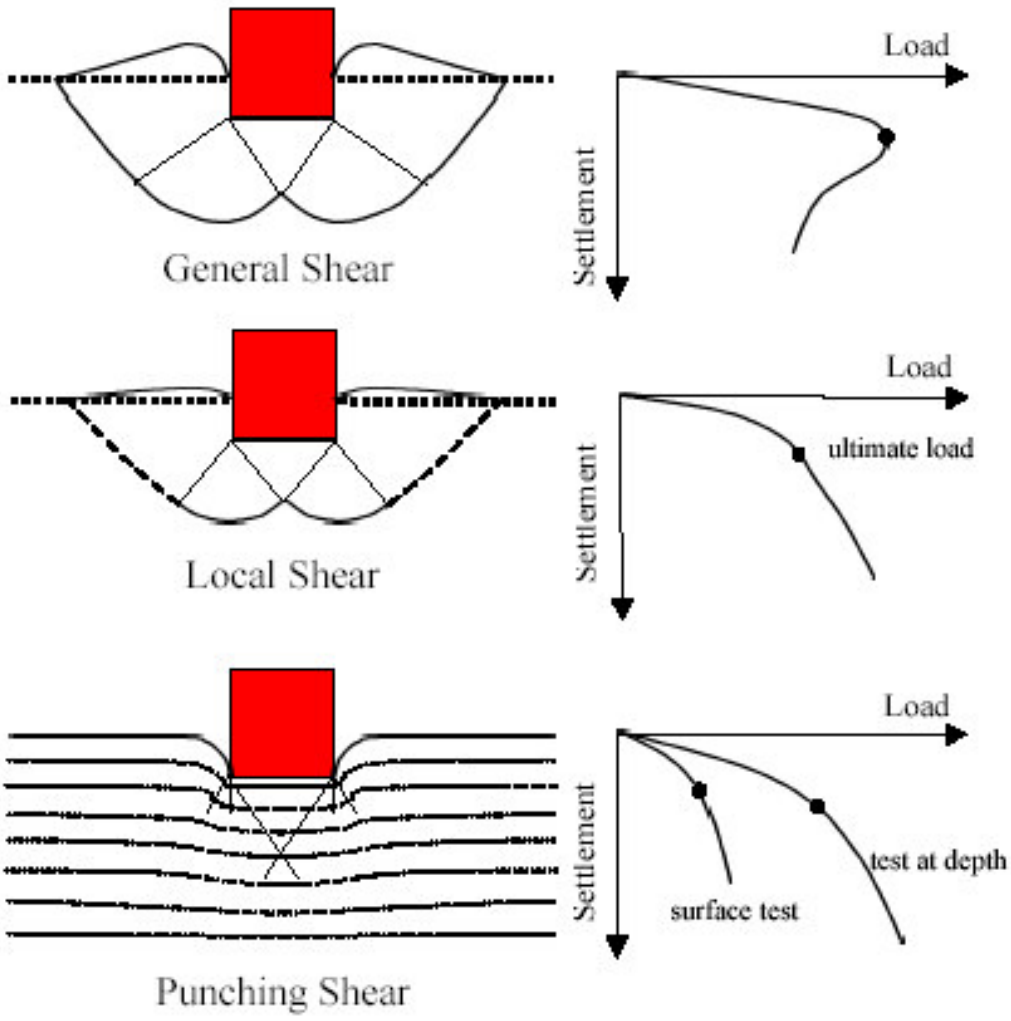

Figure 2.12 Typical failure mechanisms for a shallow foundation (after Vesic, 1973)

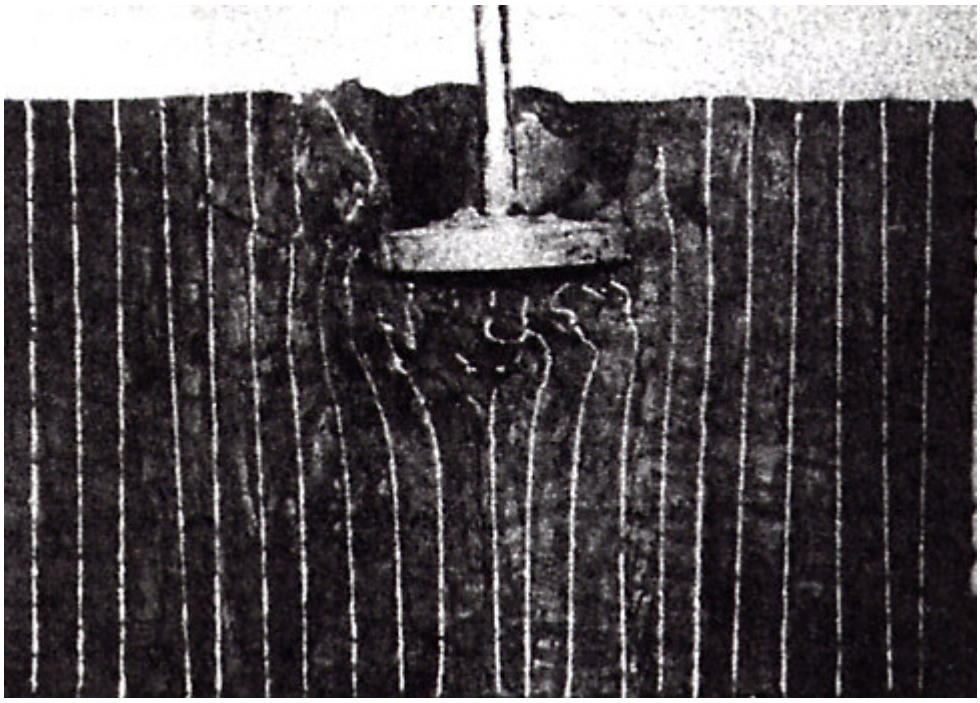

(a) d/D = 0.75

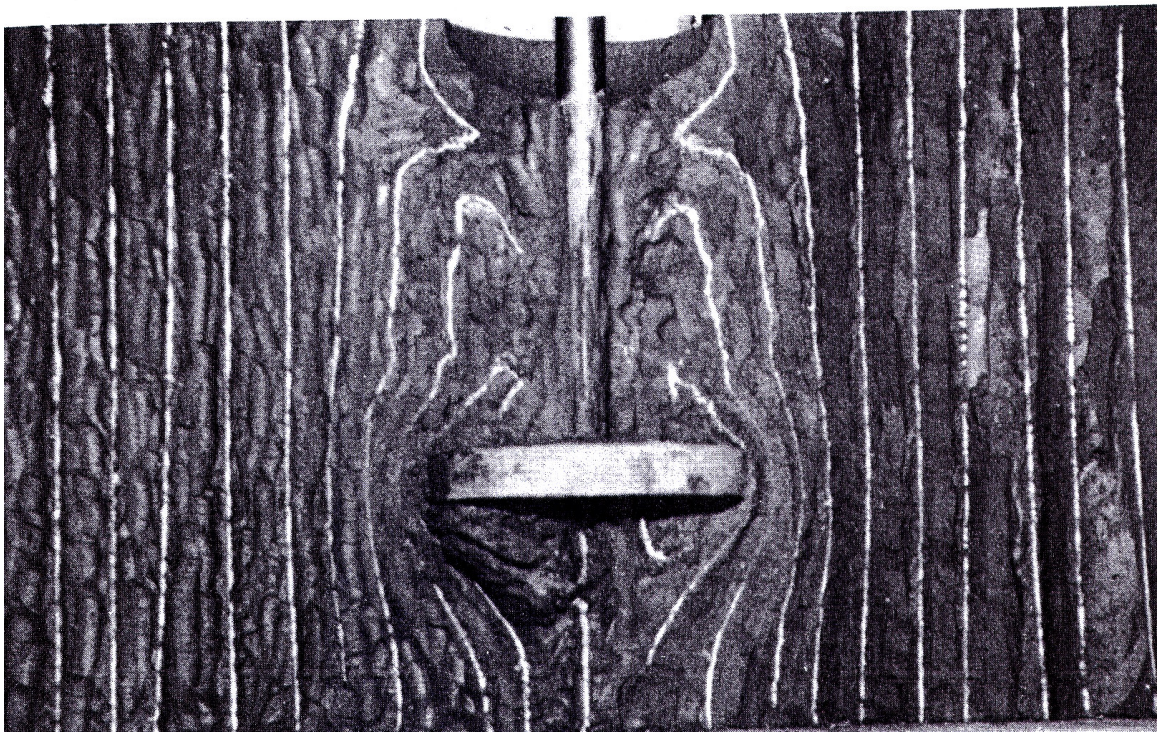

(b) d/D = 1.6

Figure 2.13 Section through model in uniform clay (after Craig and Chua, 1990, 1991)

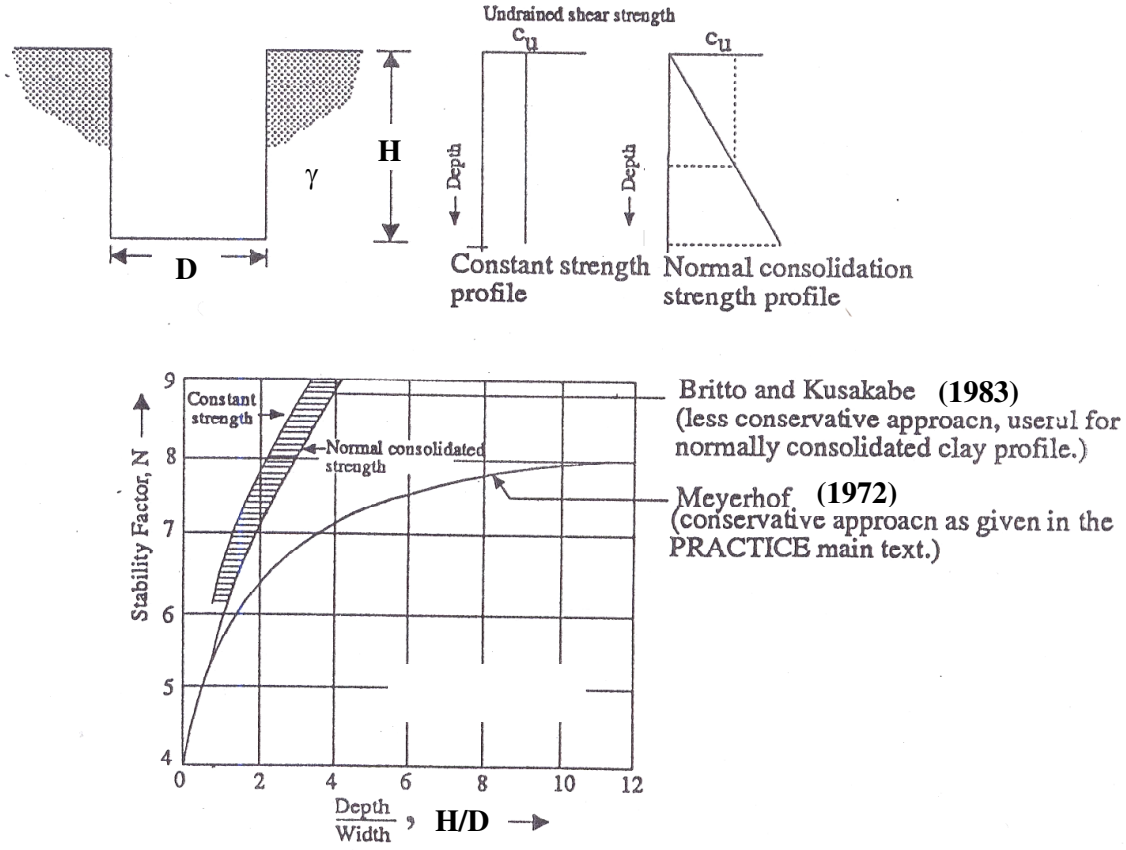

Figure 2.14 Stability numbers for cylindrical excavations in clay (after SNAME, 1997)

CHAPTER 3

PHYSICAL AND NUMERICAL MODELLING

3.1 General

The main focus of this research is to reveal the failure mechanisms of soil underneath and around spudcan foundations and its bearing response during deep penetration. Therefore, physical testing, using the drum centrifuge at the University of Western Australia, and numerical modelling, using AFENA (Carter and Balaam, 1990), are the means to investigate these aspects. The physical centrifuge modelling technique has been designed using scaling factors to obtain results close to in situ foundation dimensions and soil stress field. The numerical analysis can study the influence of isolated soil parameters with soil complex in nature. Another important aspect of this thesis is the continuous validation of the numerical modelling by comparing them with the centrifuge test results. Jack-up rigs are mobile and the offshore soils around the world exhibit a wide range of strength and classification properties. FE analysis is a key tool to reassess seabed behaviour for different sites by changing engineering parameters. This chapter discusses the details of centrifuge and numerical modelling concepts. In the investigation of soil flow mechanism during spudcan deep penetration, Particle Image Velocimetry (PIV) with close range photogrammetry is highlighted.

3.2 Experimental Concept

3.2.1 Why Centrifuge Instead of 1 g?

A 1 g test at standard earth gravity, more often called conventional model test, is easier to perform and less costly than centrifuge test. For undrained geotechnical problems such as this where the loads depend primarily on cohesive soil strength, and not on gravitational forces, reasonable modelling accuracy can be achieved without the need for centrifuge testing. However, with those problems where the loads depend on gravitational forces, 1 g test could cause problems since the gravitational field of soil is not modelled correctly under standard gravity:

- When an open cavity is created during spudcan penetration, due to the small scale of model spudcan foundation, the overburden stress level is much lower than the one in the field situation at the same H/D ratio (where, H is the height of cavity and D is the diameter of spudcan). Thus, soil back flow either never occurs or occurs at a greater depth ratio (d/D ≈ 1). Moreover, even though it occurs, the weight of the resulting infill soil will be negligible compared to the vertical bearing capacity (Martin and Houlsby, 2000).
- The bearing capacity contribution from the surcharge term is too low.

By contrast, in the operational field, there is a significant bearing capacity contribution from the overburden surcharge (provided this is not cancelled out by an extensive infilling above the penetrating footing). Also, at a typical offshore soft clay site, deep spudcan installation is usually associated with a substantial amount of infilling (Endley *et al*., 1981; Le Tirant and Pérol, 1993) which will reduce the net vertical bearing capacity. Soil infilling may have other effects on spudcan behaviour such as increased moment and horizontal load capacities, increased elastic stiffnesses and increased capacity under tensile vertical loading (Martin and Houlsby, 2001). A further consequence of infilling is that significant passive resistance can be mobilised by the embedded portion of a jack-up leg under combined (V, M, H) loading (Springman and Schofield, 1988).

Many model tests in undrained saturated cohesive soils, which can justifiably be analysed in terms of total stress, use full strength and reduced dimensions under 1 g. External loadings, e.g. the bearing stress on a surface foundation, can be brought up to prototype stress levels by mechanical means (Stewart and Randolph, 1991; Stewart, 1992). The disadvantage is that phenomena, such as tension cracking around

the periphery of a structure and surface ground heave, which are controlled by the self-weight of the foundation soils, are not correctly modelled.

In order to simulate a field situation in a laboratory, it is crucial to replicate the in-situ soil stress field properly. This can be achieved through careful centrifuge modelling of the field stress levels, on which the behaviour of soils is particularly strongly dependent. Hence an actual overburden pressure is achieved and subsequently soil failure mechanisms changing with depth, such as back flow (in uniform clay) and wall collapse (in NC clay), can be modelled properly. Centrifuge model testing therefore allows the use of small model structures to simulate the dimensions of a full size prototype, e.g. 10-20 m diameter of spudcan for a jack-up, whilst maintaining field stress levels. Therefore, centrifuge modelling is chosen to perform the experimental work instead of conventional modelling at 1 g.

3.2.2 Visualisation of Soil Flow

In practice, spudcans are generally circular or polygonal in plan. If similitude of stresses and strains is assumed, then a model-scale axisymmetric circular footing is the ideal representation of these field-scale problems.

In a laboratory, to visualise the flow mechanisms during footing penetration into soil (a non-transparent medium), it is necessary to build a strongbox with a transparent window and to penetrate the footing against the window. To perform this operation, a circular axisymmetric model needs to be bisected vertically along the centre. The half-spudcan model penetrates into soil with the central plane facing the strongbox window, i.e. half space spudcan penetration test.

However, it is not an easy job to penetrate a half-spudcan tightly with the Perspex window against a gradually increasing high resistance of soil. Any ingress of soil between the spudcan and the window will cause the spudcan to deviate from the vertical plane hence losing contact with the window. The penetration mechanism can then no longer be observed. In addition, if the soil finds any path to flow vertically

between the spudcan and the window, it will not flow laterally and hence the actual failure mechanisms will not be revealed.

These problems can be circumvented for plane strain conditions by maintaining a tight fit between the front and rear faces of the strongbox. However, the plane strain setup is far away from the field spudcan penetration situation, which is purely axisymmetric. Subsequently, it would incur to build a spudcan footing as long as the strongbox width.

Development against soil ingress

After considering the relative merits of axial symmetry and plane strain, it was decided to take the challenge of performing axisymmetric tests without any ingression of soil. In order to find the way of blocking the ingression of soil, six sets of tests were conducted with as illustrated in Figure 3.1: (a) spudcan alone (Figure 3.1(a))- the soil squeezed→ (b) extruded metallic wiper glued along the bottom edge (Figure 3.1(b))- the wiper broken→ (c) polyethylene foam with abrasion resistant polyethylene film glued on the central plan face (Figure 3.1(c))- the soil squeezed→ (d) polyethylene foam with abrasion resistant polyethylene film glued on the central plan face and a stiffener fitted rare side of the shaft- the amount of soil squeezing reduced→ (e) a 1 mm rubber 'O' ring fitted into the grove cut along the periphery of the contact face of the spudcan and the stiffener as well (Figures 3.1(d), Figure 4.8)- provided satisfactory results i.e. penetration without any soil ingress. It is important to note that the stiffener bottom must be angled and tight fit with the spudcan top conical profile, as shown clearly in Figure 4.8, so that the heavy moment that creates during deep penetration, which is responsible for the spudcan deviation from the window, can be counter balanced.

3.3 Centrifuge Modelling

3.3.1 Introduction

Centrifuge testing involves the study of geotechnical events using small-scale models subjected to acceleration fields that provides a magnitude of many times the Earth's

gravity (g). Centrifuge modelling plays a major role in resolving geotechnical issues relating to offshore structures (Rowe, 1975, 1983; Rowe *et al.*, 1976; Ko, 1988; Bassett *et al.*, 1981). "With this technique, self weight stresses and gravity dependent processes are correctly reproduced and observations from small-scale models can be related to the full-scale prototype situation using well established scaling laws. Centrifuge model tests have proved to be particularly valuable in revealing the mechanisms of soil deformation and collapse and in providing data for validating numerical analyses." (Taylor, 1995).

Laboratory modelling has a major role to play in geotechnical engineering. Physical modelling is designed to replicate an event comparable to what might exist in the prototype. "A special feature of geotechnical modelling is the necessity of reproducing the soil behaviour both in terms of strength and stiffness. In geotechnical engineering there can be a wide range of soil behaviour relevant to a particular problem. There are two principal reasons for this: (i) soils were originally deposited in layers and so it is possible to encounter different soil strata in a site which may affect a particular problem in different ways; and (ii) in situ stresses change with depth and it is well known that soil behaviour is a function of stress level and stress history. Clearly, in any generalised successful physical modelling it will be important to replicate these features. It is for the second reason that centrifuge modelling is of major use to geotechnical engineering." (Taylor, 1995).

3.3.2 Principles

The basic principles of centrifuge modelling for geotechnical purposes have been described in detail by Schofield (1980) and Taylor (1995). "If the same soil is used in the model and prototype and if a careful model preparation procedure is adopted whereby the model is subjected to a similar stress history ensuring that the packing of the soil particles is replicated, then for the centrifuge model subjected to an inertial acceleration field of N times of the Earth's gravity the vertical stress at depth h_m will be identical to that in the corresponding prototype at depth hp where $h_p = N\ h_m$. This is the basic principle of centrifuge modelling, that stress similarity is achieved at

homologous points by accelerating a model of scale 1/N to N times the Earth's gravity." (Taylor, 1995).

3.3.3 Scaling Laws and Relationships (after Taylor, 1995)

In order to correctly replicate a prototype response in a small-scale model it is necessary to develop scaling relationships, which link the model behaviour to that of the prototype. In order to derive these relationships the various physical factors that determine the prototype response must be identified and scaled accordingly in the model. Scaling laws can be derived by making use of dimensional analysis (see, for example, Langhaar, 1951) or from a consideration of the governing differential equations. However, as discussed above, the basic scaling law is derived from the need that ensures stress similarity between the model and the corresponding prototype. Schofield (1980) and Taylor (1995) discussed in detail the modelling laws that apply to centrifuge testing. Presented below is a summary of the laws applicable to model spudcan penetration in clay.

Linear dimensions: If an acceleration of N times of the Earth's gravity (g) is applied to a material of density ρ, then the vertical stress, σ_v at depth h_m in the model (using subscript 'm' to indicate the model) is given by:

$$\sigma_{vm} = \rho N g h_m \qquad (3.1)$$

In the prototype, indicated by subscript 'p', then:

$$\sigma_{vp} = \rho g h_p \qquad (3.2)$$

Thus for $\sigma_{vm} = \sigma_{vp,}$ then $h_{m} = h_p N^{-1}$ and the scale factor (model: prototype) for linear dimensions is 1: N. Since the model is a linear scale representation of the prototype, then the displacements will also have a scale factor of 1: N. It follows therefore that strains have a scale factor of 1:1 and so the part of the soil stress-strain curve mobilised in the model will be identical to the one in the prototype.

Consolidation (diffusion) and seepage: Consolidation relates to the dissipation of excess pore pressure and is a diffusion event. It is easiest to examine the scaling law for the time of consolidation using a dimensional analysis. The degree of consolidation is described by the dimensionless time factor T_v defined as:

$$T_v = \frac{c_v t}{H^2} \tag{3.3}$$

where c_v is the coefficient of consolidation, t is the time and H is the distance related to a drainage path length. For the same degree of consolidation, T_v will be the same in model and prototype and so:

$$\frac{c_{vm}\ t_m}{H_m{}^2} = \frac{c_{vm}\ t_p}{H_p{}^2} \tag{3.4}$$

Since $H_p = N\ H_m$, then:

$$t_m = \frac{1}{N^2}\frac{c_{vp}}{c_{vm}} t_p \tag{3.5}$$

Hence, if the same soil is used in model and prototype (which is usually the case) then the scale factor for time is 1: N^2. The scale factor would need to be adjusted, as indicated by the above equation, if for some reason the coefficients of consolidation were not the same in model and prototype. Thus a consolidation event lasting 400 days in the prototype can be reproduced in a one-hour centrifuge run at 100g. Following the analysis as above, the other scaling relationships can be shown below:

a) $\text{mass}_p = \text{mass}_m \times N^3$
b) $\text{velocity}_p = \text{velocity}_m \times N$ (considering diffusion event)
c) $\text{force}_p = \text{force}_m \times N^2$
d) $\text{density}_p = \text{density}_m$

All of these relations are summarised in Table 3.1.

3.3.4 Mechanics of Model (after Taylor, 1995)

The Earth's gravity is uniform for the practical range of soil depth encountered in civil engineering. When using a centrifuge to generate the high acceleration field required for physical modelling, there is a slight variation in acceleration through the model. This is because the inertial acceleration field is given by $\omega^2 r$, where ω is the angular rotational speed of the centrifuge and r is the radius to any element in the soil model. This apparent problem turns out to be minor if care is taken to select the radius at which the gravity scale factor N is determined.

The distribution of vertical stress in the model and corresponding prototype are shown in Figure 3.2. These distributions of vertical stress are compared directly in Figure 3.3 where they are plotted against corresponding depth; note that the non-linear variation of stress in the model is shown exaggerated for clarity. Based on this distribution, Taylor (1995) made the following argument. There is an exact correspondence in stress field between the model and the prototype at two thirds of the model depth ($h_i = 2/3\ h_m$) and the centrifuge radius should be measured from the central axis to one-third the depth of the model ($R_e = R_t + h_m/3$). The maximum error is ($h_m/6R_e$). For most geotechnical centrifuges, h_m/R_e is less than 0.2 and therefore the maximum error in the stress profile is minor and generally less than 3% of the prototype stress. It is important to note that even for relatively small radius centrifuges (say 1.5 m effective radius), the error due to the non-linear stress distribution is quite small for moderately large models of say 300 mm height. In this research effective radius was always maintained at one-third of the soil sample depth.

3.3.5 Scaling Effects (after Taylor, 1995)

Centrifuge modelling is often criticised as having significant scaling errors due to the non-uniform acceleration field and the difficulty of representing sufficient detail of the prototype in a small-scale model. It is clearly important to have a proper appreciation of the limitations of a modelling exercise.

In physical modelling studies, it is seldom possible to replicate precisely all details of the prototype and some approximations have to be made. It is important to recognise that model studies are not perfect and to inquire into the nature of any shortcomings, often referred to as scaling effects, and to evaluate their magnitude. Some examples of scaling effects are discussed below. Some others aspects may be relevant in any particular centrifuge study. And it is recommended that it is the centrifuge worker's responsibility to establish for any particular project the extent to which the model test results can be extrapolated to a prototype scale.

Particle size effects: The most common question asked of centrifuge workers is, how can centrifuge modelling be justified if the soil particles are not reduced in size by a factor of *N*. In increasing the model scale to the prototype in the mind's eye, it might appear sensible to also increase the particle size. Thus a fine sand used in a 1:100 scale might be considered as representing a gravel. By the same argument, a clay would then be considered as representing a very fine sand. This argument is clearly flawed since a clay has very different stress-strain characteristics to a fine sand. There could be a problem if an attempt is made to a model test at a high acceleration level and hence at a very small scale in an event where a prototype soil consists mainly of a coarse soil (gravel). In this case, the soil grain size would be significant when compared to model dimensions and it is unlikely that the model would mobilise the same stress-strain curve in the soil as would be the case in the prototype. Local effects of the soil grains would influence the behaviour rather than the soil appearing like a continuum as would be the case in the prototype.

To avoid particle size effects on foundation response, it is therefore sensible to follow simple guidelines on the critical ratio of a major dimension (such as foundation dimension) to the average grain diameter in the model test. Ovesen (1979) investigated the performance of circular foundations on sand by undertaking a series of experiments using different sized models at different acceleration levels such that they corresponded to the same prototype. The data were generally internally consistent, which validated the centrifuge technique. However, it was noted that there was some deviation from the common behaviour when the ratio of foundation diameter to grain size was less than about 15. The important point is to recognise that in some circumstances particle size effects may be important and the

model tests series should include sufficient relevant investigation to assess its significance in the problem being studied.

Rotational acceleration field: While a centrifuge is an extremely convenient method of generating an artificial by high gravitational acceleration field, problems are created by the rotation about a fixed axis. The inertial radial acceleration is proportional to the radius which leads to a variation with depth in the model; as discussed in Section 3.3.4. This acceleration is directed towards the centre of rotation and hence in the horizontal plane of the centrifuge, there is a change in the acceleration direction relative to the vertical direction of the sample across its width. There is therefore a lateral component of acceleration. This effect needs to be recognised. This can be quite significant if the major testing area is away from the radius of the channel. Therefore, it is good practice to ensure that major events occur along the radius of the channel where the error due to the radial nature of the acceleration field is minimal.

3.3.6 Centrifuge Modelling vs Field/In Situ Tests

The centrifuge modelling technique is now firmly established in the field of Geomechanics. This method is particularly useful for problems involving self-weight loading and consolidation or other diffusion processes. Self weight loading is generated automatically by the enhanced weight of the soil and diffusion processes occur rapidly due to the small dimensions of the model.

Centrifuge models have major advantages over full-scale field trials: comparatively cheaper, well controlled, more easily and accurately instrumented and with more uniform soil conditions in areal extent. However, this does not mean that field trials are unwarranted and the applicability of the observed model behaviour should be confirmed by reference to field observations or known behaviour. Additionally, the complex configurations of soil may not always be modelled properly. For instance, a soil strength profile related to the specific site conditions such as: the proportion of soil particles which are organic, the influence of long term chemical effects and

secondary compression (which will lead to higher strengths-Bjerrum, 1972) are not present in the model test.

Systematic studies of spudcan response during static and dynamic load tests are generally too expensive and risky to conduct in the field. The high cost of field-testing necessitates that such studies are undertaken, at least initially, at model scale where the associated costs are at least 2 orders of magnitude lower.

3.3.7 Modelling of Models (after Taylor, 1995)

A good technique for checking for scale effects is 'modelling of models'. It is particularly useful when no prototype is available for verifying the model test results. Centrifuge models of different scale (say N_1 and N_2) are tested at an appropriate acceleration level such that they then correspond to the same prototype. The models should predict the same behaviour (the product of length times acceleration is the same: $l_1 N_1 = l_2 N_2$) and thus provide a useful internal check on the modelling procedure.

3.4 Numerical Modelling Concept

3.4.1 Two-Dimensional or Three-Dimensional Analysis?

During operation and storm, spudcan foundations are subjected to horizontal (H) and moment (M) loading in addition to vertical loading (V). Performance under such combined loading can be evaluated using multi-dimensional yield functions (Martin, 1994; Cassidy, 1999; Martin and Houlsby, 2001). Three-dimensional numerical analysis is essential to build this yield function and to simulate in situ stresses and strains.

During installation and in a perfectly calm sea, however, the vertical load (V) is the only loading on the spudcans. To depict the spudcan or soil behaviour under such monotonic loading, two-dimensional analysis is sufficient. This research

concentrated only on spudcan installation. Hence, it was decided to perform two-dimensional numerical analysis that is axisymmetric.

3.4.2 *H*-Adaptive Finite Element Method

When finite element method is used in numerical analysis, the domain analysed has to be discretized into many small elements. This discretisation will bring in some calculation error to the solution, which will reduce the accuracy of the calculation. To minimise this discretization error, the element size needs to be small enough. However, the smaller the elements, the finer the mesh, the more costly will be the calculation. *H*-adaptive mesh generation is to adjust the element size by the discretization error, so that the element size need only be reduced in a high error region.

For non-linear elasto-plastic analysis, Hu & Randolph (1998[2]) have proposed an SPR-strain error estimator that is shown as follows,

$$e_i^* = \left[\left\{ \int_{\Omega_i} \left(\varepsilon^* - \varepsilon^h\right)^T \left(\varepsilon^* - \varepsilon^h\right) d\Omega \right\} / \Omega_i \right]^{1/2} \tag{3.6}$$

in which Ω_i is the area of element *i* in two dimensional analysis (or volume for three dimensional analysis), ε^h are the strains from the FE solution, ε^* are the strains recovered by SPR (Superconvergent Patch Recovery, Zienkiewiez & Zhu, 1993). The non-dimensional characteristic of this error estimator makes it easy to use.

When the discretization error is estimated using Equation 3.6, the initial coarse mesh can be refined. The detailed procedure on mesh refinement and minimum element size selection has been published by Hu & Randolph (1998[1]). The following is a brief description:

1. Generate an initial coarse mesh.
2. Compute an initial strain field ε^h on integration points.
3. Compute recovered strain field ε^* using SPR.

4. Calculate estimated error for each element using Equation 3.6.
5. Find e^*_{imax} over the entire mesh.
6. Halve the element size ($h_{new} = 0.5\ h_{old}$) in the area with $e^*_i > 0.5e^*_{imax}$.
7. Create a new mesh with updated mesh density function (h_{new}).
8. Use this new mesh to repeat steps 2-7, until h_{min} is achived. The number of cycles needed depends on the initial element size and the minimum element size required (h_{min}).

The above method for mesh refinement has been proved to work well in producing an optimal mesh for FE analysis in foundation response calculation.

3.4.3 *H*-Adaptive RITSS Method

H-adaptive RITSS (Remeshing and Interpolation Technique with Small Strain) method is used in continuous penetration analysis. In the RITSS method, a large deformation problem is solved using incremental small strain analyses by frequent remeshing and interpolation of stress field and soil properties over the analysed domain. The above *h*-adaptive mesh generation cycle is used to create an initial optimal mesh and for remeshing after each updated domain boundary. The procedure used in large penetration analysis by the *h*-adaptive RITSS method is summarised below. The details can be found in Hu and Randolph (1998[2]).

1. Generate an initial optimal mesh using the above *h*-adaptive mesh refinement cycles.
2. Calculate FE results with N steps of incremental small strain analysis using the AFENA.
3. Re-generate a new mesh using the updated domain boundary.
4. Check if the penetration has reached the desired value; if not, go to step 2, otherwise stop.

In step 2, the number of increments is designed so that the total deformation between each remeshing remains in a small strain range.

3.4.4 Bearing Capacity Analysis

Finite element analyses have been conducted using the AFENA finite element package (Carter & Balaam, 1990), developed at the University of Sydney, with implemented *h*-adaptive mesh generation. The geometry of the spudcan is shown later in Figure 4.9. However, in order to compare FE results with 100 g and 200 g centrifuge test results all linear dimensions were increased 100 and 200 times respectively (Table 3.1 and Table 4.1). The considered soil domain was 6 D in radius and 10 D in depth (D is spudcan diameter in prototype, Mehryar, 2002). The soil was modelled as elasto-plastic material with Tresca yield criterion. All the analyses simulated undrained conditions and hence Poison's ratio $\nu = 0.49$, friction and dilation angles $\phi = \psi = 0$, and a uniform stiffness ratio $E/s_u = 500$ (where E is the Young's modulus, s_u undrained shear strength) were adopted.

Small deformation analyses were performed under three conditions: (i) Fully Open Cavity — where no backflow occurs into the punched cavity during spudcan penetration; (ii) Cavity with Partial Backflow — where soil starts to flow back into the cavity after flow failure which fills the lower cavity with the top cavity open; (iii) Full Backflow — where soil starts to flow back from shallow penetration, therefore no cavity forms. Nine homogeneous soil cases were considered in the FE analyses (see Table 3.2). Cases I - IV are to simulate centrifuge test results without water on top and Case V is to simulate the centrifuge test a submerged clay bed. Cases VI –IX are to investigate the effect of soil strength, soil density and footing size. In the bearing capacity analyses, pre-embedment ratios have been varied from d/D = 0.025 to 2.27 (Figure 2.3), with both smooth and rough soil-spudcan interfaces. Large deformation with continuous penetration analyses was also performed for a few cases to compare the results with the ones from small deformation analyses and centrifuge tests.

To ensure accuracy of the FE analyses, the minimum element size, h_{min} and displacement increment of δ were calculated using following criteria (Hu and Randolph, 1998[2]):

$$h_{min} = 0.005D \tag{3.7}$$

$$\left(\frac{\delta}{D}\frac{E}{s_u}\right) * \left(\frac{kD}{s_{u0}}\right)^{0.8} = 0.03 \tag{3.8}$$

where kD/s_{u0} is taken as one for homogeneous soil, where $k = 0$ is the gradient of s_u and $s_{u0} = s_u$ is the soil surface undrained shear strength.

3.5 Particle Image Velocimetry (PIV) Analysis

3.5.1 Introduction

White (2002) and Take (2002) together developed a new system for precise measurement of soil movement around a foundation in physical testing. Although it has been developed primarily for their projects, the new system is widely applicable throughout geotechnical testing and offers a flexible technique for non-contact measurement of soil deformation at pre-failure strain levels without recourse to target markers. The system combines three technologies: digital still photography, Particle Image Velocimetry (PIV) and close range photogrammetry.

3.5.2 Digital Photography

"The first step in a video-based analysis system is to digitise the video image, using a PC frame-grabbing card. In the digitised form, a monochrome image consists of a two dimensional integer matrix containing the intensity (brightness) recorded at each CCD[1] pixel. A typical 8-bit frame grabbing card records brightness on an integer scale from 0 to 255. Colour images consist of three matrices: one for each colour channel. Image analysis techniques for displacement measurement such as centroiding operate on these integer matrices." (White, 2002).

[1] CCD: Charge Coupled Device. This is the flat element within the camera on which the image is formed. In digital photography a CCD is used to capture the image, instead of photographic film.

There are two types of camera used in this research: mini video camera and digital still camera. Image frames, acquired from a European standard (PAL[2]) mini video camera, have a nominal resolution of around 720 × 576 pixels. This mini video camera was used in Event 1 to Event 5 testing (Chapter 5) in this research (Figure 4.7). In contrast, digital still camera offers significantly higher pixel resolution. In Event 6 of this research, a Cannon PowerShot S40 digital still camera was used to capture images (Figure 4.6). This camera has a pixel resolution of 2270 × 1704 pixels. Compared to PAL video camera, this resolution represents a 3.1 times reduction in object-space pixel size, with a corresponding increase in precision. Digital still cameras offer another benefit over video cameras: the resulting images are stable since they are converted to digital signal within the camera rather than frame-grabbing card (or any other way of later digitisation). This avoids line-jitter and the additional noise associated with an analogue transmission.

Most digital cameras can be controlled via a PC link using native control software (e.g. Cannon Remote Capture), allowing remote adjustment of camera settings and downloading of images. This feature reduces the likelihood of accidental camera movement during operation, which leads to an apparent displacement. The S40 camera can be interfaced with a PC using a Universal Serial Bus (USB) connection, allowing faster image downloading than a conventional RS232 serial link.

However, a major drawback of digital still photography is the low frame rate. A full cycle of image capture includes digital conversion, JPEG image compression, and transmission through USB link to the hard disk of computer; which must be completed before capturing a subsequent image. A capture rate of 10 seconds per frame (0.1 Hz) can be achieved by the S40 in maximum resolution mode, although slower performance results if more than one camera is connected to the PC. Whereas a significantly higher capture rate of 0.02 seconds per frame (50 Hz) can be achieved by the mini video camera in maximum resolution mode.

Additionally, the images downloaded through the centrifuge sliprings are unreliable. In order to eliminate these effects, the camera was modified by attaching a small

[2] PAL (720 × 576 pixels): Phase Alternating Line. Video signal standard used in Europe like NTSC (720 × 480 pixels): National Television Standards Committee, used in United States and Japan.

weight to the shutter. Under centrifuge acceleration, this weight presses the shutter and triggers the continuous shooting mode of the camera. This modified system eliminates the necessity of transferring captured images through centrifuge sliprings and connecting the camera with the computer. This allows images to be captured reliably and at a higher rate of approximately 0.4 Hz, until the memory card of the camera (512 MB) is full (discussed in Section 4.2.4). The images are then downloaded after the centrifuge test. If a 7.4 v. power is unavailable on the ring channel, the camera can be operated from the battery. In a continuous shooting mode the battery lasts for about 60 minutes. Therefore, this system applies a limitation on the time of continuous image capturing and hence on the time of centrifuge testing. An optimisation of test plan is necessary to fully utilise the 60 min image capture time.

3.5.3 Particle Image Velocimetry (PIV) (after White and Take, 2002)

Particle Image Velocimetry (PIV) analysis has been performed using GeoPIV. The GeoPIV software, which implements the principles of PIV in a style suited to the analysis of geotechnical tests, was written by White and Take (2002) during their PhD research at Cambridge university.

PIV is a velocity-measuring procedure originally developed in the field of experimental fluid mechanics (Adrian, 1991). GeoPIV uses the principles of PIV to gather displacement data from sequences of digital images captured during geotechnical model and element tests. GeoPIV is a MatLab module, which runs at the MatLab command line. The development and performance of the software were described in detail by White (2002) and Take (2002). Concise details are presented in White *et al.* (2001[1], 2001[2], 2003).

The principles of PIV analysis are summarised in Figure 3.4. The analysis process used in GeoPIV is indicated by the flowchart shown in Figure 3.5. PIV operates by tracking the texture (i.e. the spatial variation of brightness) within an image of soil through a series of images. The initial image is divided up into a mesh of PIV test

patches. To find the displaced location of a patch in a subsequent image, this single patch, located at coordinates (u_1, v_1) in image 1 (Figure 3.4) is considered in the following operation:

1. The correlation between the patch extracted from image 1 (time = t_1) and a larger patch from the same part of image 2 (time = t_2) is evaluated.
2. When the location of the highest correlation is found, it indicates the displaced position of the patch (u_2, v_2), in which the location of the correlation peak is established to a sub-pixel precision by fitting a bicubic interpolation around the highest integer peak.
3. This operation is repeated for the entire mesh of patches within the image, then repeated for each image within the series, to produce complete trajectories of each test patch.

The MatLab module requires two input files (a launcher and an initial mesh file) which are prepared in ASCII format by the user. Simple MatLab scripts can be used to assist the preparation of these input files. The output files are in ASCII format, and can be manipulated by the user in MatLab or a spreadsheet to produce displacement and strain data.

3.5.4 Close Range Photogrammetry

The spatial variation in image scale leads to errors if the displacement vectors measured by PIV are converted from image-space (pixels) into object-space (mm) using a single scaling factor. Most previous geotechnical researchers, with the notable exceptions of Taylor *et al.* (1998), Ethrog (1994), White (2002) and Take (2002) have overlooked image distortion, assuming that the image scale factor is constant throughout the image.

"However, to increase an order-of-magnitude in image-space measurement precision, PIV must be accompanied by some corrections for image distortion if the improved precision is to be exploited. The process of correcting image distortion is known as camera calibration. Instead of the straightforward single scaling factor to link pixel

(u, v) with object-space *(X)* coordinates, a mathematical framework is used to describe the transformation *(u, v)* $\Rightarrow \underline{x} \Rightarrow \underline{X}$." (White, 2002).

This mathematical framework is based on the principles of close-range photogrammetry, and accounts for a number of sources of image distortion. These sources are described below (after White, 2002).

Non-coplanarity: The coordinate systems of the CCD and the object plane are rotated relatively to each other by the Euler angles θ, ϕ, and φ, such that the normals to the image and object planes are not parallel. Take (2002) reported that the enhanced self weight of a typical digital still camera during centrifuge testing at 100 g leads to an apparent 3°. rotation of the CCD. Even without centrifuge acceleration, a precise alignment of the CCD and object plane is difficult, perhaps leading to a 1-2% spatial variation in image scale.

Radial and tangential lens distortion: The pinhole camera model, signified by the bundle of light rays passing straight through a single point to form a perspective projection of the object on the camera CCD, is an approximation. Radial lens distortion causes the light ray to be deflected radially from the normal to the lens (Slama, 1980). This distortion is commonly known as fisheye.

A second error arises since the centres of curvature of the lens surfaces through which the light is refracted are not always perfectly collinear. This is particularly the case for cameras with optical systems that contain multiple lenses. This creates decentring distortion, which has both a radial and a tangential distortion component (Slama, 1980). The tangential component is commonly known as barrelling.

CCD non-squareness: A further source of variation in image scale is the non-squareness of CCD pixels. Although small, this error is a linear scaling factor, and so can be easily incorporated into the transformation from pixel coordinates to image space coordinates. The aspect ratio, α, is defined as the height of a pixel divided by the width, and is typically in the range 1 ± 0.004 (Heikkila and Silven, 1998; Ahmad and Chandler, 1999), and is considered to be constant over the CCD.

Refraction through a viewing window: A further variation in image scale arises when the object is behind a viewing window. This causes the light rays to be refracted. An apparent change in object size arises. This apparent scaling depends on the thickness and refractive index of the window, which do not vary across the image, and the inclination of the rays to the normal of the window, which does vary across the image. Snell's Law is used to model this refraction.

Table 3.1 Centrifuge scaling laws

Parameter	Scaling Relationship (model / prototype)
Gravity	N
Stress	1
Strain	1
Length	1/N
Force	$1/N^2$
Density	1
Mass	$1/N^3$
Velocity	N
Time (consolidation)	$1/N^2$

Table 3.2 Case studies in FE analyses

		s_u (kPa)	γ (kN/m^3)	D (m)	Notes
Without water on top	Case I	13	17	6	100 g centrifuge
	Case II	16.5	17	6	100 g centrifuge
	Case III	18	17	12	200 g centrifuge
	Case IV	20	17	12	200 g centrifuge
With water on top	Case V	12	7	6	100 g centrifuge
	Case VI	18	7	12	Numerical comparison
	Case VII	9	17	12	Numerical comparison
	Case VIII	18	17	6	Numerical comparison
	Case IX	9	17	6	Numerical comparison

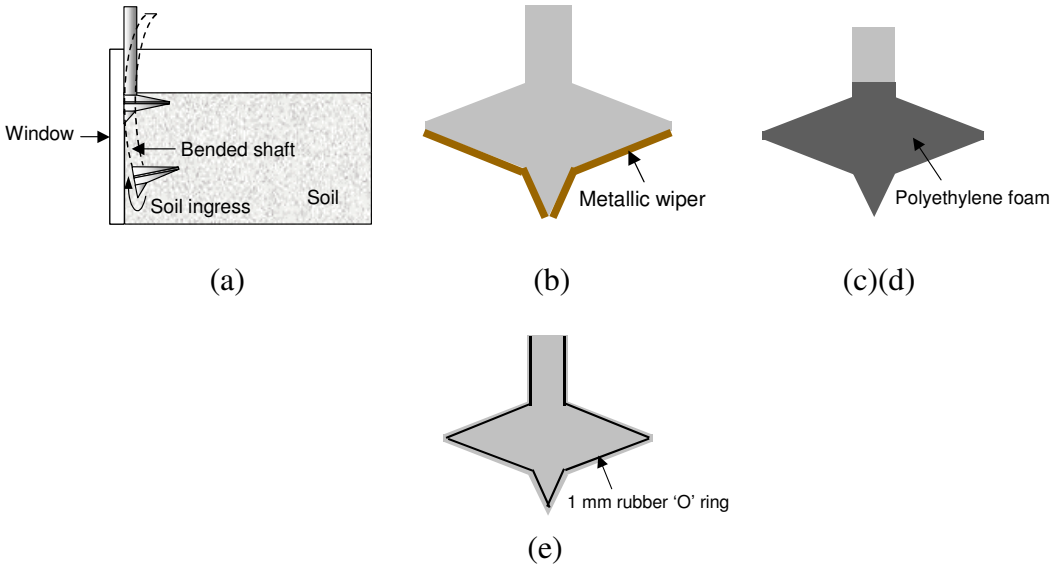

Figure 3.1 Development against soil ingress: (a): spudcan alone; (b): spudcan with metallic wiper; (c): spudcan with polyethylene foam; (c): spudcan with polyethylene foam and stiffener; (e): spudcan with 'O' ring and stiffener

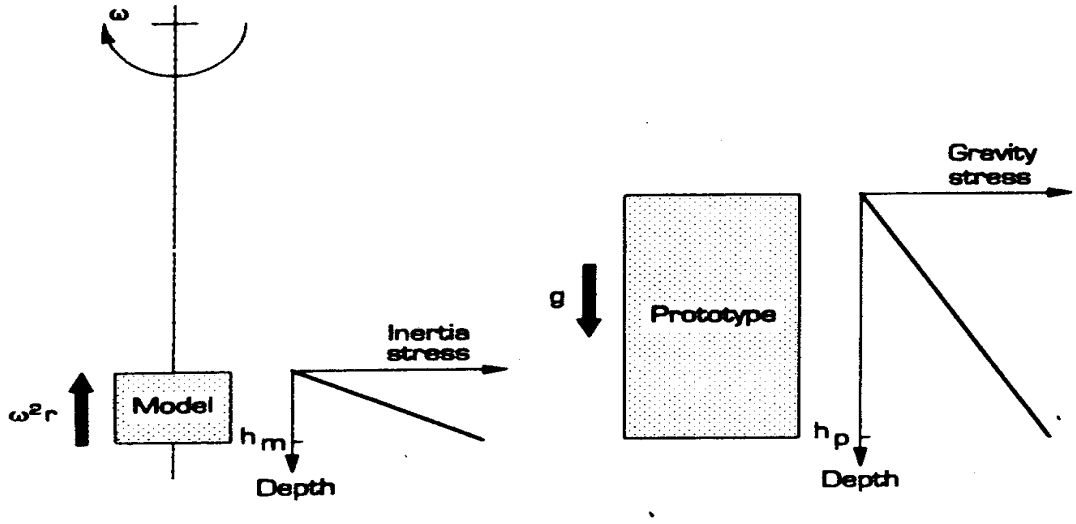

Figure 3.2 Inertial stresses in a centrifuge model induced by rotation about a fixed axis vs the gravitational stresses in the corresponding prototype (after Taylor, 1995)

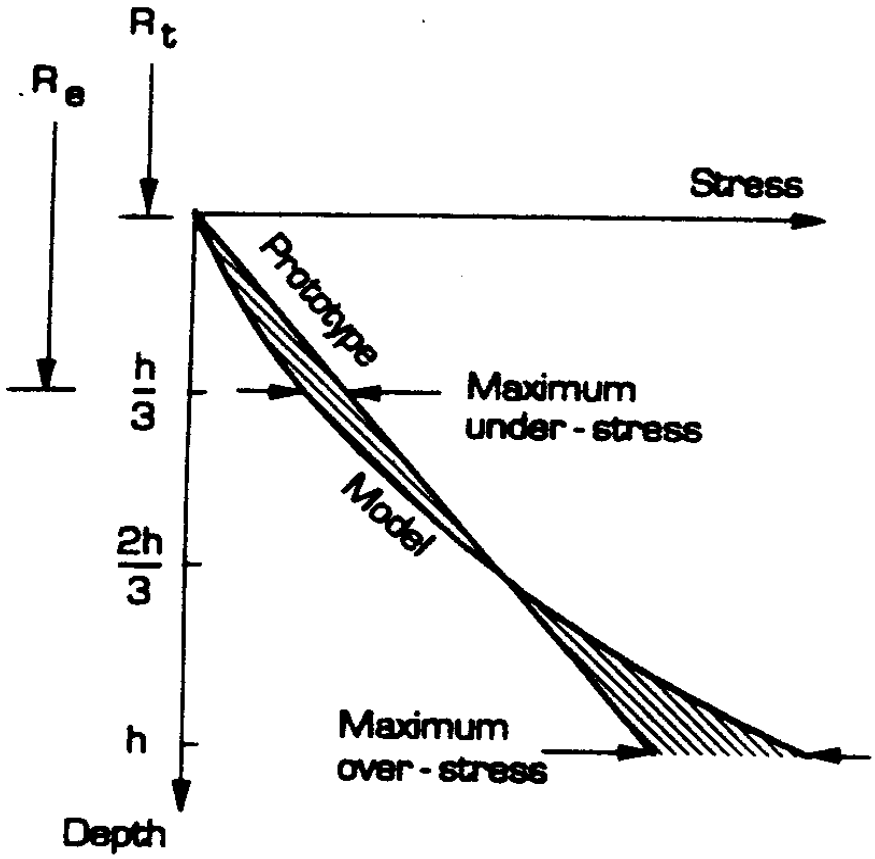

Figure 3.3 Comparison of stress variations with depth in a centrifuge model and its corresponding prototype (after Taylor, 1995)

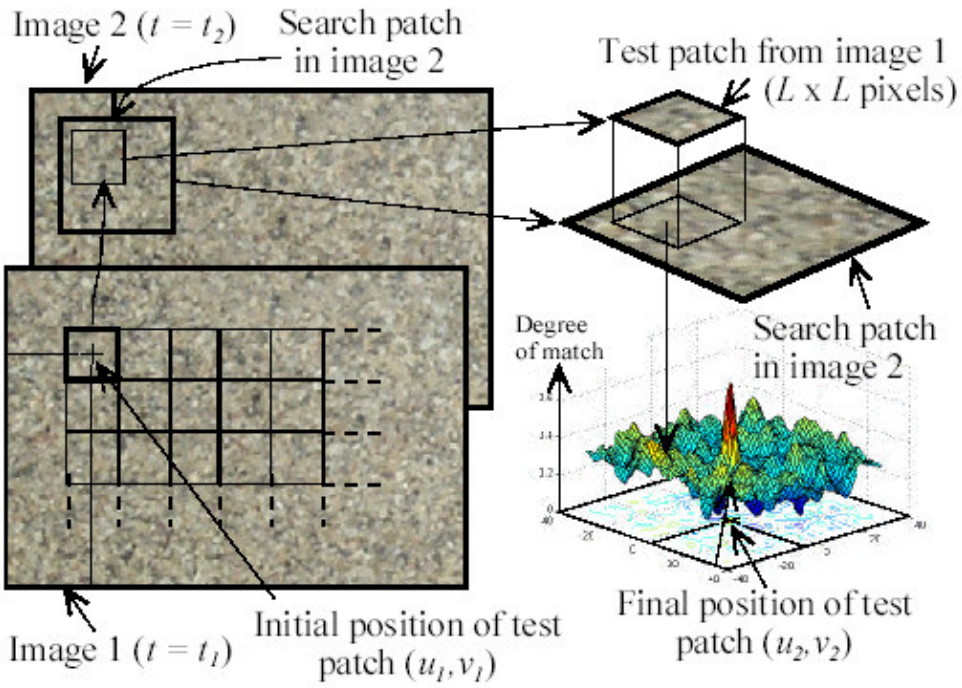

Figure 3.4 Principles of PIV analysis (after White and Take, 2002)

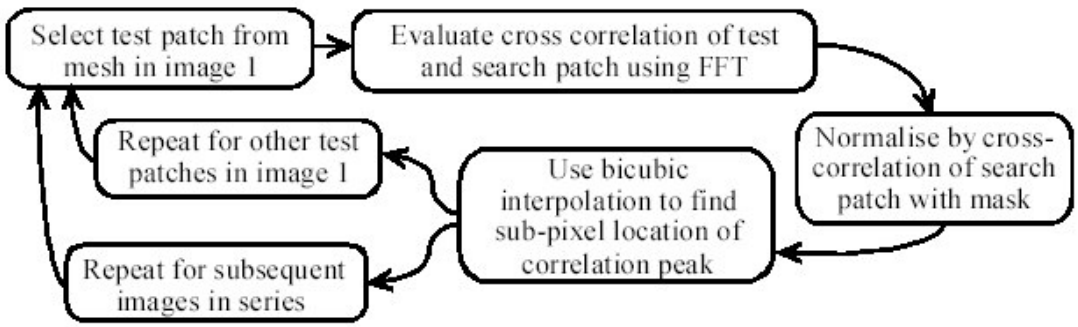

Figure 3.5 Flow chart of the GeoPIV analysis procedure (after White and Take, 2002)

CHAPTER 4

EXPERIMENTAL SET-UP AND CLAY SPECIMEN

4.1 General

Firstly, this chapter outlines the design, construction and operation of testing apparatus. The arrangements for load and displacement instrumentation, data acquisition and computerised control of the apparatus are summarised. Secondly, this chapter describes the testing soil used in centrifuge modelling and sample preparation. Thirdly, this chapter discusses the techniques of capturing good quality images using a digital camera during centrifuge testing. Finally, test strategies and test procedures from Event 1 to Event 6 in this study are presented, together with a focus on the tests design with a water layer on top of the soil specimen in the drum centrifuge.

4.2 Experimental Set-Up

4.2.1 Drum Centrifuge

The tests described here were performed in the drum centrifuge located at the University of Western Australia (Figure 4.1). This facility, installed in 1997, has a 1.2 m diameter and a maximum acceleration level of 485 g. A central set of actuators provides vertical and radial motions that, combined with a fixed load cell (described below), allow a combined vertical, horizontal and moment motion to be applied to the footing. By using two concentrically driven shafts connected by a Dynaserv motor, a relative motion between the outer channel and the central tool table (see

Figure 4.2) can be achieved and controlled. The system has been designed such that the tool table can be stopped and raised out of the main testing area while the channel with soil sample continues to rotate. This allows the instrument testing tools that are fixed to the actuator to be modified or changed without affecting the acceleration level on the soil. This was done between each test on the same soil sample, allowing for the half-spudcan, full-spudcan, T-bar and hosepipe (for sprinkling water) to be cleaned and interchanged.

The outer channel of the drum centrifuge has a 300 mm vertical height and a 200 mm radial depth. In this study pre-consolidated soil specimens were placed into the drum centrifuge strongbox (described below) fitted in its position within the channel. The depth of soil sample in the strongbox can be up to 130 mm. The strongbox base has a radius of 560 mm in flight.

There are two on-board data acquisition systems: one is fitted on the channel and the other is fitted on the tool table. The basic systems can record a total of 32 direct signals, transferred through the sliprings, on both the channel and the tool table. Each system comprises an onboard computer with A/D conversion board and a pair of 8 channel instrumentation amplifiers. Digital signals from each onboard computer are transferred to a single data acquisition computer in the control room (Figure 4.3) via a RS232 link. The off-board computer stores the data to the disk, and allows control over sampling frequency and signal integration, synchronises sampling from the two systems, and transfers the saved data to a second computer for real time graphics display. Further technical details of the drum centrifuge can be found in Stewart *et al.* (1998).

4.2.2 Strongbox

A specially made strongbox (Figure 4.4) was used in this study. The box consisted of a plexiglass window at one side in order to record soil movement during spudcan penetration and dural walls on all other sides. The box has an internal size of 258 (length) × 80 (width) × 160 (depth) mm. It was restrained in position by four plates bolted to the ring channel (top and bottom) so that the mid-plane of the box was on a

radius. However, for half-spudcan tests an extra base plate was added so that the inner surface of the plexiglass window was on radius.

4.2.3 V-H-M Load Cell

For half-spudcan and full-spudcan tests, a V-H-M load cell (Figure 4.5) was used to measure load-penetration response. Spudcan was attached to one side of the load cell and fixed to the main radial actuator of the centrifuge during testing. Thus the spudcan acted as a loading leg. The load cell, properly strain gauged, is sensitive against vertical, horizontal and moment loading. Vertical and horizontal displacements can be obtained from the loading actuator. However, this study concentrated on the vertical loading and corresponding displacement response only. The moment reading was also used to set the flat face of the half-spudcan model against the strongbox window.

4.2.4 Camera

In Event 1-5, a mini video camera (resolution: 720 × 576 pixels and frame rate: 50 Hz) was used to capture the images. The camera was mounted on a wedge support in the ring channel positioning at the centre of the channel so that the centre of the images was lined up with the mid-height of the strongbox (along which the spudcan was installed). In this position, the camera field of view was 257 mm wide and 206 mm high with the bottom of the strongbox just visible. This camera was used not only to capture the images of soil failure mechanisms but also to monitor the installation of the spudcan to ensure the half-spudcan was tightly against the window during penetration. The video camera transmitted an analogue signal through the centrifuge sliprings to feed into a videotape in the control room. There was also another camera mounted on top of the actuator loading leg to record the cavity formation on top of the penetrating spudcan and to view and fix the test position of the probe on the soil specimen.

In Event 6, ‘Cannon PowerShot S40’ digital camera (Figure 4.6, resolution: 2272 × 1704 pixels and frame rate: 0.4 Hz) was used, along with the aforementioned mini

video cameras, to capture the images. The mini video cameras here played the role of fixing the testing positions of the probes. A specially made cradle was used to set the digital camera in front of the strongbox in the drum channel. The cradle was mounted fully forward in the central slots so that the centre of the images was lined up with the mid-height of the channel (Figure 4.7). Camera stage was positioned at a right angle to the plexiglass window, to avoid lens distortion, with the swinging stops tightened level with the inscribed lines. In this position, the view field of the camera was 193 mm wide and 144 mm high with the bottom of the soil specimen just visible. The digital camera was modified by attaching a small weight to the shutter (as shown in Figure 4.6). Under centrifuge acceleration, this weight would press the camera shutter, thus trigger the continuous shooting mode of the camera. This allowed images to be captured at a rate of approximately 0.4 Hz, until the memory card (512 MB) was full or the battery was flat. Note, the rechargeable battery lasts for about 60 minutes. After centrifuge testing, the captured images were downloaded (using scanner and camera wizard) by connecting the camera with the Windows XP PC in the drum control room using the USB connection cable. As an alternative to using the weighted shutter, the USB connection combined with the Cannon Remote Capture software could be used to control the camera through sliprings. Thus, the images could be transferred to the PC during image capture. However, the images through the sliprings are unreliable in terms of quality. Additionally, since each image is downloaded after being taken and before the next shot, the capture rate is approximately four times lower than the continuous shooting mood with the weighted shutter.

4.2.5 Lighting

Two 60 v globe lights were mounted on both sides of the testing channel (Figure 4.7), facing slightly (depends on the sample height) towards the axis of the drum, to avoid excessive reflections on the images captured. The area surrounding the strongbox window was painted white to improve the lighting conditions, hence the quality of images.

4.2.6 Spudcan Model

In this study, circular full-spudcan, half-spudcan and half-plate models were used (Figure 4.8). The geometry of the spudcan model is shown in Figure 4.9 and all linear dimensions are in proportion with corresponding diameters. For realistic comparison, the footing sizes at model and at enhanced acceleration are reported in Table 4.1.

A full-spudcan of 30 mm diameter and half-spudcans of 30 mm and 60 mm diameter were used with a 13° shallow conical underside profile and a 76° protruding spigot. Similar type of spudcans, with small variation in either diameter or shape, were used by Byrne and Cassidy (2002), Dean *et al.* (1998), Houlsby and Martin (1992), Martin (1994), Martin and Houlsby (2000), Martin and Houlsby (2001), Noble Denton and associates (1987), Santa Maria (1998) and Vlahos *et al.* (2001). The full-spudcan was used to measure load-penetration response and the half-spudcan was used to reveal soil failure mechanisms during spudcan installation. The half-spudcan was prepared by splitting a full-spudcan down the central vertical plane. This was to facilitate penetration tightly against the plexiglass window of the strongbox so that video/digital camera could capture the resulting mechanisms of soil flow. In order to avoid soil squeezing in between the plexiglass window and the spudcan model, thick foam on the central flat face of the spudcan and eventually 1 mm rubber "O" ring along the periphery of the spudcan with a stiffener on the back side of the spudcan shaft were used. Spudcan models were polished to have a smooth surface and they were made from dural. Both full-spudcan and half-spudcan models were smooth black coloured (anodised), without increasing / affecting the surface roughness, to distinguish it from white kaolin clay during filming. Figure 4.10 and Figure and 4.11 illustrate full-spudcan and half-spudcan respectively fitted with the actuator- ready for penetration tests. Note that a half-plate of 60 mm was also used with a small sharp protruding spigot (Figure 4.8).

4.2.7 T-Bar Penetrometer

The T-bar, as shown in Figure 4.12, is commonly used in centrifuge testing at UWA to measure clay strength. It is a penetrometer to test the undrained shear strength of soft soils. It has been used in site investigation and in the centrifuge testing. The advantage of the T-bar penetrometer is that it incorporates the advantages of the cone penetrometer (which gives a continuous profile of "strength") and the vane shear device (which gives an "exact" or direct measure of shear strength) and is relatively simple to construct and use. The principle of this and other types of 'flow- round' penetrometers (such as ball-penetrometer and plate-penetrometer) is to force the soil to flow around the probe in order to minimise the relative magnitude of volume expansion of the soil due to insertion of the device. In this way, correction of the measured penetration resistance due to the overburden stress is minimised (Watson *et al.*, 1998).

The model T-bar penetrometer developed for the centrifuge comprises a cylindrical cross bar, of 5 mm diameter and 20 mm long, attached at a right angle (to form a T) at the end of a vertical shaft, which narrows to 4.5 mm diameter behind the T-bar (Figure 4.13). When the T-bar is pushed into the soil, the penetration resistance is measured by a highly sensitive load cell (± 100 N maximum range) situated immediately behind the bar. The cylindrical surface of the T-bar was sand blasted to create a relatively rough surface, while the ends of the bar were machined smooth to minimise end effects. The T-bar can be used with conventional cone penetration equipment by just unscrewing the 60° cone tip and replacing it with the T-bar.

The analytical value of bearing capacity factor for T-bar, N_{ctb} (Randolph and Houlsby, 1984 and Stewart and Randolph, 1991) is dependent on the surface roughness of the cylinder, described by its adhesion factor, α (with $\alpha = 0$ for smooth and $\alpha = 1$ for rough). The upper and lower bounds of the plasticity solution coincide at approximately 12 for a fully rough bar and diverge slightly at lower values of α, with a minimum about 9. It is unlikely that the adhesion factors can be either 0 or 1 exactly in any test, despite the fact that the cross-bar was sand blasted. Therefore, an intermediate value of N_{ctb} was recommended as 10.5 for general use (Randolph and

Houlsby, 1984; Watson, 1999). This value has been used in interpreting soil strength in this study.

4.2.8 Hosepipe

In order to perform centrifuge tests with water on top of the soil specimens, a nylon hosepipe was mounted just above the spudcan fitted leg of the tool table (Figure 4.14 and Figure 4.15). Water was sprinkled over the soil specimen through the hosepipe at lower acceleration (15 g) level to avoid injection-induced distortion of the soil sample. After adding sufficient amounts of water, the tool table was stopped and parked and the pipe was removed carefully when the drum channel was still spinning. Then the tool table was swung up again and when it reached 15 g, it was synchronised and locked with the channel. The speed was then ramped up to the desired gravity level for probe penetration test.

4.3 Preparation of Clay Sample

4.3.1 Speswhite Kaolin Clay

The footing tests were performed on soft, heavily overconsolidated specimens of Speswhite kaolin clay. This clay has been used in numerous laboratory studies involving small-scale physical model tests, including work on:

- Piles (Randolph *et al.*, 1979; Steenfelt *et al.*, 1981; Martins, 1983; Gue, 1984).
- Tunnels (Mair, 1979; Kim, 1994).
- Shallow/deep foundations (Santa Maria, 1988; Santa Maria and Houlsby, 1988; Craig and Chua, 1990, 1991; Houlsby and Martin, 1992; Martin, 1994; Dean *et al*., 1998; Martin and Houlsby, 2000).
- Reinforced soil (Love, 1984; Fannin, 1986).

At UWA, Speswhite kaolin has also been used by-

- ✦ Stewart (1992) → Pile bridge abutments.
- ✦ Watson (1999) → Skirted foundations for offshore structures.
- ✦ Vlahos *et al.* (2001) → Spudcan foundation.
- ✦ Cassidy and Byrne (2001, 2002) → Spudcan and caisson foundation.

The principal reason for the popularity of Speswhite kaolin is that, for a clay, it has a relatively high coefficient of permeability, of the order of 10^{-9} m/s (Al-Tabba, 1987; Smith, 1993), which allows rapid consolidation of large specimens from reconstituted slurry. Because of its widespread use in research, its key properties are well established and they are presented in Table 4.2.

4.3.2 Preparation of Kaolin Slurry

Clay samples were prepared by consolidating kaolin slurry. Homogeneous slurry was obtained by mixing kaolin powder with 120 % deionised water (approximately twice the liquid limit) in a conventional barrel mixer (Figure 4.16). The mixer was equipped with a vacuum pump via a jubilee connection (Figure 4.17). Each sample was mixed in the mixer for 4 hours. A vacuum of 80 kPa was maintained throughout the mixing period to de-air the slurry.

4.3.3 Consolidation into Conventional Tank

After slurry mixing, the slurry was then pumped into fully assembled consolidation tanks (Figure 4.18) under 100 mm water. This was to prevent desiccation and air entrapment. The consolidation tank consisted of two identical cylinders, of 394 mm inside diameter and 400 mm high, and a circular base plate, which were all bolted together and sealed by rubber gaskets (Figure 4.18). Geo-fabric mats with drainage to atmospheric pressure were provided at both ends of the slurry. A piston, consisting of a ram and a circular base plate with central drainage tube, was pushed on top of the upper geo-fabric. The consolidation tank was covered by a circular plate, which was bolted together with top cylinder and sealed by a rubber gasket. The ram was

sealed together with piston base plate and tank cover plate by 4 rubber "O" rings. Air pressure was controlled by a yellow pressure gauge. It was applied in the space between the piston and the cover plate through a plastic tube that was fitted with the cover plate. Figure 4.19 shows the cross-section of the consolidation tank to illustrate all internal assembles.

The consolidation pressure was applied in stages of: 25 kPa, 50 kPa, 100 kPa, 150 kPa, 200 kPa (final pressure depended on the required consolidation pressure). Each increment was applied when the rate of consolidation fell below 1 mm/h. During the final pressure increment, primary consolidation was considered to have been achieved when the rate dropped to 0.1 mm/h. The sample was then unloaded to 100 kPa and 50 kPa and finally to atmospheric pressure. The total time required for consolidation was two and a half weeks.

The sample was then removed from the consolidation tank (Figure 4.20). The resulting clay sample was about 250-280 mm deep (from slurry of 50 kg kaolin powder), with a moisture content of approximately 50%. Test specimens were prepared by cutting the pre-consolidated clay sample to the size of the strongbox. Six specimens were obtained at required size: 258 mm (length) × 80 mm (width) × 125 mm (depth) (Figure 4.21). The time elapsed between unloading the pre-consolidation pressure and prior to centrifuge test was about 10 hours. Each typical centrifuge test lasted 4-5 hours.

4.3.4 Consolidation in Centrifuge Strongbox

Layered consolidation

The strongbox itself was used as a consolidation cell (as shown in Figure 4.22 (a)). The slurry was placed by hand in layers into the cell to minimise air entrapment. Geo-fabric mats with drainage to atmospheric pressure were provided at both ends of the slurry (Figure 4.23). A piston, which consisted of two rams and a rectangular base plate with central drainage tube, was pushed on top of the upper geo-fabric mat. The rams were screwed together with piston base plate at equal distance from the plate centre (Figure 4.22 (a) and Figure 4.23). Weights were applied evenly on the

top of the rams to avoid any tilting. Thus the applied pressure could be distributed evenly on the slurry surface (Figure 4.23).

The weights were applied in four stages: 10 kg, 20 kg, 40 kg and finally 52.5 kg so that consolidation pressure was applied in stages roughly of 5 kPa, 10 kPa, 20 kPa and finally 25 kPa. Each increment was applied when the rate of consolidation became sufficiently low. Weights and piston were then removed, then the second layer of slurry was placed on top of the consolidated layer in the similar manner. Consolidation pressures were applied in the same systematic way. Specimen of sufficient height was obtained by repeating this procedure up to three layers. After placing the final (third) layer, each increment of consolidation pressure was applied when the rate of consolidation dropped below 1 mm/h. During the final pressure increment, primary consolidation was considered to have been achieved when the rate dropped to 0.1 mm/h. The sample was then unloaded to 20 kPa and 10 kPa and finally to atmospheric pressure. The total time required for consolidation in the strongbox was about four weeks.

Single layer consolidation

In order to consolidate the soil sample in a single layer and to avoid effects related to layered consolidation, the consolidation cell was made by assembling the strongbox with a guide collar on top (as shown in Figure 4.22 (b)). The slurry was placed by hand in layers into the cell to minimise air entrapment. With collar, the set-up procedures were similar to that stated in the above section.

The weights were applied in four stages: 10 kg, 20 kg, 40 kg and finally 52.5 kg so that consolidation pressure was applied in stages roughly of 5 kPa, 10 kPa, 20 kPa and finally 25 kPa. Each increment was applied when the rate of consolidation dropped below 1 mm/h. During the final pressure increment, primary consolidation was considered to have been achieved when the rate dropped to 0.1 mm/h. The sample was then unloaded to 20 kPa and 10 kPa and finally to atmospheric pressure. The total time required for consolidation was two and a half weeks.

Specimen

The resulting clay sample was 125 mm deep (from about 250 mm slurry), with a moisture content of approximately 50 %. A single sample was obtained under each consolidation to form a specimen used size: 258 mm (length) × 80 mm (width) × 125 mm (depth). The elapsed time between removing the consolidation pressure and prior to centrifuge test was about 6 hours. Each typical centrifuge test lasted 4-5 hours.

4.3.5 Soil Strength Profile

Soil characterisation tests were performed using a T-bar penetrometer (Stewart and Randolph, 1991) of projected area 100 mm^2 (explained in Section 4.2.7). These tests were performed at a rate of 1 mm/sec so that undrained behaviour was obtained. This can be assessed by examining the dimensionless velocity group, vD/c_v, as suggested by Finnie (1993), where v is the penetration velocity, D is the appropriate length dimension (that is T-bar diameter here), and c_v is the coefficient of consolidation. Finnie (1993) suggests that if vD/c_v is below 0.1 drained behaviour dominates whilst if vD/c_v is above 10, undrained behaviour dominates. In this case vD/c_v is about 80, well above the minimum value (10) for ensuring undrained condition. The bearing capacity factor of T-bar has been studied extensively by Stewart (1991), Stewart and Randolph (1991) and Watson (1999). A well established value N_{ctb} = 10.5 has been applied here to calculate soil strength profile.

4.4 Specimen Preparation from Consolidation Tank to Strongbox

The specimen preparation procedures from soil samples in a consolidation tank to a specimen in strongbox are listed below:

1. The sample from the pre-consolidation tank was cut using greased (Shell Snow White petroleum jelly) cutting blades (required specimen size: 258 mm × 80 mm × sample height).

2. The window of the strongbox was removed and all inner surfaces were lubricated with the grease up to specimen height/depth.
3. The specimen was slid down into the box.
4. For direct observation of soil deformation during the test, square grids were drawn on the soil specimen facing the strongbox window using "STAEDTLER LUMOCOLOR", when a mini video camera was used to capture soil flow images.
5. Alternatively, black 'flock' modelling material was sprinkled over the soil specimen facing the strongbox window for PIV analysis to reveal soil movement, when a digital camera was used in testing. The black 'flock' was applied via a 300-micron sieve, until an even mixture of white (clay) and black (flock) was visible.
6. The window glass was screwed back onto the front of the strongbox;
7. The strongbox with soil specimen (Figure 4.24) was placed in the channel of the drum centrifuge.
8. The actuator was then driven down and the digital camera was mounted on the support cradle (see Section 4.5 below on using the digital camera).
9. The drum centrifuge top hat was placed over the centrifuge.

Note: In strongbox consolidation, a single sample resulted. The window was taken off carefully as the soil was very soft. The grids were drawn or flock materials were sprinkled gently. After cleaning the strongbox inner surfaces above the soil specimen, the strongbox window was screwed back onto the strongbox. A slightly greasing on the inside of the window glass was to reduce the friction between the soil specimen and the window during the spudcan penetration test.

4.5 Experimental Strategy

4.5.1 Event 1-5

In this series of tests, half-spudcan and full-spudcan tests were conducted at 100 g and 200 g. The half-spudcan was penetrated along the centre but with the flat face set

tightly against the window in order to prevent soil squeezing in between the spudcan and the window. This is because once soil squeezed in between the spudcan and the window, the images of soil flow only showed the movement of the squeezed soil instead soil flow around the spudcan. The soil sample was grid-lined on the side facing the plexiglass. Soil flow images were captured continuously by a mini video camera focusing on midheight of the window. The deformation of the grid lines was used to analyse the soil flow mechanism. Although the half-spudcan tests were filmed for soil deformation and measured on load-penetration response, the friction between the half-spudcan and the plexiglass was difficult to estimate. Thus, full-spudcan tests, to measure the load-penetration response, were conducted along the vertical centreline of the strongbox to minimise boundary effects from the strongbox. In-flight T-bar tests were performed, to measure the soil undrained shear strength, immediately after the completion of spudcan penetration tests.

4.5.2 Event 6

In this series of tests, half-spudcan and full-spudcan tests were conducted at 50 g, 100 g and 200 g. Instead of drawing gridlines to view the soil deformation, coloured flock was sprinkled on the soil specimen so that the images captured by the digital camera could be used for PIV (Particle Image Velocimetry) analysis for a quantitative soil deformation evaluation. Soil flow images were captured continuously by the digital camera facing the midheight of the window. Full-spudcan tests were again conducted along the vertical centreline of the strongbox for load-penetration responses. T-bar tests were performed before and after each spudcan penetration test to evaluate soil softening and strengthening effects in-flight at different g-levels.

Similar tests were also performed when a 30 mm water layer was present on top of the specimens to simulate seabed conditions. Water was sprinkled over the soil sample through the hosepipe at lower acceleration (15 g) to avoid injection induced distortion of the soil specimen. Lying above soil specimens, 30 mm water imposes a water pressure of 30 kPa on the soil surface under 100 g acceleration.

4.5.3 Velocity of Spudcan Penetration

The rate of penetration was chosen so that the non-dimensional velocity index, vD/c_v was in the region of undrained behaviour. In all events half-spudcan and full-spudcan were run at a constant rate of 0.2 mm/sec except in half-spudcan tests with digital camera, in which spudcan penetrated at a vertical displacement rate of 0.05 mm/sec in order to capture more images and to evaluate soil deformation more precisely (selection of footing penetration rate has been discussed in Appendix 2). All these velocities have ensured an undrained condition with $vD/c_v > 30$. However, the total time required, in prototype scale ($T_p = N^2 \times T_m$), for loading up to d/D = 1.67-3.33 was longer than typical preloading time at field scale (see Appendix 2).

4.5.4 Typical Procedures of Submerged Soil Test

When a submerged soil specimen was tested, the typical test procedures, which were followed in this study, are discussed below:

1. Set effective radius (up to 1/3 of sample depth) and calibration file for half-spudcan test.
2. Spin both the tool table and the drum channel up to 15 g.
3. Sprinkle sufficient water on top of soil sample using hosepipe.
4. Stop and park tool table and then remove the hosepipe while the channel is still spinning.
5. Ramp tool table up to 15 g so that it synchronised with, and can be locked to, the channel.
6. Begin data acquisition (slow logging rate), and data plotting.
7. Drive the half-spudcan model fitted with the actuator close to the top of the soil sample using actuator.
8. Drive the spudcan tightly against the window using the Dinaserv.

   Note: By positioning the spudcan prior to the testing gravity level, the operating time of the camera is minimised. This will reduce the possibility of the battery running flat at mid-test.
9. Turn off all drum centrifuge room lights, to provide better view of images, except control room lights.

10. Spin up to 100 g [camera activates at ≈ 25 g].
11. Increase the logging rate to maximum value.
12. Drive actuator with half-spudcan foundation out at a chosen penetration rate up to about 100 mm into the specimen (Figure 4.27).
13. Retract the spudcan in a similar rate until no longer in contact with water [camera will stop somewhere during spudcan extraction due to either a flat battery or a full memory card].
14. Stop data logging.
15. Stop and park tool table while channel continues to rotate.
16. Remove spudcan and set T-bar.
17. Change cal file for data logging for T-bar test.
18. Ramp tool table up to 100 g so that it can be locked to the channel.
19. Begin data acquisition (slow logging rate), and data plotting.
20. Drive T-bar fitted with actuator out, at a chosen penetration rate up to about 100 mm into the specimen [increase the logging rate to maximum value when the T-bar is close to touch the water surface], vertically at the test position T-bar 1 (T-bar 1 in Figure 4.27).
21. Retract T-bar in a similar rate until no longer in contact with water surface.
22. Stop data logging.
23. Stop and park tool table while channel continues to rotate.
24. Remove T-bar and set full-spudcan.
25. Ramp tool table up to 100 g so that it can be locked to the channel.
26. Change cal file for data logging for full-spudcan test.
27. Begin data acquisition (slow logging rate), and data plotting.
28. Drive full-spudcan fitted with actuator out, at a chosen penetration rate up to about 100 mm into the specimen [increase the logging rate to maximum value when the T-bar is close to touch the water surface], vertically at 125 mm above from the test position of T-bar 1 and along the centre of the box (full-spudcan in Figure 4.27).
29. Retract full-spudcan in a similar rate until no longer in contact with water surface.
30. Stop data logging.
31. Stop and park tool table while channel continues to rotate.
32. Remove spudcan and set T-bar.

33. Change cal file for data logging for T-bar test.
34. Ramp tool table up to 100 g so that it can be locked to the channel.
35. Begin data acquisition (slow logging rate), and data plotting.
36. Drive T-bar fitted with actuator out, at a chosen penetration rate up to about 100 mm into the specimen [increase the logging rate to maximum value when the T-bar is close to touch the water surface], to the test position of T-bar 2, vertically at 91.5 mm above from the home position of tool table and along the centre of the box (T-bar 2 in Figure 4.27).
37. Retract T-bar in a similar rate until no longer in contact with water surface.
38. Stop data logging.
39. Spin down tool table and channel.
40. Remove the head of drum centrifuge.
41. Remove digital camera and download images.
42. Use reverse of previous procedure (Step 7 in Section 4.4) to remove strongbox from channel without removing tool table.

Table 4.1 Spudcan diameter in prototype

Acceleration Level	Half-Spudcan	Full-Spudcan
1 g	60 mm	30 mm
50 g	3 m	1.5 m
100 g	6 m	3 m
200 g	12 m	6 m

Table 4.2 Kaolin clay properties (after Stewart, 1992)

Property	Value
Liquid Limit, LL	61 %
Plastic Limit, PL	27 %
Plasticity Index, I_p	34 %
Specific gravity, G_s	2.6
Angle of internal friction, ϕ'	23°
Critical state frictional constant, M	0.92
Voids ratio at $p' = 1$ kPa on critical state line, e_{cs}	2.14
Slope of normal consolidation line, λ	0.205
Slope of swelling line, κ	0.044
Parameter $\Lambda = (\lambda - \kappa)/\lambda$	0.785
Spacing ratio, r	2.14
Consolidation Coefficient (mean), c_v	2 m^2/year

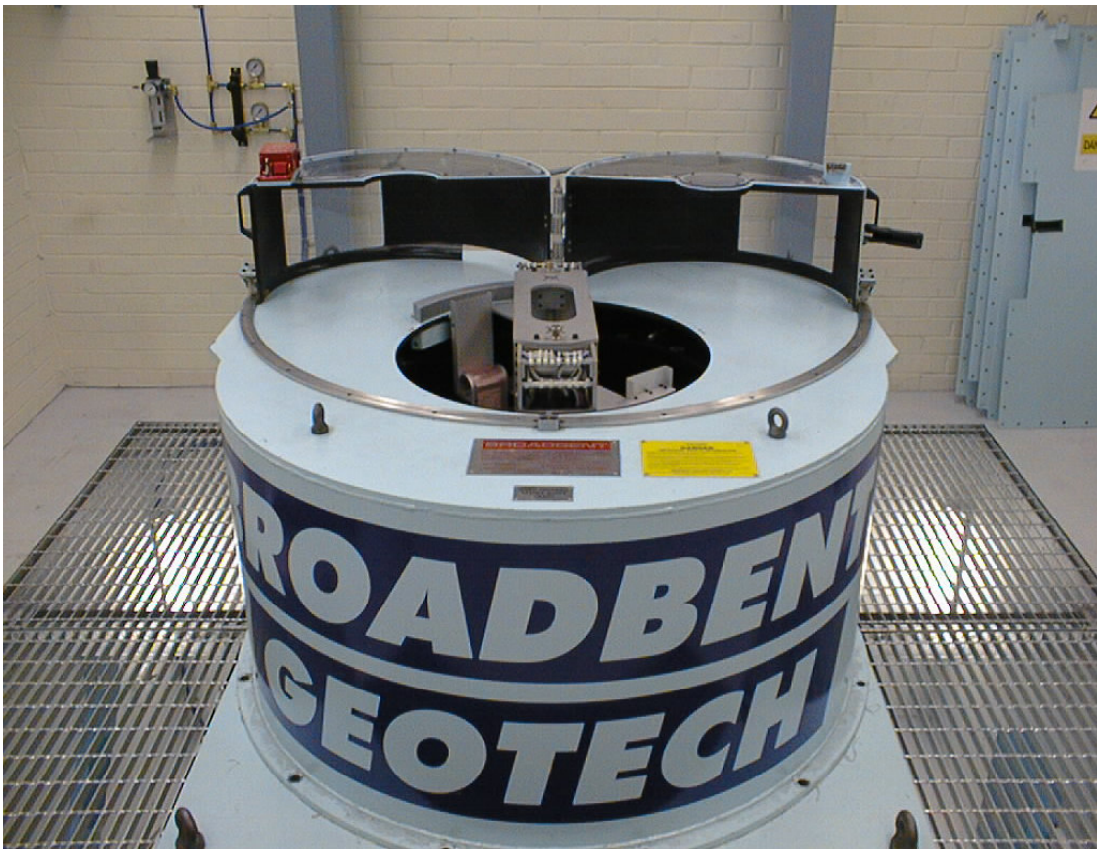

Figure 4.1 The UWA Drum centrifuge

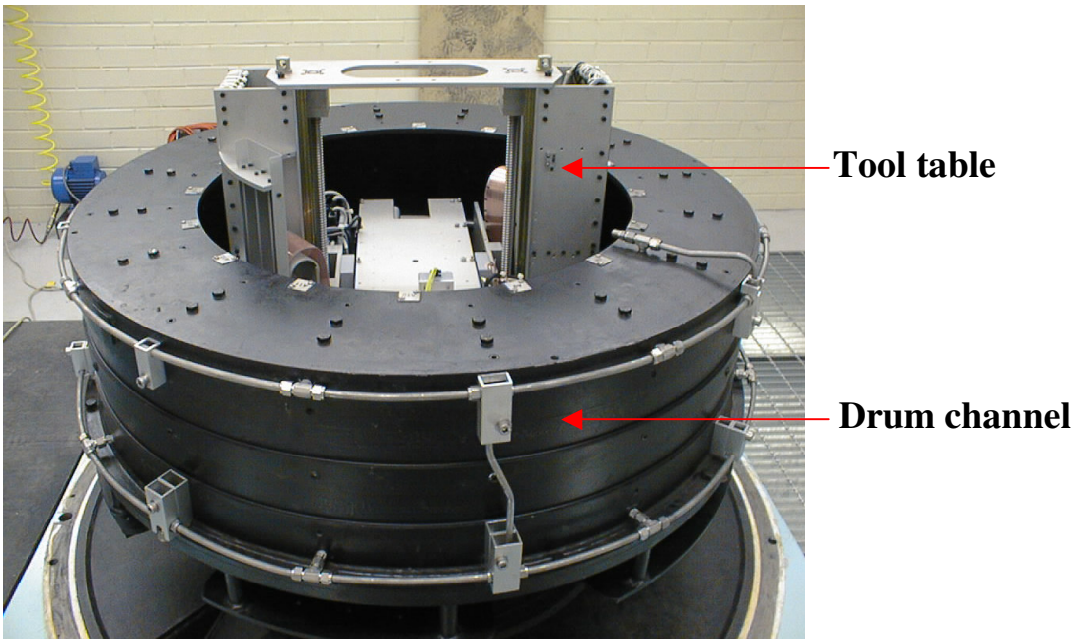

Figure 4.2 Drum channel and tool table

Figure 4.3 Drum centrifuge control room

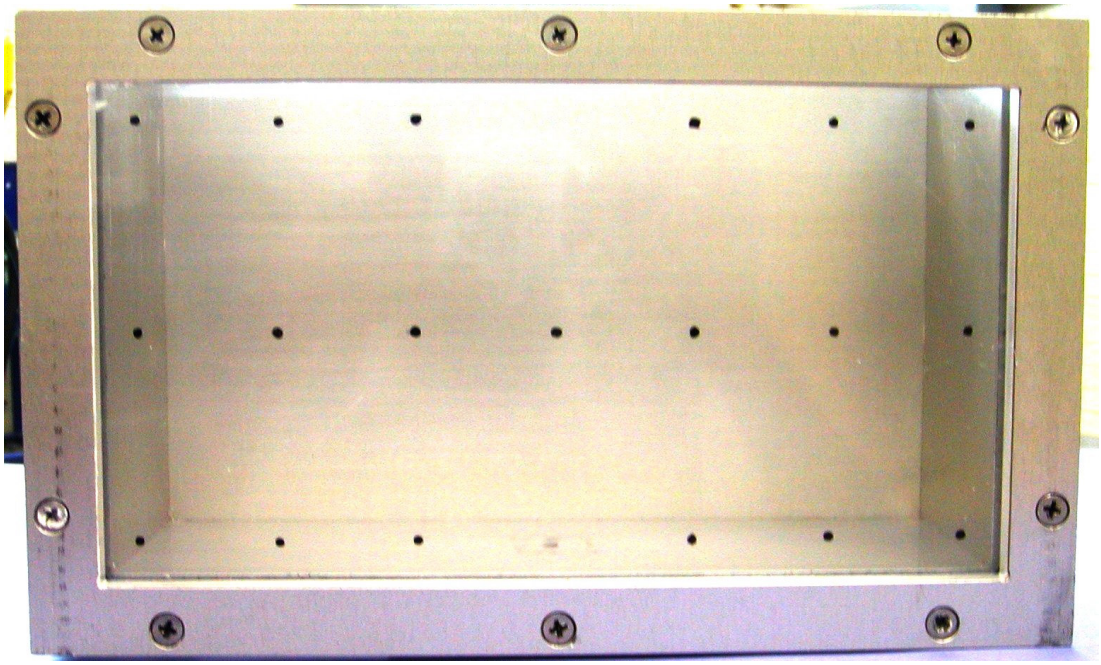

Figure 4.4 Strongbox with plexiglass window

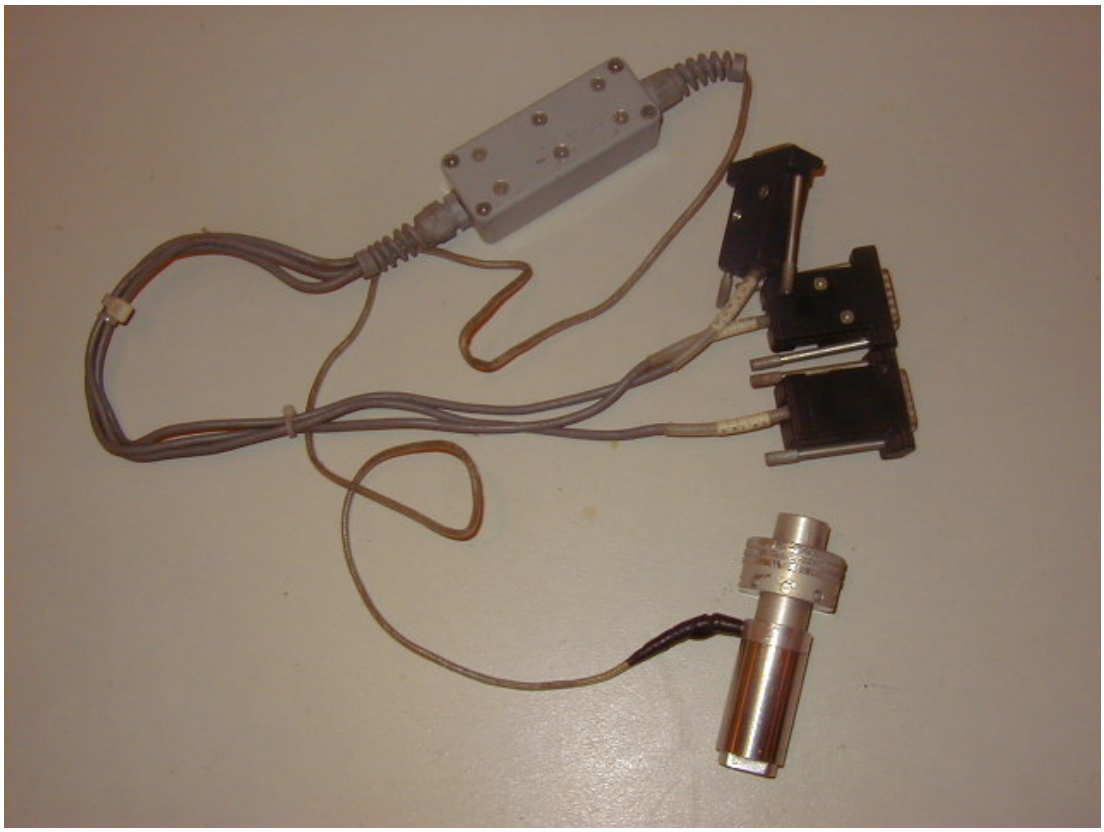

Figure 4.5 V-H-M load cell

Figure 4.6 Digital camera (Canon PowerShot S40)

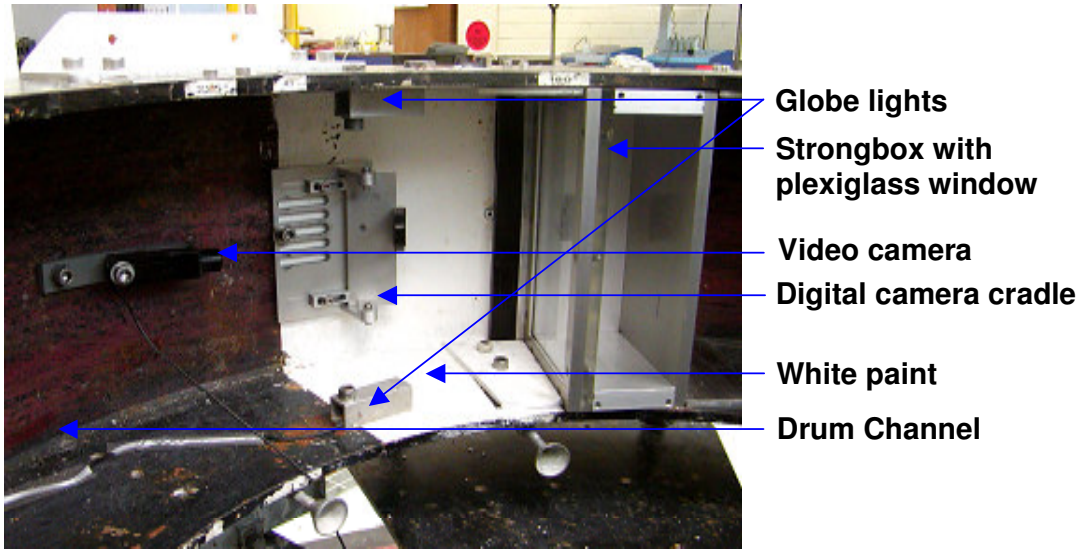

Figure 4.7 View of channel set-up in the drum centrifuge

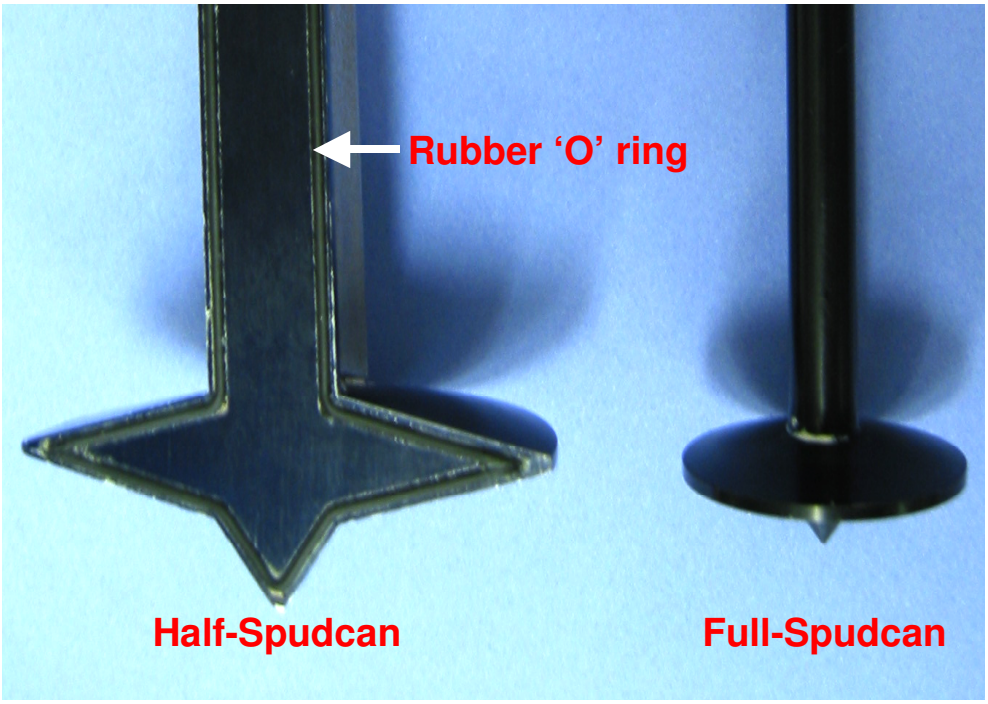

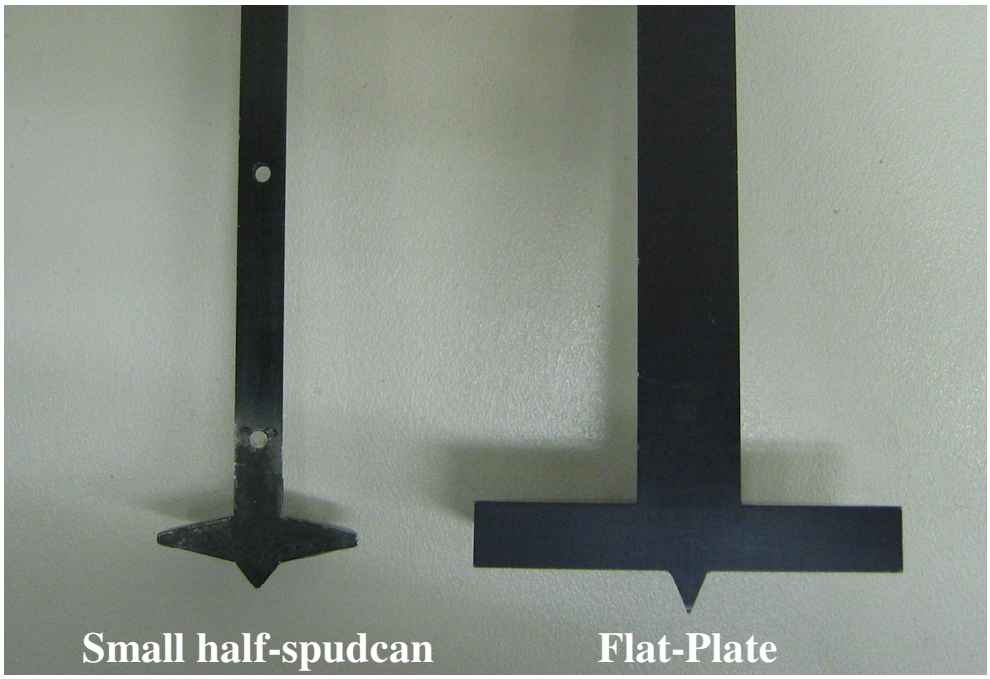

Figure 4.8 Spudcan models

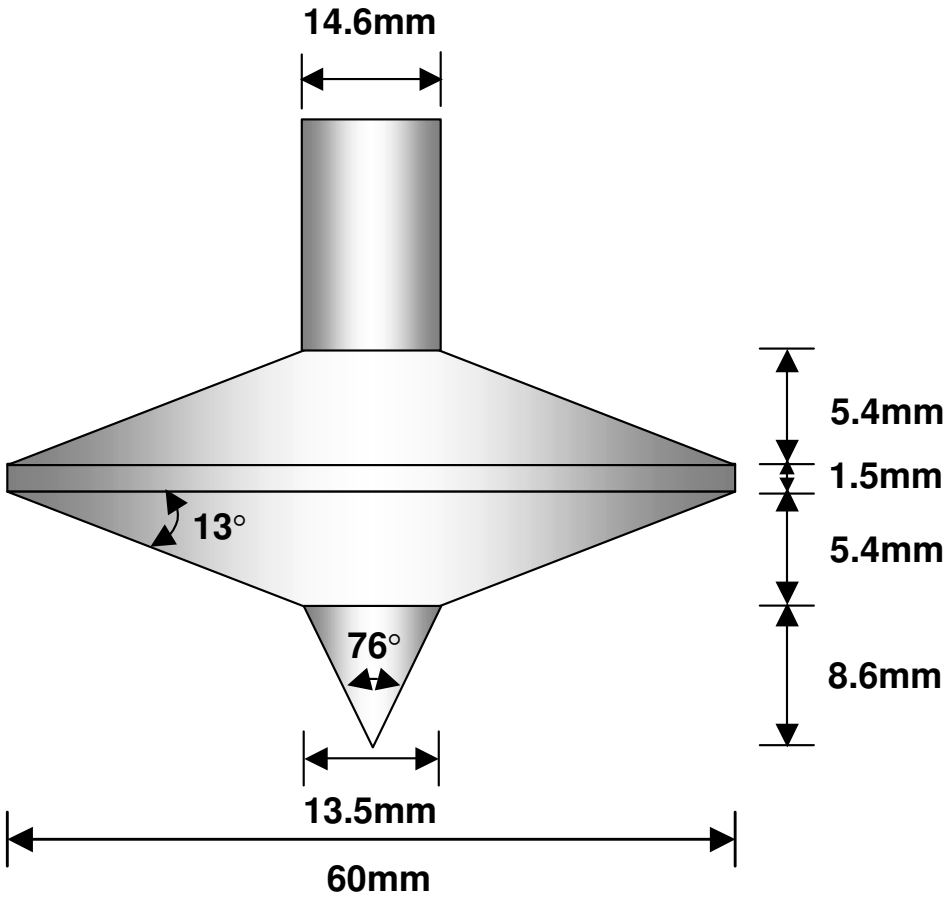

Figure 4.9 Dimensions of half-spudcan model

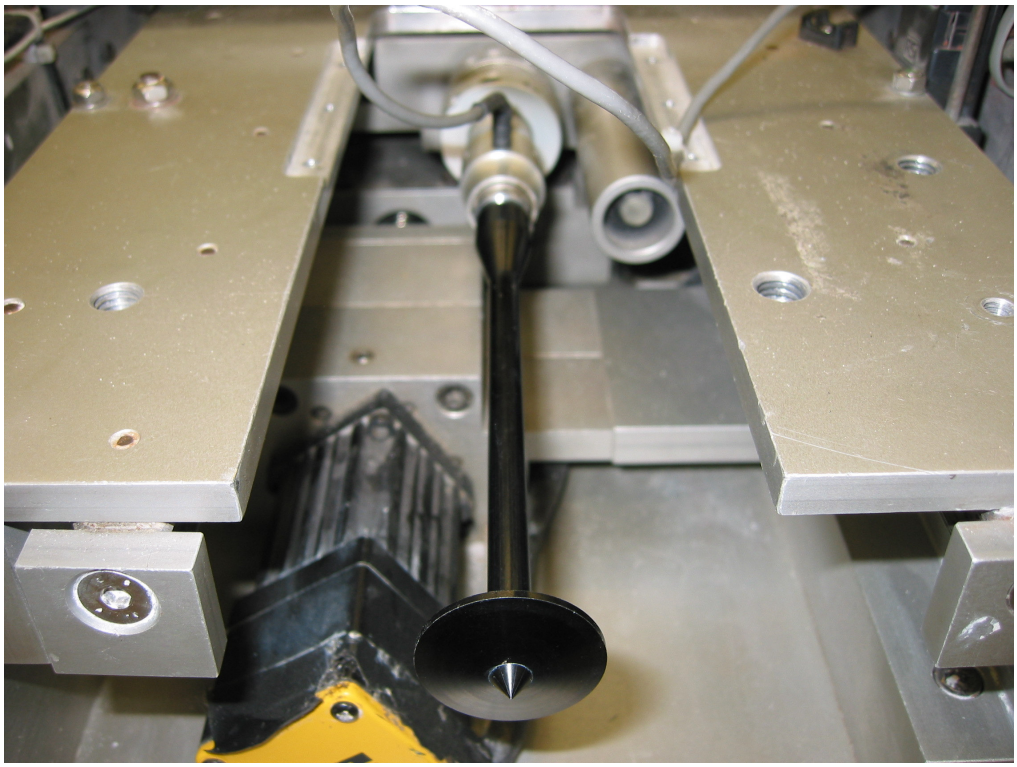

Figure 4.10 Full-spudcan fitted with the actuator

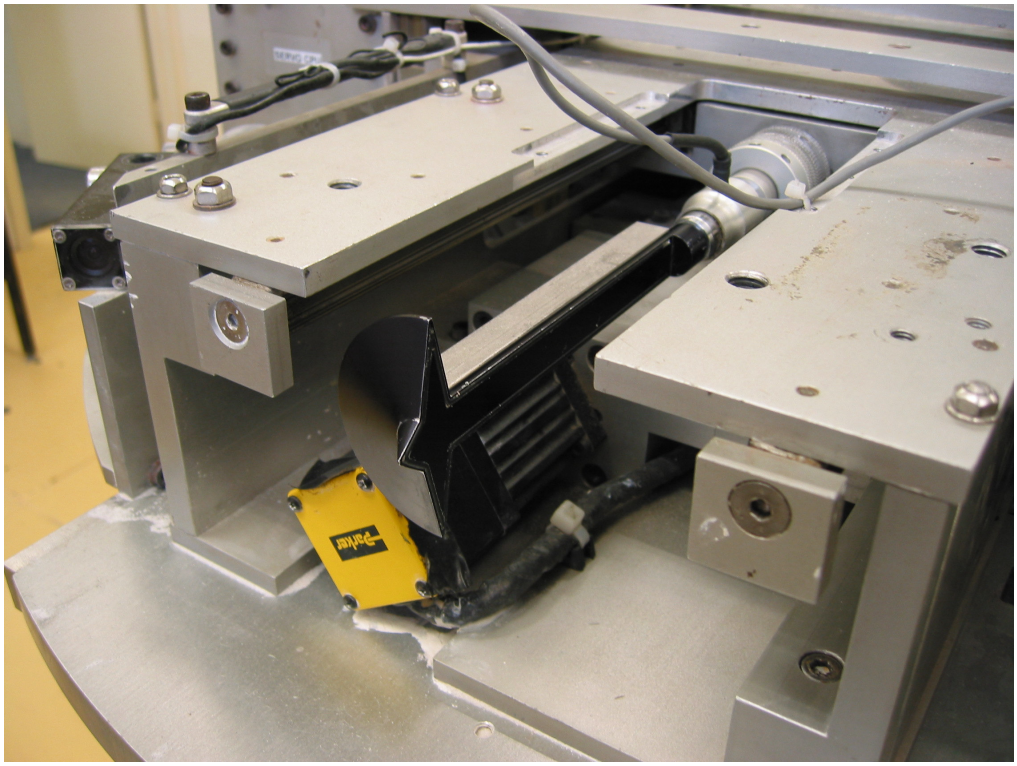

Figure 4.11 Half-spudcan fitted with the actuator

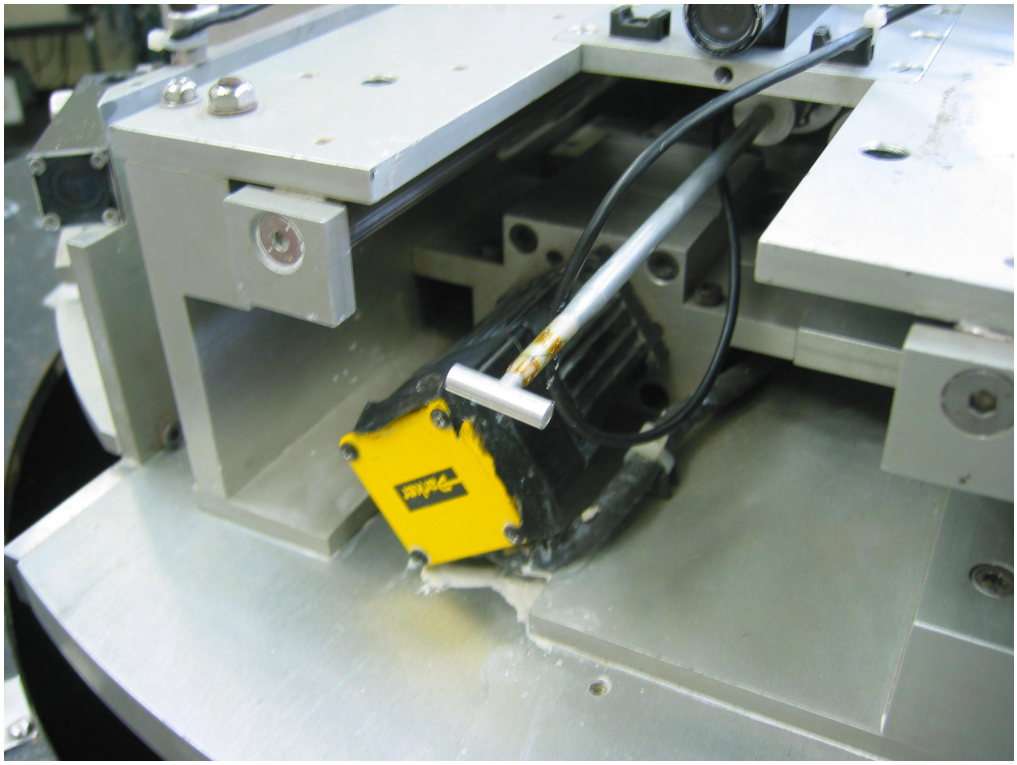

Figure 4.12 T-bar fitted with the actuator

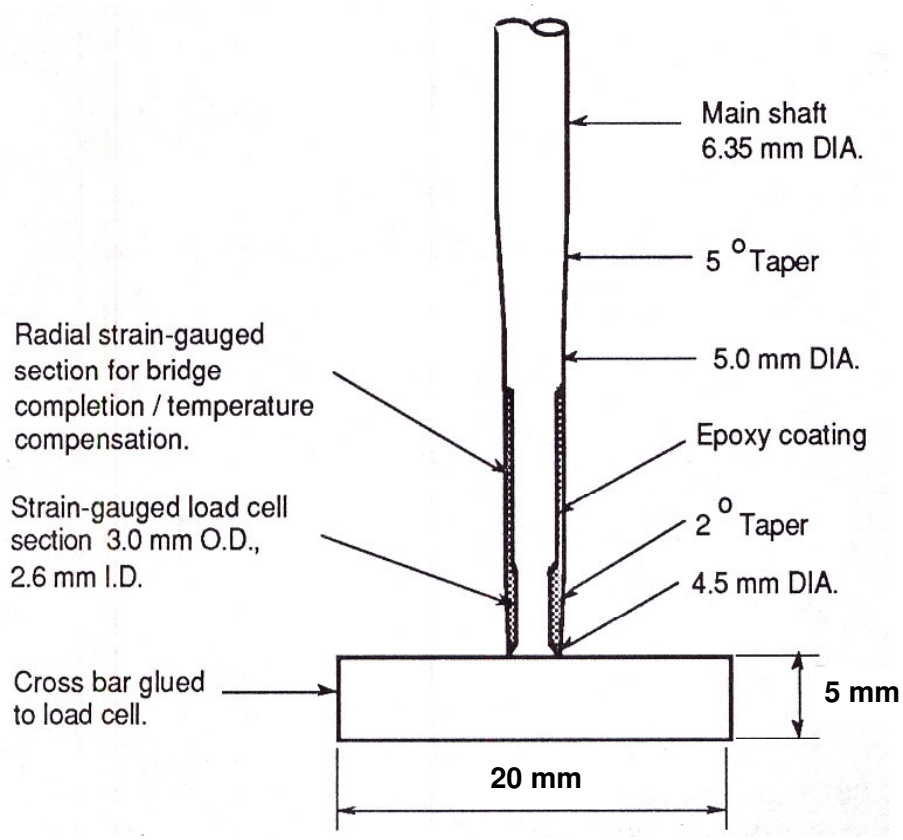

Figure 4.13 Schematic diagram of T-bar penetrometer (after Stewart, 1992)

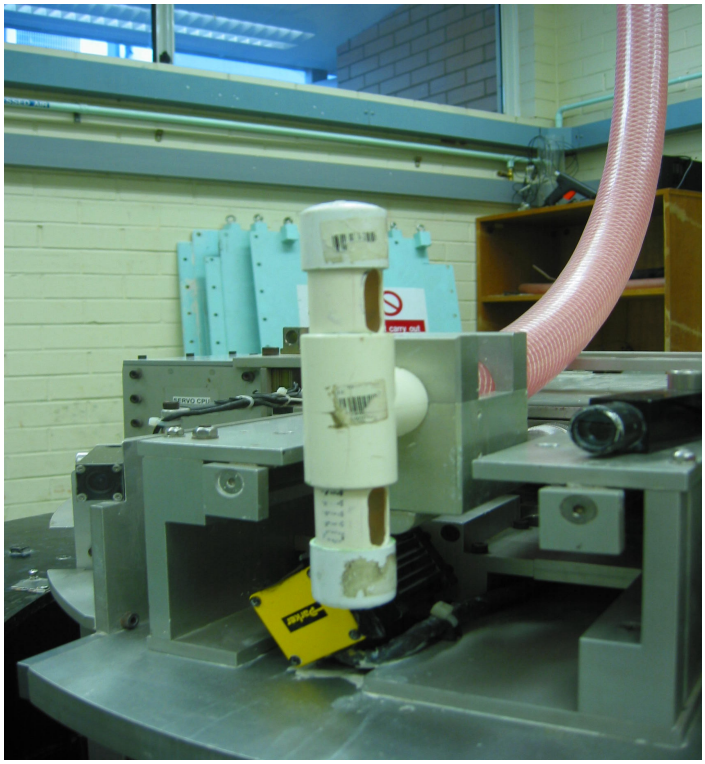

Figure 4.14 Mouth of hosepipe with two openings for injecting water

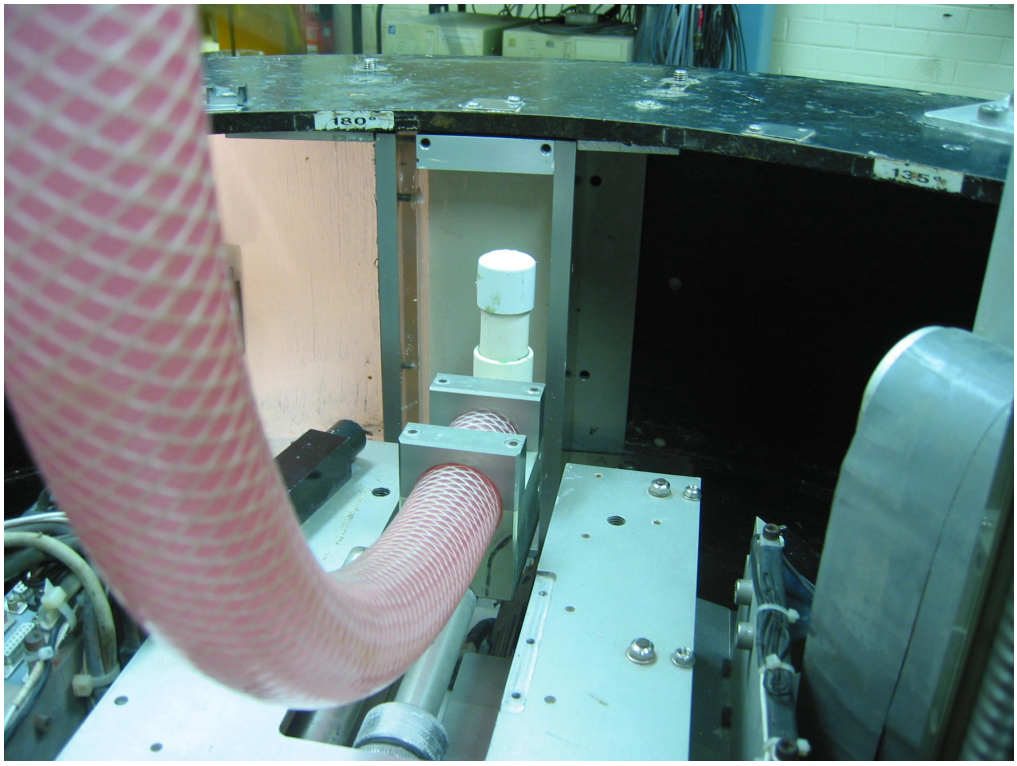

Figure 4.15 Hosepipe fitted with the actuator

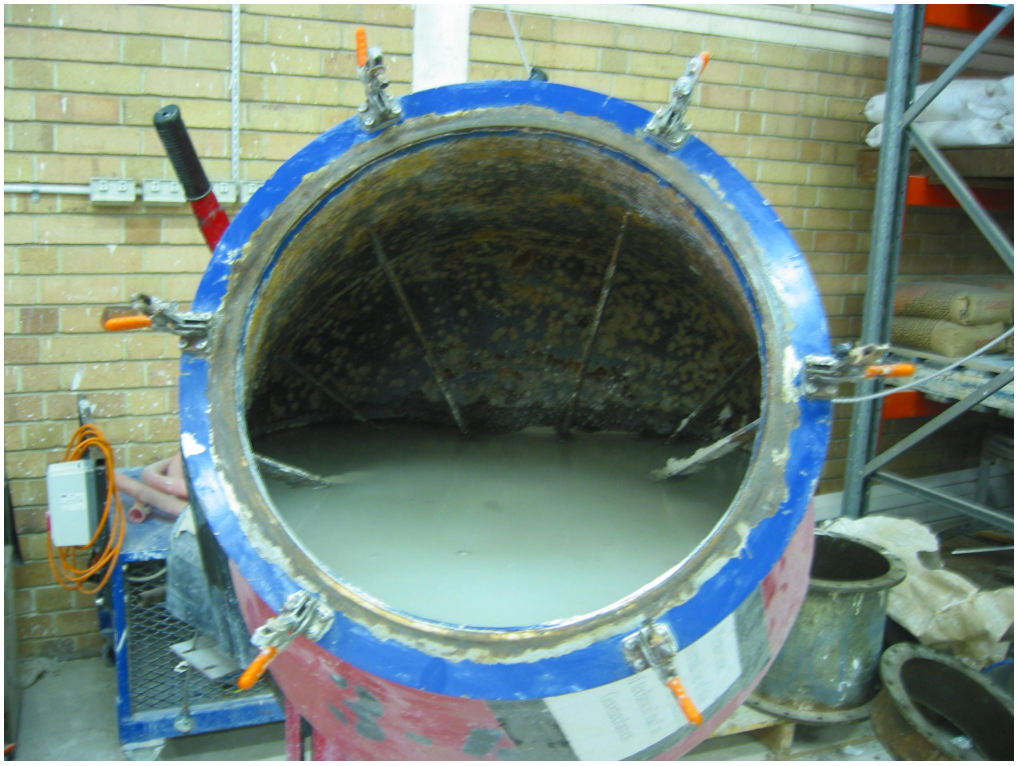

Figure 4.16 Conventional mixture barrel, kaolin slurry is in

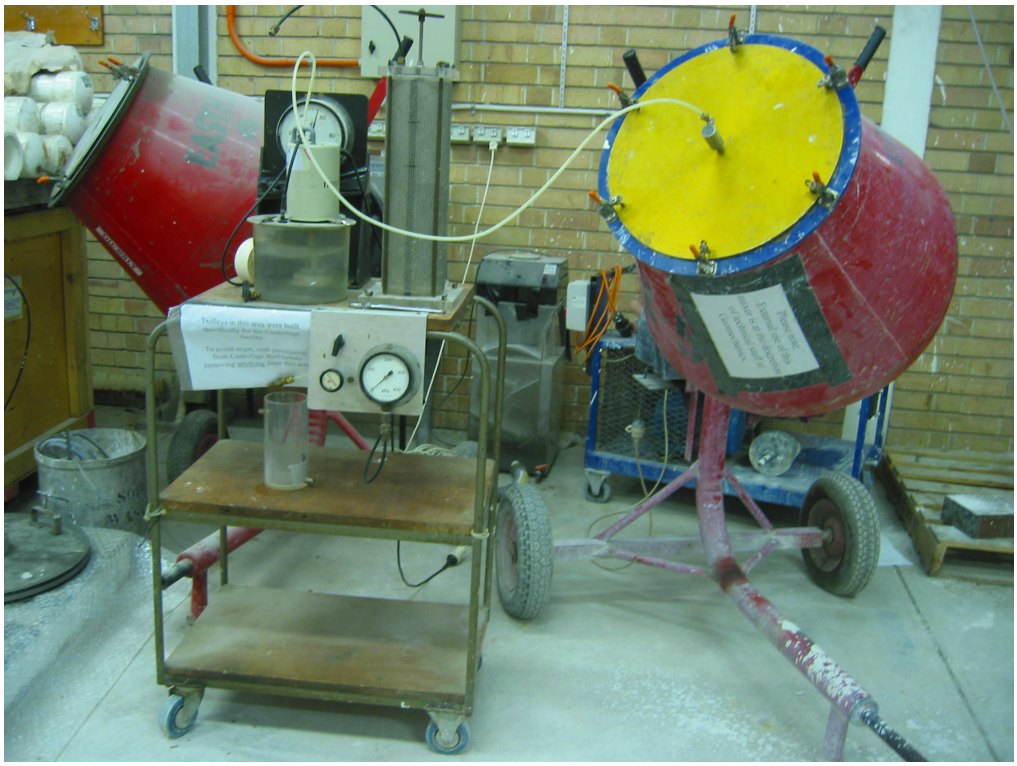

Figure 4.17 Conventional barrel mixture equipped with vacuum pump

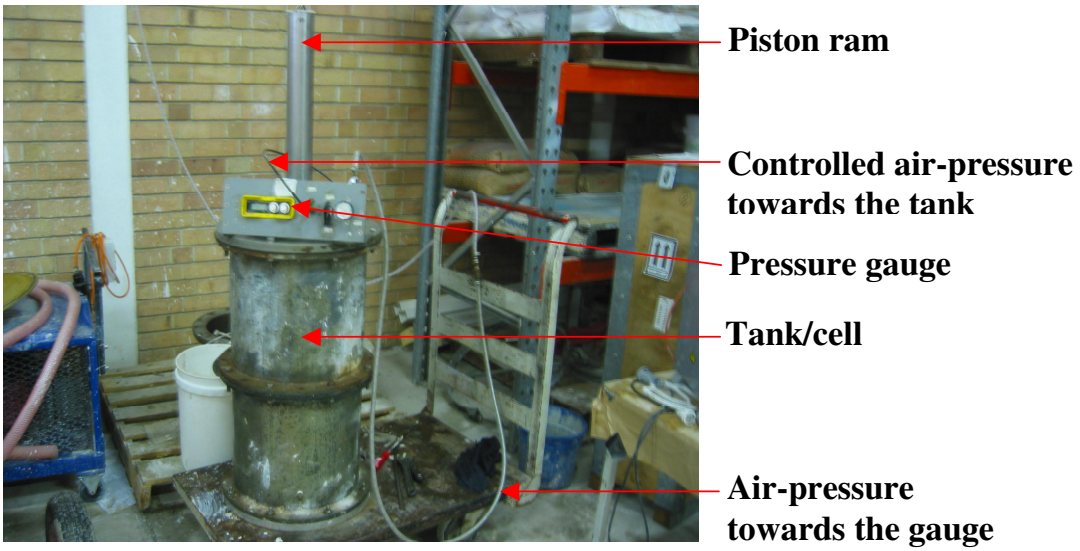

Figure 4.18 Conventional consolidation tank with kaolin slurry under consolidation

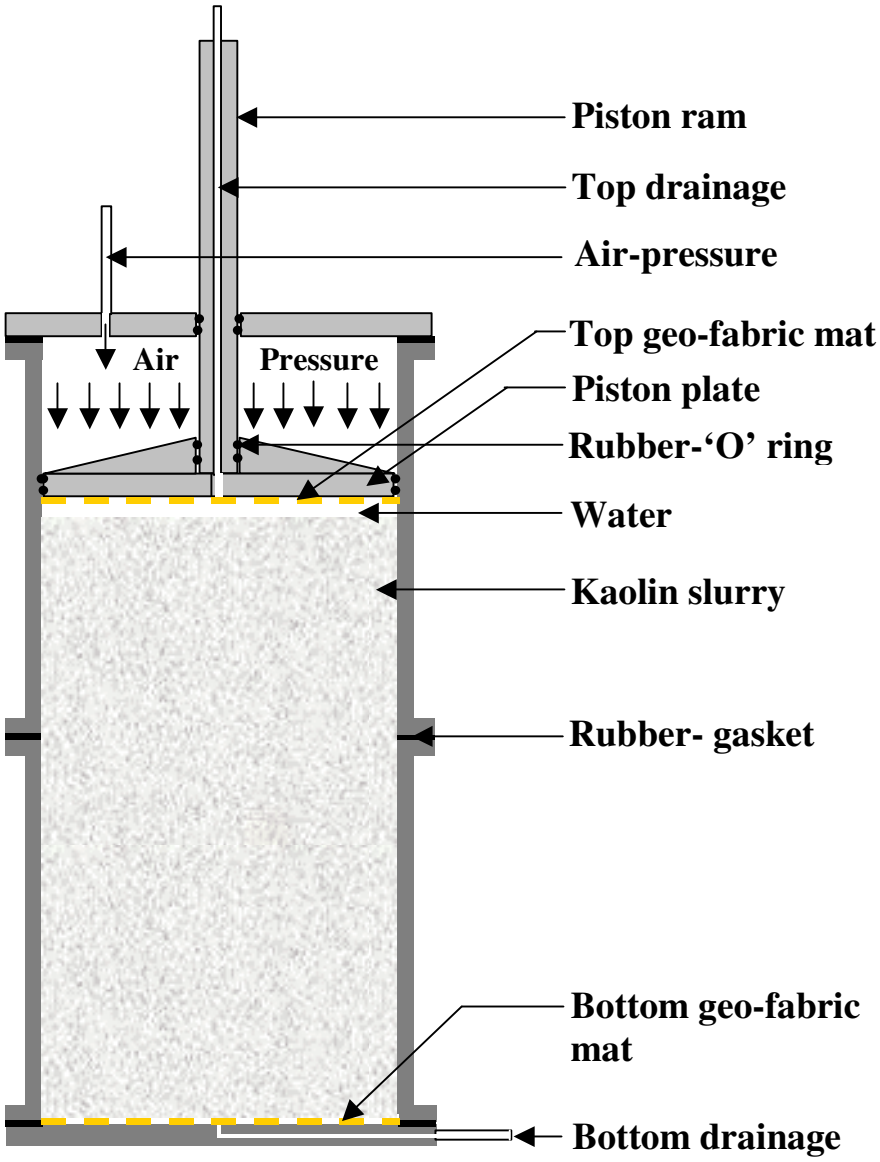

Figure 4.19 Schematic diagram of the conventional consolidation tank

Figure 4.20 Soil sample after consolidation

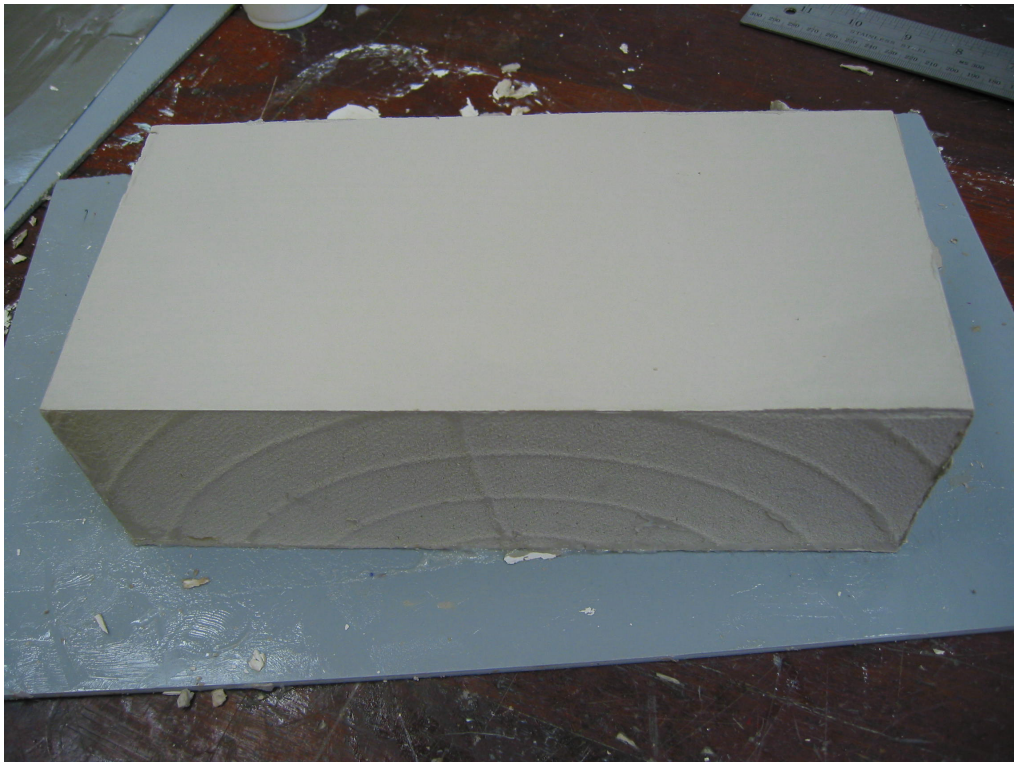

Figure 4.21 Clay Specimen (258 mm × 80 mm × 125 mm)

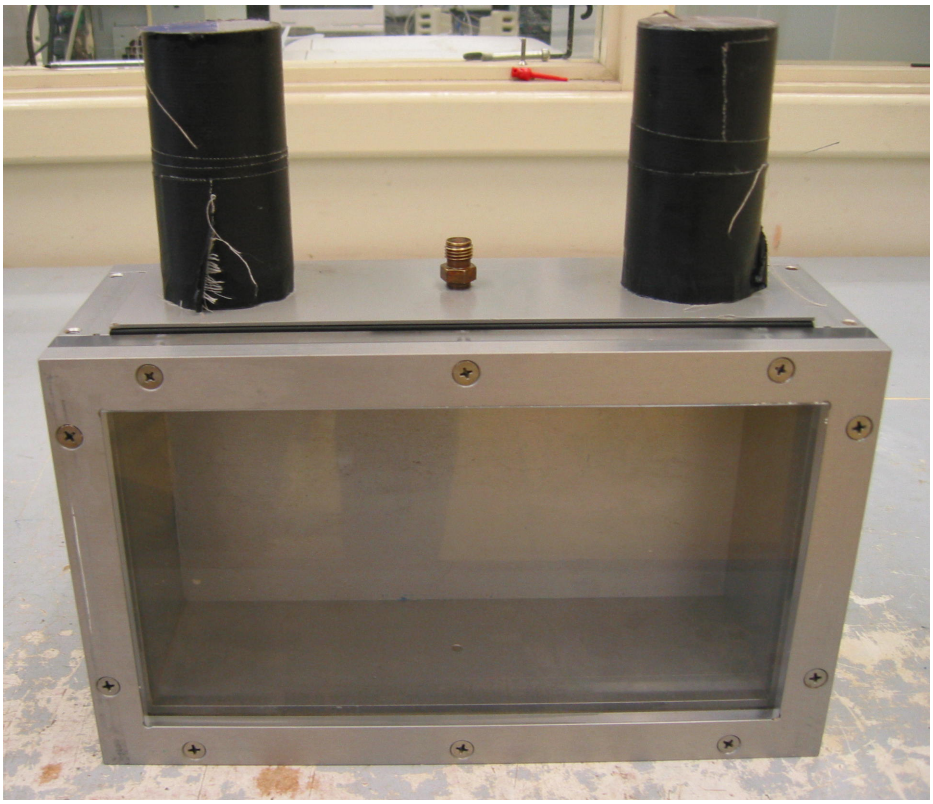

Figure 4.22(a) Strongbox with piston on top

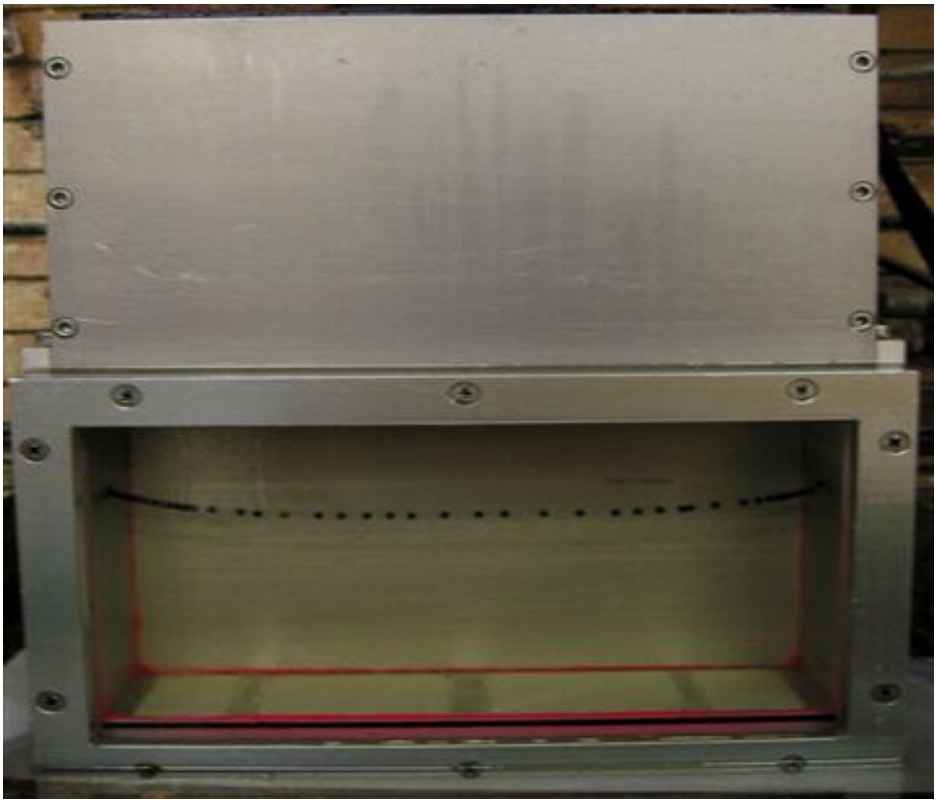

Figure 4.22(b) Strongbox with collar/guide

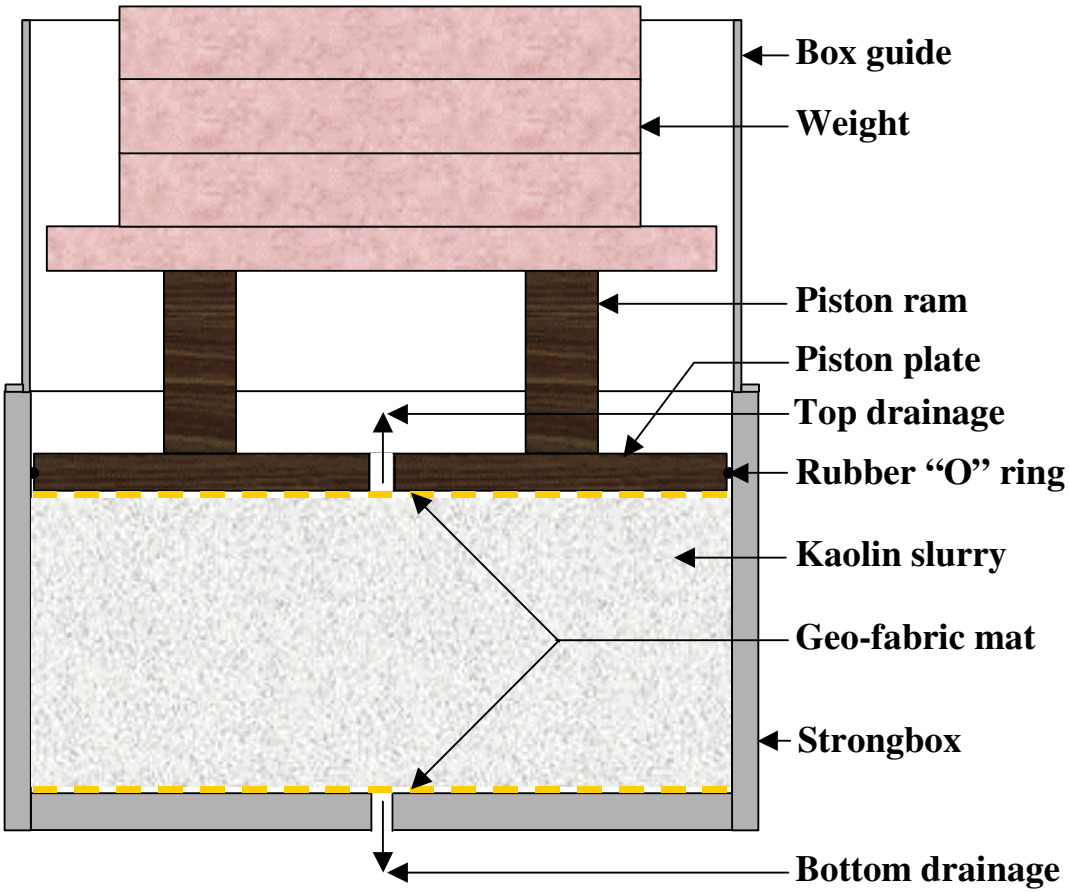

Figure 4.23 Schematic diagram of strongbox consolidation

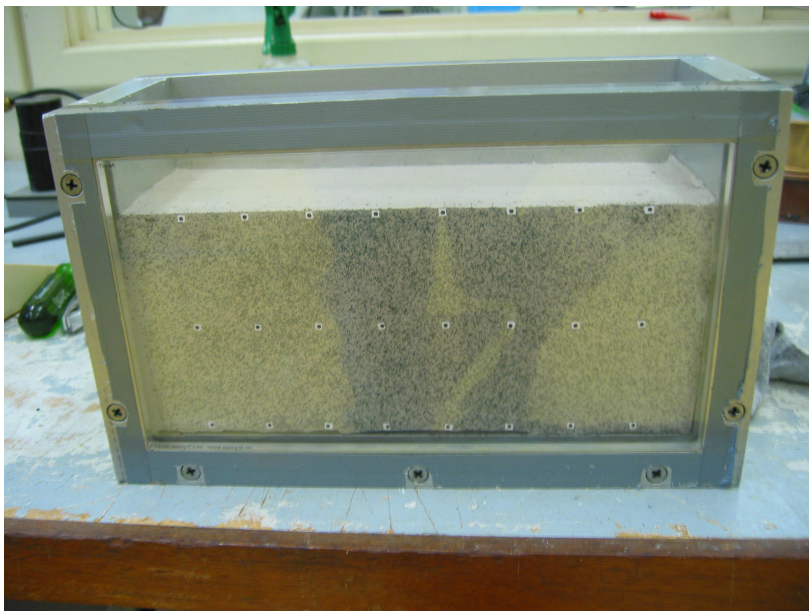

Figure 4.24 Strong box, clay specimen with black flock on window side before testing

Figure 4.25 Camera display settings for g-level triggering on drum centrifuge

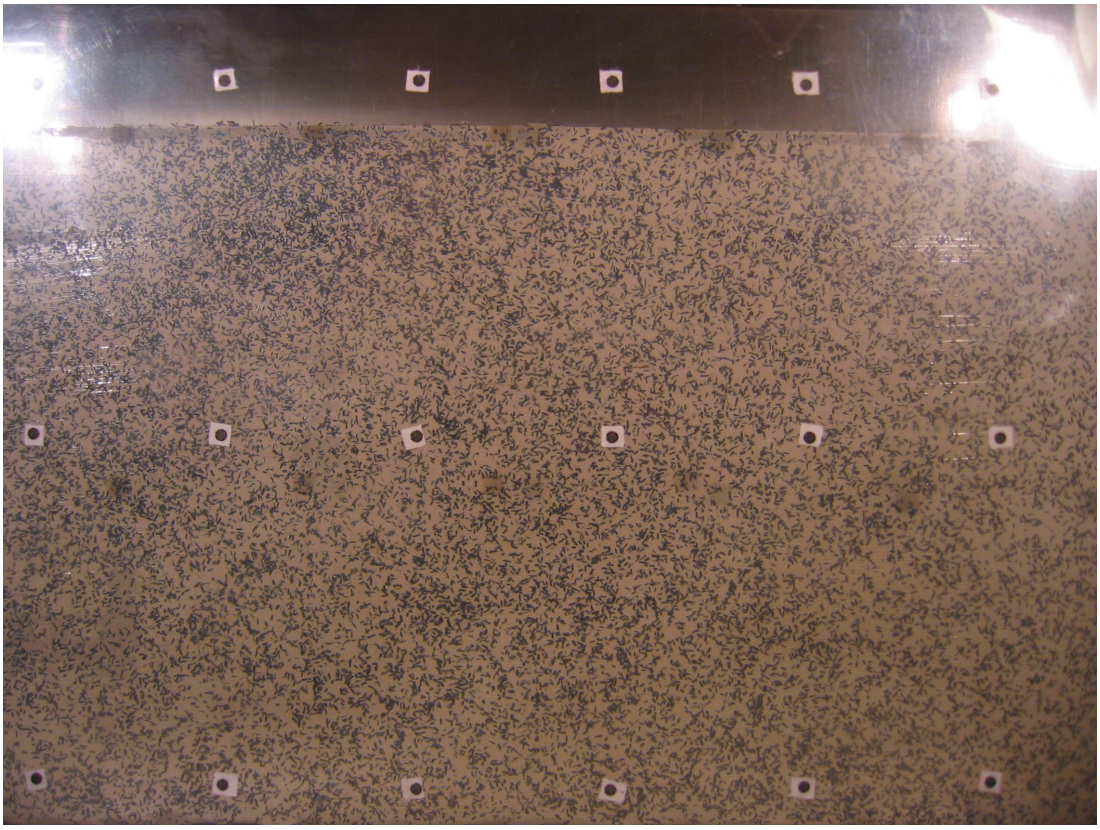

Figure 4.26 An image of soil specimen captured by digital camera

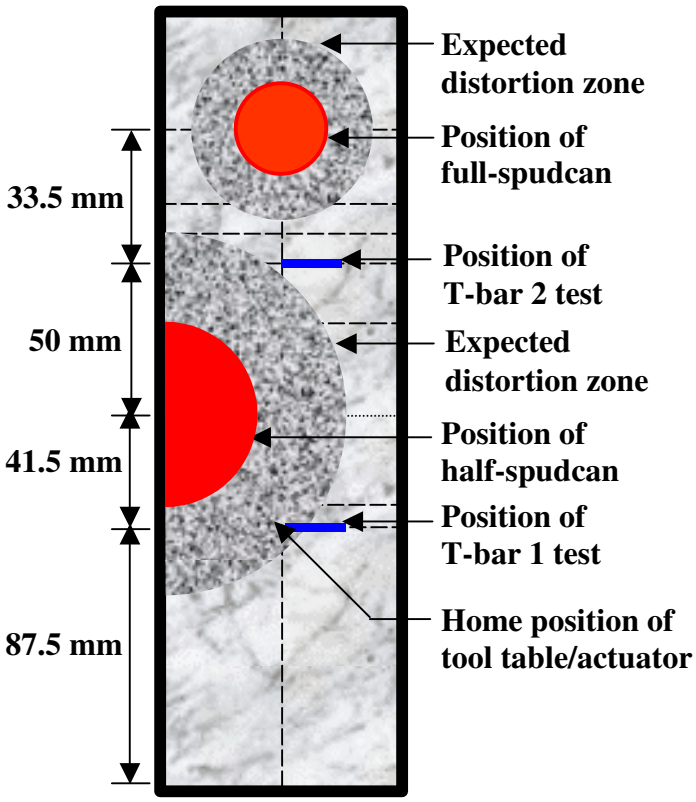

Figure 4.27 Top view of typical test arrangement in a strong box

CHAPTER 5

RESULTS AND DISCUSSION: EXPERIMENTAL AND NUMERICAL ANALYSIS

5.1 General

This Chapter describes the results of centrifuge tests performed using the apparatus, strategies and procedures described in Chapter 4. The main aim is to study soil failure mechanisms along with related soil strength and spudcan bearing capacity. Soil properties were switched from soft clay to very soft clay then again soft clay. In this Chapter, the word "Event" refers to the group of individual footing experiments ("Tests") carried out on the "specimens" obtained from the same "sample" after consolidation in the conventional consolidation tank. Six Events of experiments were carried out. Each test is named as Event→Test→Footing type→No (if any). Some examples with their meanings are displayed below:

- E1T1HS: Half-Spudcan (HS) test (T) on specimen 1 of Event (E) 1.
- E1T2FP: Flat-Plate (FP) test (T) on specimen 2 of Event (E) 1.
- E4T3FS: Full-Spudcan (FS) test (T) on specimen 3 of Event (E) 4.
- E5T1SHS: Small Half-Spudcan (SHS) test (T) on specimen 1 of Event (E) 5.
- E6T2TB1: 1st T-Bar (TB1) test (T) on specimen 2 of Event (E) 6.

HS indicates a half-spudcan model with 60 mm in diameter, and SHS indicates a small half-spudcan model with 30 mm in diameter. A few tests were also carried out in normally consolidated (NC) clay. Table 5.1 summarises information of pre-consolidation and centrifuge testing conditions for all the tests conducted.

Besides the observations in drum centrifuge testing, finite element (FE) analysis can provide more detailed and accurate results by varying each individual parameter.

Both small and large deformation FE analyses have been performed using the FE package AFENA (Carter and Balaam, 1990). In small deformation analyses, three types of cavity condition, which may form in practice, were considered: (i) Fully Open Cavity — where no soil backflow occurs into the punched cavity during spudcan penetration; (ii) Cavity with Partial Backflow — where soil starts to flow back into the cavity after flow failure which fills the lower cavity with the top cavity open; (iii) Full Backflow — where soil starts to flow back from shallow penetration therefore no cavity forms. These three cavity conditions are illustrated in Figure 5.1. Then the results of FE analysis are discussed. The design chart for cavity depth estimation proposed in the Offshore Design Guideline (SNAME, 1997) is introduced. Based on the new findings in this research, a new design chart has been developed and compared with the conventional one proposed in SNAME (1997).

Overall, the results presented in this Chapter are divided into two parts. The first part describes all the preliminary centrifuge tests, which ultimately failed to reach the goal designed but were the foundation to develop the successful test that followed. In the second part, the results from successful centrifuge tests and FE analyses are discussed together, so that some significant conclusions can be drawn.

5.2 Preliminary Centrifuge Tests (E1-E5)

5.2.1 Event 1-2 (E1 & E2)

5.2.1.1 Background

The key plan of these tests was to reveal the soil failure mechanisms during spudcan foundation penetration using the newly developed technique in the drum centrifuge. Kaolin slurry was consolidated, in a conventional consolidation tank, under a maximum pressure of 200 kPa in Event 1 and 100 kPa in Event 2 (procedures in Section 4.3.3). Six specimens, of size 258 mm × 80 mm × model height, from each sample were cut after consolidation. In Event 1, the half-spudcan and the half flat-plate models were used to observe the soil flow mechanisms as well as to measure the bearing response. In Event 2, only the half-spudcan model was used. In all cases,

footing penetration tests were run at a constant velocity of 0.2 mm/sec. Soil flow images were captured continuously using a mini video camera. To obtain the soil strength profile, T-bar penetration tests were undertaken, at a velocity of 1 mm/sec right after the completion of each footing test. Note that none of the tests reached the goal successfully in terms of capturing clear pictures of soil flow around spudcan and measuring spudcan load penetration response accurately. However, the reasons and some interesting preliminary findings are discussed in the following sections.

5.2.1.2 Soil strength

Figure 5.2 and Figure 5.3 illustrate the T-bar test results from 100 g and 200 g drum centrifuge tests respectively. These are from Event 1 tests. TB1 and TB2 indicate the sequence of T-bar tests conducted after footing tests on each specimen. Note that the in-flight time which elapsed between these two tests was about 7-10 minutes. The horizontal axis shows the undrained shear strength, s_u and the vertical axis represents the soil depth (z) in prototype. In order to investigate the effect of gravity level (or T-bar size) and elapsed time on strength characteristics, the 100 and 200 g tests results are summarised in Figure 5.4. The vertical axis is non-dimensionalised as z/D by the half-spudcan diameter (D), where z/D = 0.083 refers to the penetration depth of the full bar. It is clear that the soil strength of each specimen stays consistent with different T-bar tests in flight. A summary of the findings is as following:

- As the T-bar touches the soil surface, the strength measurement remains almost zero. But it increases sharply after the full bar penetrates into soil.
- In the 100 g tests, almost uniform strength of s_u = 18-19 kPa was obtained. This type of profile is typical for overconsolidated homogeneous clay.
- In the 200 g tests, the soil strength increases with the depth in the lower half (normally consolidated). This non-uniform profile indicates the soil was subjected to a re-consolidation. This is because the self weight pressure in the lower part of the soil under 200 g exceeded the pre-consolidation pressure (200 kPa). Reconsolidation effect is significant here as the tests were carried out after footing tests which took about 2 hours to perform. For this reason, E1T4TB1 shows uniform strength even though it was conducted at 200 g as the test was performed right after the centrifuge reached at 200 g prior to footing test.

- By comparing the results of 100 g and 200 g tests, the soil strength at 200 g is about 20-25% stronger than that at 100 g. The reasons could be: (a) the effect of re-consolidation pressure that is higher under higher acceleration level and longer elapsed time, (b) the effect of T-bar size (length and dia) which is double at 200 g.

Figure 5.5 illustrates the undrained soil strength associated with 200 g tests in Event 2. These results clearly demonstrate the effect of elapsed time under higher g-level; the longer the time under higher g-level, the higher will be the soil strength. Moreover, the following discussions should be noted:

- Unlike the Event 1 tests, two half-spudcan tests were carried out on a single specimen. 1st T-bar test (E2T3TB1) was performed after completion of the first spudcan installation. Then 2nd footing installation was performed followed by 2nd T-bar test (E2T3TB2). For the reason of more time elapsing in flight, a higher strength (s_u = 15 kPa) appears in E2T3TB2 than that (s_u = 13 kPa) appears in E2T3TB1 (15%). In E2T3TB2, a slightly stronger soil close to the surface might be attributed to the soil compaction and re-consolidation as two half-spudcans, of 60 mm model dia, penetration tests were undertaken prior to this test within the limited space of strongbox.
- By comparing with the Event 1 results at 200 g (s_u = 23-24 kPa), about half soil strength is resulted (s_u = 13 kPa, E2T3TB1). This correlates well with the applied pre-consolidation pressure (200 kPa in E1 and 100 kPa in E2).

5.2.1.3 Soil flow

Figure 5.6 displays the images captured by mini video camera. The images were fed directly into a video tape followed by digitisation to CD (converts the PAL video signal into an 8 Bit digital format and generates 320 × 240 pixels image), during half-spudcan penetration test at 100 g acceleration. The grids are 15 × 15 mm square in size. Figure 5.7 shows the images from 200 g test. The size of grid in the central part of the soil specimen was halved (7.5 × 7.5 mm square). This is to detect the soil deformation more precisely and to measure the distortion zone more accurately. Figure 5.6(a) and Figure 5.7(a) illustrate that a cavity is formed in the initial stage of the penetration and the soil flows plastically around the spudcan from underside

towards the soil surface. This causes soil heave close to the footing edges. With further penetration, the soil starts to flow back on the exposed top of the spudcan with the initial cavity open (Figures 5.6(b) and 5.7(b)). The stable cavity depth in prototype under 200 g is higher than the one under 100 g test. This is because that, at 200 g test, spudcan diameter in prototype, hence cavity diameter, is larger (Table 4.1), and soil strength is higher (Figure 5.4). At deep penetration, the spudcan is obscured by the ingression of soil, thus the soil flow mechanism cannot be evaluated.

Figure 5.8 illustrates the same mechanisms of Figure 5.6 but with monochrome video images directly digitised using PC frame-grabbing card (converts the PAL video signal into an 8 Bit digital format and generates 450 × 470 pixel image). Although image quality is improved, the effects of lens distortion and curvature are significant.

On the way to capture better images and to get clearer visualisation of soil flow mechanisms, some obstacles were encountered.

- Soil ingression in between the spudcan and the window: in this case, the picture does not show the true soil flow mechanism around the spudcan but an image of the movement of the ingress soil.
- Low quality of images due to:
    a. use of low resolution video camera,
    b. presence of lens distortion and curvature,
    c. transfer of images through centrifuge sliprings,
    d. presence of centrifuge vibration,
    e. improper position of camera.

All of the above mentioned features are from Event 1 tests. In order to prevent the ingression of soil, it was decided to use thin but spongy polyethylene foam* glued to the flat face of the half-spudcan in Event 2 test, so that the spudcan could be placed tightly against the window by the pressure applied by the Dynaserv.

* Self Wound, Abrasion Resistant, Polyethylene Foam Tape.

Albeit thin foam helped to prevent soil squeezing initially, soil started to squeeze in after a few mm penetrations and hence the spudcan disappeared from the image again. Therefore, the images have not been illustrated here.

5.2.1.4 Bearing capacity

From Figures 5.6-5.8, it is apparent that the soil squeezed in between the spudcan/plate and the window. This affected not only the observation of soil flow mechanisms around the spudcan during penetration, but also the measurement of bearing capacity of the spudcan, since the squeezed-in soil can create extra friction. Thus the measured bearing capacity values can be higher than the actual ones. Therefore, the bearing capacity factor, N_c, is not discussed here. However, some characteristics of bearing capacity response can still be observed.

E1T1HS

E1T1HS was performed at 100 g using half-spudcan of 60 mm dia. Figure 5.9 (a) shows the corresponding result. Bearing capacity (horizontal axis) is presented as a function of spudcan tip penetration depth, d_t/D in prototype. As the sharp conical tip of the spudcan first penetrates into the clay (as the early part of the bearing capacity curve) the bearing capacity remains low because of the small contact area. Once the main conical part of the footing begins to penetrate the clay the contact area increases rapidly with further penetration, so the bearing capacity rises sharply. After penetration of a full diameter there is no further increase in contact area but the bearing capacity continues to rise, although at a very low rate, partly because of changing geometry due to footing embedment below the soil surface and partly because of increasing overburden pressure with depth. Meanwhile, there was an abrupt drop of bearing capacity at the point when soil flowed back on top of the spudcan and applied pressure on the exposed top of the spudcan. It rises shortly as the overburden pressure, around the spudcan, increased with increase in penetration depth.

E1T2FP

E1T2FP was performed at 100 g but using half flat-plate of 60 mm dia. Figure 5.9(b) presents the corresponding result. The bearing capacity increases very slowly as the small sharp conical tip or spigot penetrates into the clay. After that, it rises abruptly

to almost the ultimate value due to penetration of full diameter. In flat-plate footing, after small conical tip there is no blunt conical underside (Figure 4.8) like spudcan, and hence the bearing area changes drastically. A sudden drop of bearing capacity is also present here, due to the back flow soil as discussed above.

E1T3HS and E1T4HS

E1T3HS and E1T4HS were performed using half-spudcan of 60 mm dia but at 200 g. According to the scaling law, the prototype diameter of spudcan and penetration depth is doubled at 200 g compared to 100 g. Figure 5.10 illustrates these tests results and shows almost identical bearing capacity as was expected. The sudden drop in bearing capacity due to soil back flow shows a stronger impact at 200 g than that at 100 g (Figure 5.9).

Effect of footing shape on bearing capacity

In order to investigate the effect of footing shape on bearing capacity, the results of test E1T1HS and E1T2HP are plotted together on Figure 5.11. The initial discrepancy is due to the absence of the bottom blunt conical underside in flat-plate, as stated above. After penetration of a full diameter, the flat-plate gives higher bearing capacity than the conical spudcan. It is well understood from mechanics that vertical pressure on flat surface is higher than that on conical surface (considering identical smooth surface). Another reason for higher bearing pressure could be the presence of a greater cylindrical shear area on the sides of the flat-plate (Figure 4.8). It should also be mentioned that the abrupt drop in bearing capacity occurred at closely identical depths in both cases, which means there was no significant effect of footing shape on the depth of backflow, when the same diameter was used in spudcan model and plate model. However, the soil backflow impact is weaker for spudcan than for plate.

5.2.2 Event 3 (E3)

5.2.2.1 Background

In order to improve the quality of the test, soft soil specimens were prepared. This was designed to reduce the chance of soil squeezing in between the spudcan and the

window. Kaolin slurry was consolidated, within the strong box, under maximum pressure of 25 kPa (explained in Section 4.3.4). Single specimen, of 125 mm height, was obtained after consolidation of three slurry layers. Four specimens were prepared in this way, with two tested at 100 g and the other two at 200 g. Half-spudcan penetration tests were performed at a constant velocity of 0.2 mm/sec. Soil flow images were captured continuously using a mini video camera. An in-flight T-bar test was undertaken in the specimen, at a velocity 1 mm/sec, right after the completion of each footing test.

5.2.2.2 Soil strength

Figure 5.12(a) and Figure 5.12(b) present the results from 200 g and 100 g testing respectively. In order to investigate the effect of gravity level and elapsed time on strength characteristics, 100 and 200 g tests results are summarised on Figure 5.13. After completion of in-flight T-bar tests at 100 g, a test was also conducted after ramping down the centrifuge at 1 g. It has also been included in Figure 5.13. Soil depth (z) in vertical axis is non-dimensionalised by half-spudcan diameter (D) as depth ratio, z/D, where z/D = 0.083 refers to the penetration depth of the full bar.

From Figure 5.13, it can be seen that the soil strength of the bottom layer was not affected by the g-level. However, the soil strength of top and middle layer were strongly influenced by g-level. At 100 g, the soil strength profile rises sharply to a peak value of 6 kPa at z/D = 0.35 followed by dropping back slowly to a residual value of 4 kPa at z/D = 1 and then again increasing sharply to 10.5 kPa at z/D = 1.54. Similar characteristics but with a slightly higher strength resulted at 200 g: shear strength rises sharply to a value of 7.5 kPa at z/D = 0.35 followed by a slow drop and almost merges with 100 g strength profile at z/D = 1. It should be noted that this strength profile with stronger soil (top layer) underlaid by soft soil (middle layer) leaves open the possibility of punch through failure. In post-test at 1 g, a uniform strength of 4.5 kPa for top and middle layers was obtained. The following points can be made from the results presented: (a) layering effect and (b) consolidation drainage effect. Firstly, since the soil was preconsolidated in three layers, this may have affected the final consolidation and created a layered deposit instead of a single layer deposit and therefore uniform strength profile. Secondly, drainage was provided only at the top and bottom plate centre through geo-fabrics (see Figure 4.22(a) and Figure

4.23). The top (plate of ram) and bottom (base of strong box) plate were not lined towards the centre which could also have hampered a uniform consolidation. In addition, no lateral or vertical sand drain was provided. Due to layered consolidation and faulty drainage the whole soil sample may not have been consolidated uniformly, i.e. the top and the bottom layer might have been consolidated more since they are closer to the drainage layers hence higher strengths resulted. However, the middle layer might have encountered difficulty in consolidating hence soft soil resulted.

It is also obvious during testing at elevated gravity, specimens were subjected to a reconsolidation due to overburden pressure. The overburden pressure exceeded the preconsolidation pressure (25 kPa) at very shallow depth of z/D = 0.24 and at z/D = 0.12 under 100 g and 200 g acceleration respectively. This is the reason why higher strengths resulted in these zones compared to the 1 g strength (under which acceleration, the soil depth was insufficient to exceed preconsolidation pressure). A slightly higher strength in the 200 g tests compared to that in the 100 g test might be due to the effect of more elapsed time in-flight (prototype). The soil strength at 1 g (post-test) is uniform in the top and middle layers and marginally lower than the other results, which highlights the gradual swelling (and strength reduction) of clay during swingdown. After z/D = 1, all strength profiles almost merged together and rise sharply to a normally consolidated clay. This is the typical soil strength profile under reconsolidation. More investigations are necessary to look into these layer effects and reconsolidation effects.

5.2.2.3 Soil flow

In Event 3, a thin metallic wiper was glued around the bottom conical and spigot edges of spudcan. The wiper itself was stiff but flexible and protruded slightly along the spudcan periphery which helped it to fit tightly against the window. Unfortunately, during the tests, the wiper was broken due to the high resistance from the soil. Thus, this attempt to obtain a clear soil flow pictures failed.

5.2.2.4 Bearing capacity

E3T1HS, E3T2HS and E3T3HS

E3T1HS was performed at 200 g and E3T2HS and E3T3HS were performed at 100 g using the half-spudcan of 60 mm dia. Figure 5.14 and Figure 5.15 show the

corresponding results respectively. In all three tests, the bearing capacity rises to the peak value at $d_t/D = 0.5$. After this peak point, the bearing capacity has stayed below this value until $d_t/D = 1.0$. It has shown the potential of punch through failure. This is due to the non-uniform consolidation i.e. non-uniform and soft soil at this (middle layer) zone.

5.2.3 Event 4 (E4)

5.2.3.1 Background

The chief aim of Event 4 was to eliminate the effect of layered soil. From the results of Event 3 tests, it was suspected that a layered clay was deposited (strong layer over soft layer) due to consolidation by layering. Kaolin slurry was consolidated, within the strong box, under a maximum pressure of 25 kPa in a single layer (explained in Section 4.3.4). Two specimens were prepared and tested in this Event. Due to the limited space of the strong box (258 mm long, but due to home position of tool table only (170.5 +D/2) mm can be used), another small half-spudcan (SHS) was made to perform two effective tests on one specimen. This was to fit more half-spudcan tests in one soil specimen, since one specimen was obtained after two and half weeks-consolidation within the strong box. Additionally, in the effort to catch clear images of soil deformation during half-spudcan penetration, half-spudcan model needs to be placed tightly against the window when penetrating. Thus it was inevitable to include the friction between spudcan and plexiglass in load response measurement. It was decided to measure the load-penetration response separately from the half-spudcan test. A full-spudcan model with 30 mm diameter was made to record actual bearing capacity of the spudcan. As such the half-spudcan model was only used for image capturing. Unlike the half-spudcan test, the full-spudcan model was penetrated along the centreline of the box (Figure 5.16). Half-spudcan and full-spudcan penetration tests were performed at a constant velocity 0.2 mm/sec. Soil flow images were captured continuously using the mini video camera. After the completion of half-spudcan and full-spudcan penetration tests, T-bar tests were conducted at a velocity of 1 mm/sec.

5.2.3.2 Soil strength

Figure 5.17 shows the measured undrained shear strengths of soil specimens at 100 g. A normally consolidated soil strength profile was obtained at deep soil layer. The soil strength rises initially to a peak value of 6 kPa at z = 1.0 m. This is due to reconsolidation effect as the overburden pressure exceeded the preconsolidation pressure (25 kPa) at a small depth z = 1.5 m. This peak value was followed by a slow drop back to a residual value of 3.5 kPa at z = 5 m and then a further rapid increase to a value of 13 kPa at z = 9 m. In order to investigate the actual reason for this layered profile (abrupt change) of softly preconsolidated clay, all results (100 g) of Event 3, consolidated by layering, and Event 4, consolidated in single layer, are plotted together on Figure 5.18. Similar soil strength profiles are shown. This means layered consolidation is not responsible for this profile. Therefore, effect of drainage i.e. non-uniform consolidation, explained above, along with the effects of reconsolidation, desiccation and boundary might be the crucial reasons.

5.2.3.3 Soil flow

In the above previous tests (E1, E2, E3), it was observed that the model of half-spudcan alone, half-spudcan with thin polyethylene foam and half-spudcan with metallic wiper failed to resist the soil ingression properly. In this Event, half-spudcan, of 30 mm dia, was glued with thick polyethylene foam with abrasion resistant polyethylene film. Figure 5.19 shows the images captured, by mini video camera, at 100 g acceleration. The grids are 10 × 10 mm square in size. Figure 5.19(a) illustrates clearly that a cavity was formed in the initial stage of penetration and the soil flowed plastically around the spudcan from underside to the soil surface. Therefore soil heave occurred close to the spudcan edges. With further penetration, soil started to flow back on the exposed top of the spudcan (Figure 5.19(b)). At deep penetration, the spudcan become fully embedded with the initial cavity open (Figure 5.19(c)).

However, it was realised that, with this small half-spudcan model, the shaft was too flexible to penetrate with high Dynaserv pressure (moment). In addition, the soil deformation is not so clear, as the diameter is apparently too small to detect the soil deformation clearly, particularly on these hazy images.

On the way to a clear visualisation of soil flow mechanisms, some obstacles can still be detected:

- Soil ingress, caused by the flexible shaft of small half-spudcan (Figure 4.8).
- Low quality of images due to:
    (i) line of collimation was not perpendicular to the strongbox; lens distortion and curvature are profound,
    (ii) use of low resolution video camera,
    (iii) transfer of images through centrifuge sliprings.

5.2.3.4 Bearing capacity

Effect of spudcan-plexiglass friction on bearing resistance

Figure 5.20 presents load-penetration response from half-spudcan and full-spudcan tests together, conducted at 100 g. The overall responses from half-spudcan and full-spudcan agree very well. However, the difference between half-spudcan and full-spudcan has clearly shown the influence of friction between the spudcan and the plexiglass window. Therefore, it was decided that to quantify bearing capacity or to calculate N_c value, only full-spudcan results would be used.

5.2.4 Event 5 (E5)

5.2.4.1 Background

In Event 4, it was found that the shaft of the small half-spudcan (SHS) is too flexible to penetrate tightly against the window. In addition, it was very difficult to track the soil deformation clearly around the small spudcan. Therefore, in Event 5, the original half-spudcan (D = 60 mm) was used with sponge tape glued on the spudcan face. In this event, Kaolin slurry was consolidated, in a conventional consolidation tank, under a maximum pressure of 150 kPa (explained in Section 4.3.3). Soil flow images were captured continuously using two mini video cameras. The additional one is to capture the plan (top) view of soil flow images. Half-spudcan and full-spudcan tests were run at a constant rate of 0.2 mm/sec. T-bar tests were conducted of a velocity of 1 mm/sec immediately after the completion of spudcan footing tests. One T-bar test was also undertaken at 1 g, before ramping up the centrifuge to conduct footing

penetration tests. In addition, full-spudcan tests were also undertaken in air and water alone (without any soil deposit) in order to investigate the effect of centrifuge acceleration on spudcan self-weight in air and in the presence of water so that its effect could be taken into account in the bearing capacity analysis of soil.

5.2.4.2 Soil strength

The soil strength results are presented and discussed later in Section 5.3.1 (Figure 5.25).

5.2.4.3 Bearing capacity

Effect of spudcan-plexiglass friction on bearing resistance – more evidence

In order to investigate the effect of spudcan-plexiglass interface frictions, due to being penetrated tightly against the window to prevent ingress of soil, full-spudcan tests were performed along the centreline of the box. Figures 5.21 and 5.22 present load-penetration response from half-spudcan and full-spudcan tests together, conducted at 100 g and 200 g respectively. After penetration of full-diameter, 30%-40% higher bearing resistances can be obtained from the half-spudcan tests. This was caused by spudcan-plexiglass interface friction. The higher friction, in comparing to Event 4, was attributed to the higher contact pressures in Event 5.

It was further proved that to quantify actual bearing capacity or to calculate N_c value, only full-spudcan results would be used.

Effect of footing weight and presence of water

In order to quantify the effect of footing weight, two full-spudcan tests have been undertaken at 100 g and 200 g in air alone (without any soil deposit) and the results are shown in Figure 5.23. This increase of load (-ve) with penetration depth is due to increase of radial distance of the centroid of the penetrating spudcan. Surprisingly, an identical resistance resulted which can be idealised as linearly increasing with depth having a gradient of -1.6 kPa/m. This is completely due to the weight of the spudcan (in model ≈ 30 gm, $\gamma = 26.87$ kN/m^3) acting vertically downward.

A test was also conducted in water at 100 g to quantify water resistance i.e. the effect of buoyancy. Tests results (at 100 g), conducted in air and water, are plotted together on Figure 5.24. There was an abrupt drop of resistance, from –7.8 kPa to –6.15 kPa, at the point where the footing tip touched the water surface and the bottom conical surface penetrated into water. This is due to the resistance of water i.e. the buoyant force which acts vertically upwards, opposite to the weight of footing. After this sudden drop, the rate of decrease increased very slowly with the depth of water.

The increase –1.6 kPa/m is due to the rotation radius of centrifuge. The gravity increases with increase of radius. This is why the spudcan becomes heavier with radius. In Figure 5.24, the reduction of negative bearing resistance is due to the buoyancy of the spudcan in water. However, the gradient of spudcan under water is not the same as the one in air. This is mainly associated with the increasing spudcan submerged volume as the shaft was penetrating into water. These effects took into account in bearing capacity calculations in the Sections 5.7.1 and 5.8.4. The test range within the soil deposit in the drum channel is also labelled on Figure 5.24.

After the few trials in centrifuge testing (E1-E4), the modifications on the half-spudcan test allowed the subsequent success in centrifuge testing (E5-E6). Together with numerical simulations, the following discussion (Section 5.3-5.7) has focused on (a) soil strength, (b) image analysis, (c) soil flow mechanisms, (d) cavity stability, and (e) bearing capacity.

5.3 Soil Strength

5.3.1 Event 5

Figure 5.25 shows the measured undrained shear strengths, assuming N_{ctb} = 10.5, of soil specimens at different gravity levels. Herein, soil depth (z) in vertical axis is non-dimensionalised by full-spudcan diameter (D) as depth ratio, z/D, where z/D = 0.167 refers to the penetration depth of the full bar. The following discussion summarises the results.

By comparing with the soil strength at 1 g after consolidation, it is seen that the soil gradually becomes weaker at 100 g but stronger at 200 g. This can be explained as that the soil was heavily overconsolidated under 150 kPa preconsolidation pressure before centrifuge testing. When the clay sample was open to air after consolidation, it might have experienced a pore suction and tried to suck air (or water if available) from the exposed surfaces. Subsequently, at elevated gravity, specimens were subjected to a reconsolidation due to overburden pressure. However, under the 100 g acceleration the vertical overburden pressure (self weight) up to z/D = 3 was less than the preconsolidation pressure. This allowed a gradual swelling of the specimen, with a uniform strength obtained over the depth of penetration. On the other hand, under the 200 g acceleration, overburden pressure exceeded the preconsolidation pressure at z/D = 1.25. This caused the soil specimen to be reconsolidated in the lower part of the specimen. Thus the soil strength increased with depth in the lower part. Moreover, the soil specimen, particularly at the exposed periphery, gradually became dry by evaporating water, as it was open to atmosphere. Obviously, at enhanced gravity level this effect was higher (Phillips, 1997) due to high speed spinning. Although the soil sample was wrapped up by plastic sheets most of the time, the desiccation effect might not have been prevented completely. This is why slightly higher strength resulted in the top part of the soil specimen. Note that all aforementioned effects are related to the time which elapsed between the release of pressure after preconsolidation and the start of in-flight penetrations. The time elapsed in model between a T-bar test under 1 g (prior footing test) and a T-bar test under 100 g or 200 g (right after completion of footing test) was about two hours and 30 minutes.

5.3.2 Event 6

In Event 6, kaolin slurry was consolidated, in a conventional consolidation tank, under a maximum pressure of 150 kPa (explained in Section 4.3.3). Soil characterisation tests were performed by in-flight T-bar penetration tests. These tests were undertaken, before and after each footing test, at a rate of 1 mm/s. To simulate a seabed condition, similar tests were then also performed with about 30 mm water covering the top of the specimens.

Figure 5.26 shows the measured undrained shear strengths of three soil specimens under different g-level when no water layer was placed on the top of the soil specimen. Soil depth (z) in vertical axis is non-dimensionalised by half-spudcan diameter (D) as depth ratio, z/D, where z/D = 0.167 refers to the penetration depth of the full bar. By comparing the results at elevated g-level with the soil strength at 1 g after consolidation, almost identical (within 1 kPa) soil strengths were obtained at 50 g and 100 g and therefore the swelling effect, as explained above, is not obvious. It is probably due to the careful measurement carried out. However, at 200 g, still slightly higher strength was resulted. This is attributed to the reconsolidation effect of soil specimen at 200 g and the slight desiccation as discussed above. The longer elapsed time before the 200 g test has enhanced this effect.

Figure 5.27 shows the strength profile of soil specimen with water layer on top. There were three soil specimens tested. On specimen I, a full-spudcan along with a T-bar tests were conducted at 50 g. With the same specimen, centrifuge gravity was increased to 100 g, and a full spudcan and a T-bar tests were carried out. The T-bar results of specimen I in Figure 5.27 have shown that the soil has a relatively higher strength at 50 g and a lower strength at 100 g. This is associated with the shorter in-flight elapsed time at 50 g, with less strength loss (14%, Table 5.2). Whereas, with the longer in-flight elapsed time at 100 g, greater strength loss occurred (44%, Table 5.2). It should be noted that in Table 5.2, the percent of loosing/softening of soil strengths are evaluated with respect to the 1 g soil strength in absence of free water on the top of the specimen (Figure 5.26).

On specimen II and specimen III, the same sequence was followed at 50 g in specimen II and 100 g in III: half-spudcan test → T-bar test → full-spudcan test → T-bar test. Since the T-bar tests on the specimen II and III were conducted after half-spudcan tests, a rather long and similar elapsed time, before T-bar tests, induced the same softening effect as on specimen I in 100 g test (14%, Table 5.2). Therefore, the in-flight lapse time is crucial to the soil strength profile particularly when free water is present on the top of the soil specimen (Table 5.2). Thus the in-flight elapsed time between tests needs to be strictly controlled to obtain a designed soil strength profile.

In order to investigate the softening effect at testing gravity on soil strength more precisely, all T-bar test results, which were conducted before and after footing tests, at different gravity are summarised in Figure 5.28. In the absence of free top water, the softening effect is not so profound (Figure 5.28(a) and (b)). However, there are swelling (under 100 g) and reconsolidation and desiccation (under 200 g) effects observed. In the presence of free top water, the softening effect is obvious. Figure 5.28(c) and (d) depict a decrease in strength of 15-20% both at 50 g and 100 g testing. This softening effect is due to the absorbed water into the specimen with the time. Therefore, average strengths were used in N_c value calculations.

5.4 Image Observations

5.4.1 Event 5

Figure 5.29 shows the images captured, by the mini video camera, during a half-spudcan penetration test at 100 g acceleration. The grids are 10 × 10 mm square in size. Figure 5.30 shows the images from 200 g test. A smaller size grid 5 × 5 mm square was drawn at the zone of interest to detect the soil particle movement more clearly and to measure the distortion zone more accurately.

Figure 5.29(a) and Figure 5.30(a) show the soil deformation when the spudcan was shallowly embedded. By inspecting the grid deformation, it can be seen that underneath the spudcan, soil has been pushed down to a large depth, up to 1 D. At the same time, soil has heaved up at both sides with a heave range up to 1.5 D. With further penetration, soil starts to flow back on top of the spudcan (Figure 5.29(b) and Figure 5.30(b)). The cavity formed at the initial penetration remains open. The backflow occurs at H/D = 0.32 at 100 g and at H/D = 0.27 at 200 g. The reason for the different H/D could be (a) the reduction of applied stress (F/A, F is the applied vertical load and A is the spudcan effective area) with the increase of diameter or effective area, (b) the stronger material resulted at 200 g testing (see Figure 5.25). The soil flow mechanism becomes totally localized when the penetration was deep (Figure 5.29(c) and Figure 5.30(c)). There was no wall failure observed although it

was suggested in design guidelines. This was further confirmed by the top view during spudcan penetration (Figure 5.31). There was no enlargement of the cavity diameter, thus there was no sign of wall failure.

5.4.2 Event 6

For better images of soil flow around the spudcan, black flock powder and a high resolution digital still camera were deployed in this event of tests. To ensure a tight contact between the half-spudcan and the window, a 1 mm "O" ring around the periphery and a thickened stiffener at the rear side of the spudcan shaft were used (Figures 4.8 and 4.11). The black 'flock' modelling material was sprinkled over the plexiglass face. This is to suit the images captured by the digital camera for subsequent PIV analysis. It was observed, from Event 1-5, that the quality of images captured by the video camera was very low. The main reasons were the use of a low resolution video camera and transferring the images through the centrifuge sliprings. To overcome these two obstacles and to provide clearer soil movement images for PIV analysis, soil flow images were captured by a high resolution (2270 × 1704 pixels) digital still camera (based on the probable solutions as discussed in Appendix 1). Moreover, the camera was modified by attaching a small weight to the shutter so that, under centrifuge acceleration, it would capture images continuously on board (i.e. there is no need to transfer through the centrifuge sliprings). The camera position, set-up and the lighting in the drum channel have been carefully designed (details in Section 4.2.4 and 4.2.5).

Half-spudcan penetration tests were conducted at a lower rate (0.04 mm/sec) to obtain more images at a given penetration (see rate selection in Appendix 2). Thus a more detailed soil movement can be obtained by the PIV analysis. To simulate a seabed situation, similar tests were then also performed with about 30 mm water on top of the specimens where the half-spudcan was lowered at a slightly higher rate of 0.05 mm/sec due to additional time requirement in sprinkling water (see Appendix 2).

Due to the initial concern of the workability of a digital camera at high acceleration levels, the first half-spudcan penetration test was conducted at 50 g. Similar types of failure mechanisms, as stated above, were visualised, but of course with a clearer visualization of the zone of interest (Figure 5.32) due to use of the high resolution digital camera.

In the tests without water on top, the cavity depth ratio (or the depth ratio of backflow) of H/D = 0.53 at 50 g (Figure 5.32) for flow failure lies above the corresponding depth ratios of Event 5 tests at 100 g and 200 g (Table 5.4). Note, the footing diameter is lower at 50 g but the soil is stronger compared to 100 g (Table 5.4). Therefore, footing size might be a comparatively more crucial factor for soil backflow.

In order to study the seabed situation, centrifuge tests were also carried out successfully on submerged clay beds at 50 g and 100 g accelerations. Figure 5.33 and Figure 5.34 have displayed the digital images of a half-spudcan penetrating into soil at 50 g and 100 g gravity respectively. The stable cavity depth ratios can be observed of H/D = 0.72 and 0.48 for 50 g and 100 g testing respectively (Table 5.4). This is because the prototype spudcan diameters are different under different gravity. When these cavity depths with water on top are compared with the one without water on top at the same gravity (equal footing size), it is apparent that the ones with water on top are higher than the ones without water on top. This is because, since water filled up the cavity in the soil specimen with water on top, the cavity stability was dependent on its effective unit weight, i.e. $\gamma' = 7$ kN/m^3, and at the same time when there is not water on the top of the soil sample, the cavity was filled up with air, thus the cavity stability was dependent on its total unit weight, i.e. $\gamma = 17$ kN/m^3. Therefore, a deeper depth was required with the soil buoyant unit weight (γ') to flow back into the cavity and hence a deeper cavity depth (H) was obtained in the test of soil under free water. Another interesting feature is that greater and hence more profound soil heaves are created in the presence of free top water. This is associated with the same reason, that the effective unit weight controls the soil flow. It should be noted that the depth of cavity (or the depth of soil above the spudcan) and the soil heaves play a key role in evaluating the bearing capacity of a penetrating footing.

5.5 Soil Flow

5.5.1 PIV Analysis

Figures 5.35-5.37 show the displacement vectors from PIV analysis which correspond to the images in Figures 5.32-5.34. This is from the digital images, captured during Event 6 testing. Figures 5.35(a)-5.37(a) display the general bearing capacity failure for a shallow footing. It can be seen that there is a significant vertical downward movement underneath the blunt spigot. Around the spudcan shoulder, there is a transitional movement from laterally to vertically upward. Soil flow towards the ground surface is the reason for soil heave near the spudcan edges. With increase in penetration depth, the upward soil flow towards the surface changed its direction to flow back on top of the spudcan (Figures 5.35(b)-5.37(b)). When penetration is deeper, a fully localised shear failure, i.e. a deep failure mechanism appears (Figures 5.35(c)-5.37(c)).

In addition, it can be observed that: (a) at the shallow penetration of the spudcan, a large amount of soil underneath the spudcan moves downward, and only a small amount of soil near the spudcan shoulder flows around the spudcan; (b) at the deep penetration of the spudcan, the area of soil downward movement underneath the spudcan is decreased to (0.5 D), and the rest of the soil underneath the spudcan forms a backflow on top of the spudcan. The lateral deformation zone extends to 1.5~1.6 D for the surface footing and 1.26~1.32 D for the deeply embedded footing. These phenomena have also been found in Event 5 when the deformed grids were inspected (Figures 5.29 and 5.30).

5.5.2 Numerical Analysis

5.5.2.1 Small deformation analysis

In small deformation finite element study, firstly, a fully open cavity above the spudcan foundation was considered (Figure 5.1(a)). With different embedment of the spudcan, it is to perceive the occurrence of flow failure and cavity wall failure. Figure 5.38 shows the soil failure mechanisms with the fully open cavity. The soil

parameters were chosen as the Case III centrifuge test (Table 3.2). In this case, soil unit weight was γ =17 kN/m^3, soil uniform strength was s_u = 18 kPa and spudcan diameter was D = 12 m. Both smooth and rough soil-spudcan interfaces were analysed. In this study, the soil weight was used to provide an initial stress field. Then the spudcan is penetrated into the soil using displacement control.

It is apparent that at shallow embedment, soil initially heaves up (Figure 5.38(ai) & (bi)). However, for spudcan pre-embedment beyond a certain depth, i.e. the cavity wall reaches a certain height (H_F), soil failure occurs by flowing back on top of the spudcan. This forms flow failure (Figure 5.38(aii) & (bii)). This failure is due to the penetration movement of the spudcan and has also been observed in centrifuge testing (Figures 5.35(b)-5.37(b)). In reality, the cavity will keep the height at this point. When the spudcan is placed deeper, soil will keep flowing back on top of the spudcan, which was what occurred in centrifuge testing. However, in order to study the cavity wall height for wall failure, as was stated in the design guideline (SNAME 1997), a spudcan with a deeper cavity was simulated.

At a certain depth (H_W), a wall failure mechanism was obtained in Figure 5.38(aiii) & (biii). This wall failure is due to the initial stress field imported from soil self weight, i.e. the wall failure is due to soil gravity. It is apparent that to initiate a wall failure a deeper open cavity is needed than to initiate a flow failure. This is why the wall failure mechanism has never been observed in the centrifuge tests. From Figure 5.38, it can also be seen that the flow failure is due to the penetration action of spudcan foundation, and the wall failure is due to the gravity of wall that is too high to stand. Comparing the results of smooth spudcan and rough spudcan analysis, the cavity wall height at flow failure and wall failure is not influenced by the spudcan roughness, though the soil failure zone underneath the spudcan is larger for the rough spudcan. Rough interface causes a lateral distortion zone of 0.33-0.5 D whereas smooth spudcan causes a distortion zone of 0.17-0.2 D from the spudcan edges.

To investigate the effect on cavity depth in different soils with different spudcan diameter, more case studies with a fully open cavity above the spudcan were carried out numerically. All of them experienced similar failure modes: surface failure, flow failure at H_F and wall failure at H_W and in all cases $H_W > H_F$.

In a very soft clay deposit, extensive backfilling could fill the cavity completely immediately after the spudcan penetrates into clay. Figure 5.39 illustrates the results of the embedded spudcan with a full backflow, i.e. there is no cavity during spudcan penetration. Both smooth and rough interfaces were investigated. With increasing embedment depth, the soil flow mechanism varies from a shallow failure mechanism to a localised deep failure mechanism.

In order to simulate the flow mechanisms observed in the centrifuge tests, numerical investigations were also conducted assuming a cavity with partial backflow. The soil properties and spudcan dimensions are the same as the above. The results are illustrated in Figure 5.40. Before the backflow starts, the simulations are the same as the one with the fully open cavity. However, once soil starts to flow back on top of the spudcan, the spudcan becomes fully embedded. At deep penetration, however, the flow becomes fully localized and the wall failure has no chance to occur i.e. the cavity remains open near the soil surface. These results agree very well with the observations from centrifuge tests.

5.5.2.2 Large deformation analysis

Soil flow mechanisms have been depicted above assuming three probable cavity conditions above the penetrating spudcan. All of these are from pre-embedded spudcan analyses with the spudcan foundation wished in place. However, to reveal a continuous penetration process, large deformation analyses were also performed. Figure 5.41 shows the agreeable results of a perfectly smooth spudcan case. Similar features are observed as in the centrifuge tests (from PIV analysis) and small deformation FE analyses (with a cavity and partial backflow). As the spudcan is penetrating into a uniform clay, a clean cavity is formed above the spudcan. The soil flow towards the ground surface causes soil heave near the spudcan edges. When penetration is deeper, the cavity depth increases with increasing spudcan penetration depth until soil backflow occurs. After this point, the cavity depth stays constant, and soil flows back onto the top of the spudcan continuously. When penetration goes further, the failure mechanism becomes fully localised. The cavity formed initially remains open and no wall failure is observed. In addition, by comparing the results from the continuous penetration analysis with the one from the small strain analysis

with a cavity and partial backflow, interestingly the same penetration depths have been found for the change of failure mechanisms.

Under the same soil conditions, a buoyant unit weight of clay (γ' = 7 kN/m^3) was used to simulate the submerged seabed. Interestingly more profound features can be seen in Figure 5.42. By comparing with the results with saturated soil unit weight (cavity filled with air) (Figure 5.41), greater soil heave is found and a cavity is sustained to deeper penetration. Additionally, it leads to significant increase in the depth of backflow and the depth of localised flow and therefore a deeper cavity remains open above the spudcan. This demonstrates that soil deforming under water has a significant effect on the amount of ground surface heave, the depth of cavity formed and the depth before fully localised deep failure. This phenomenon was also observed in centrifuge tests (Figures 5.33 and 5.34), in which a significant deeper cavity was formed during the penetration of the spudcan with a water layer on top of the soil specimen.

5.6 Stability Number of Cavity

5.6.1 Cavity Stability

Due to the formation of the cavity above the spudcan foundation during penetration into uniform clay, the soil backflow mechanism plays an important role in estimating the open cavity depth (or the depth of soil above the spudcan). The soil infill into the cavity above the spudcan can be projected in two ways: flow failure and wall failure. The flow failure is caused by the combined action of penetration pressure and overburden pressure. During penetration, spudcan pushes the underneath soil to flow plastically around the foundation towards the top (such as Figure 5.38(ai) & (bi)). However, when the overburden pressure becomes sufficient, due to the penetration depth, to counteract this flow pressure (pressure applied by the penetrating footing), the soil is forced to flow towards the cavity (Figure 5.38(aii) & (bii)).

The wall failure is caused by the gravity of the cavity wall. When the cavity wall is too high to stand, the soil from the cavity wall slides into the cavity (see Figure 5.38(aiii) & (biii)). This failure occurs without the influence of spudcan penetration. Whatever the mechanisms of infill above the penetrating spudcan, its effect will be (a) to reduce the net vertical bearing capacity and hence increase the penetration depth, (b) to increase the available moment and horizontal load capacities, (c) to increase elastic stiffness and (d) to increase soil foundation interaction capacity under tensile vertical loading. A further consequence of the infilling is that a significant passive resistance can be mobilised by the embedded portion of a jack-up leg under combined loading (Springman and Schofield, 1998).

The cavity wall failure has been investigated extensively by Britto and Kusakabe (1982, 1983) and Meyerhof (1972). These analytical solutions are for wall failure during axisymmetric excavation. Offshore design guideline SNAME (1997) recommends to using stability factors of Meyerhof (1972) for uniform clay and that of Britto and Kusakabe (1983) for normally consolidated clay for conservative evaluation of depth of backflow during spudcan foundation penetration.

The FE results of soil flow mechanism with a fully open cavity above the spudcan have clearly been discussed in Section 5.5.2.1. It is apparent that the soil flow failure, i.e. the soil backflow due to the penetration process, occurred at a shallower depth than the one for wall failure, i.e. the soil backflow due to the gravity wall failure. This difference is made clear when all the deduced cavity stability numbers in centrifuge tests and FE analyses for nine cases (Table 3.2) are plotted in Figure 5.43, together with suggested criteria from SNAME (1997) design guidelines. The stability number (N_s) has been calculated using Equation 2.11 considering H as the depth of maximum bearing area of spudcan and s_u as the local soil strength at that depth (assuming uniform profile over the penetration depth). It is confirmed that: (1) for wall failure, the FE results agree well with the analytical solutions suggested by SNAME (1997); (2) for flow failure, the FE results match well with the centrifuge measurements. However, the curve of flow failure is totally different from the curve of wall failure. At certain cavity depth (H), the N_s number from flow failure stays much lower than that from wall failure. Thus the design curve needs to be modified.

Table 5.5 has also summarised the stability numbers to provide a better view for quantitative comparison. By comparing the cavity depth, it shows clearly that the wall failure (H_W) has overestimated the cavity depth by up to 4 times compared with the value for flow failure (H_F). Thus, a new design curve is imperative.

5.6.2 New Design Curve

As the soil backflow is caused by a totally different failure mechanism- flow failure, rather than the one suggested in SNAME – wall failure, a series of parametric study using FE were conducted to investigate the cavity depth and the corresponding stability number. Soil unit weights γ = 17 kN/m^3 and 7 kN/m^3 were chosen for soil without water on top and with water on top respectively. Spudcan diameter D = 18 m, 12 m and 6 m were considered to examine the foundation size effect. Therefore, six combined cases with different unit weight and footing size were analysed. In all the cases, the soil undrained shear strength was varied from 1 kPa to 60 kPa to investigate the corresponding effect on cavity stability. Since no significant variation in the depth of backflow considering smooth and rough interface has been found, only the smooth soil-spudcan interface is considered in these analyses. Note that both small and large deformation analyses were performed.

Figure 5.44 shows the results using the conventional coordinate system in the design chart. Remarkably all the results stayed fairly close together to form a unique curve. A small discrepancy only appears in the area H/D < 0.2, where the soil strengths are very low (s_u = 1-9 kPa). This is because the definition of the stability number N_s = $\gamma H/s_u$; since s_u is small, a small change in H can cause a large change in N_s. Nonetheless, a fitted curve can be obtained and used in practice:

$$N_s = f_1\left(\frac{H}{D}\right)^{f_2} \tag{5.1}$$

$$N_s = 1.01\left(\frac{H}{D}\right)^{-0.9} \tag{5.1.1}$$

where the suitable values of the empirical constants are f_1 = 1.01 and f_2 = -0.9. The centrifuge results are also plotted in Figure 5.44 and agree well with the numerical results.

In previous studies (Herdy and Townsend, 1983; Higham, 1984; Craig and Chua, 1990), the stability factor was presented as the dimensionless group $\gamma D/s_u$ (or $s_u/\gamma D$) rather than $\gamma H/s_u$. From flow failure mechanism point of view, $\gamma D/s_u$ should be more appropriate, since $N_s = \gamma H/s_u$ is used for wall failure, where wall height H is the controlling factor; however, the flow failure is caused by spudcan penetration process, thus the spudcan diameter should be the controlling factor. In addition, in offshore practice, it is usual to conduct shear vane tests or a cone penetration test and obtain samples in order to measure soil properties (s_u, γ' etc.) before assessing jack-up foundations. Therefore, for jack-up unit designers and practitioners, it is comparatively easy to predict the probable depth of backflow from the design chart of $\gamma D/s_u$ vs H/D. For the new stability number N_{sD} (= $\gamma D/s_u$), the fitted curve as mentioned above will be:

$$N_{sD} = f_1\left(\frac{H}{D}\right)^{f_3} \tag{5.2}$$

$$N_{sD} = 1.01\left(\frac{H}{D}\right)^{-1.9} \tag{5.2.1}$$

in which f_3 = -1.9. Figure 5.45 shows this design curve along with the measured values. Since the concerning range of N_{sD} for a major jack-up rig design stays between 3 and 10 (Craig & Chua, 1990), Figure 5.46 displays the data close to this range and the bound curves to give upper bound and lower bound of the data. The general equation for the bound curves can be written as:

$$N_{sD} = 0.75\left(\frac{H}{D}\right)^{-1.9} \tag{5.2.3}$$

$$N_{sD} = 1.25\left(\frac{H}{D}\right)^{-1.9} \tag{5.2.4}$$

in which f_1 = 1.25 and 0.75 for the upper bound and lower bound curves respectively. Since the cavity base is uneven in centrifuge testing, the average value of the cavity depth and its variations (bound values) are given in Figure 5.46. The average values from centrifuge tests have shown a good agreement with the bound curves defined by Equations 5.2.3 and 5.2.4. Therefore, Equations 5.2.3 and 5.2.4 can be used in practice to estimate the cavity depth or how deep the backfill soil will be above the spudcan.

5.7 Bearing Capacity Factor, N_c

The bearing capacity of spudcan foundation on undrained clay is of particular importance in offshore design. In this study, this response has been described by the non-dimensional bearing capacity factor, N_c.

5.7.1 Centrifuge Tests

Full spudcan penetration test results are used to calculate the bearing capacity factor N_c, which is expressed as

$$N_c = \frac{q_u}{s_u} \tag{5.3}$$

where s_u is the undrained shear strength of soil and q_u is the total ultimate bearing pressure on spudcan foundation, which is:

$$q_u = \frac{V}{A} \tag{5.4}$$

where V is the measured total vertical force on spudcan foundation during penetration and A is the projected horizontal area ($A = \pi D^2/4$) of spudcan, D is the diameter of spudcan (Figure 2.3). Depending on the strength profile of soil (Figures 5.25-5.27), the undrained shear strength of soil (s_u) is assumed as either constant (s_u

= s_{uo}) over the depth of penetration or slightly increasing with depth ($s_u = s_{uo} + kz$, z is the soil depth). In Equation 5.4, the contribution of overburden pressure to the vertical load capacity has not been considered separately. Thus, a total response is obtained. Note, appropriate spudcan buoyancy effect (Section 5.2.4.3) has been taken into account in the following bearing capacity calculations.

5.7.1.1 Event 5

Figure 5.47 shows the results of spudcan penetration in the 100 g and 200 g centrifuge tests. The corresponding soil strengths are shown in Figure 5.25. The ultimate bearing capacity factor reaches N_c = 11.7 and 10.2 at 100 g and 200 g test respectively. There could be two reasons: a) effect of footing weight; b) effect of s_u measurement. The effect of footing weight has been discussed in section 5.2.4.3. Thus only the s_u measurement is addressed here. From Equation 5.3, it can be clearly seen that the calculated N_c number is strongly dependent on the accurate measurement of soil undrained shear strength. All the soil strengths in Figure 5.25 were measured after the spudcan penetration tests. From Figure 5.25, it is apparent that soil becomes weaker at 100 g and stronger at 200 g with more elapsed time. Thus the measured soil strength could be lower at 100 g test and higher at 200 g test than the actually existed ones during footing penetration. Therefore, it is necessary to conduct T-bar test before and after footing penetration test so that the average value can be taken as the appropriate strength during testing.

5.7.1.2 Event 6

In this Event, full-spudcan tests were conducted, at a constant rate of 0.2 mm/sec, at 50 g, 100 g and 200 g. Soil shear strengths were measured before and after spudcan penetration test and the average of these two was used in Equation 5.3 to evaluate the bearing capacity factor. Several discussion points can be made:

Figure 5.48 shows the bearing capacity factor (N_c) in the 50 g, 100 g and 200 g centrifuge tests in absence of free water on the top of the soil specimen. Different ultimate N_c values, 10.5 ~ 11.2, appear at different acceleration g-level. Since the soil shear strength was tested before and after each spudcan penetration test, the shear strength has been carefully evaluated. This is why the difference in N_c number between different g-levels, as discussed in Event 5 tests, is reduced considerably.

For submerged clay bed, the results are shown in Figure 5.49. Interestingly, a consistent ultimate bearing capacity factor of N_c = 10.5 is obtained as penetration reaches d/D = 1.5 for all four penetration tests. Presumable, the strengths have been evaluated more accurately. The slight inconsistency observed at the beginning of the penetration (N_c = 5 ~ 8) is due to the softening effect on the soil surface with water presence. Although the soil strength (s_u), that is used in the calculation of N_c number (Equation 5.3), can be taken as the straight lines suggested in Figure 5.27, the difference between the measured s_u and suggested s_u shows a bigger gap in specimen I tests than in specimen II and III tests. This is the reason why, at the beginning of the spudcan penetration, sample I tests give lower N_c values than the N_c values from specimen II and III tests. However, when penetration reaches 1.5 times the diameter, all tests provide a consistent N_c number of 10.5, which can be recommended for design in uniform clayey marine deposit.

5.7.2 Numerical Analysis

In small deformation FE analyses, based on soil backflow during spudcan penetration, three types of cavity conditions are simulated: (i) Fully Open Cavity; (ii) Cavity with Partial Backflow; and (iii) Full Backflow. Figure 5.50 and Figure 5.51 display the bearing capacity factor of spudcan with fully open cavity above the spudcan. The spudcan diameter is of D = 12 m with smooth interface and soil unit weights are γ = 17 and 7 kN/m^3 respectively. Soil undrained shear strength (s_u) varies from 3 to 30 kPa are considered. Several discussion points can be made:

- As a typical curve ($\gamma D/s_u$ = 11.33 in Figure 5.50, or $\gamma D/s_u$ = 4.67 in Figure 5.51), it can be seen that the first part OA rises sharply since in this stage soil was yielding towards the surface. More work needs to be done with the increasing of penetration depth against higher overburden pressure.
- At point A, the soil started to flow back on top of the spudcan. This is why in the second part AB the bearing capacity remains almost unchanged. It increases again after point B, where wall failure occurs. Consequently the third part of the curve BC rises sharply again. As discussed above, these two failure mechanisms (flow failure and wall failure) are related to the stability number,

$\gamma D/s_u$. The delayed change of bearing capacity factor profile is obtained with the lower stability number.

- However, in very soft clay where $\gamma D/s_u$ is higher, considerable disagreements are found with N_c value increasing without any interruption. The reason might be that wall failure occurred right after flow failure i.e. difference between these two failures was very low.
- By comparing Figures 5.50 and 5.51, similar but delayed profiles are found in Figure 5.51 where buoyant (lower) unit weight was considered. This is associated with the lower value of $\gamma D/s_u$.

Figure 5.52 and Figure 5.53 display N_c values of the spudcan with cavity with partial backflow and full backflow above the spudcan. The spudcan diameters are of D = 12 m and 6 m respectively with perfectly smooth and rough interface. The following points can be made from the results presented:

- For the case of Cavity with Partial Backflow, as a typical curve ($\gamma D/s_u$ = 22.67 in Figure 5.52, or $\gamma D/s_u$ = 2.33 in Figure 5.53), it can be seen that the first part OA rises sharply since in this stage soil was yielding towards the surface.
- At point A, the soil started to flow back on top of the spudcan. To show the effect of soil backflow on the bearing capacity profile, this portion has been shown in greater detail in Figure 5.54. In the second part AB, the bearing capacity increases very slowly due to the presence of the uppermost conical part of spudcan. Bearing capacity increases again after the embedment of the conical part of spudcan. Consequently, the third part of the curve BC rises sharply again. Eventually, the failure mechanism alters to fully localise at point C. Therefore, the fourth part of the curve CD becomes unchanged with depth. This is associated with the attainment of ultimate bearing capacity. Note, the attainment of these break points (A and C) or the depths of change of failure mechanisms are totally dependent on the corresponding $\gamma D/s_u$ value.
- For the case of Full Backflow, the bearing capacity rises without any break until the failure mechanism becomes localised. This is due to no cavity being present above the spudcan. After that, it reaches a constant ultimate value.
- By comparing the results presented on Figures 5.52 and 5.53, the ultimate bearing capacities are obtained at lower penetration depths in Figure 5.53

where the footing diameter is lower (half). No empirical relation has been found between the depth of deep failure and $\gamma D/s_u$. However, it can be seen that this depth decreases with the footing diameter regardless of γ and s_u.

- The rough interface caused about 10-15% higher results than the ones for smooth interface. This is associated with the high frictional resistance equivalent to between soil-soil rather than spudcan-soil.

From the above results from Fully Open Cavity, Cavity with Partial Backflow and Full Backflow analyses, it can clearly be seen that N_c values of Fully Open Cavity cases are lower than that of Cavity with Partial Backflow cases as no soil was considered above the exposed top of spudcan. The results in Cavity with Partial Backflow cases are slightly lower than that in Full Backflow cases, due to the presence of open cavity (i.e. no soil).

The above mentioned results are from small strain analyses. In this range of soil strengths, the realistic case is Cavity with Partial Backflow which was approved by continuous penetration analyses and also by centrifuge tests (Figures 5.32-5.34 and Figures 5.41-5.42). The bearing capacity factors of spudcan with Partial Backflow, for diameter 6 m and 12 m, are presented together in Figure 5.55 in order investigate the effect of footing diameter. At deep penetration ($d/D > 1.5$), when the soil flow became fully localised, an excellent agreement was obtained with identical numbers, N_c = 10.7 (smooth) to 12.2 (rough). Which indicates the absence of $\gamma D/s_u$ effect on the ultimate N_c value.

Figure 5.56 presents a typical comparison of bearing capacity profile from large and small deformation analysis. For similar $\gamma D/s_u$, a fairly agreeable result obtained from large deformation analysis. Interestingly the above mentioned break points (A and B) due to soil back flow can also clearly be detected.

Table 5.5 presents the ultimate bearing capacity factors from the above mentioned centrifuge tests and small strain analyses. It also includes the results from large deformation analyses of this study and the ones for flat-plate presented elsewhere in uniform clay. In this study, interestingly, closely agreeing values can be found

considering large deformation and small deformation FE analyses for smooth spudcan and centrifuge tests. This is because the spudcan used in the centrifuge tests was sufficiently smooth.

The result for smooth plate of Wang and Carter (2002), from large deformation FE analysis, is about 8% lower than the one of Martin and Randolph (2001), from exact solution. This may be associated with the thin plate in exact solution rather than bulkier/thick plate in FE analysis. By comparing with the results of plate (both from FE and exact solution), the limit N_c values of spudcan are lower for both smooth and rough interface. This is associated with the underside geometry of footing being conical rather than flat.

5.8 Normally Consolidated Clay

5.8.1 Background

Although the focus of this report is on spudcan behaviour in over consolidated (OC) clays, there was one group of tests performed in normally consolidated (NC) soil. To prepare NC clay sample, clay slurry was spread into the drum channel and consolidated in flight by spinning the drum centrifuge. A constant pore pressure profile was taken as the completion of consolidation. Details about the sample preparation can be found in House *et al.* (2001). The sample was approximately 155 mm deep all through the drum channel. Probe tests were performed without stopping the channel after consolidation. Full-spudcan, of 30 mm diameter, penetration tests were performed at a constant velocity of 0.2 mm/sec. Then T-bar tests were conducted at a velocity of 1 mm/sec. In offshore practice, jack-up preloading on soft clays frequently leads to spudcan penetrations up to 2-3 diameters (Endley *et al.*, 1981), thus the penetration of spudcan in centrifuge tests covered a similar range. The top view of soil flow images were captured continuously using a mini video camera.

5.8.2 Soil Strength

A set of T-bar test results is shown in Figure 5.57. They show a consistent strength profile that can be idealised excellently as linearly increasing with a strength gradient of 1.0 kPa/m. This is a typical strength profile for this type (NC) of clay.

5.8.3 Soil Flow

Figure 5.58 displays the top view of soil flow mechanisms from the centrifuge tests. Since the clay was deposited all through the drum channel, it was not possible to capture the soil failure mechanisms (side view) with the penetration depth, such as the test with OC clay in the strongbox. However, From Figure 5.58 it can be seen that: (i) Figure 5.58(a) shows the spudcan foundation shoulder touching the soil surface. The soil deformation zone, 1.67 D, indicates the zone of soil heaving up around the spudcan shoulder; (ii) Figure 5.58(b) shows the partially embedded spudcan as the exposed spudcan is less than its full diameter, which displays the back flow of surface soil as the spudcan penetrates deeper; (iii) Figure 5.58(c) shows only the spudcan shaft with spudcan fully embedded in soil. The remaining lateral distortion zone is about 1.67D as created initially.

In this research, numerical analysis has not been performed with NC clay. However, the soil flow mechanisms from Hossain *et al.* (2004) are depicted in Figure 5.59 to compare with the centrifuge observation. Figure 5.59 shows soil displacement vectors from large deformation FE analysis considering smooth soil-spudcan interface. Unlike centrifuge results, it displays the side view and therefore the change of soil failure mechanisms can be detected clearly at various penetration depths. Comparing with the images from the centrifuge in Figure 5.58, they correspond well at all stages of penetration. Figure 5.59(c) shows that, after penetration d/D = 0.75, the failure mechanism becomes a fully localised deep failure mechanism. The lateral distortion is confined within a range of 1.6D, which agrees well with the centrifuge observation (1.67D).

5.8.4 Bearing Capacity

The non-dimensional bearing capacity factor, N_c is calculated using Equation 5.3. Figure 5.60 summarises the results of bearing capacity factor of spudcan with penetration depth from both centrifuge test and FE analysis. The FE results are from Hossain *et al.* (2004). The initial scattered values of N_c number are due to the low strength of surface soil. The N_c number starts to be stable after d/D = 0.5, and attains an ultimate value of N_c = 10.5 when penetration ratio (d/D) reaches 0.75. This is associated with the soil failure mechanism corresponding to deep (local) failure mechanism at this penetration depth (as discussed above).

From the FE results for smooth and rough soil-spudcan interface, the N_c number of 10.1 for smooth spudcan has shown a constant value up to d/D = 3. However, the rough spudcan result becomes higher after d/D = 1.5 and consequently shows a 10% increase in N_c number (N_c = 11.1) when penetration gets deeper. The reason for this higher value (at deep embedment) could be that a higher frictional resistance occurs for the rough interface. Nonetheless, this effect of spudcan underside interface roughness is not so profound here as in uniform (stiff) clay, which might be due to the soft surface clay being trapped underneath the spudcan during penetration.

In the centrifuge test, the ultimate value of N_c = 10.5 lies right between the smooth and rough results from FE analyses considering smooth and rough interface. The trend of the N_c curve is similar to the smooth spudcan in FE analysis, since the spudcan model used in the centrifuge testing was polished. However, it might not be perfectly smooth, thus a slightly higher N_c number is obtained.

Figure 5.60 also includes the results of Hu *et al.* (2001) of centrifuge penetration and FE analyses with plate-penetrometer in kaolin clay. This is to investigate the effect of spudcan underside geometry. In the centrifuge test, by comparing with the spudcan result, initial discrepancy was attributed to the variation of underside geometry, flat for plate and conical for spudcan. However, a closely agreeing value of N_c = 10.5 can be obtained after d/D > 0.75 from which deep failure mechanisms was achieved. This means that the footing underside geometry does not have a significant effect on its

bearing response at deep penetration into NC clay, when the failure mechanism is totally localised and the footing is fully embedded.

In FE analyses for flat-plate, a constant N_c value of 11.7 can be obtained at deep penetration independent of roughness. By comparing with spudcan results, flat plate has increased the bearing response by 10%. This result has contradicted to the conclusion above from the centrifuge test results where the footing underside effect was not found to be significant. By comparing with the spudcan, the flat underside of the plate has increased the bearing response but reduced the contact surface and thus effect of roughness. Furthermore, the flat underside of the plate has created a soil wedge, which might be equivalent to a rough conical footing response. This is the reason why the N_c = 11.7 of plate is close to the rough spudcan's result.

From the above discussion on bearing capacity (in Sections 5.7 and 5.8.4), it can be concluded that the N_c value for spudcans should be as 10.5 for use in clayey (both OC and NC) marine deposit.

Table 5.1 Summary of test Events

	Test Events						
	E1	**E2**	**E3**	**E4**	**E5**	**E6**	**E7**
Stress history[1]	HOC	HOC	LOC	LOC	HOC	HOC	NC
σ'_{vp} (kPa)	200	200	25	25	150	150	-
Consolidation conducted at	Tank	Tank	Box (layer)	Box (single)	Tank	Tank	Centrifuge
G level	100 & 200	200	100 & 200	100	100 & 200	50,100 & 200	100
Soil sample	1	1	4	2	1	1	1
Test specimen (T)	6	6	4	2	6	6	-
Water presence	×	×	×	×	×	×, √	×
Comments on capturing soil failure mechanisms	Unsuccessful	Unsuccessful	Unsuccessful	Unsuccessful	Satisfactory	Successful	Successful (plan view)

[1]Stress history: HOC – heavily overconsolidated, LOC – lightly overconsolidated, NC – normally consolidated

Table 5.2 Clay strength reduction with in-flight elapsed time in presence of free water

Specimen	G-Level	Elapsed time	Strength reduction at $z/D^1 = 1.0$ (in compare to 1 g strength in absence of free water)
I	50 g	Right after reaching at 50 g	13.5%
I	100 g	1 hour and 40 minutes [1 hour at 50 g and 40 minutes at 100 g]	44%
II	50 g	1 hour and 40 minutes	44%
III	100 g	1 hour and 40 minutes	44%

D^1 – full-spudcan diameter

Table 5.3 Depth of soil back flow from centrifuge tests

	Depth of back flow					
	G-level	D (m)	γ (kN/m^3)	s_u (kPa)	H (m)	H / D
Without water on top	200	12	17	18	3.2	0.27
	100	6	17	13	1.9	0.32
	50	3	17	17.4	1.6	0.53
With water on top	100	6	7	12	2.9	0.48
	50	3	7	15.6	2.15	0.72

Table 5.4 Stability numbers for flow and wall failure

		Flow failure				Wall failure			
			H_F	H_F/D	N_s		H_W	H_W/D	N_s
Without water on top	Case I	FE	1.86	0.31	2.43	FE	4.51	0.75	5.90
		Centrifuge	1.90	0.32	2.48	M	4.51	0.75	5.28
	Case II	FE	2.22	0.37	2.29	FE	6.07	1.01	6.25
		Centrifuge	*	*	*	M	6.07	1.01	5.59
	Case III	FE	3.24	0.27	3.06	FE	5.70	0.47	5.38
		Centrifuge	3.20	0.27	3.00	M	5.70	0.47	4.88
	Case IV	FE	3.40	0.28	2.89	FE	6.47	0.54	5.50
		Centrifuge	*	*	*	M	6.47	0.54	5.00
With water on top	Case V	FE	2.85	0.48	1.66	FE	12.17	2.03	7.10
		Centrifuge	2.90	0.49	1.69	M	12.17	2.03	6.36
	Case VI	FE	5.20	0.43	2.02	FE	17.23	1.44	6.70
		Centrifuge	*	*	*	M	17.23	1.44	5.98

* No centrifuge test data

M – Analytical solutions from Meyerhof (M)

Table 5.4 Ultimate bearing capacity factor, N_c

Authors	Geometry	Interface	Ultimate N_c	Notes
Martin and Randolph (2001)	Plate	Smooth	12.42	Exact solution
Martin and Randolph (2001)	Plate	Rough	13.31	Exact solution
Wang and Carter (2002)	Plate	Smooth	11.5	FE (large deformation)
This study	Spudcan	Close to smooth	10.5	Centrifuge tests
This study	Spudcan	Smooth	10.7	FE (small deformation)
This study	Spudcan	Smooth	10.8	FE (large deformation)
This study	Spudcan	Rough	12.2	FE (small deformation)

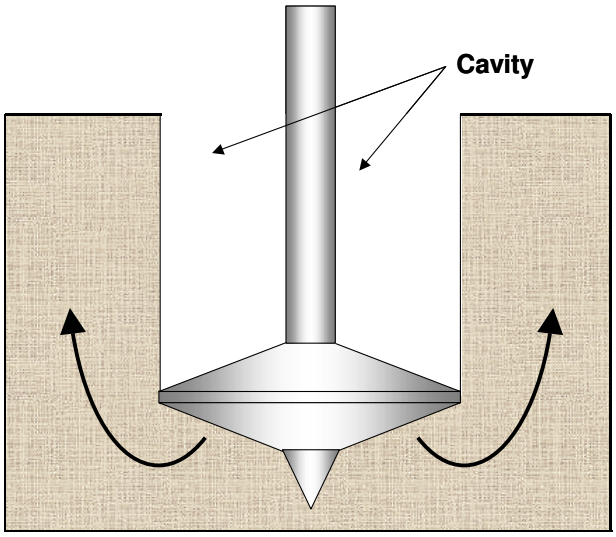

(a) Fully Open Cavity

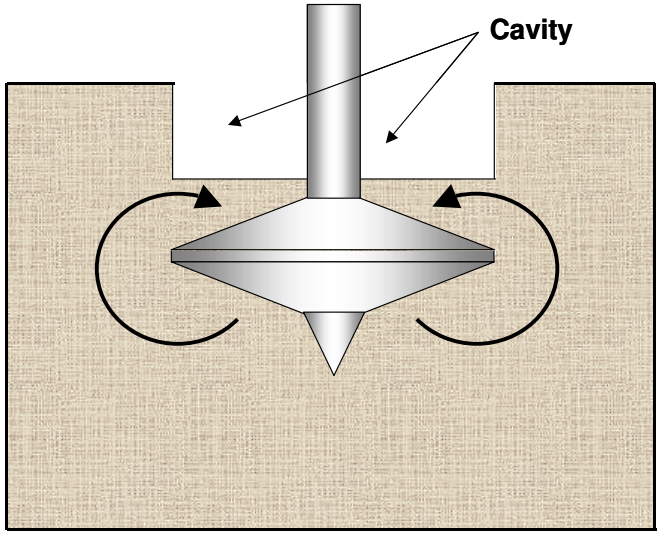

(b) Cavity with Partial Backflow

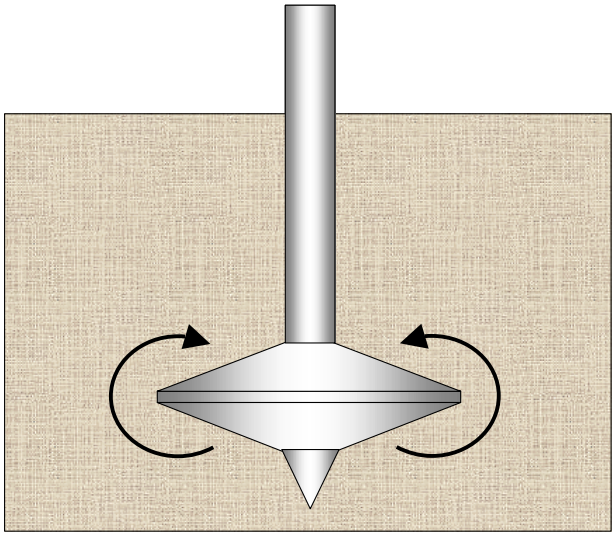

(c) Full Backflow

Figure 5.1 Three types of cavity condition in small strain FE analyses

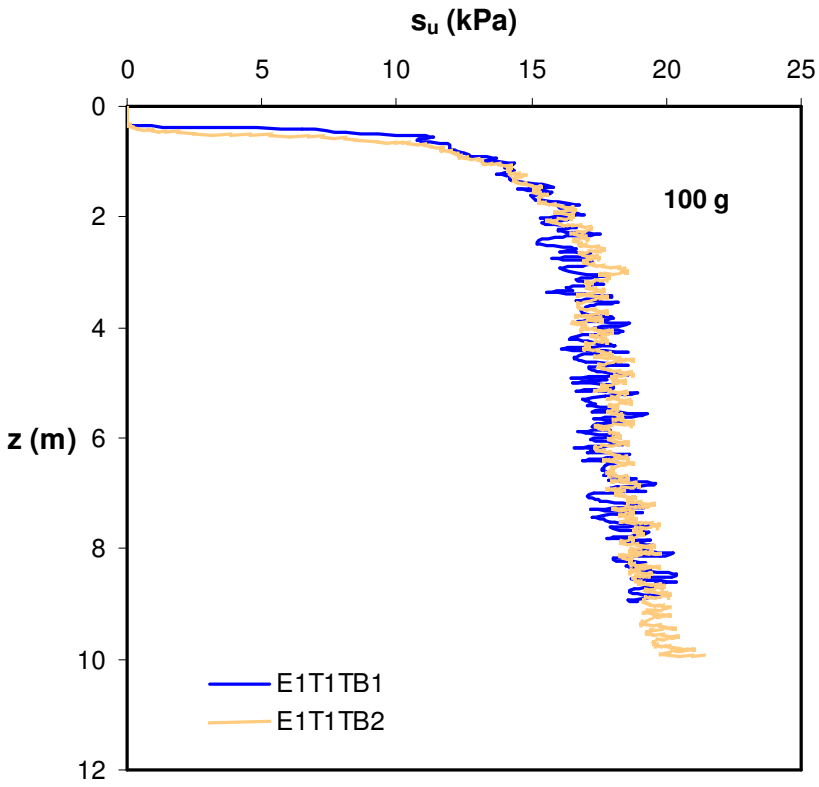

(a) Tests 1

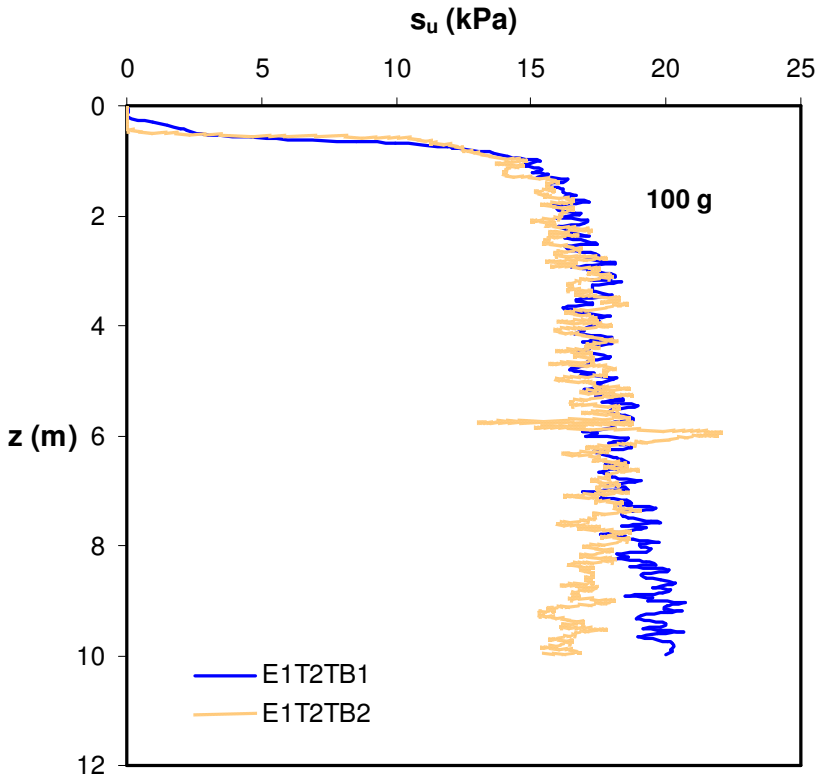

(b) Test 2

Figure 5.2 Soil strength profile in Event-1 100 g Tests

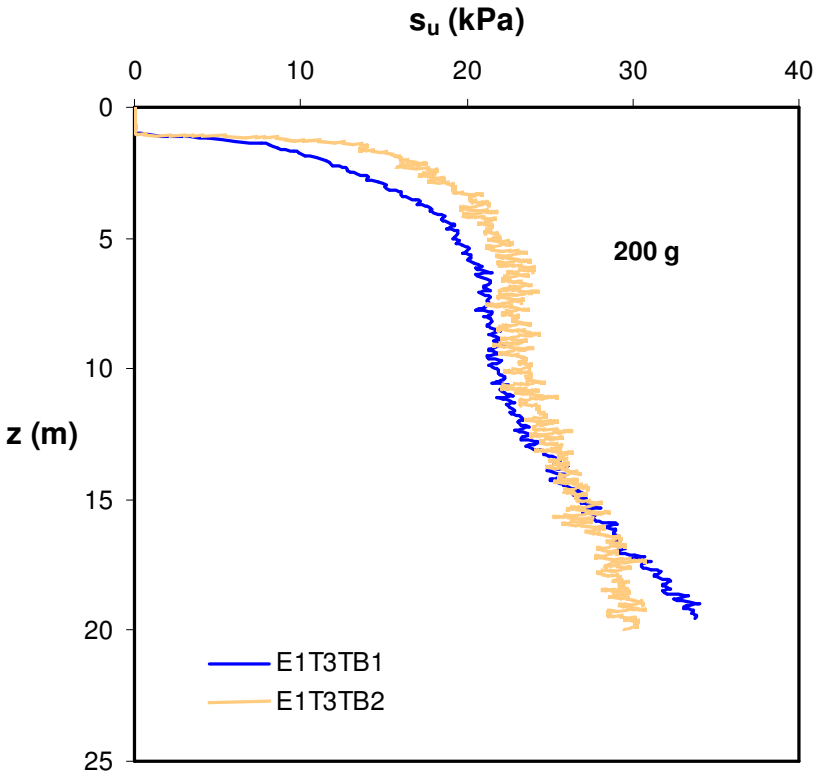

(a) Test 3

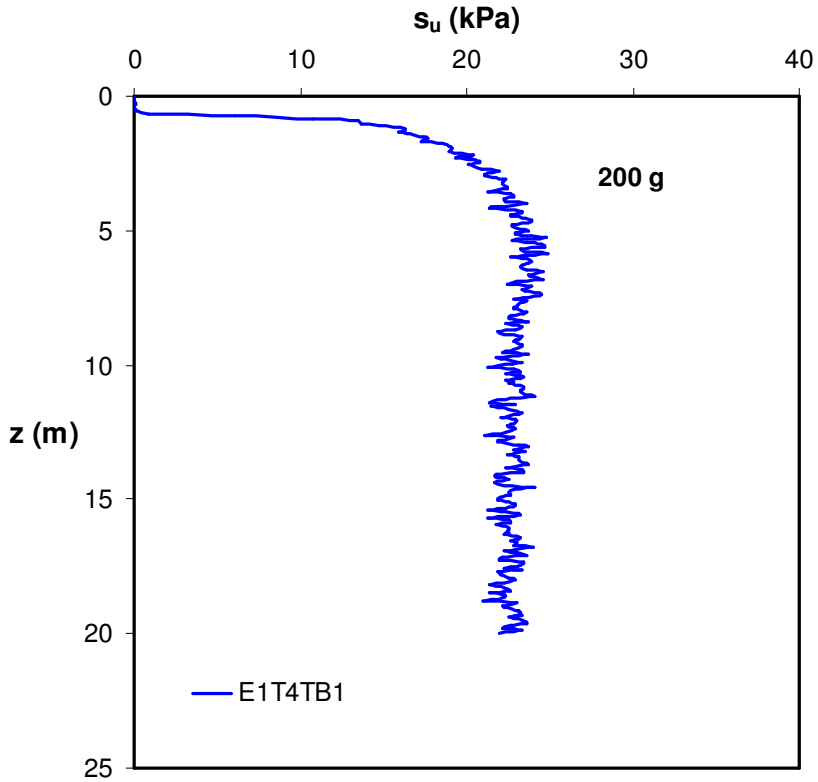

(b) Test 4

Figure 5.3 Soil strength profile in Event-1 200 g Tests

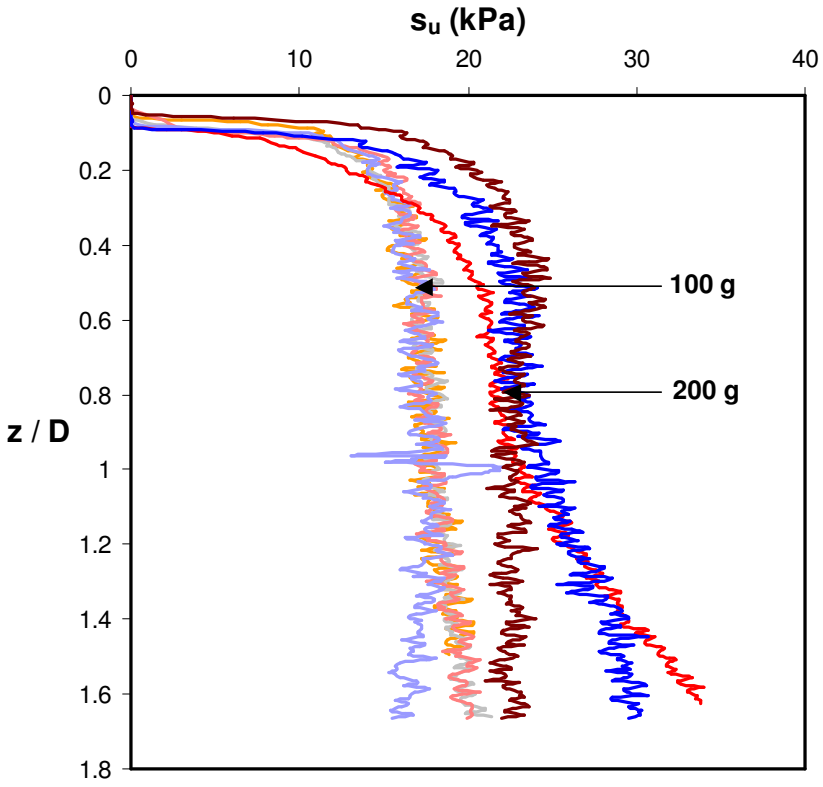

Figure 5.4 Soil strength profile in Event-1 Tests

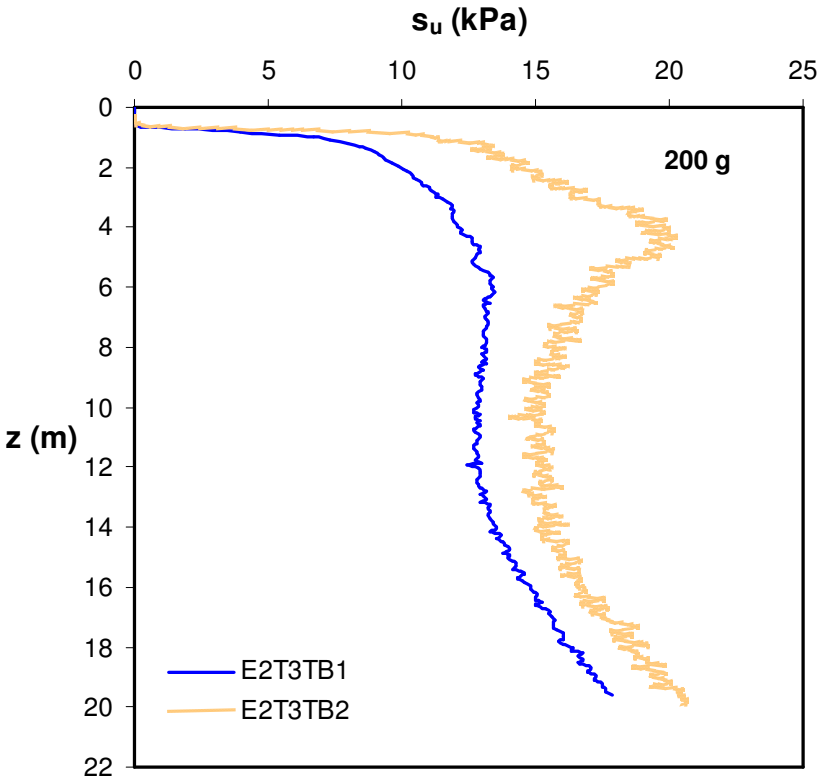

Figure 5.5 Soil strength profile in Event-2 Tests (200 g)

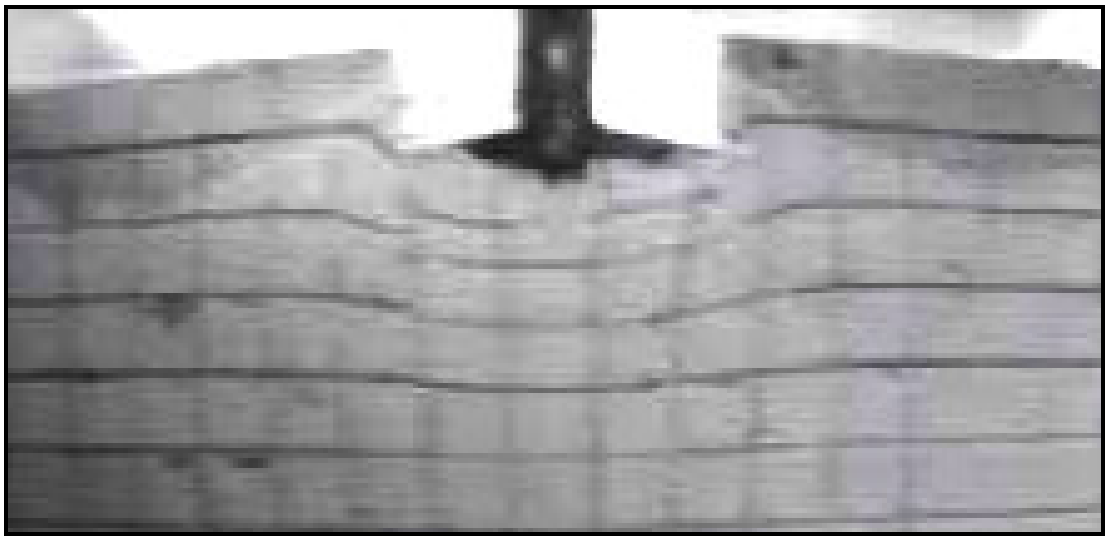

(a) d / D = 0.30

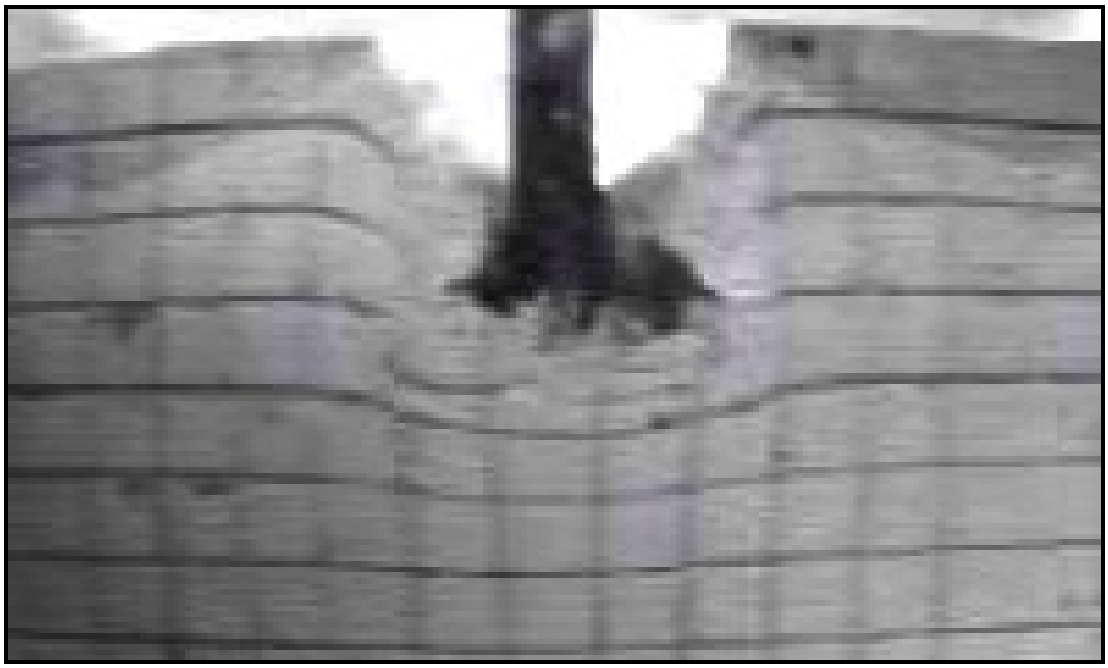

(b) d / D = 0.87

(c) d / D = 1.17

Figure 5.6 Soil failure mechanisms during spudcan penetration at 100 g (E1)

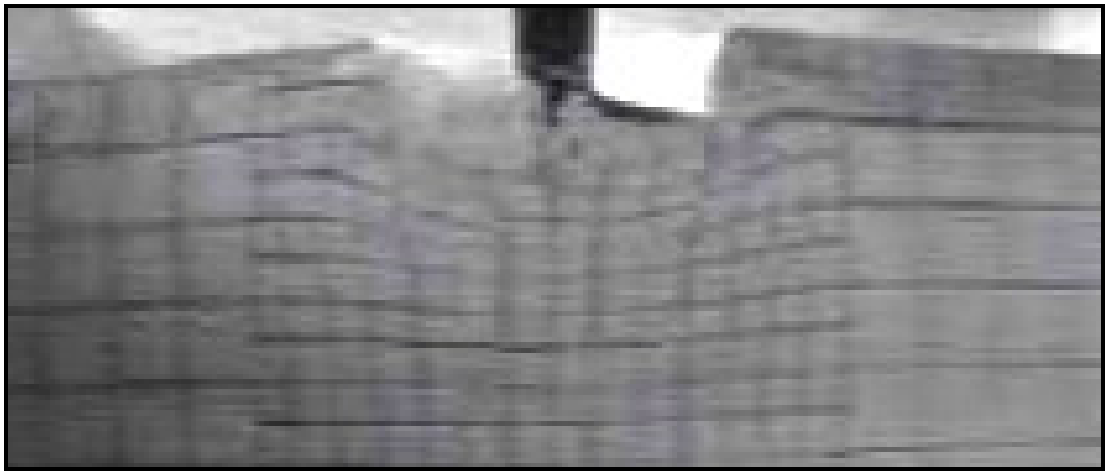

(a) d / D = 0.3

(b) d / D = 0.38

(c) d / D = 1.17

Figure 5.7 Soil failure mechanisms during spudcan penetration at 200g (E1)

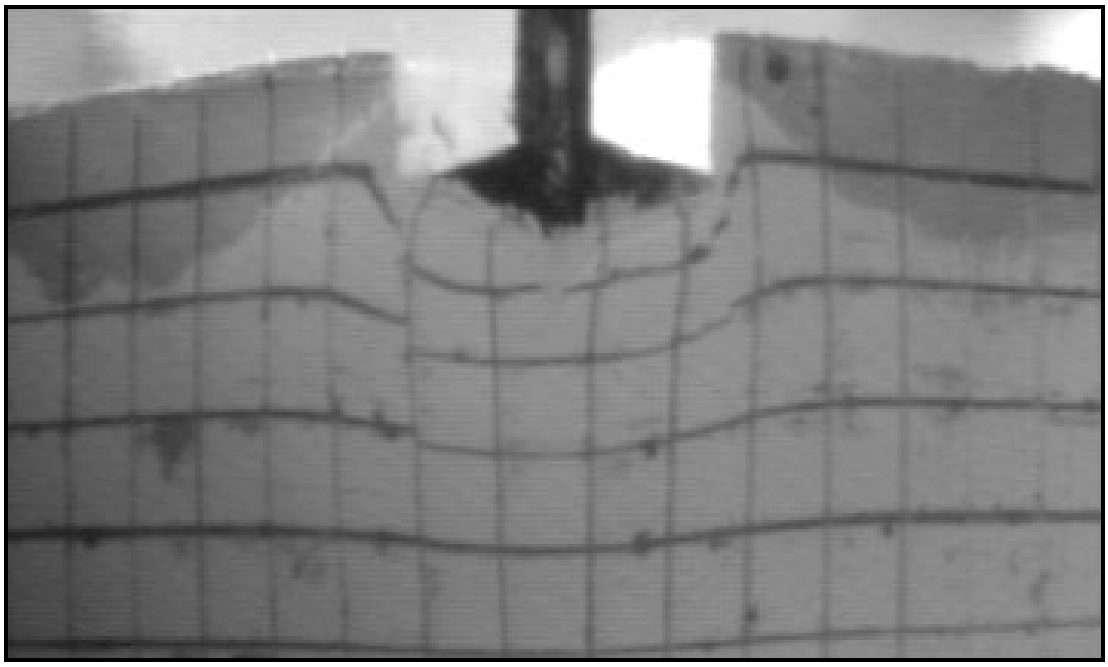

(a) d / D = 0.30

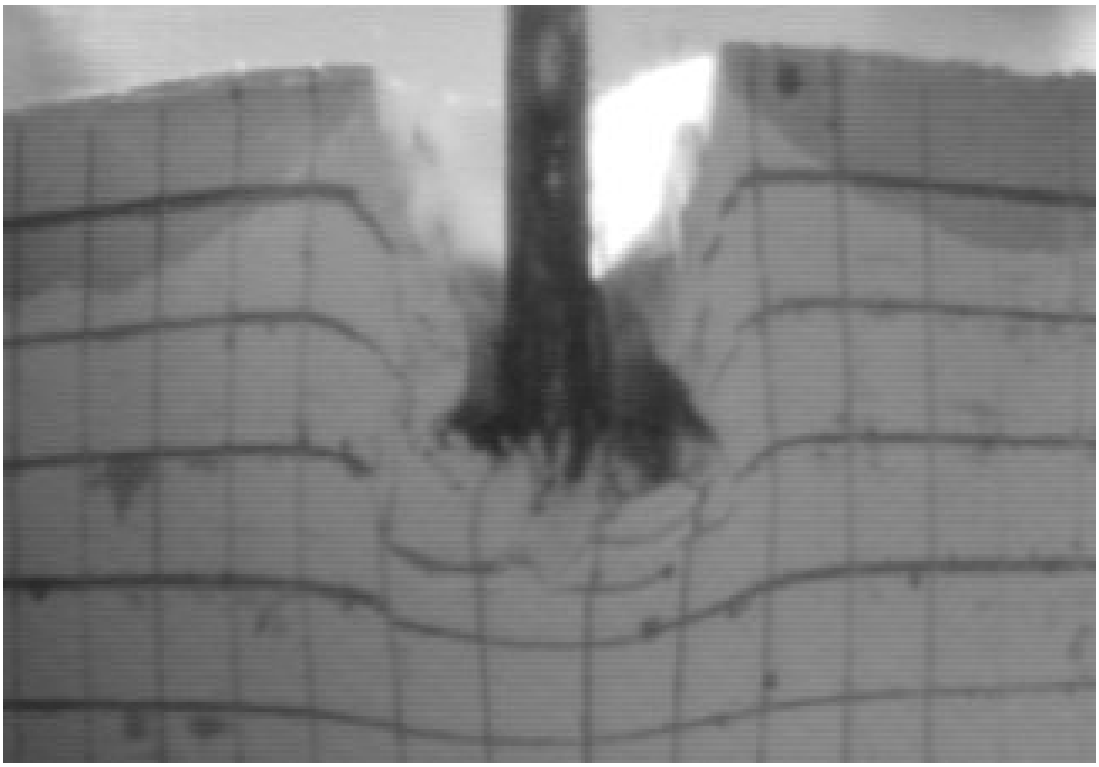

(b) d / D = 0.87

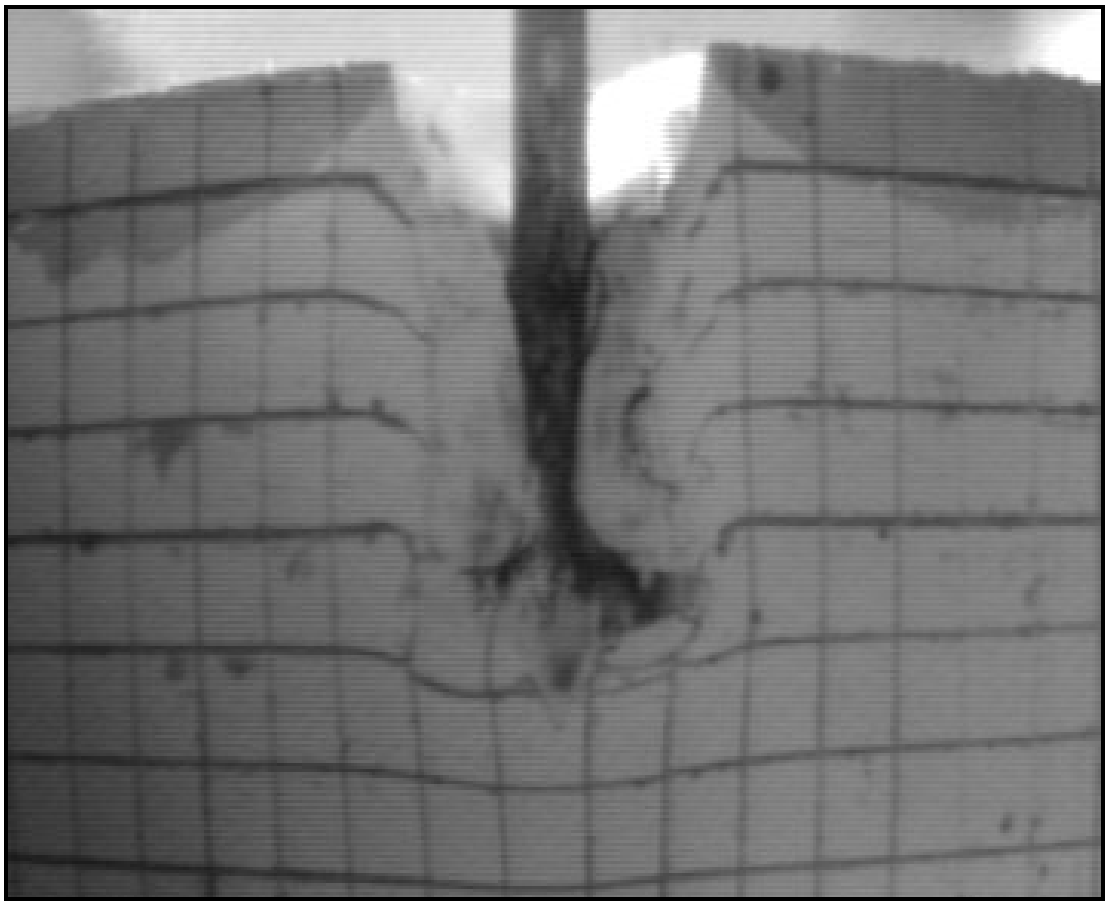

(c) d / D = 1.17

Figure 5.8 Soil failure mechanisms during spudcan penetration at 100 g, digitised by PC frame grabber (E1)

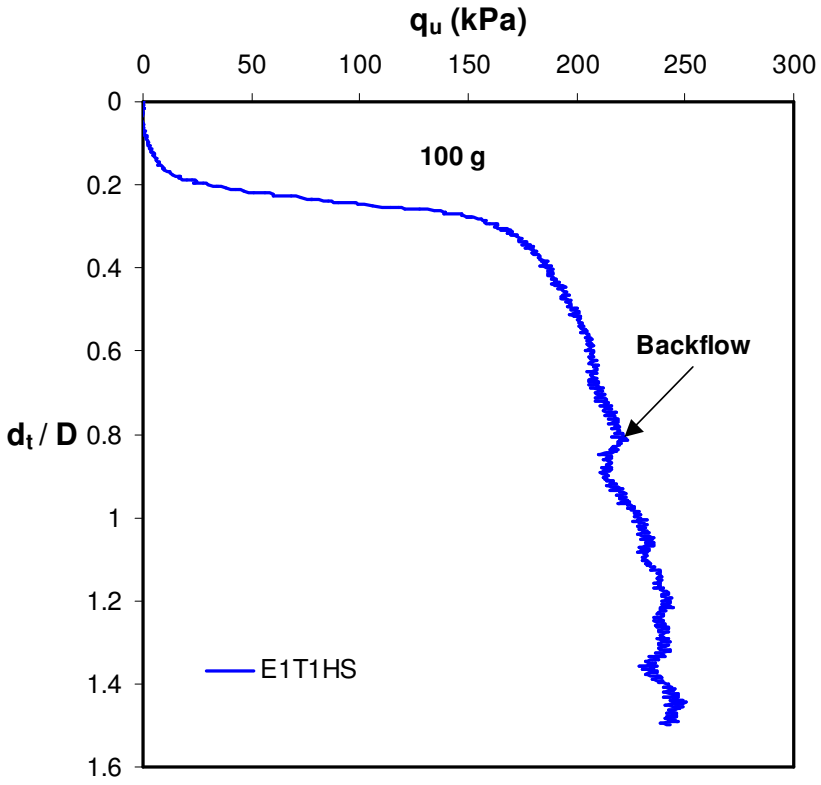

(a) spudcan

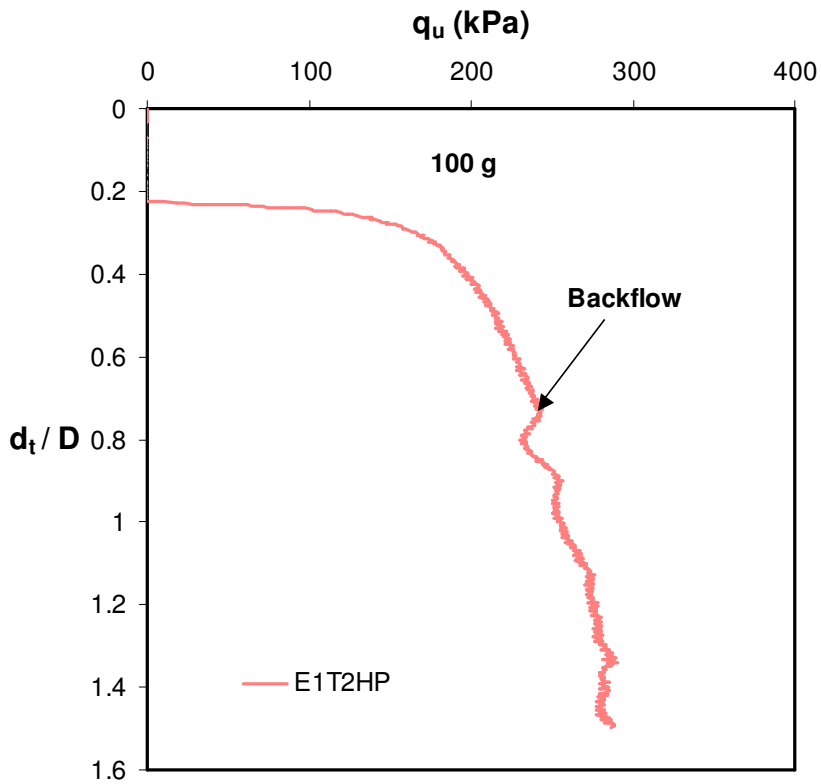

(b) flat plate

Figure 5.9 Load-penetration response in Event-1 Tests (100 g)

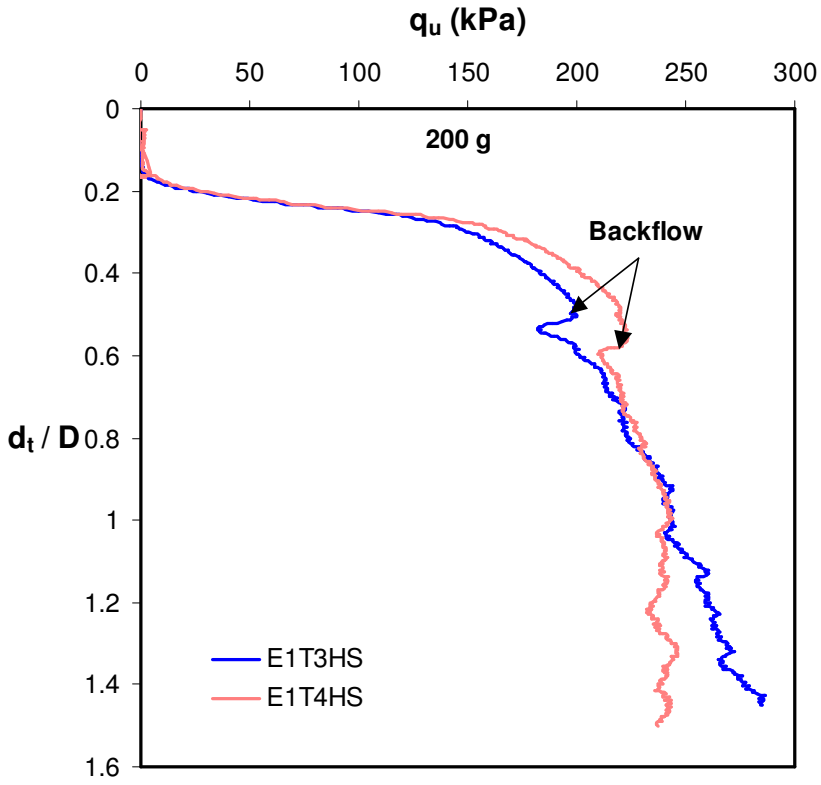

Figure 5.10 Load-penetration response in Event-1 Tests (200 g)

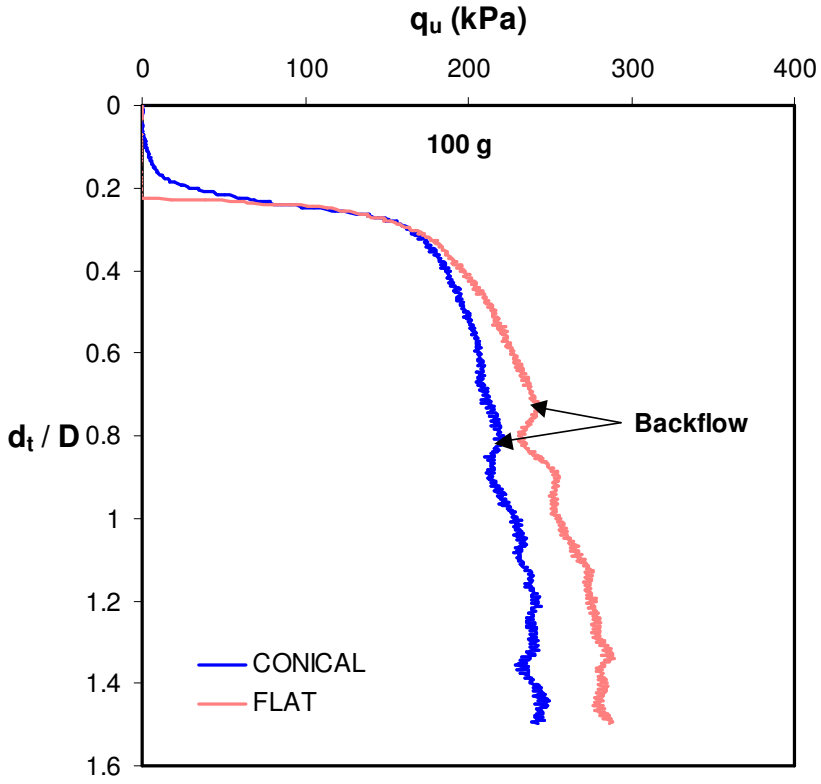

Figure 5.11 Effect of spudcan geometry on load-penetration response (E1)

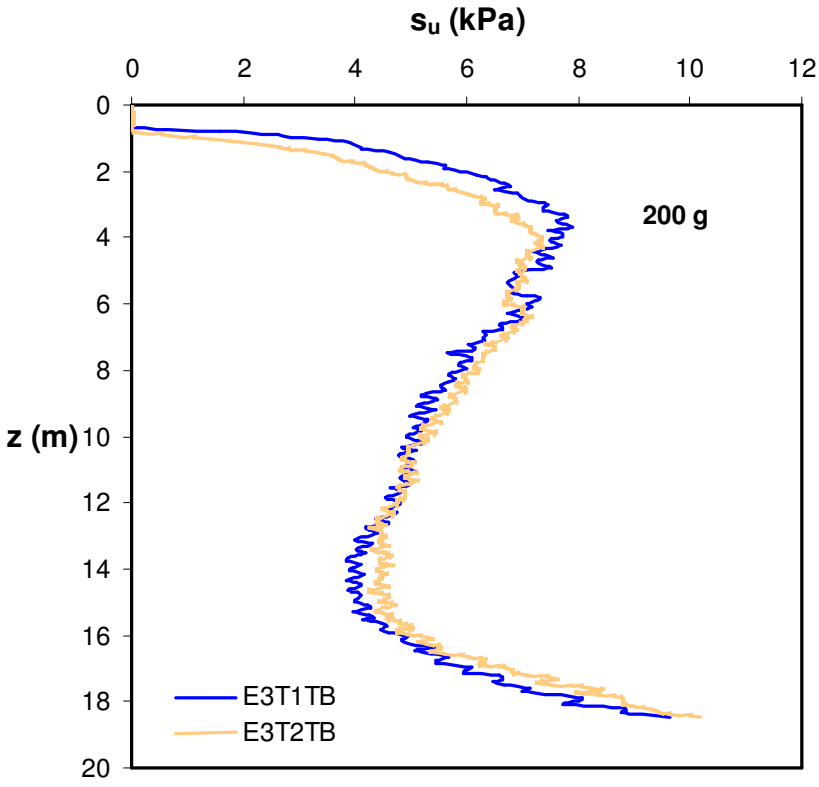

(a) Test 1 and Test 2

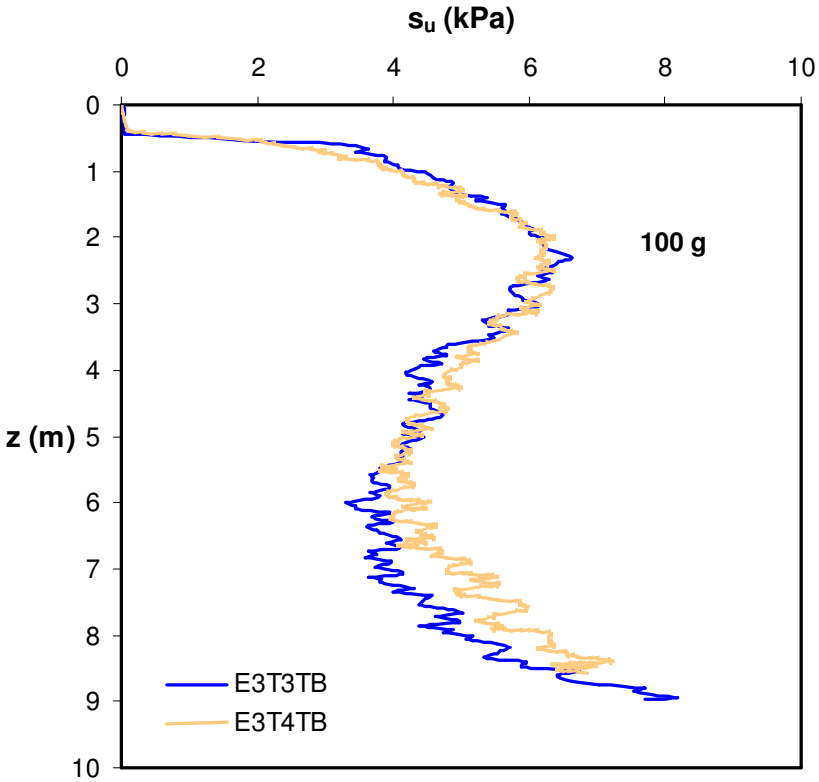

(b) Test 3 and Test 4

Figure 5.12 Soil strength profile in Event-3 Tests

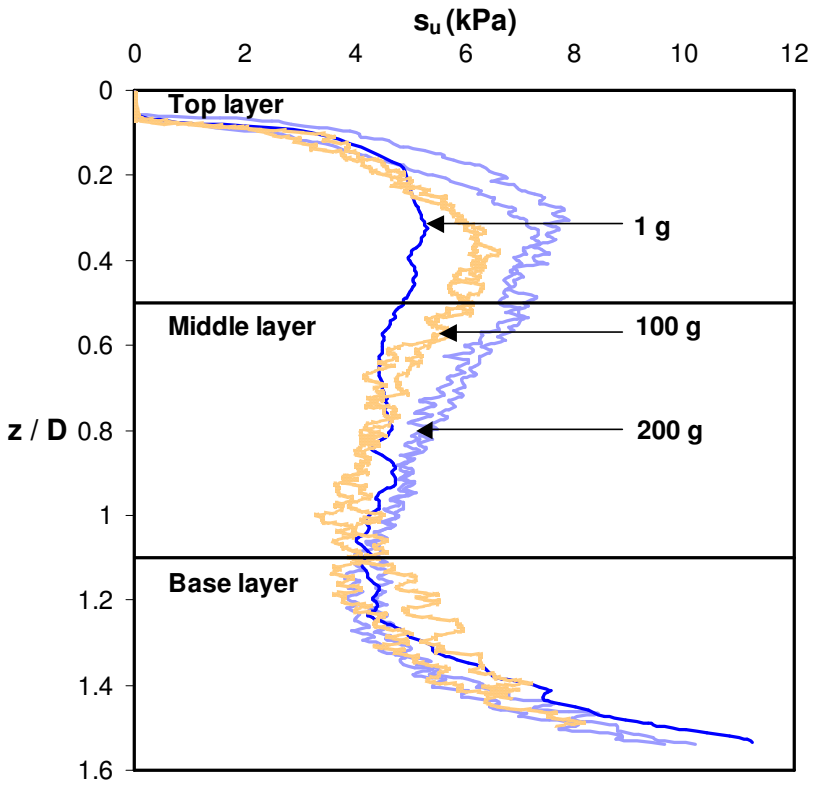

Figure 5.13 Effect of layering and gravity on measured strength and its profile (E3)

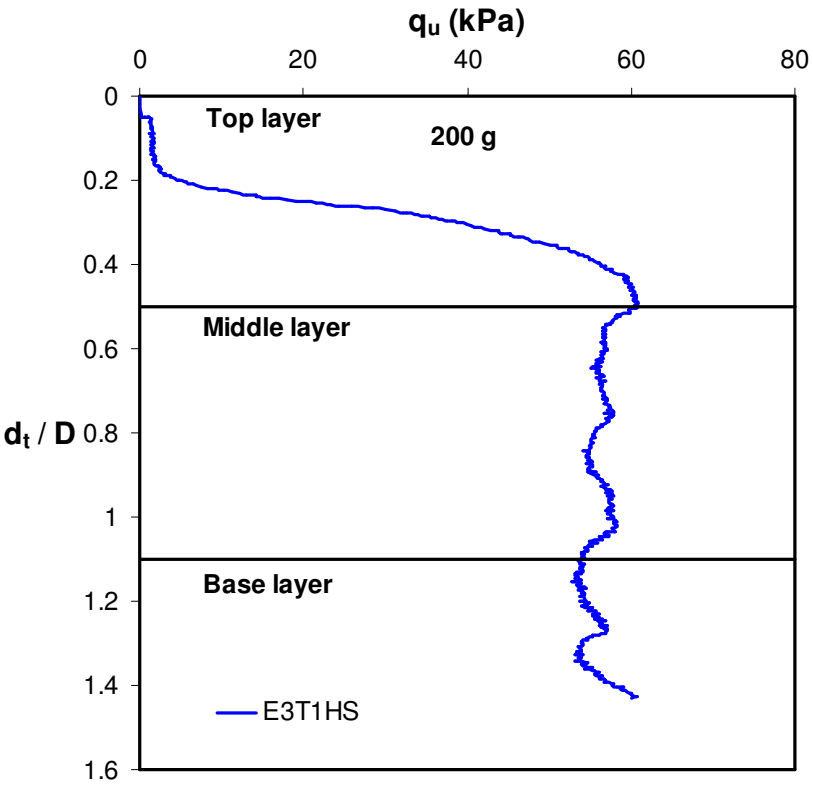

Figure 5.14 Load-penetration response in Event-3 Tests (200 g)

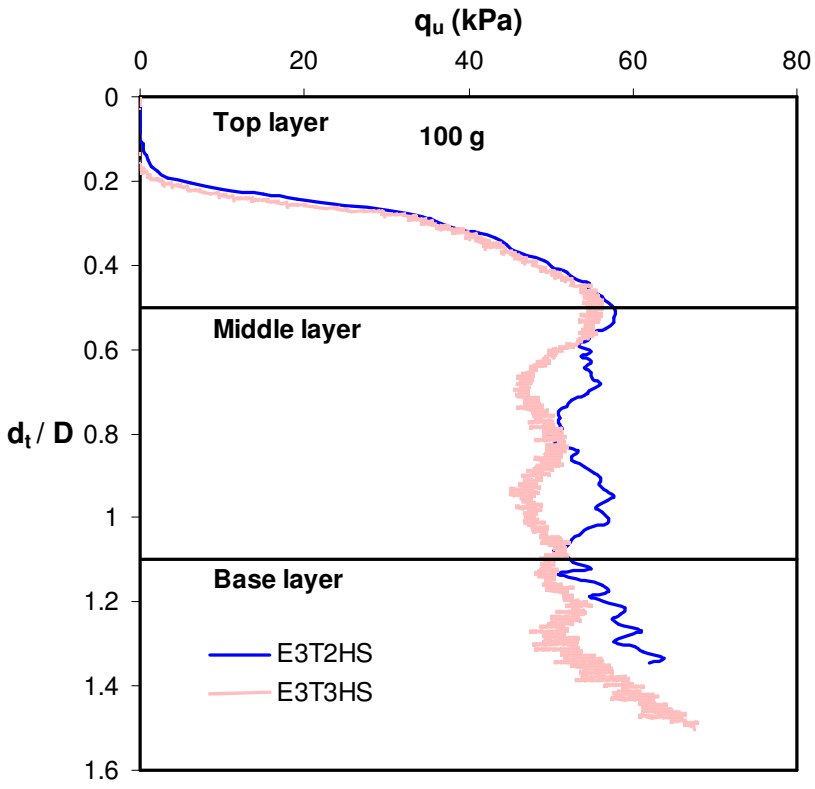

Figure 5.15 Load-penetration response in Event-3 Tests (100 g)

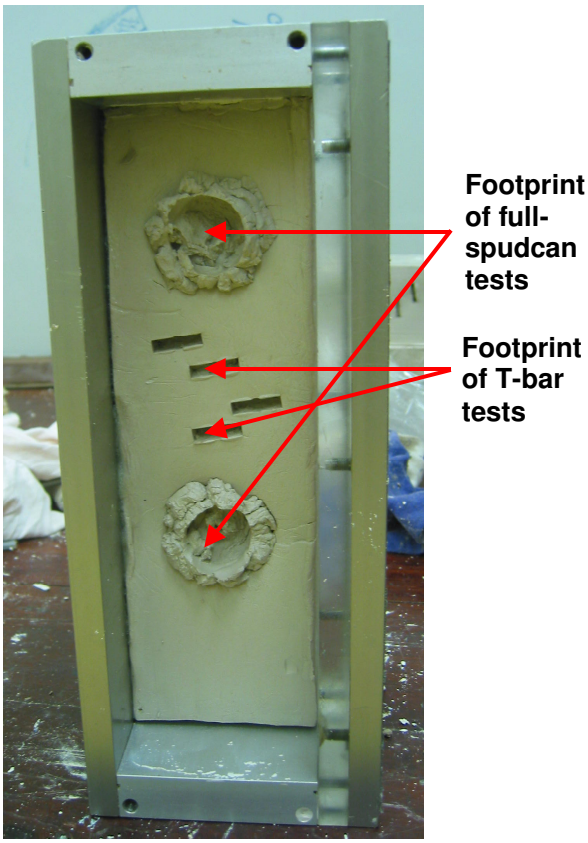

Figure 5.16 Typical position of probe tests on a soil specimen

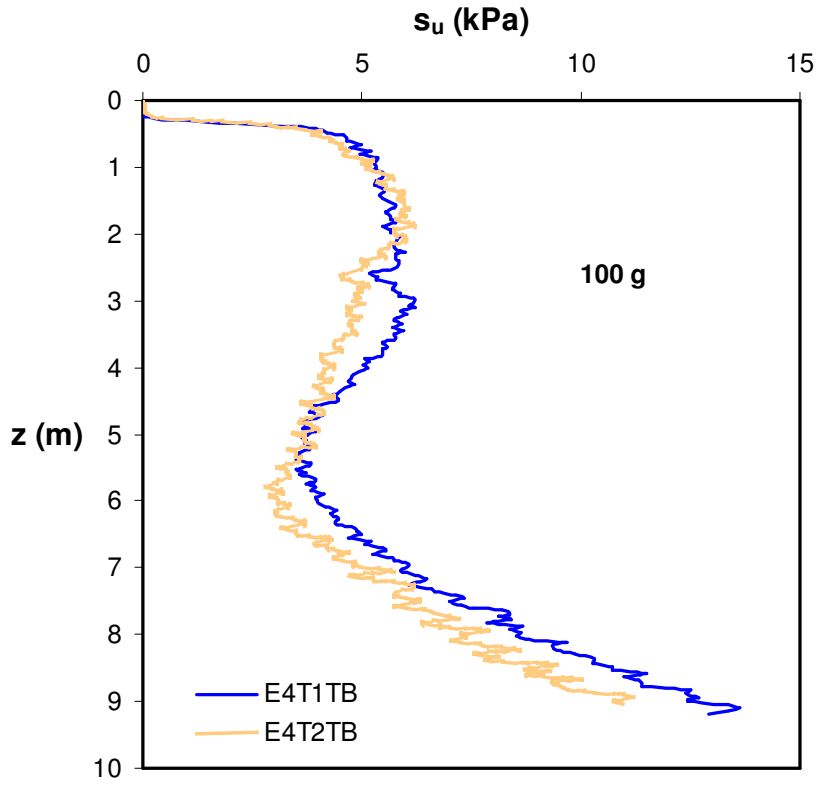

Figure 5.17 Soil strength profile in Event-4 Tests (100 g)

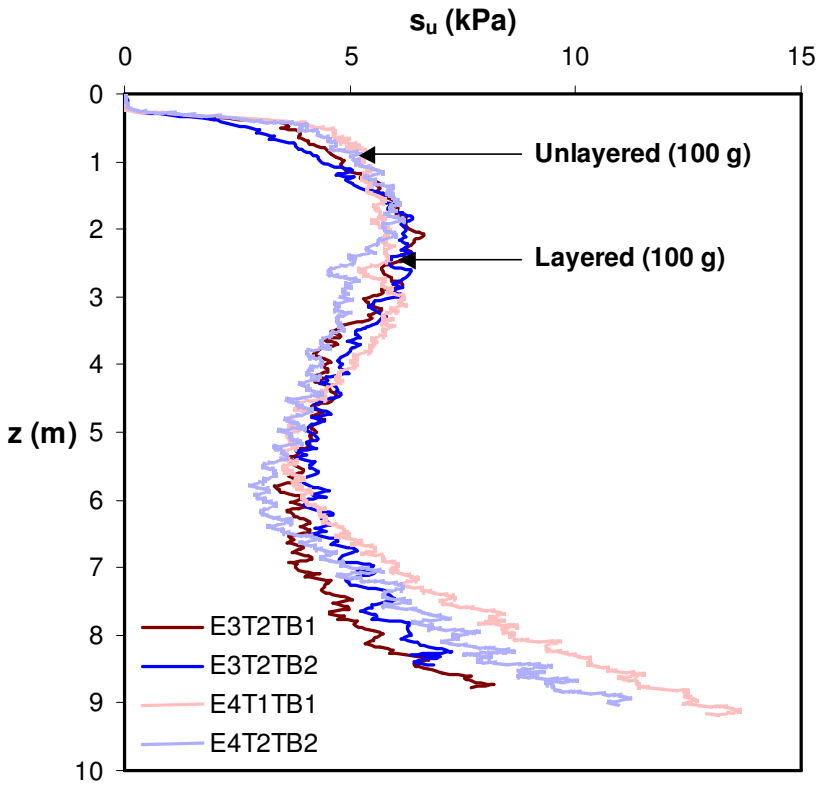

Figure 5.18 Soil strength profile of layered (Event 3) and un-layered (Event 4) soft clay (100 g)

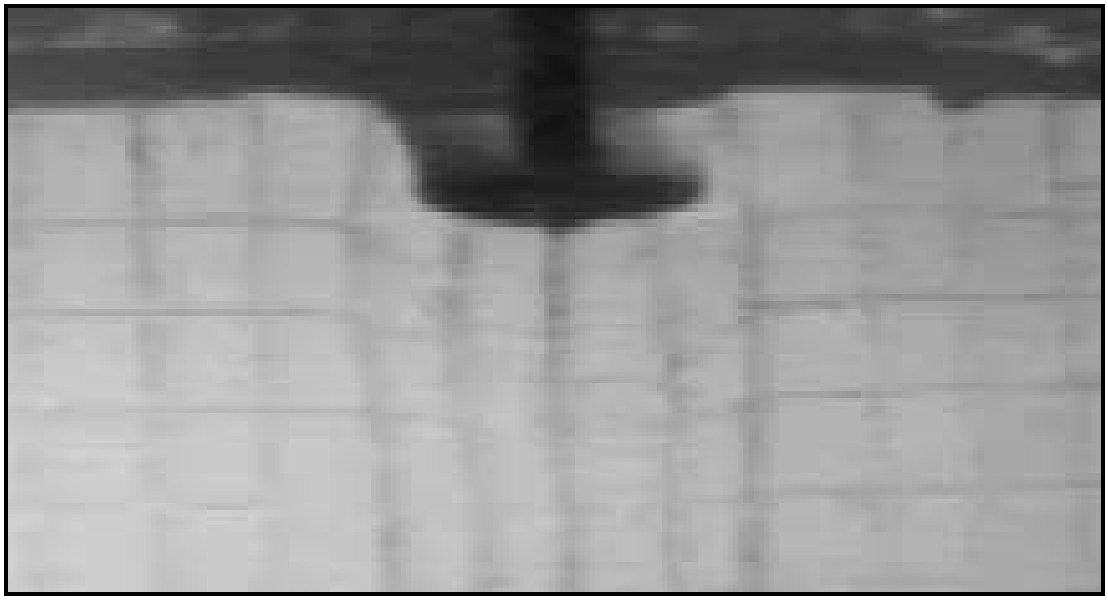

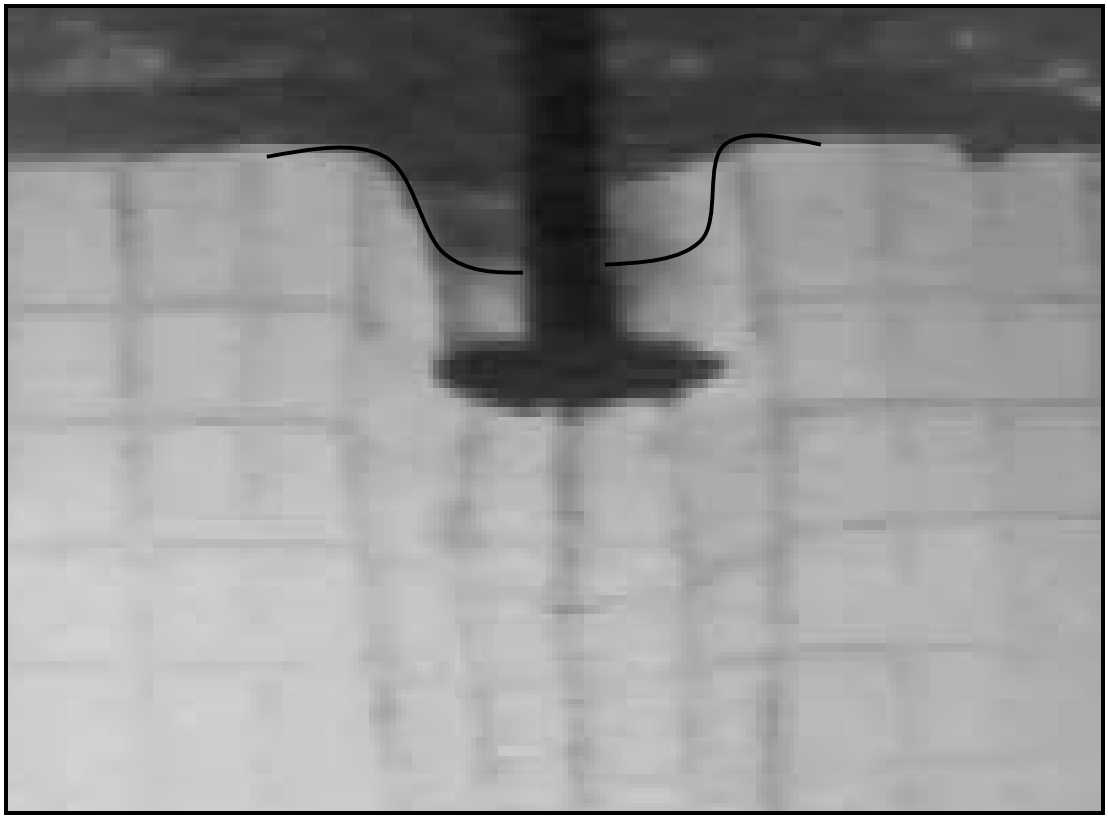

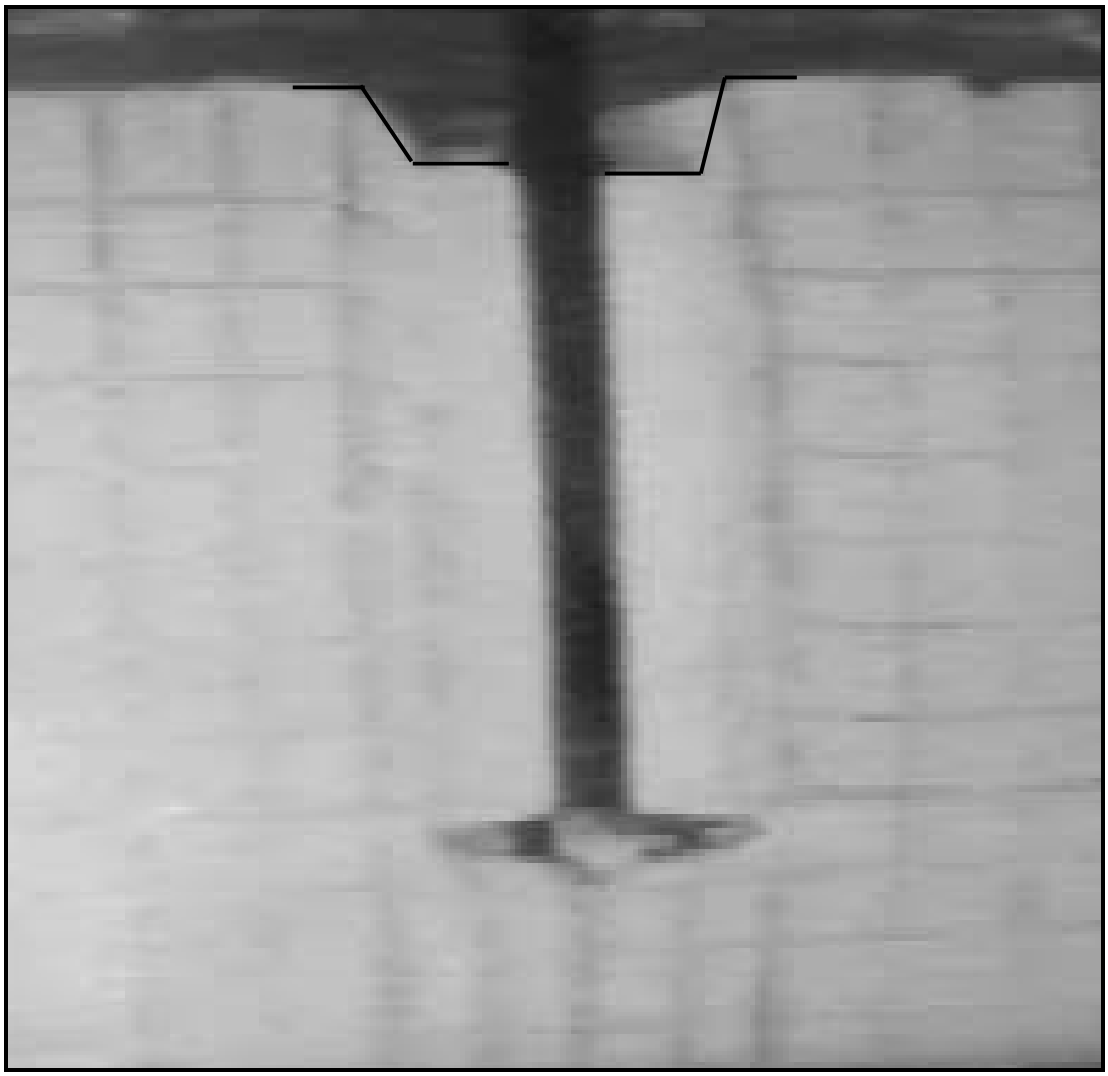

Figure 5.19 Soil failure mechanisms during spudcan (D = 30 mm) installation at 100g (E4)

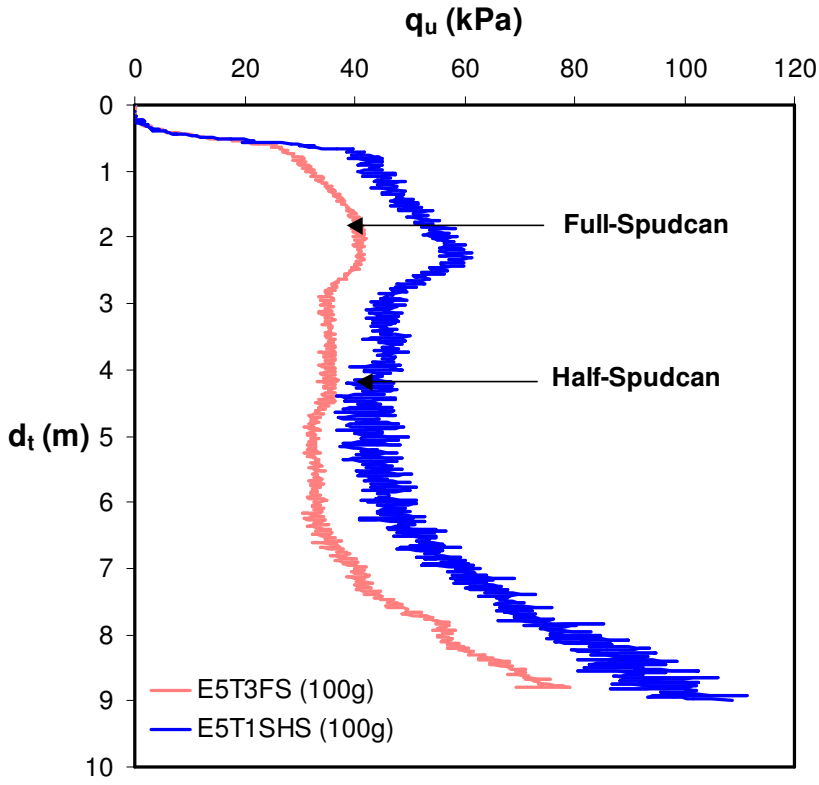

Figure 5.20 Load penetration response from half-spudcan and full-spudcan tests in Event 4

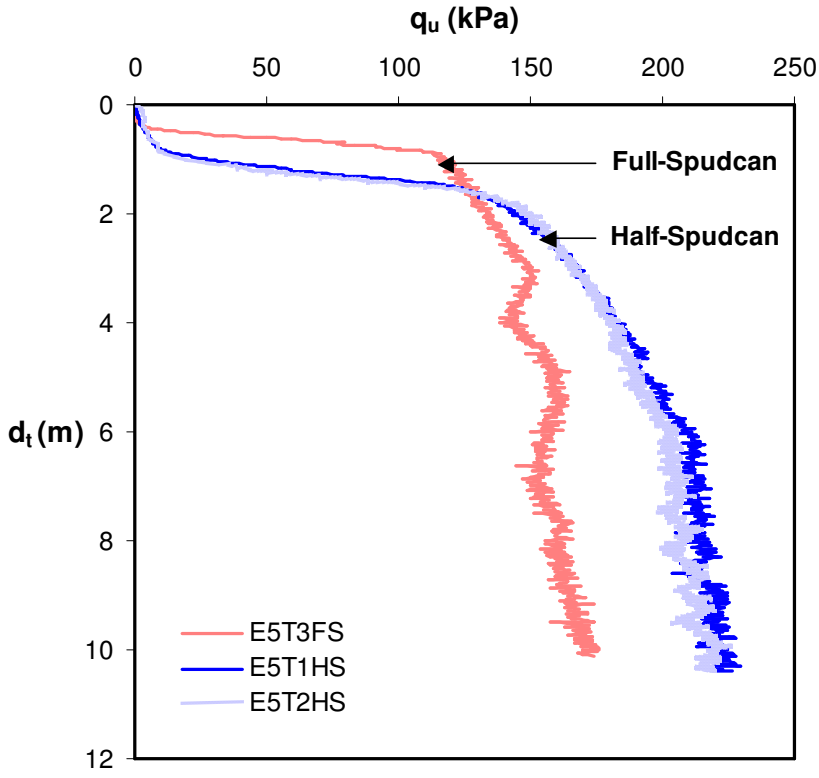

Figure 5.21 Load-penetration response from half-spudcan and full-spudcan tests in Event 5 (100g)

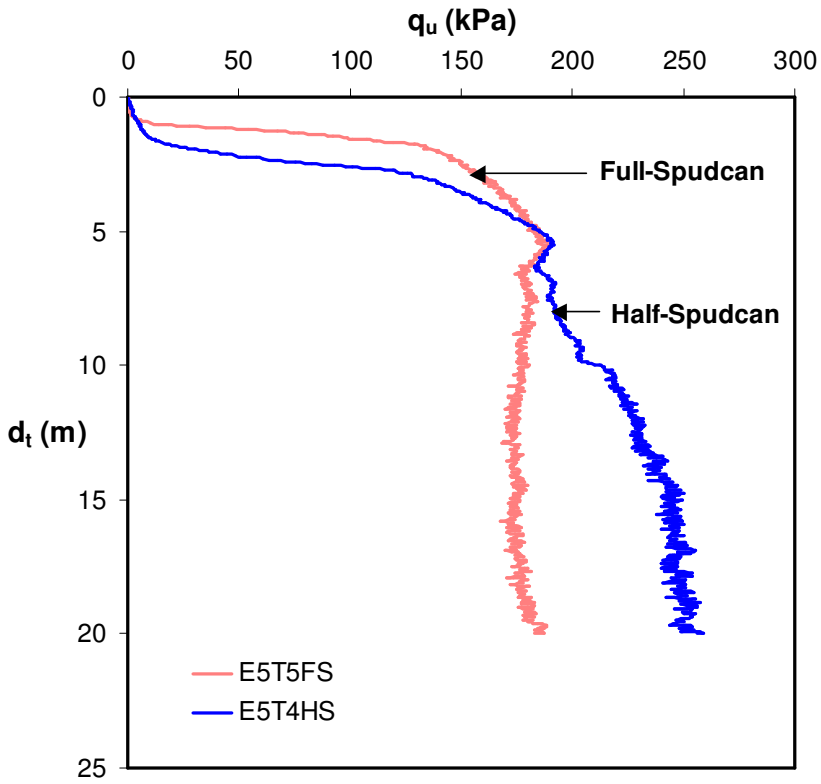

Figure 5.22 Load-penetration response from half-spudcan and full-spudcan tests in Event 5 (200 g)

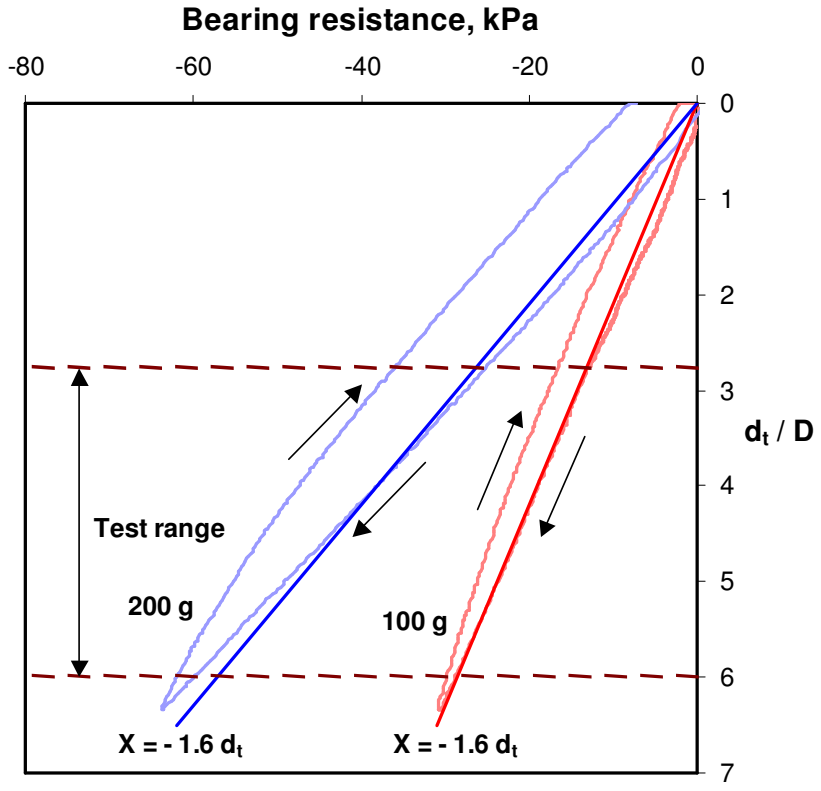

Figure 5.23 Load-penetration response during full-spudcan installation in air

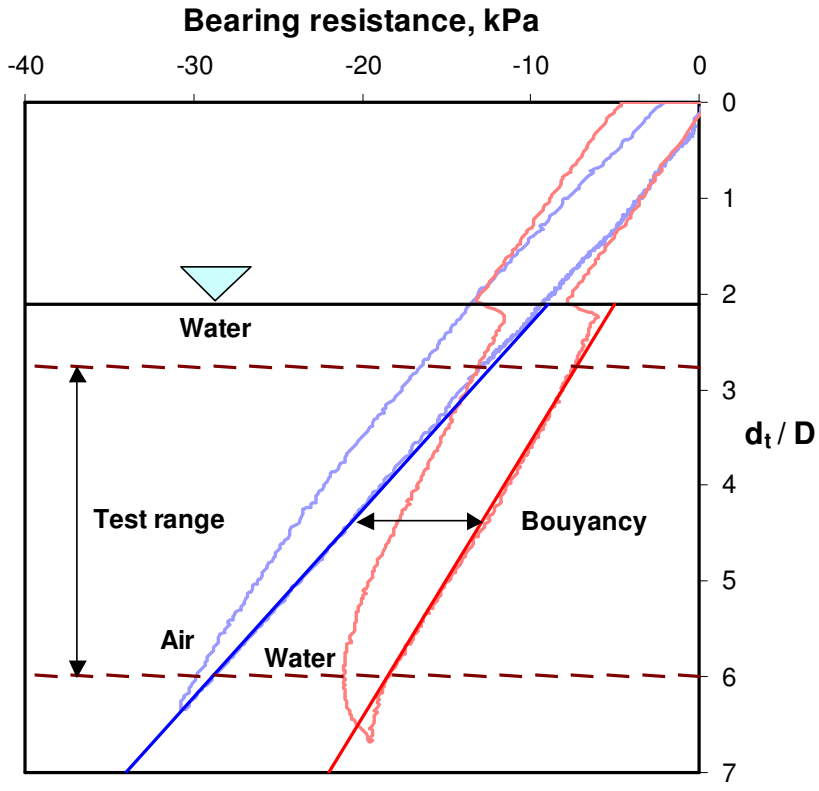

Figure 5.24 Load-penetration response during full-spudcan installation in air and water

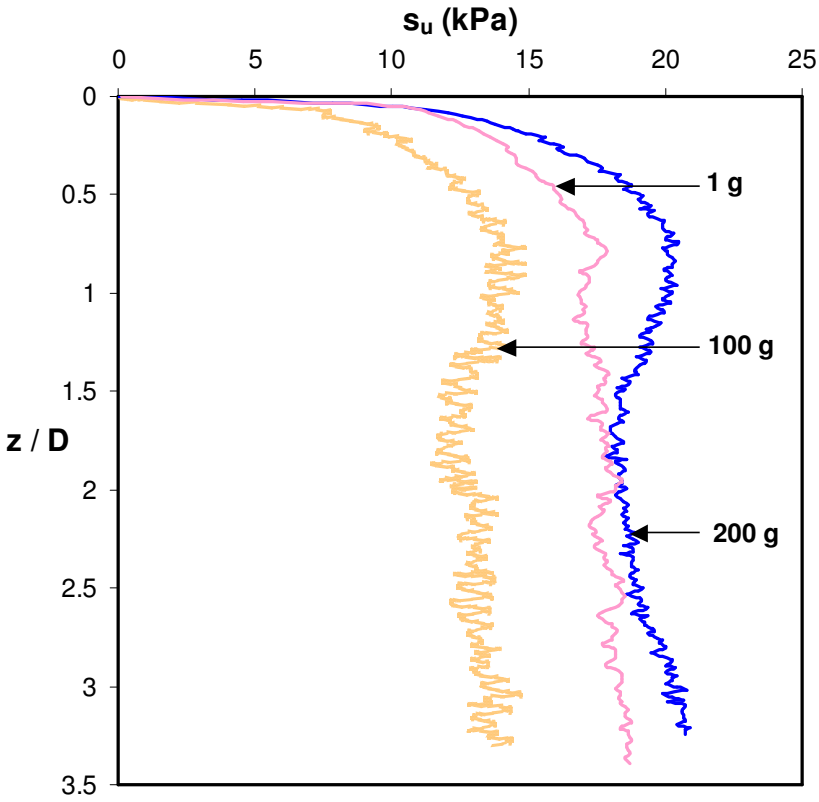

Figure 5.25 Soil strength profile in Event-5 Tests

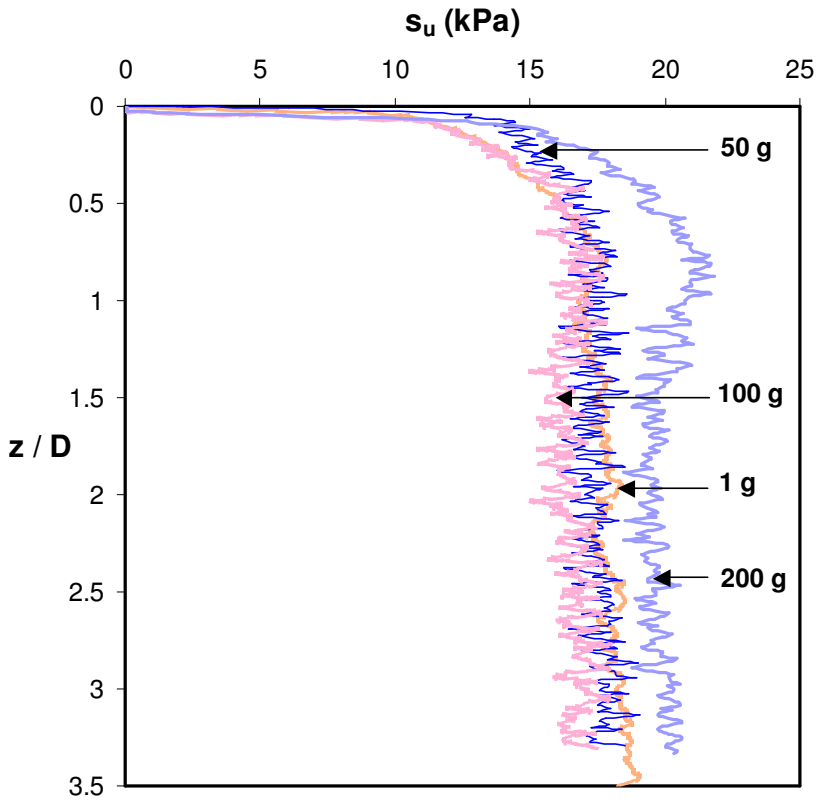

Figure 5.26 Strength profile of saturated clay bed (without water on top) in Event-6 Tests

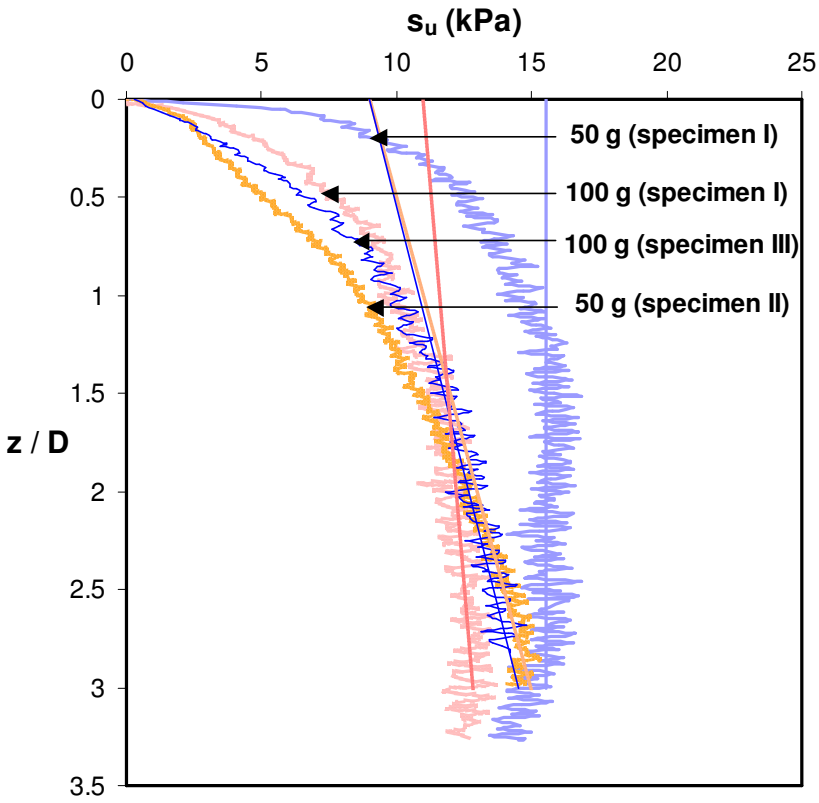

Figure 5.27 Strength profile of submerged clay bed (with water on top) in Event-6 Tests

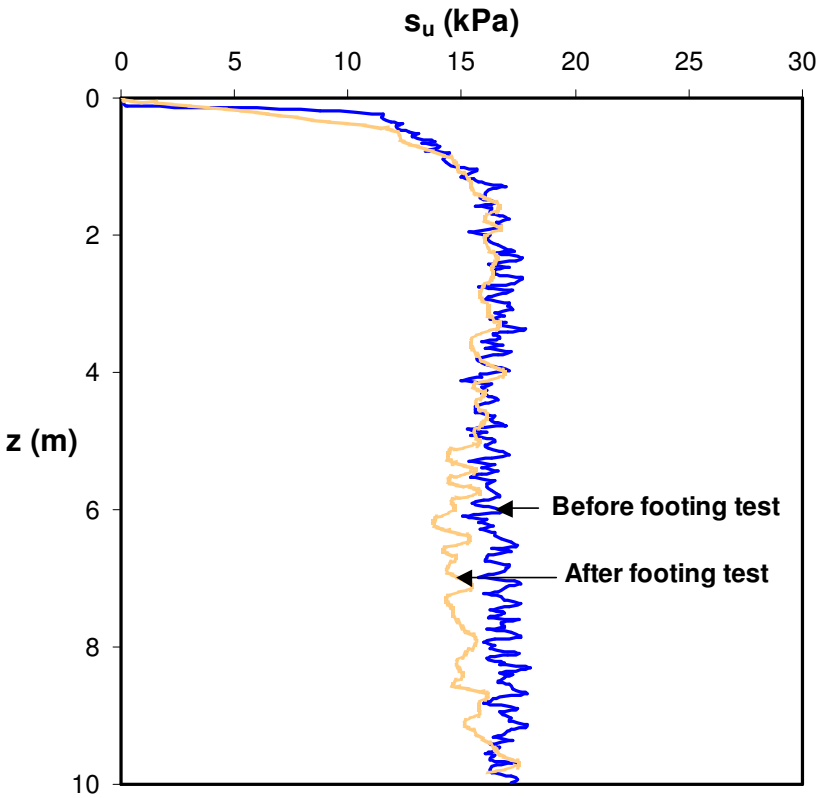

(a) without water on top (100 g)

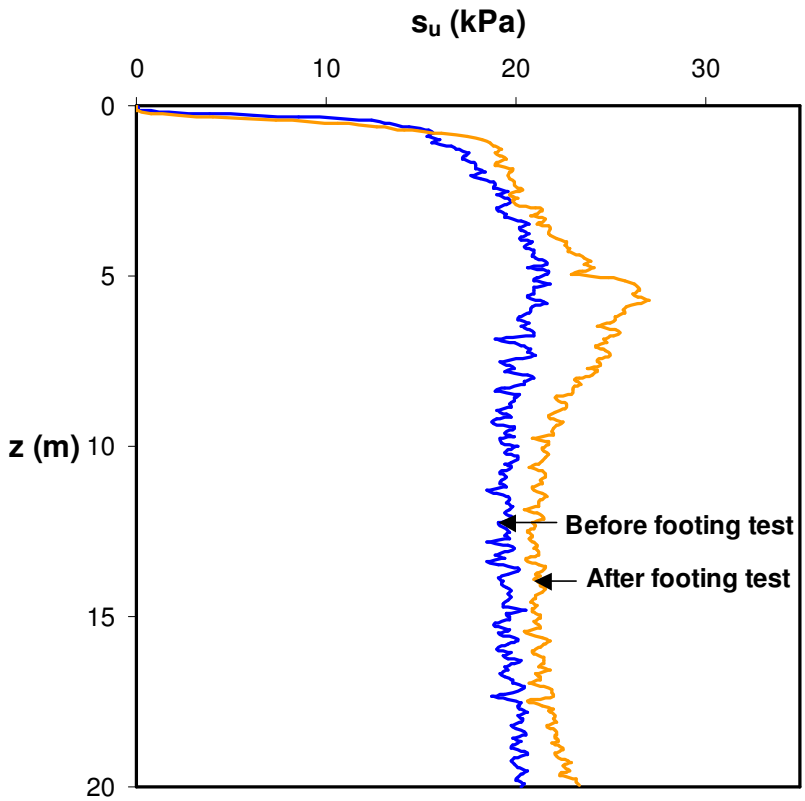

(b) without water on top (200 g)

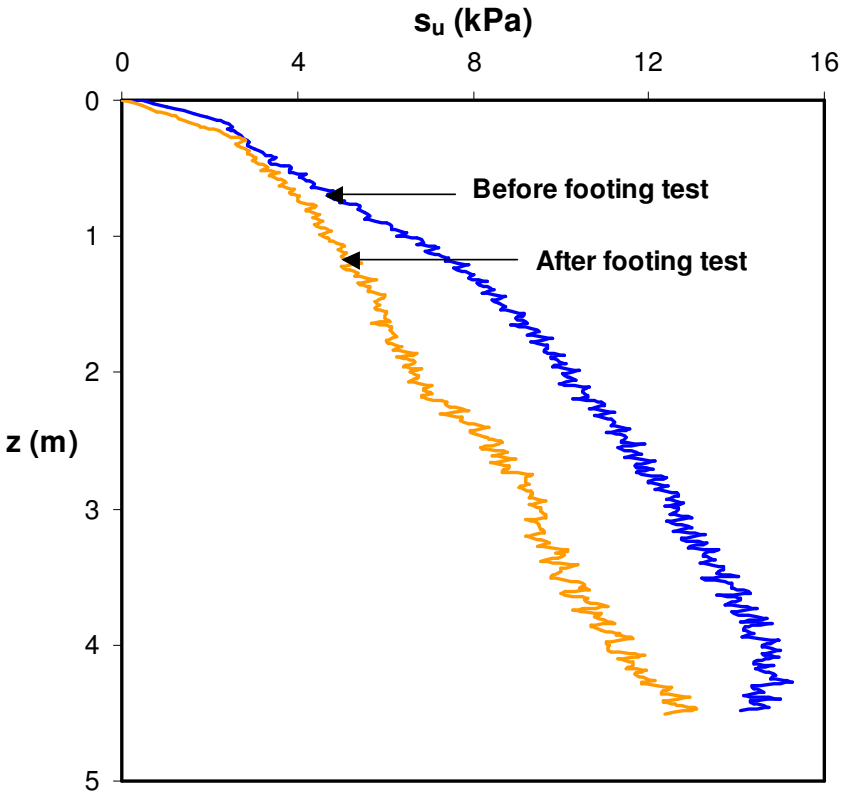

(c) with water on top (50 g)

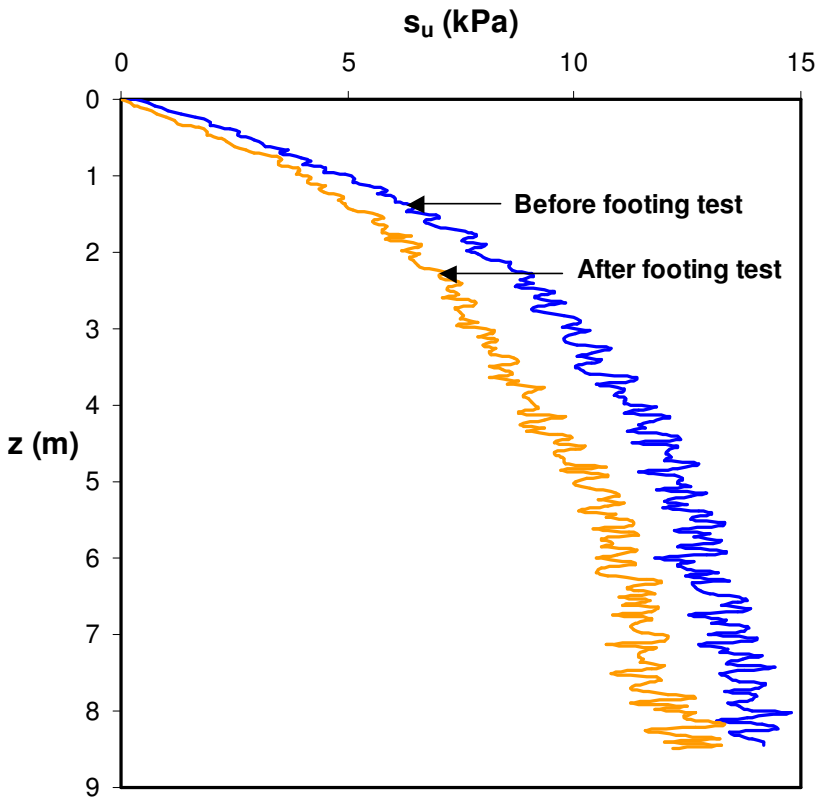

(d) with water on top (100 g)

Figure 5.28 Effect of elapsed time at elevated gravity on measured shear strength

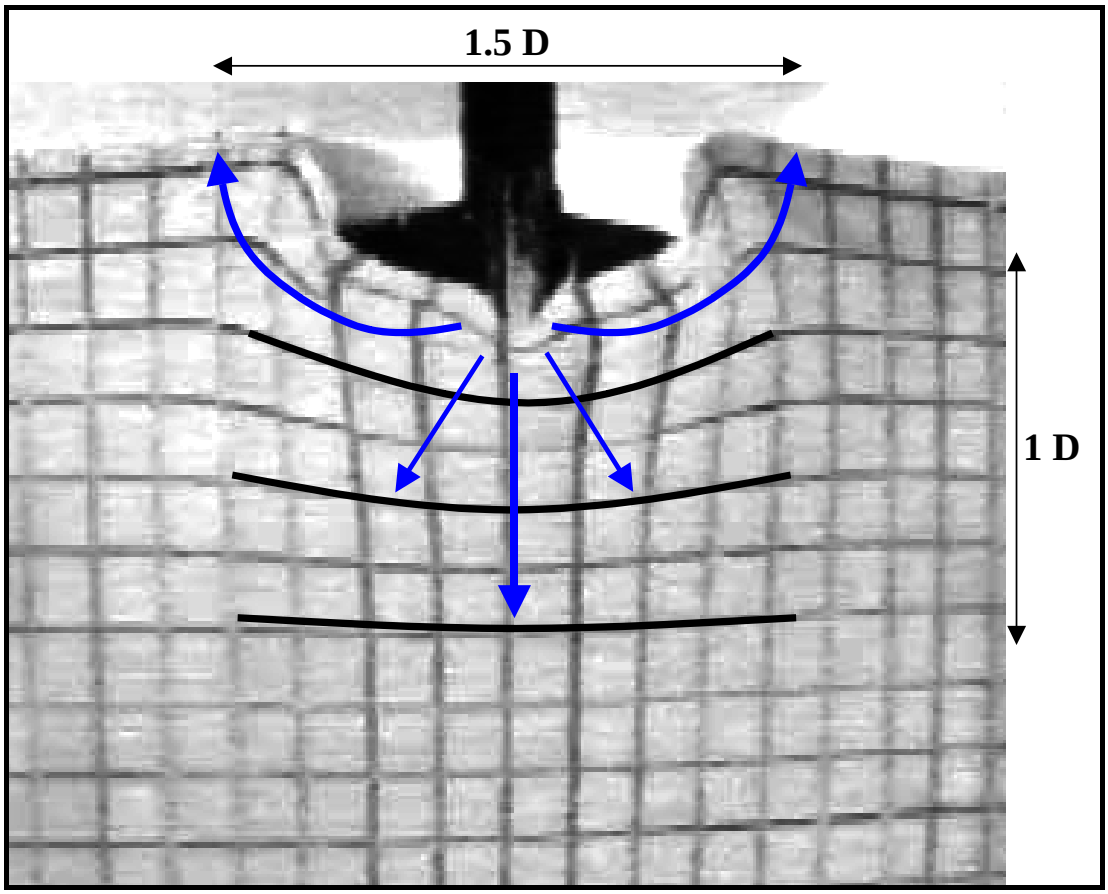

(a) d / D = 0.25

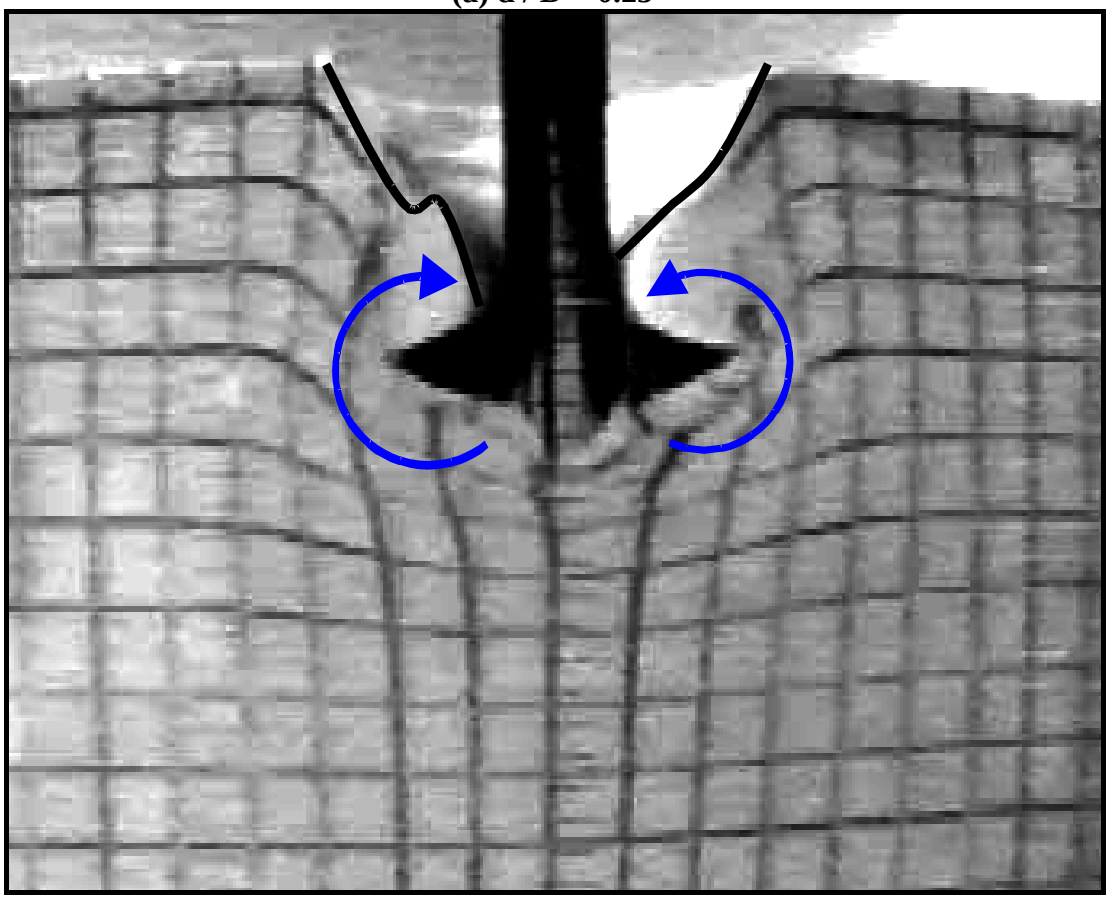

(b) d / D = 0.58

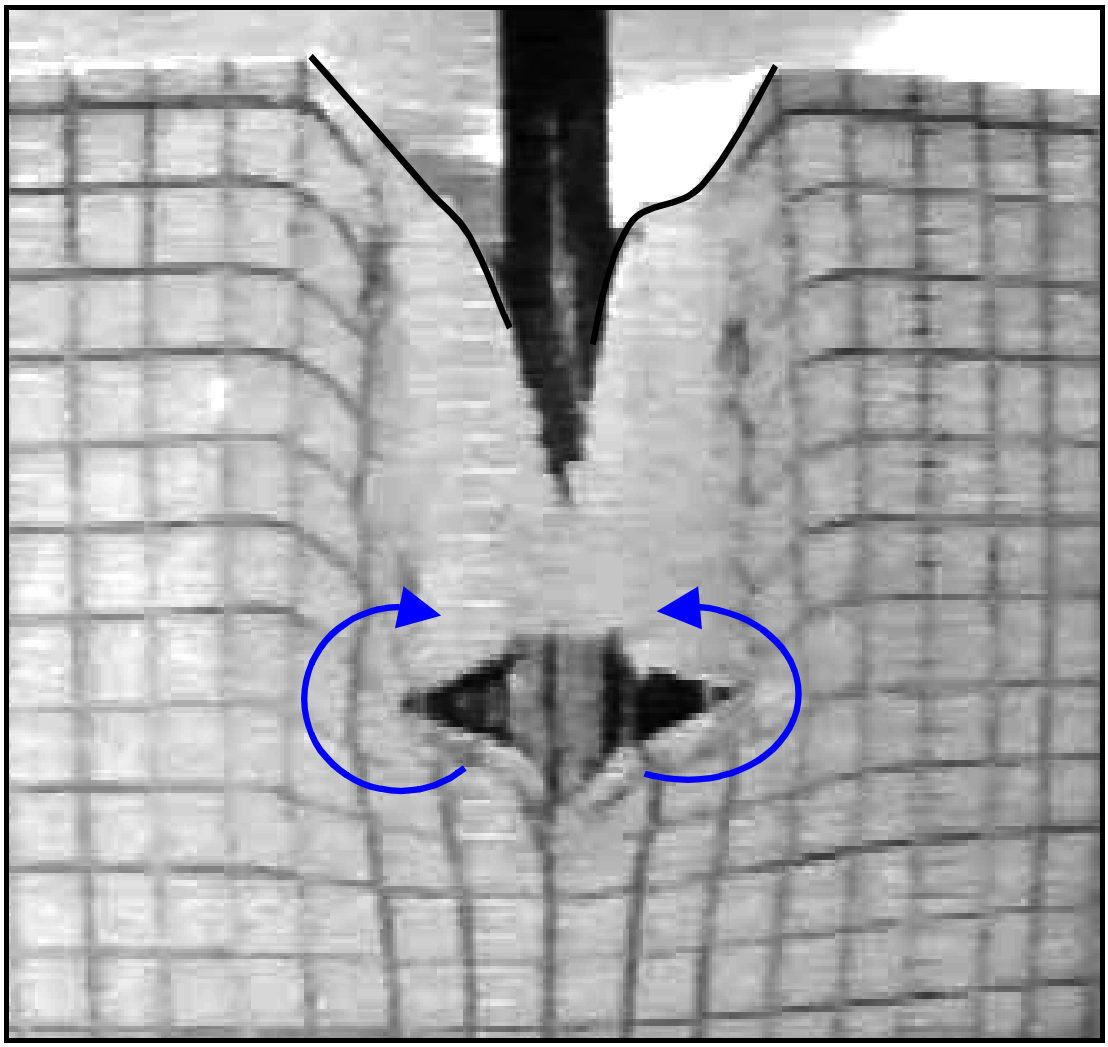

(c) d / D = 1.25

Figure 5.29 Soil failure mechanisms in Event-5 Tests (100 g)

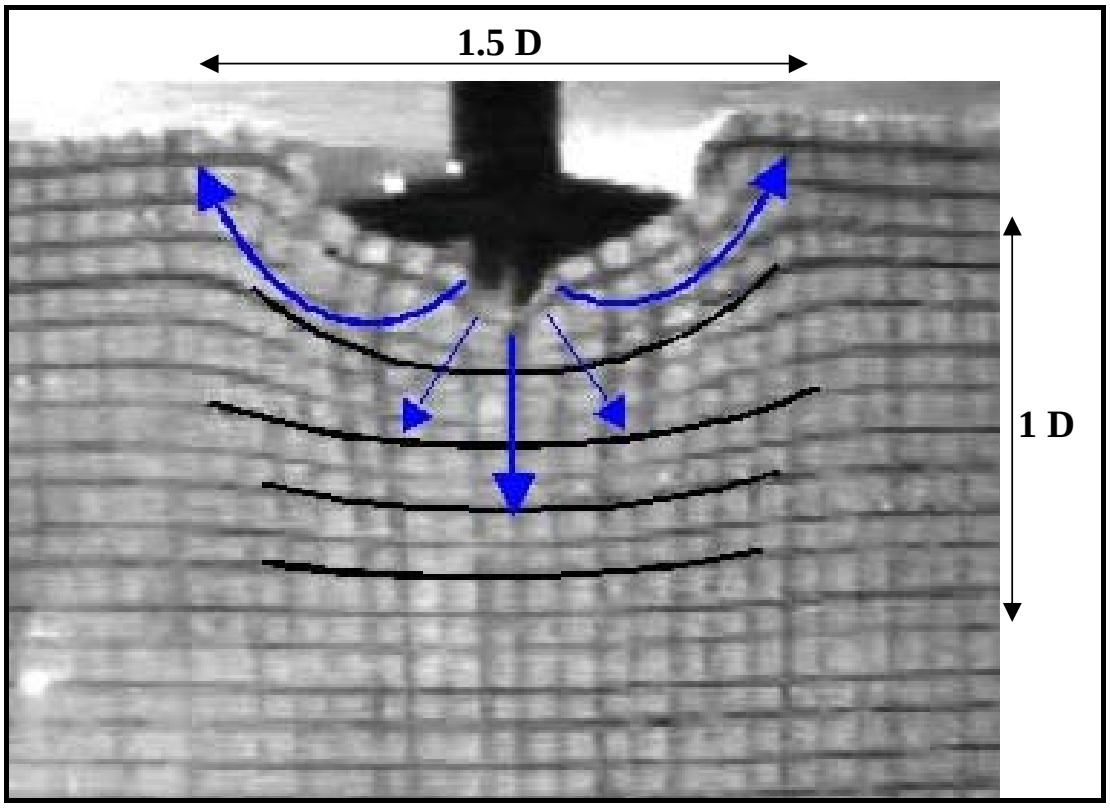

(a) d / D = 0.15

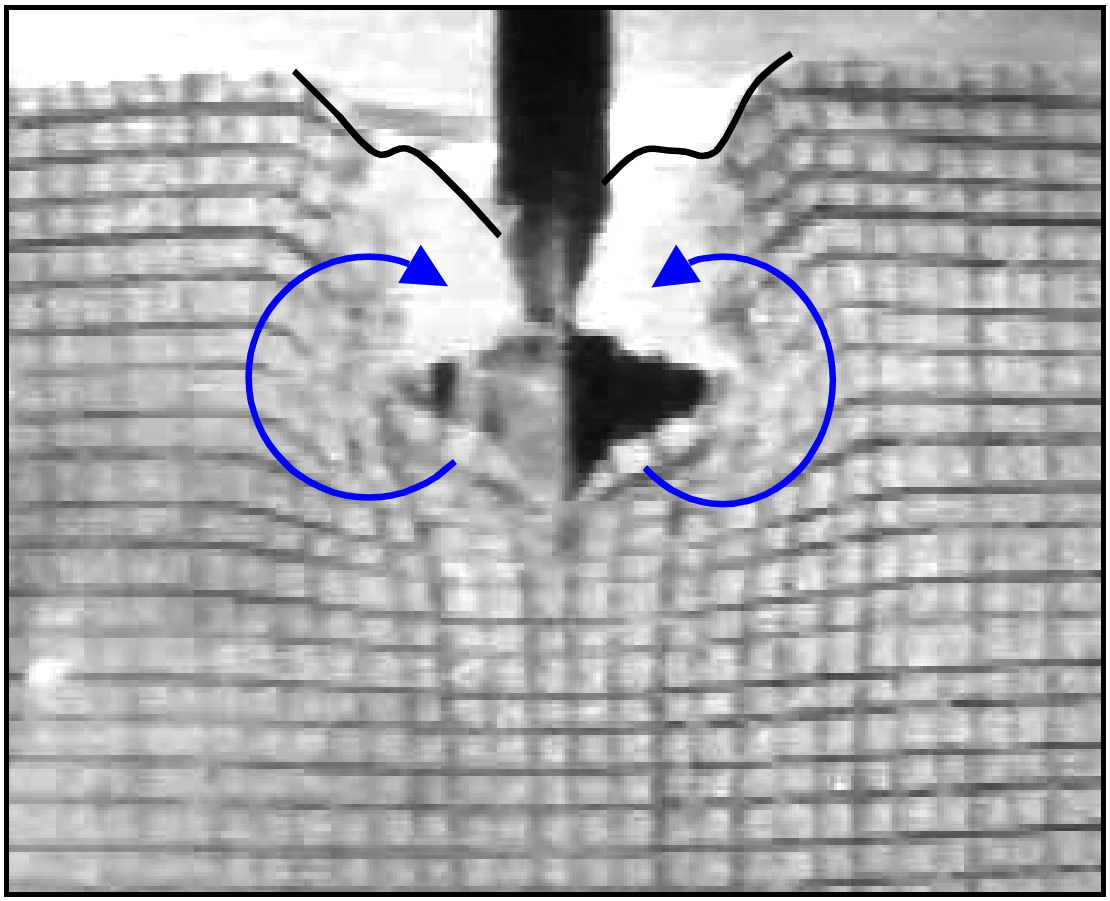

(b) d / D = 0.58

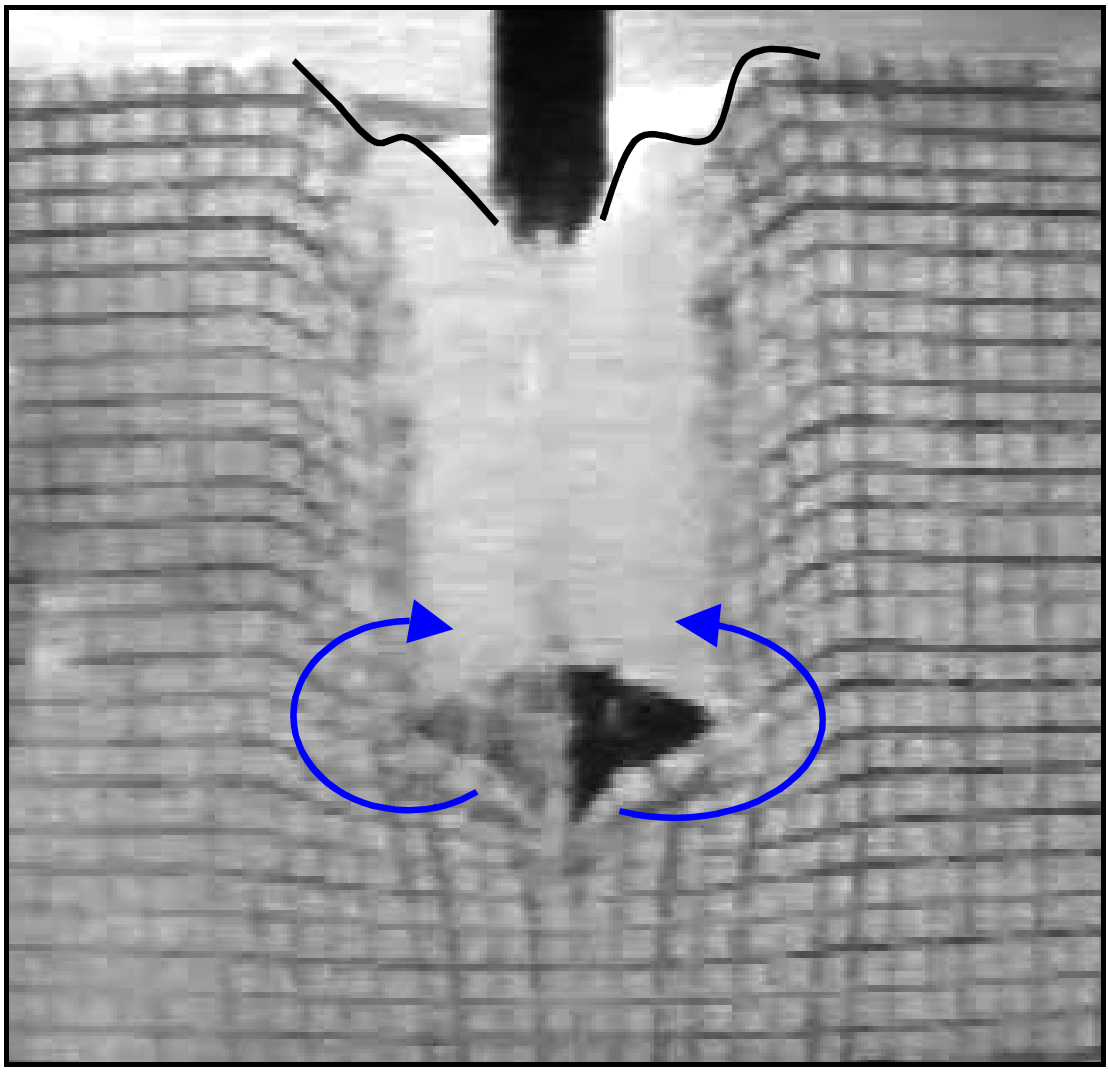

(c) d / D = 1.35

Figure 5.30 Soil failure mechanisms in Event-5 Tests (200 g)

(a) top view of flow failure

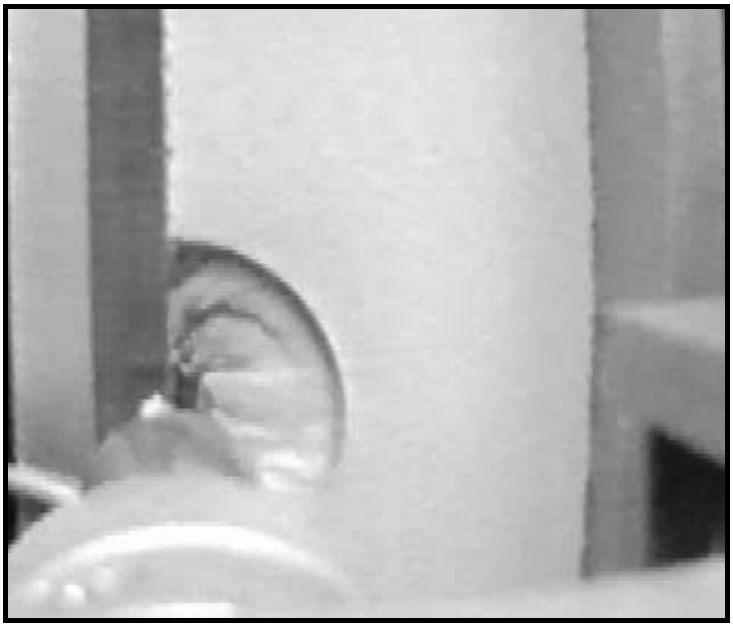

(b) top view at deep penetration

Figure 5.31 Top view of soil flow mechanisms

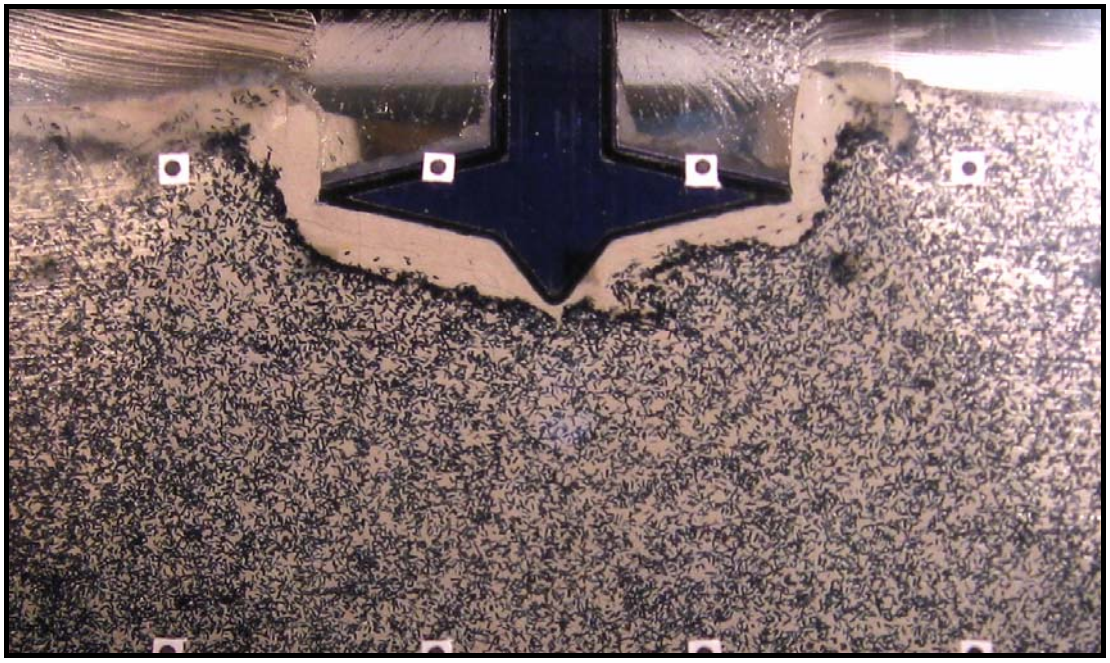

(a) d / D = 0.16

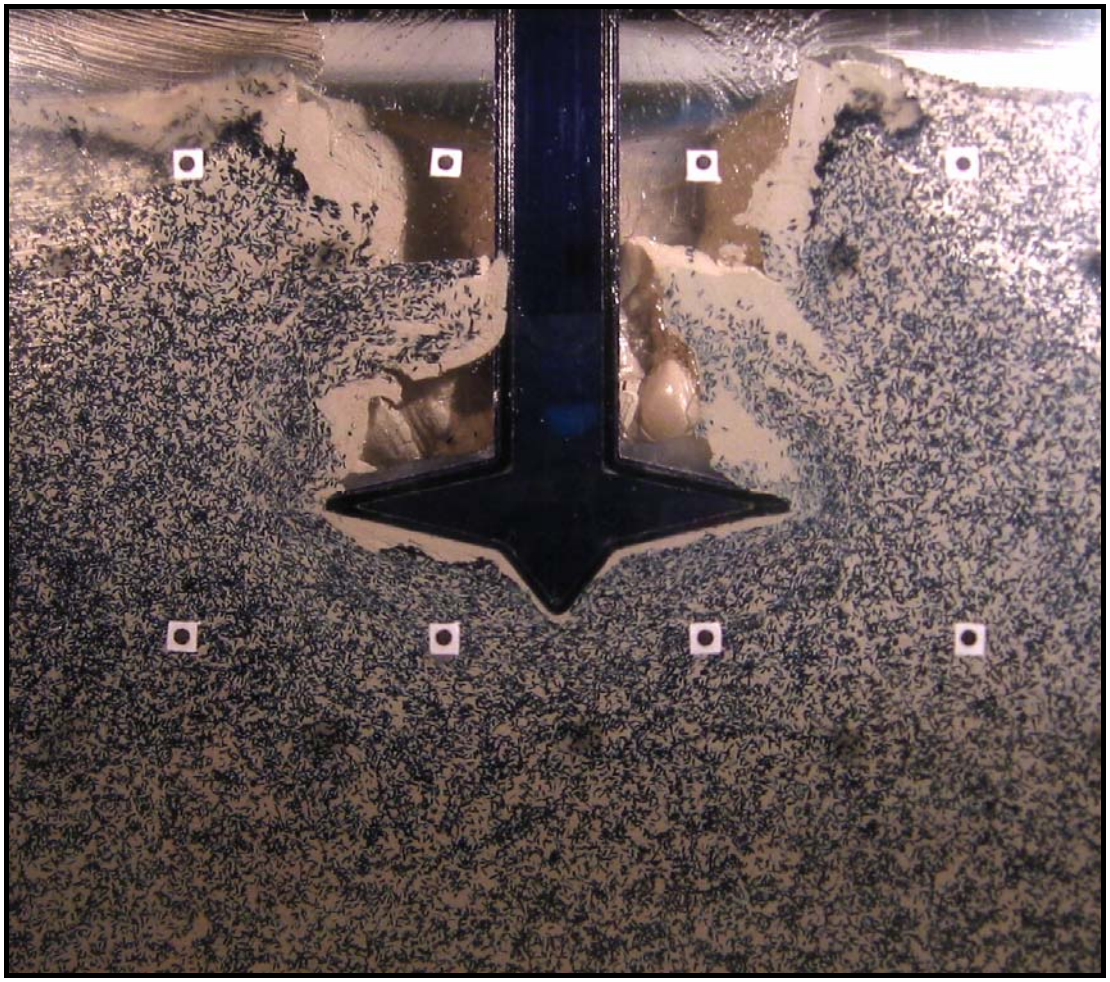

(b) d / D = 0.74

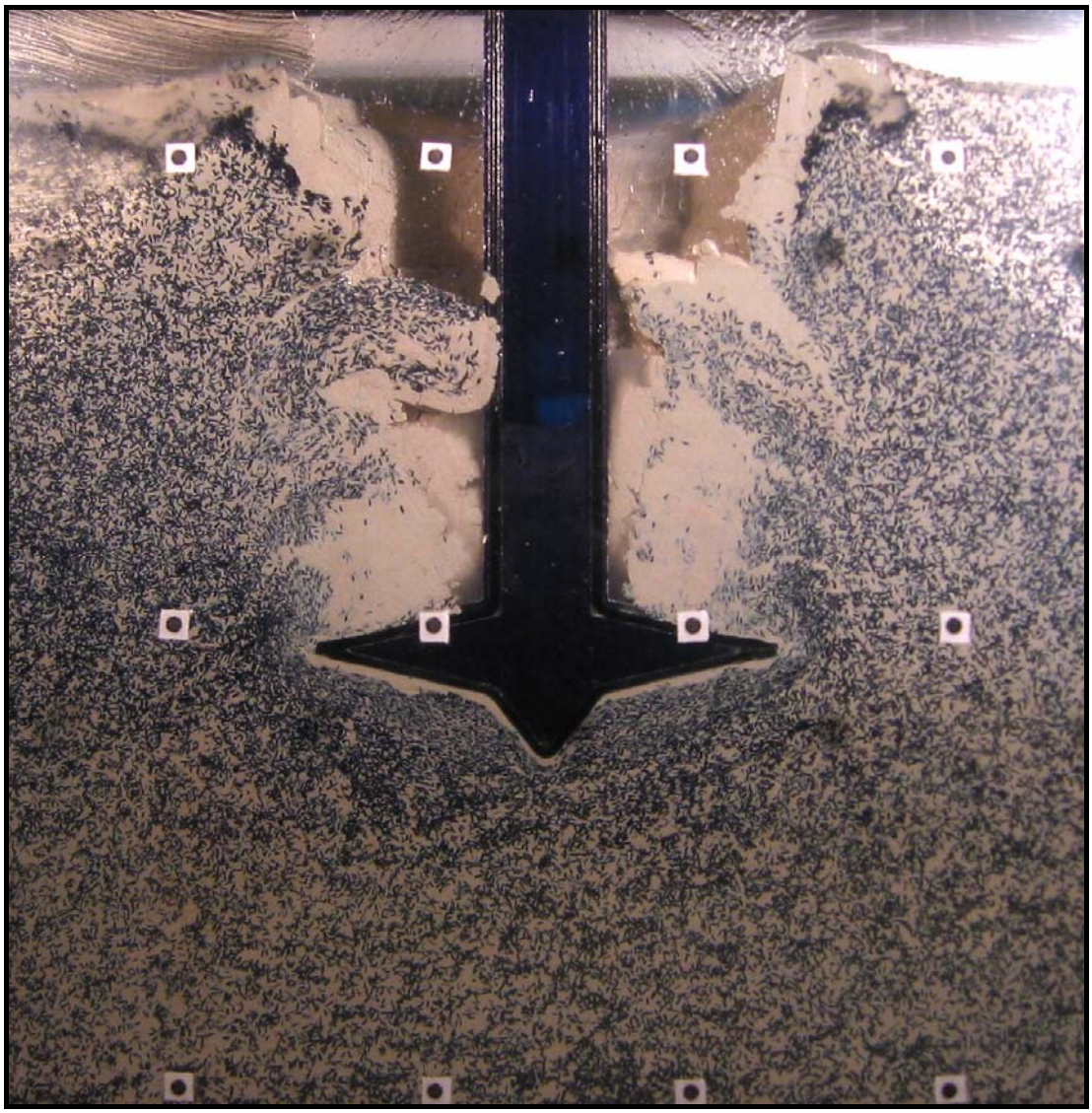

(c) d / D = 1.00

Figure 5.32 Soil failure mechanisms in Event-6 Test at 50 g (without water on top)

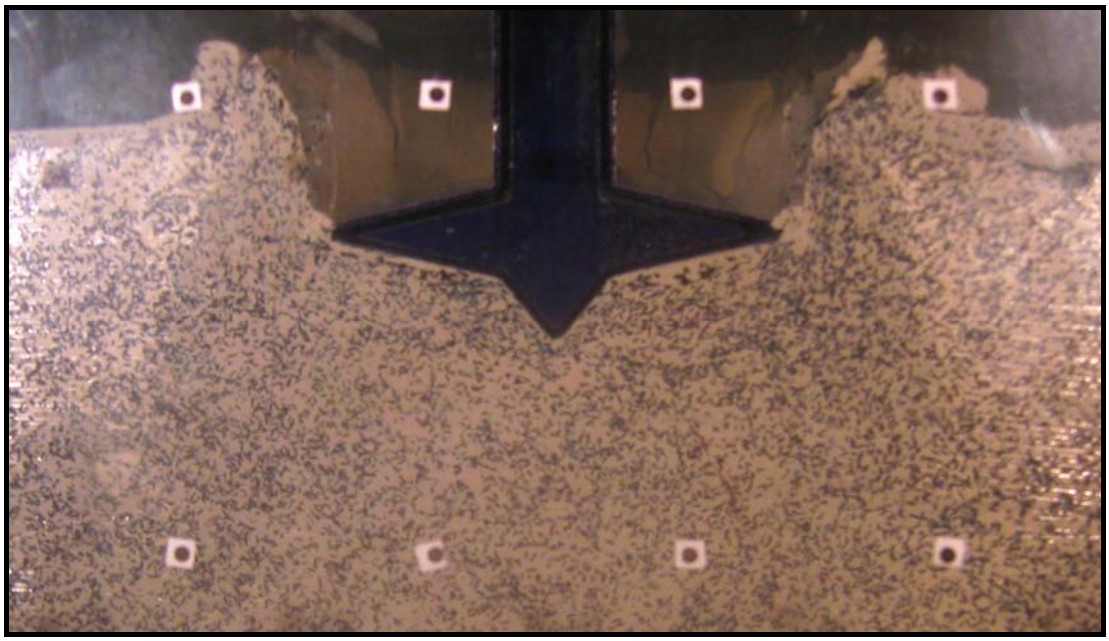

(a) d / D = 0.22

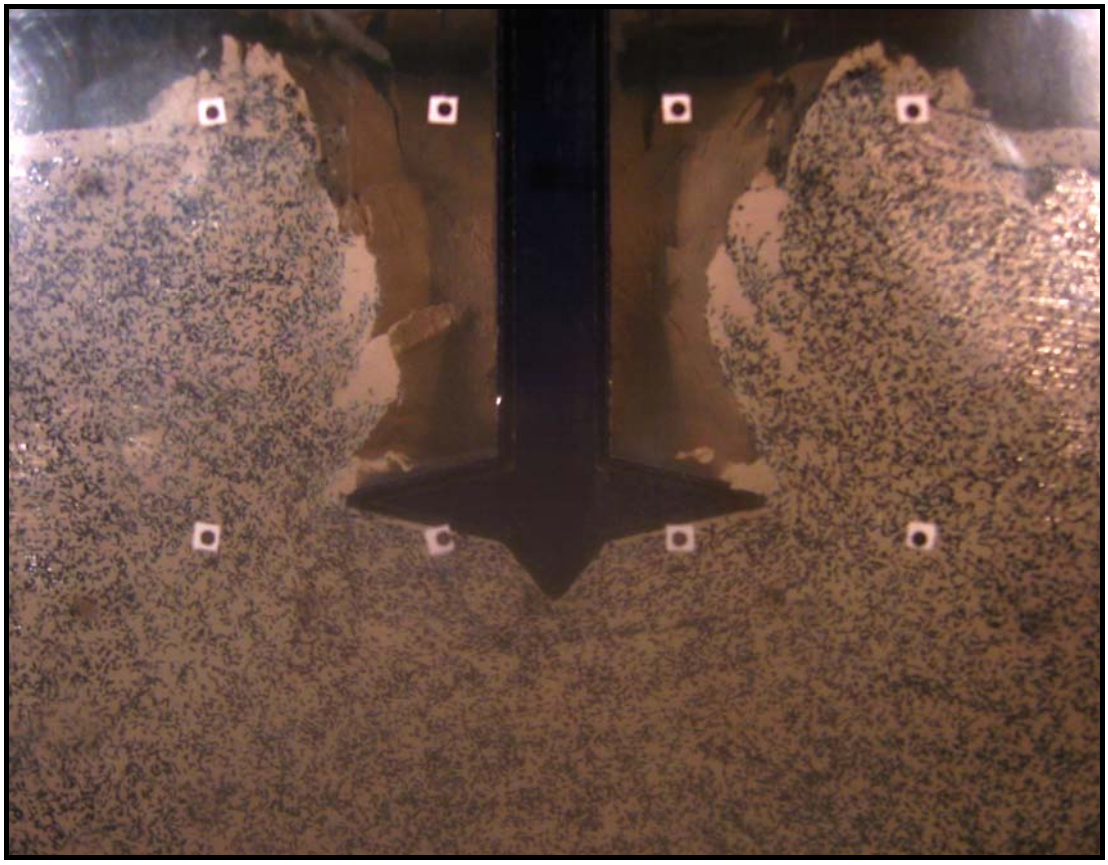

(b) d / D = 0.85

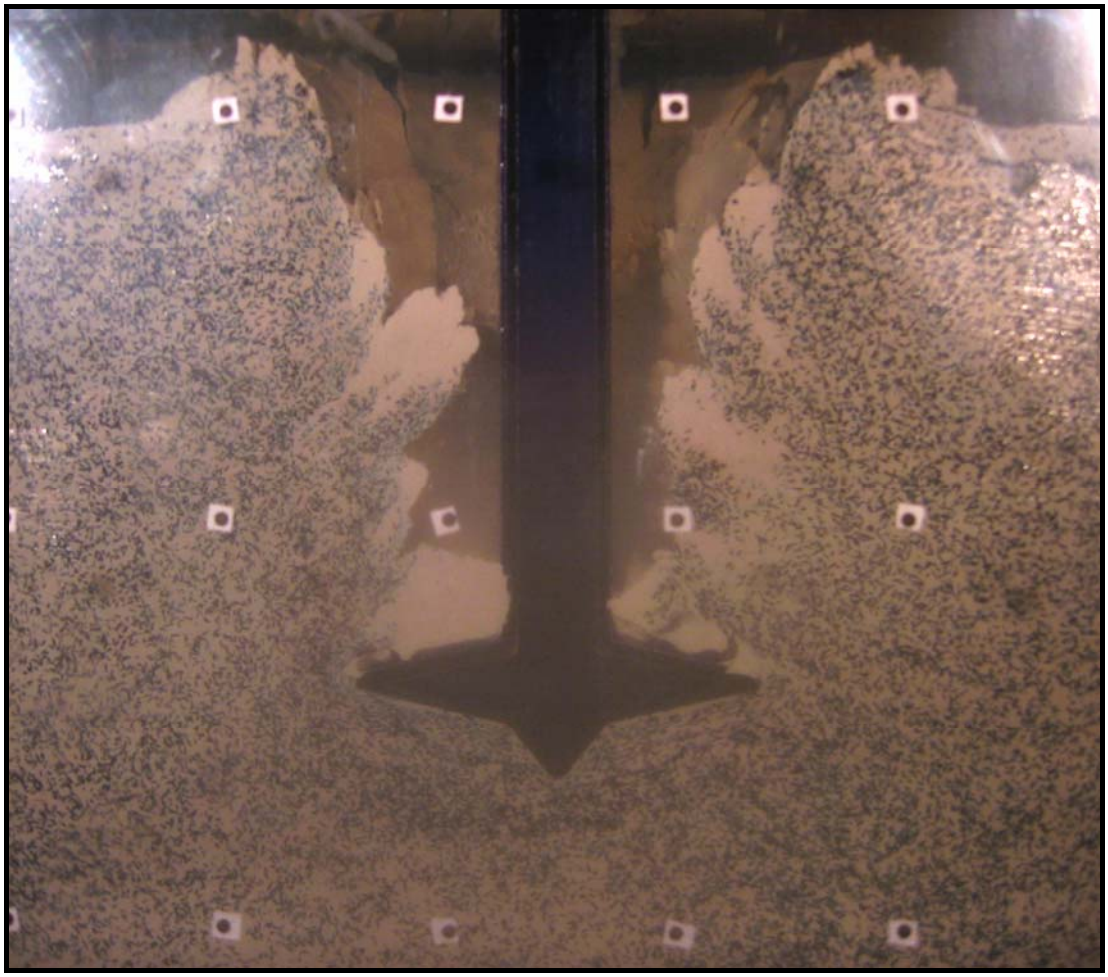

(c) d / D = 1.30

Figure 5.33 Soil failure mechanisms in Event-6 Test at 50 g (with water on top)

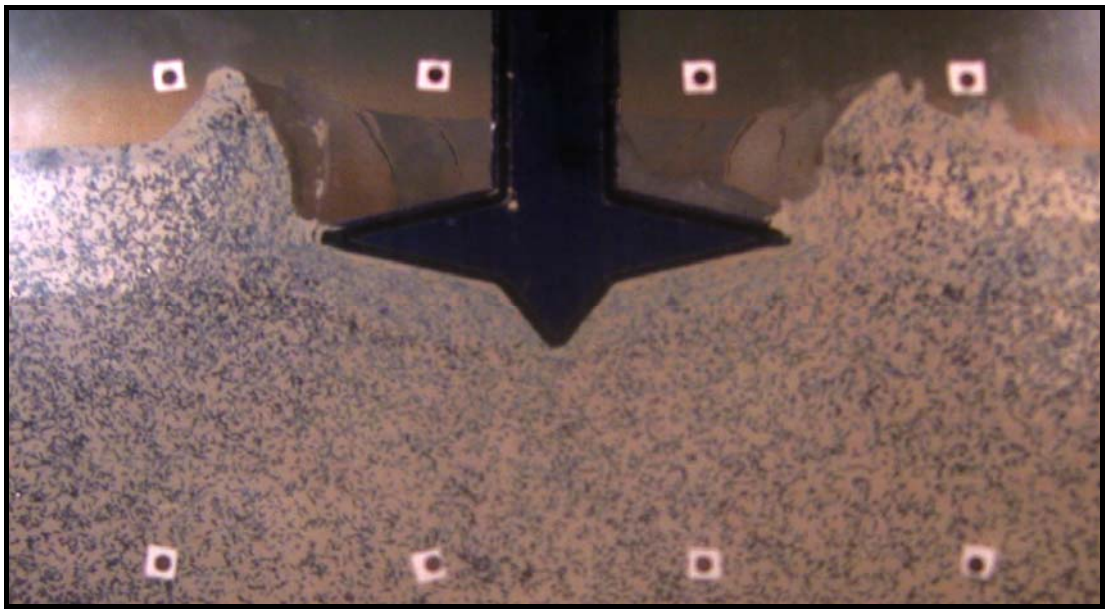

(a) d / D = 0.17

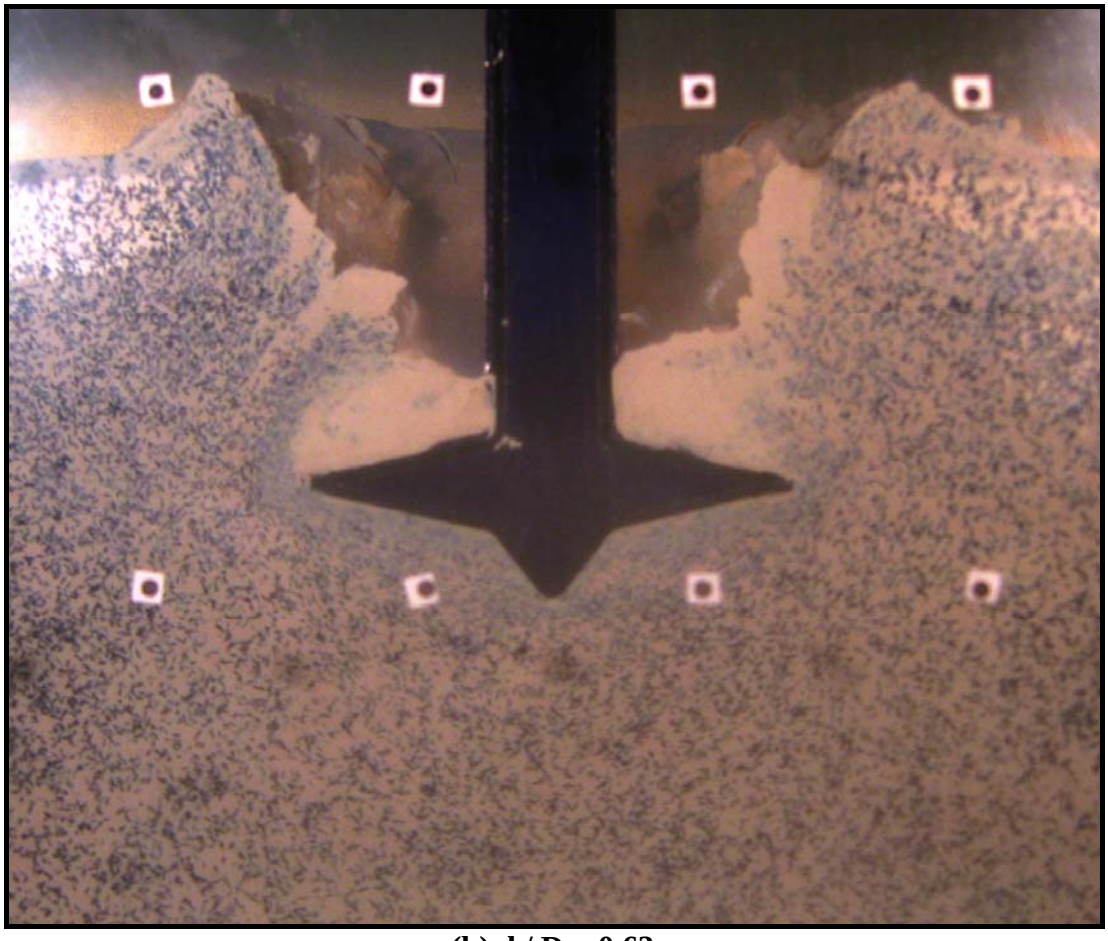

(b) d / D = 0.63

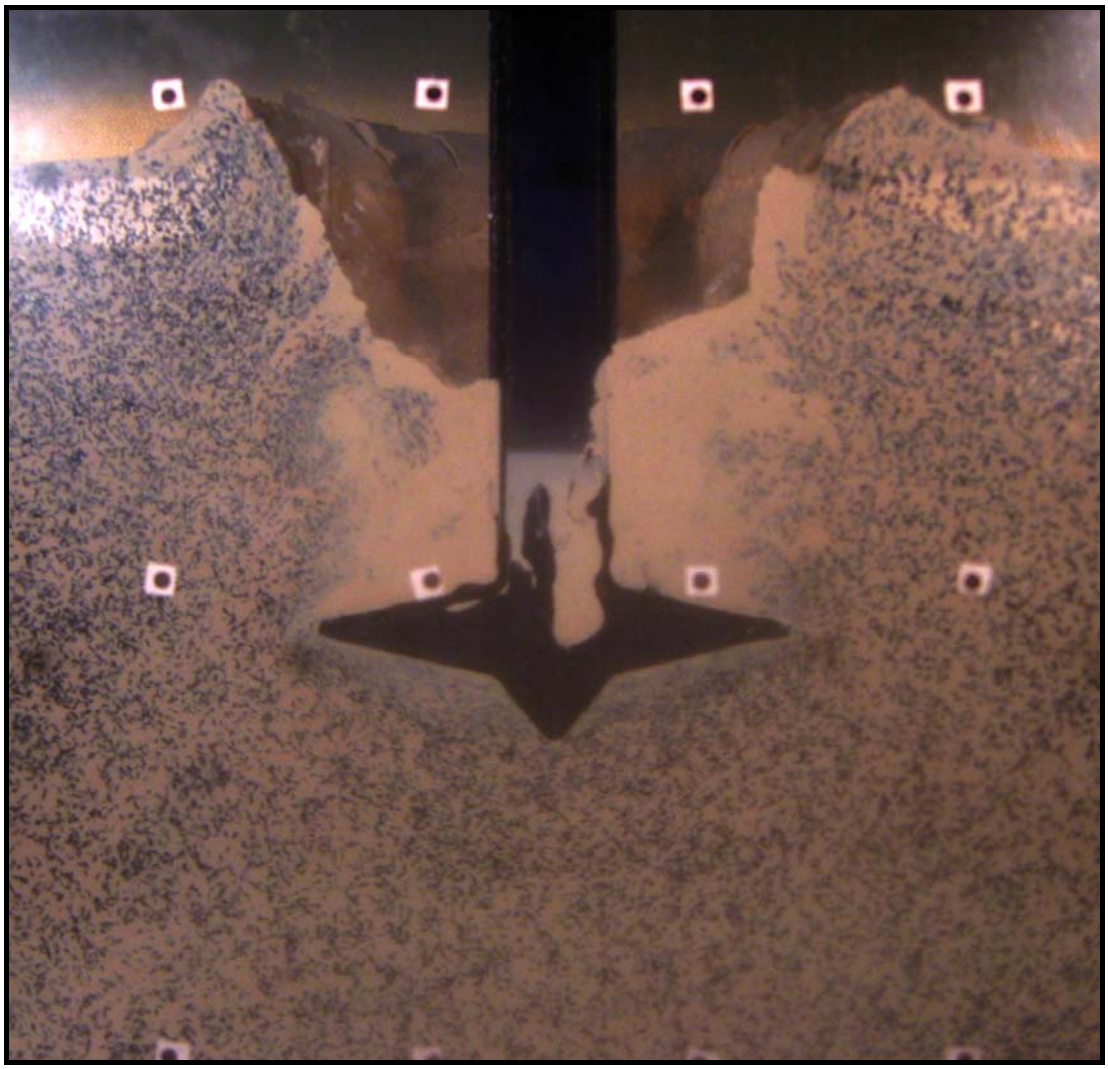

(c) d / D = 0.97

Figure 5.34 Soil failure mechanisms in Event-6 Test at 100 g (with water on top)

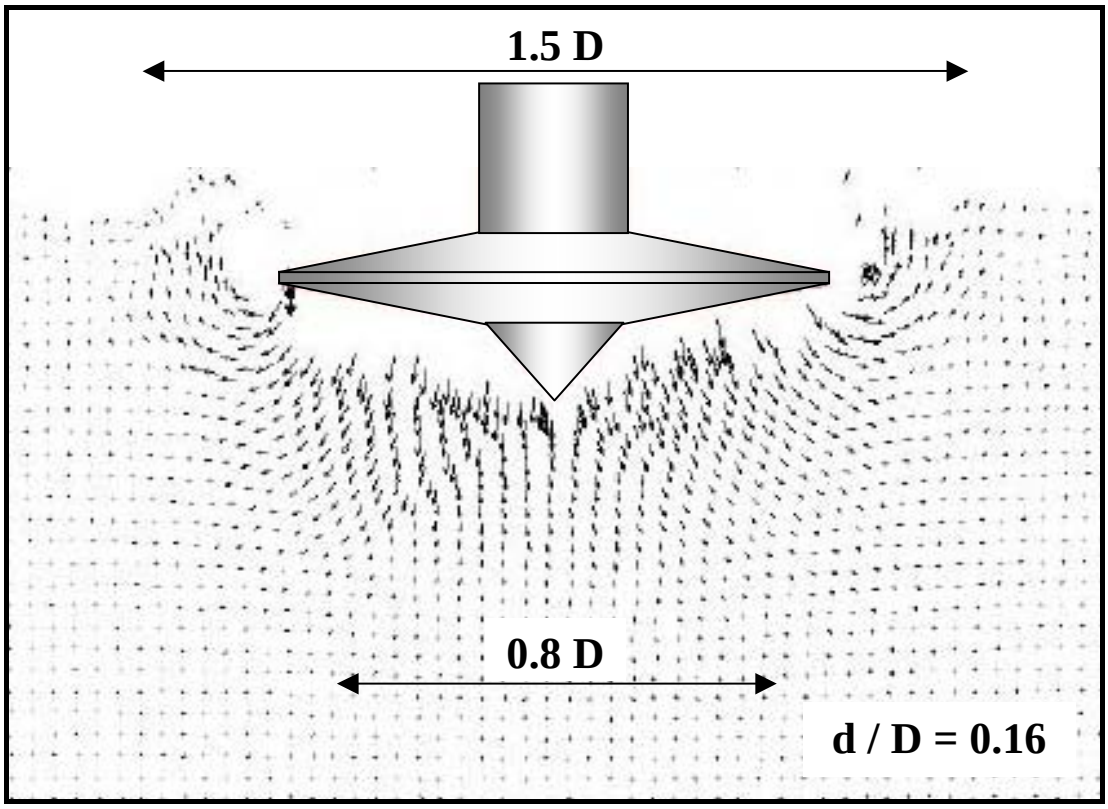

(a) surface flow

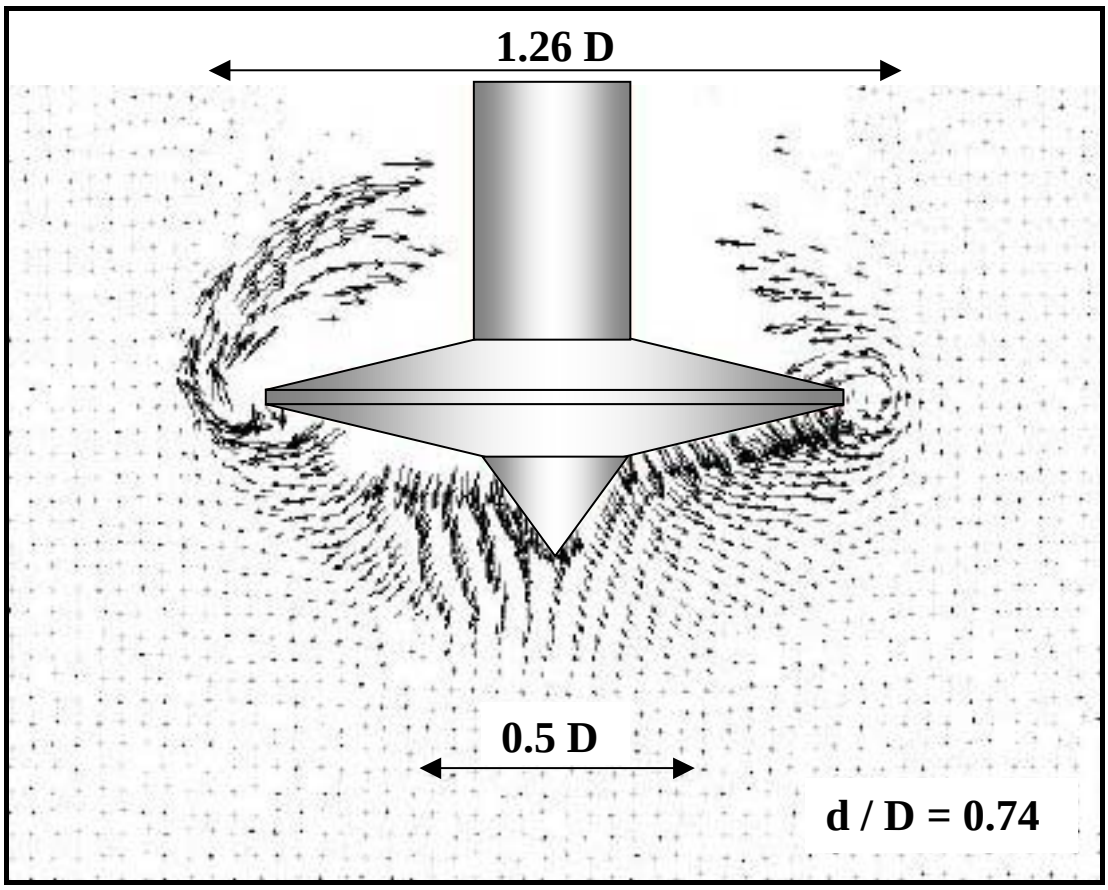

(b) backflow

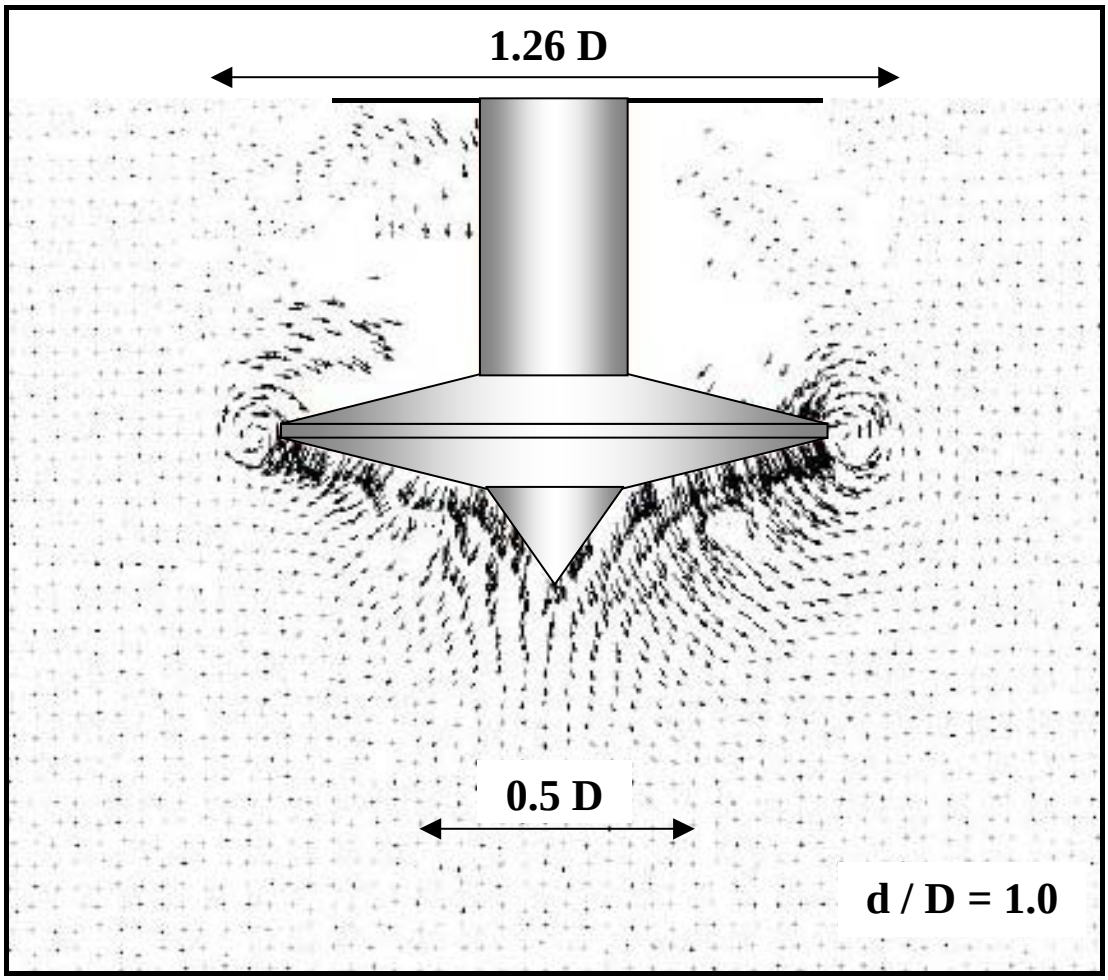

(c) deep/local flow

Figure 5.35 Displacement vectors from PIV analysis in Event-6 test at 50 g (without free water on top)

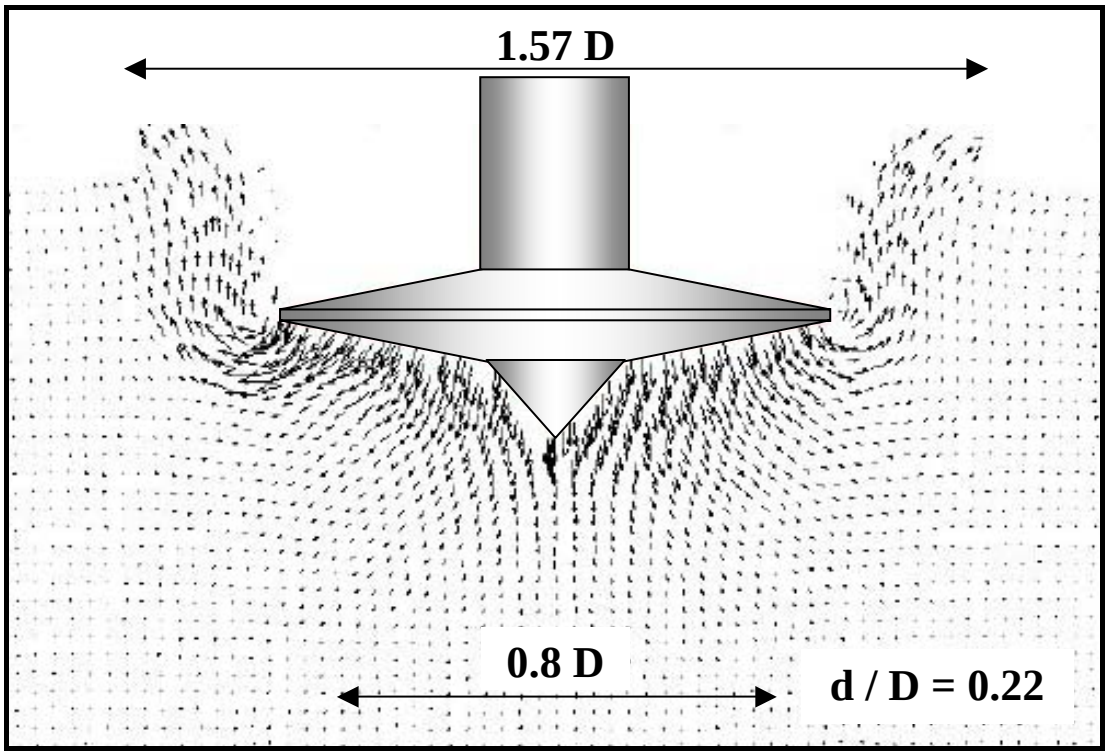

(a) surface flow

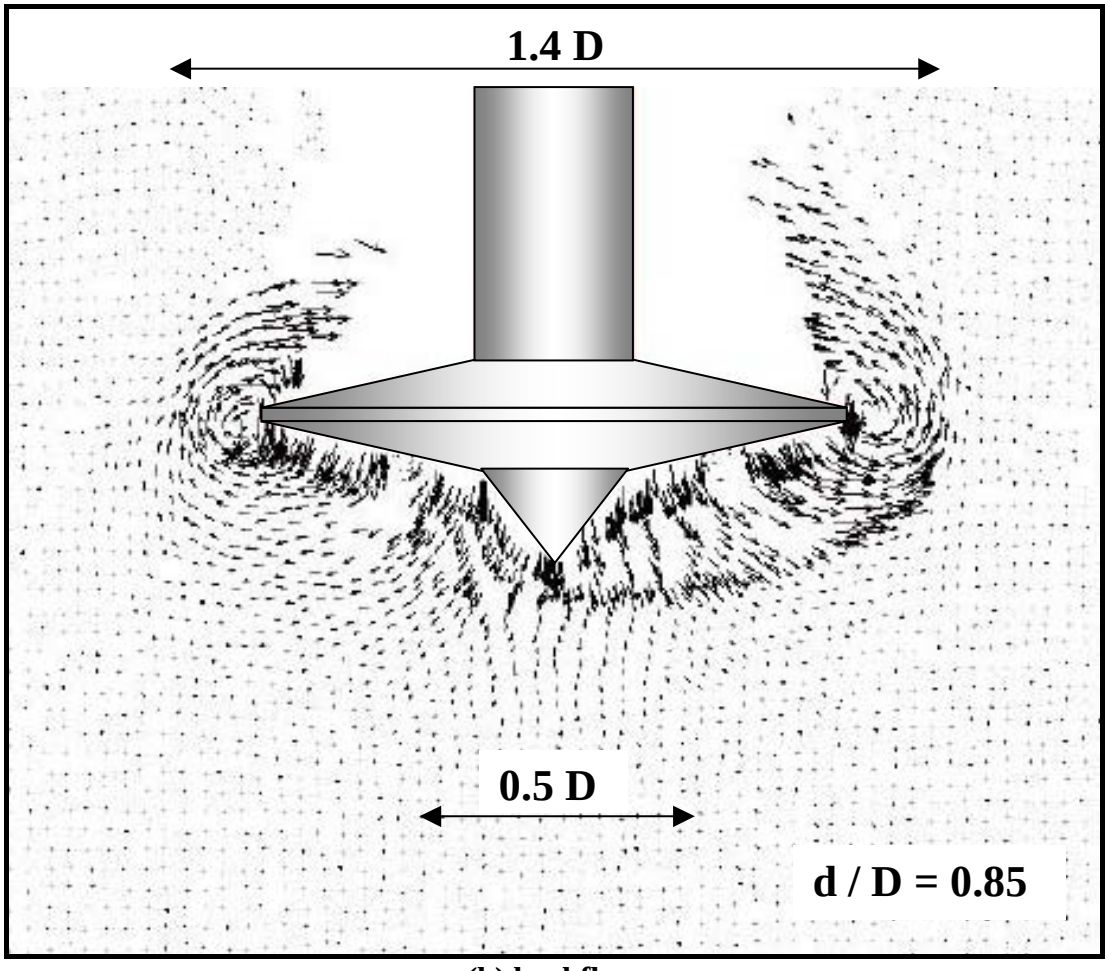

(b) backflow

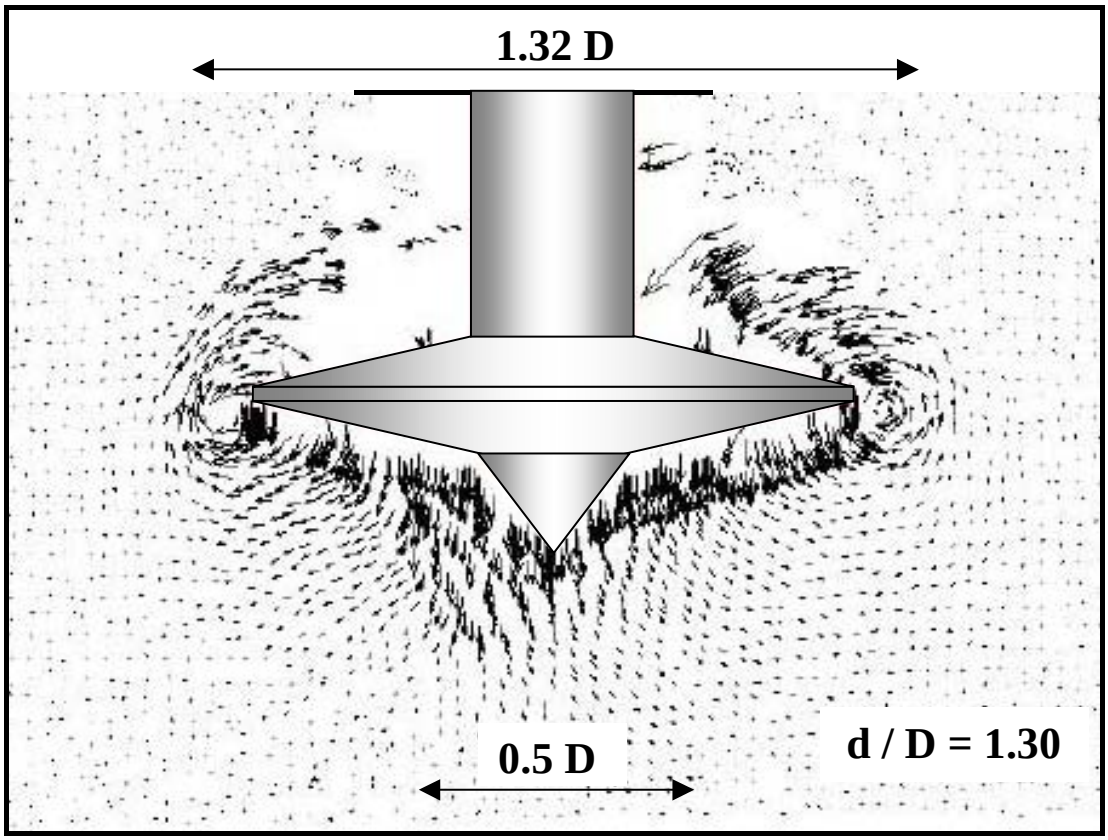

(c) deep/local flow

Figure 5.36 Displacement vectors from PIV analysis in Event-6 test at 50 g (with free water on top)

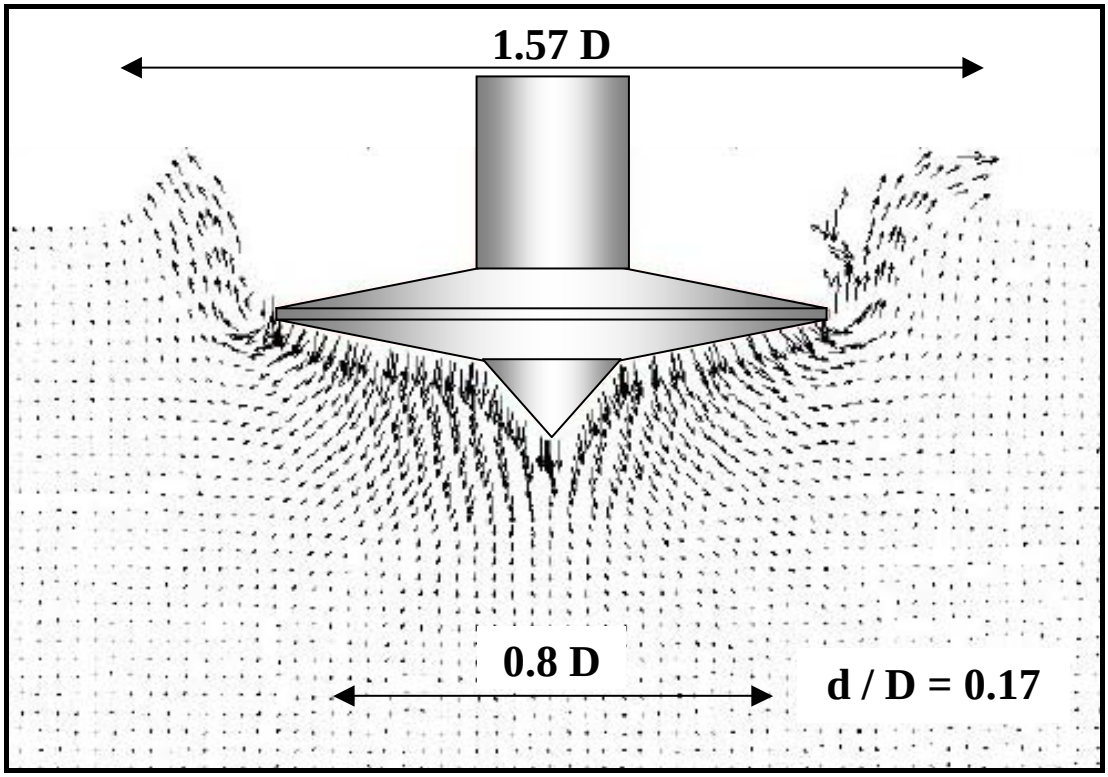

(a) surface flow

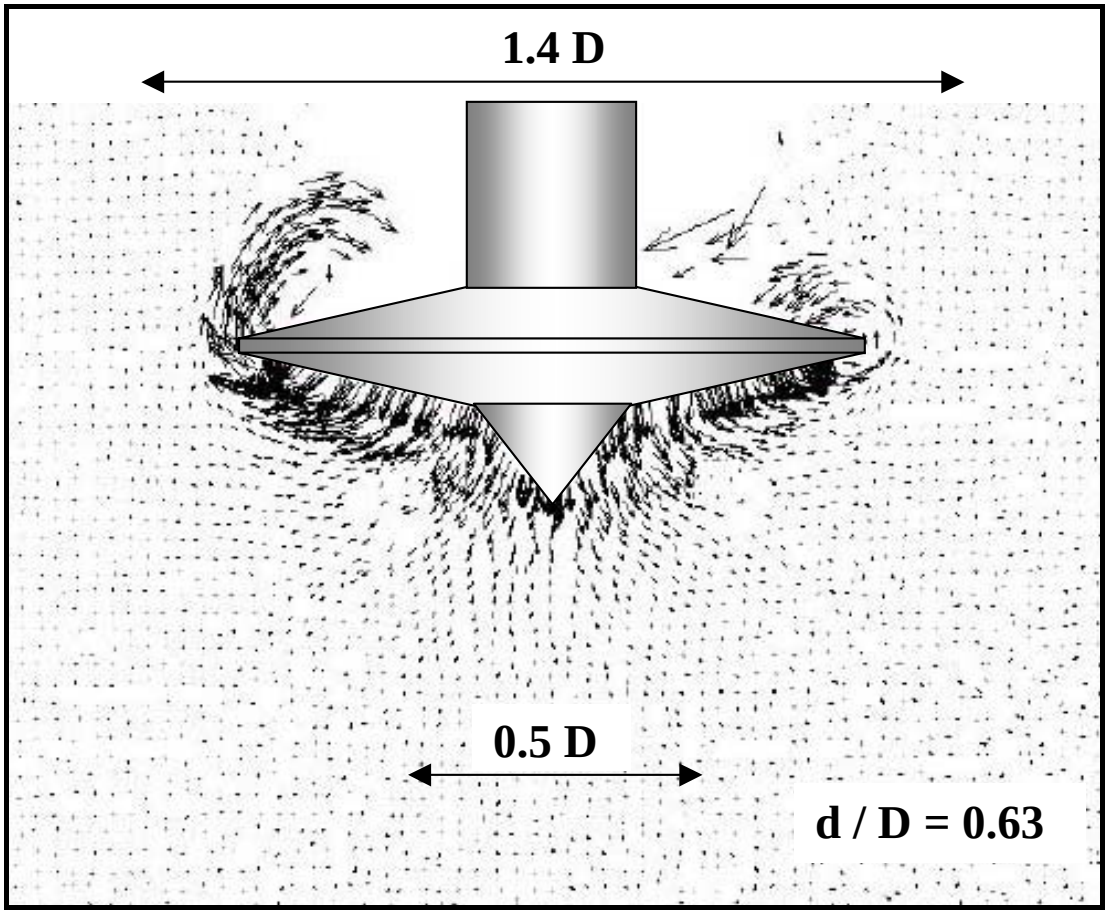

(b) backflow

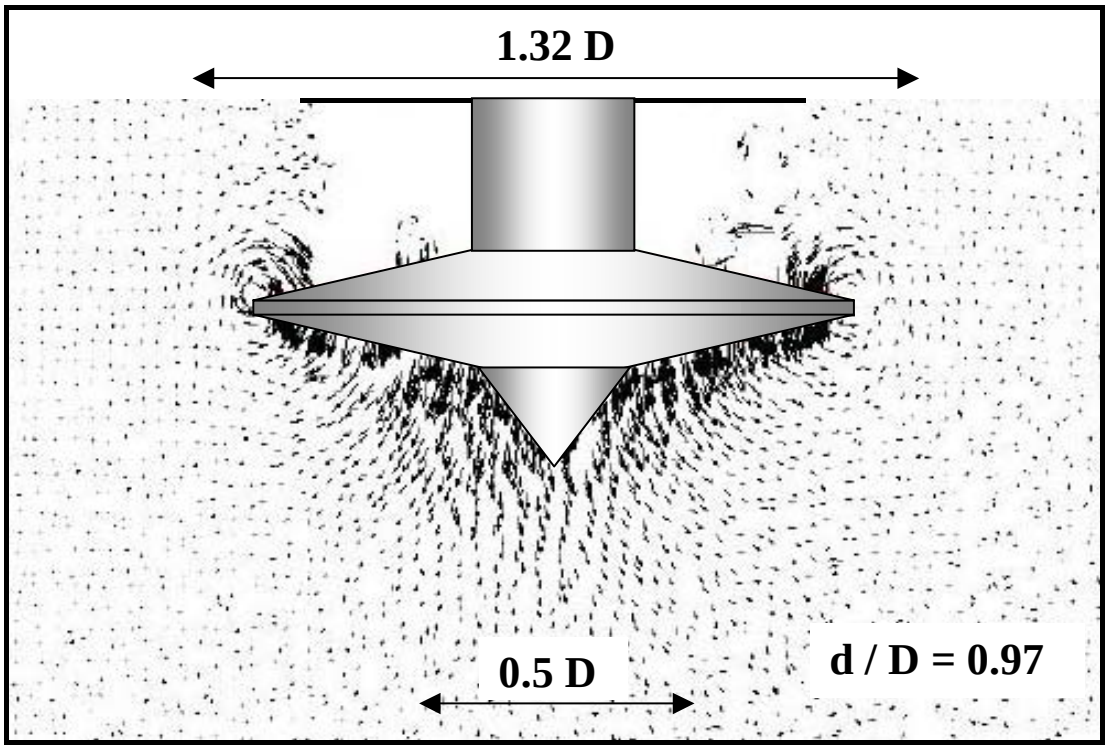

(c) deep/local flow

Figure 5.37 Displacement vectors from PIV analysis in Event-6 test at 100 g (with free water on top)

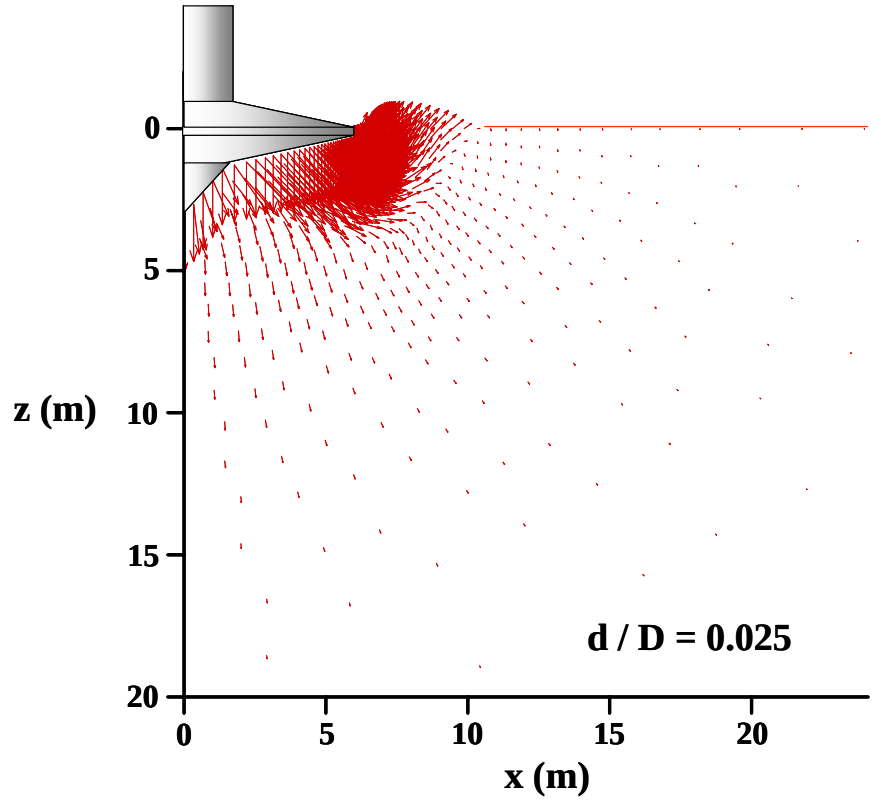

(i) soil heave formed at surface penetration

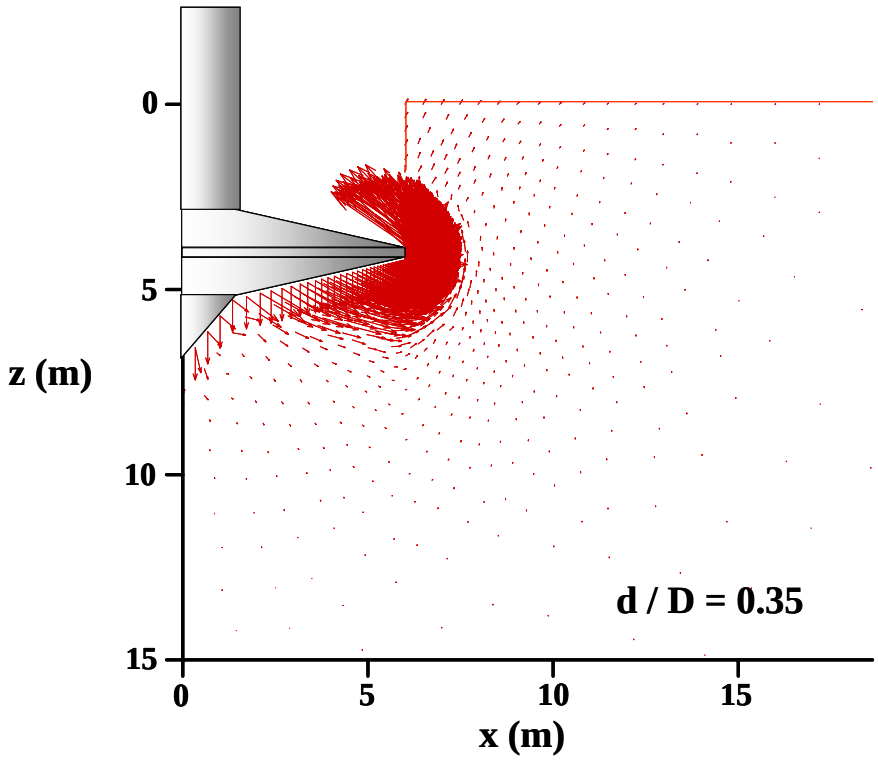

(ii) soil back flow due to flow failure

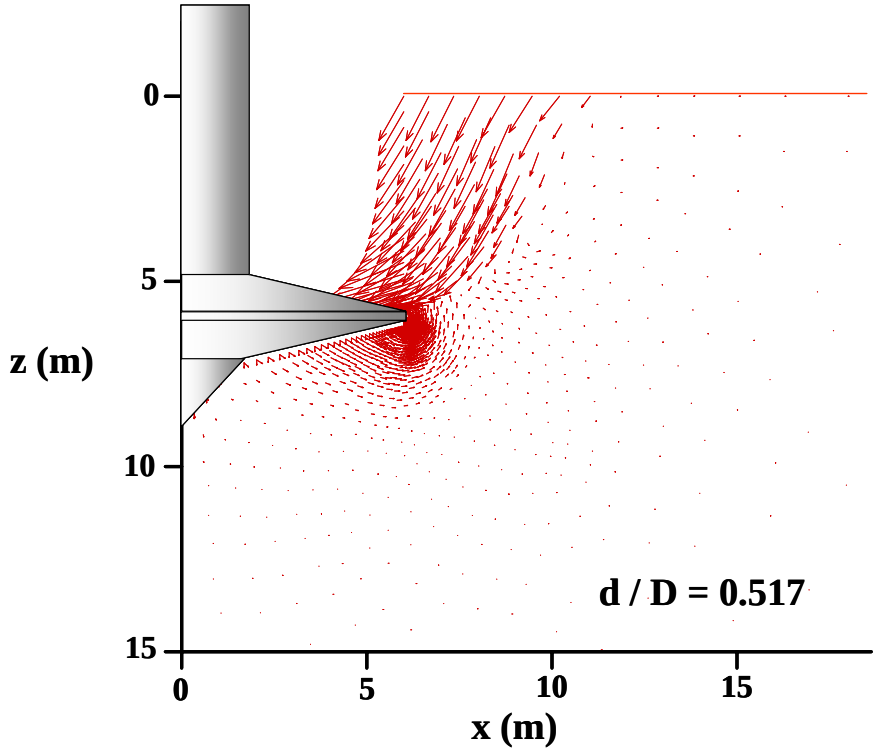

(iii) soil back flow due to wall failure
(a) smooth soil-spudcan interface

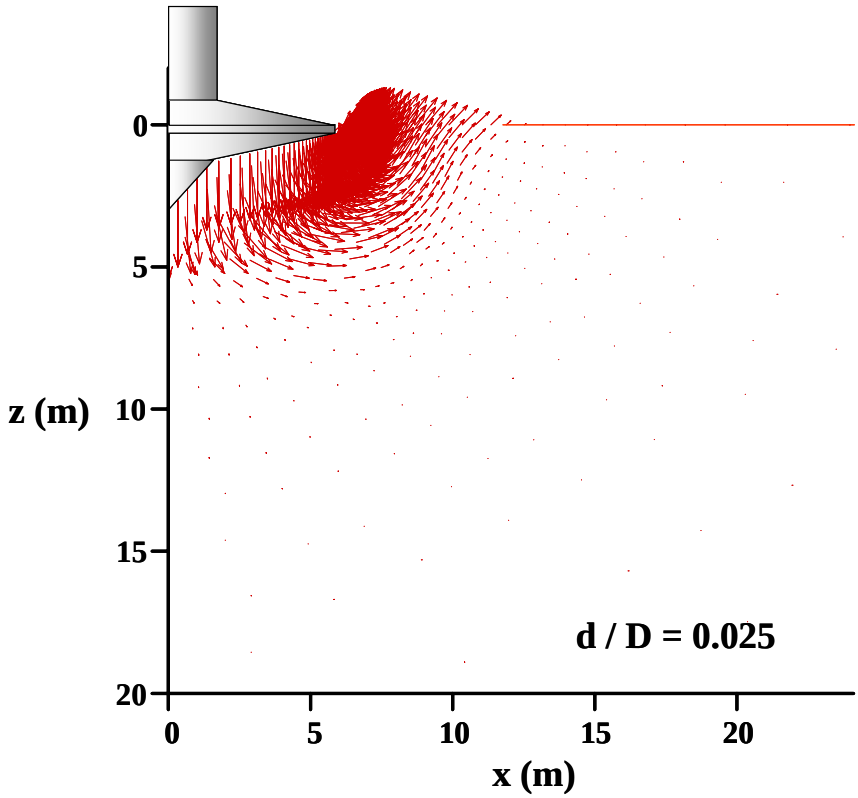

(i) soil heave formed at surface penetration

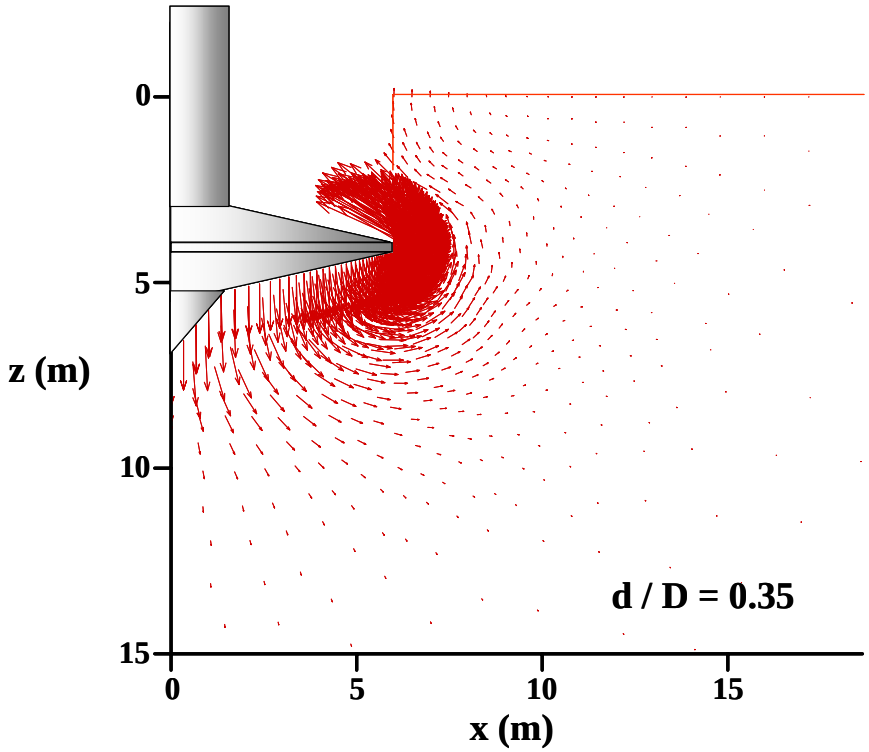

(ii) soil backflow due to flow failure

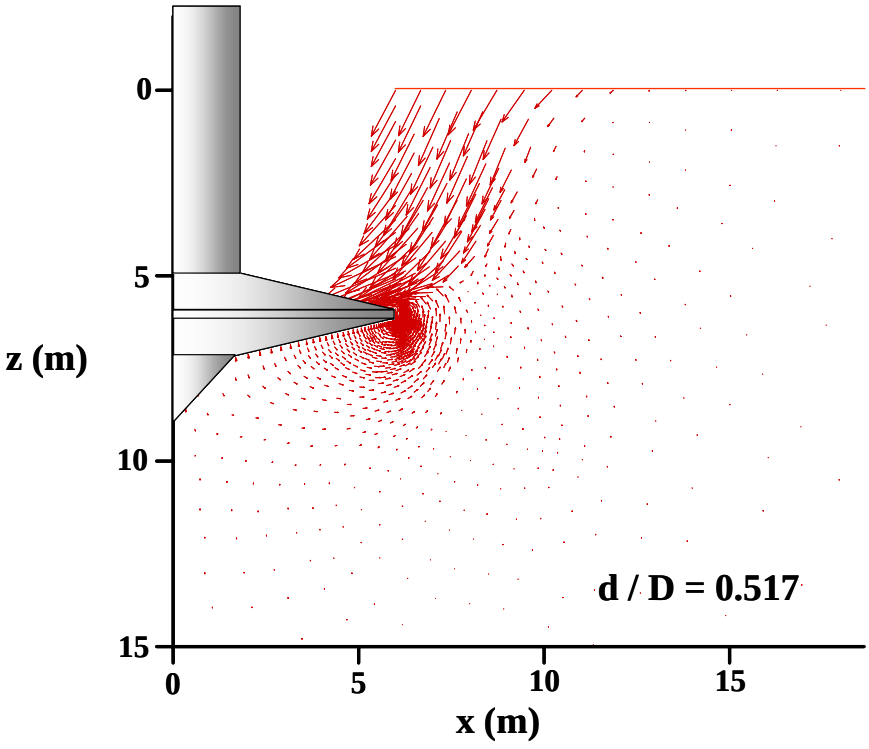

(iii) soil back flow due to wall failure

(b) rough soil-spudcan interface

Figure 5.38 Soil failure mechanisms from FE analyses with a Fully Open Cavity (Case III, Table 3.2)

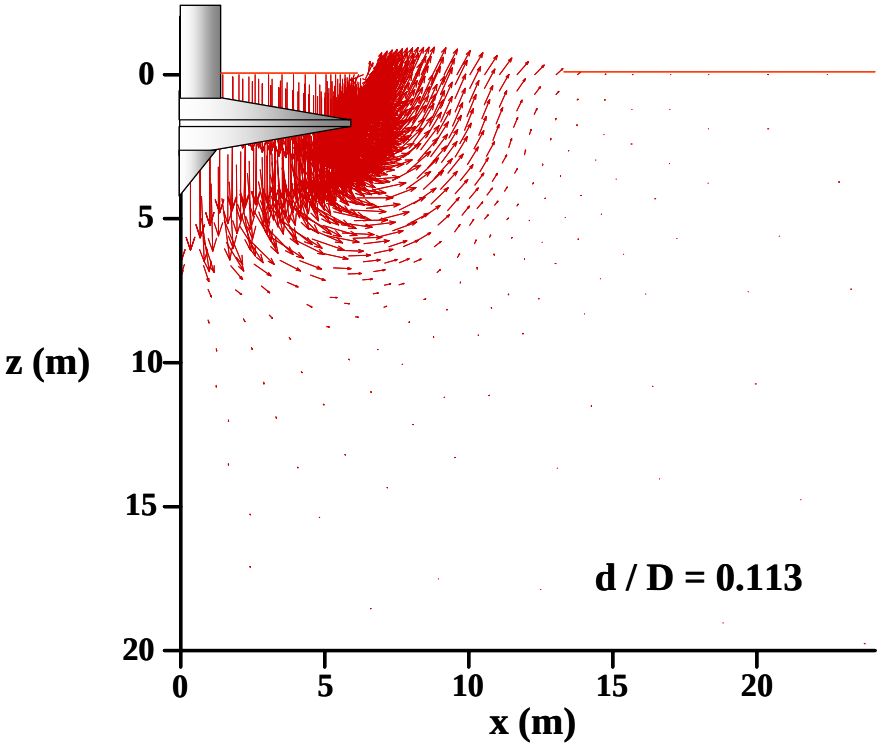
0
5
10
15
20
z (m)
0
5
10
15
20
x (m)
d / D = 0.113

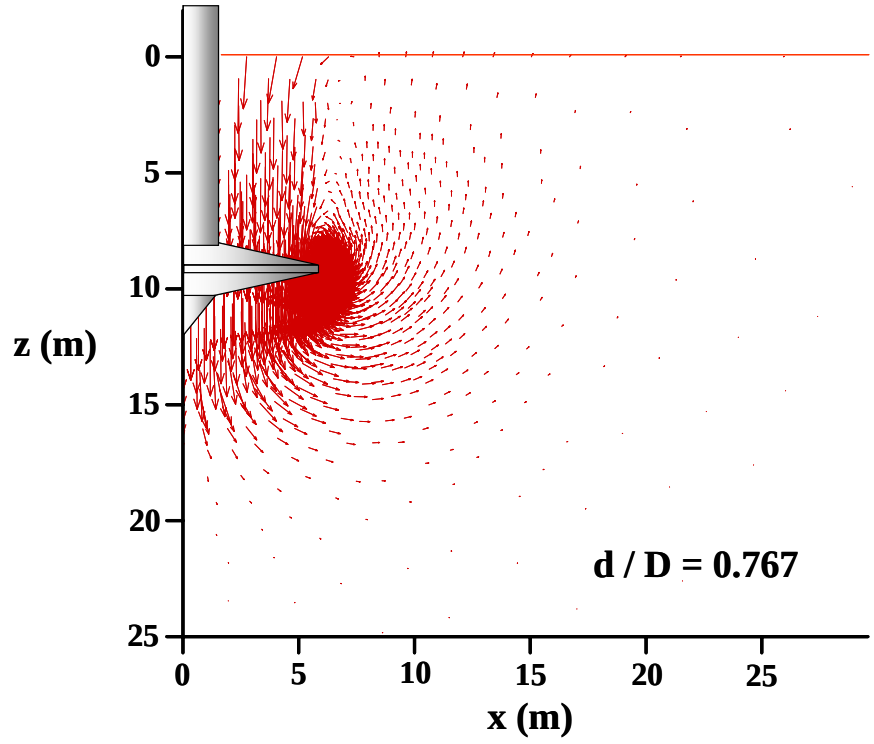
0
5
10
15
20
25
z (m)
0
5
10
15
20
25
x (m)
d / D = 0.767

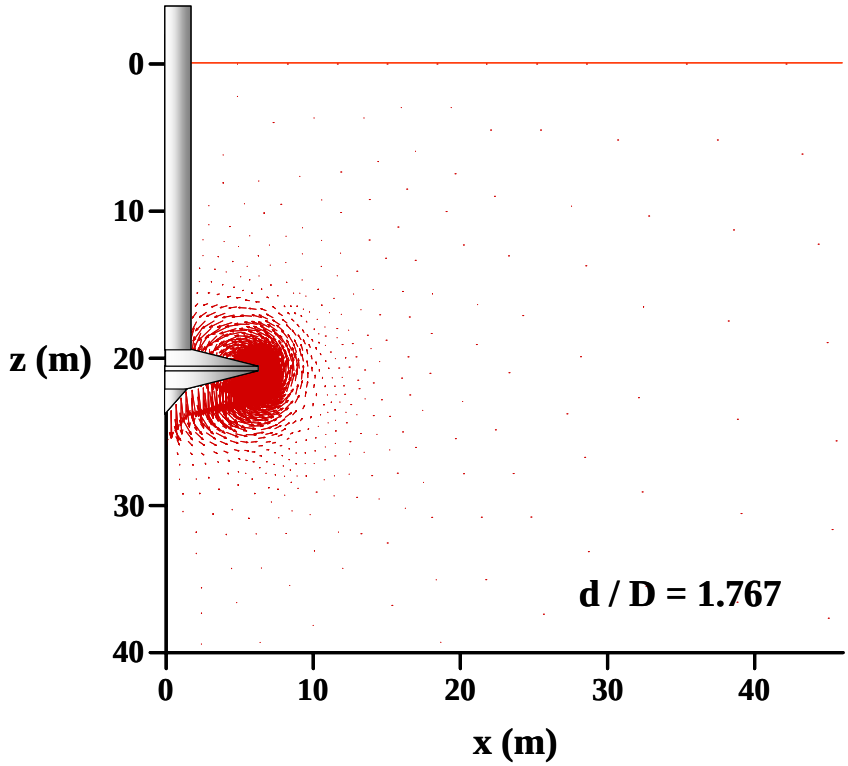

Figure 5.39 Soil failure mechanisms from FE analyses with a Full Backflow (Case III, Table 3.2)

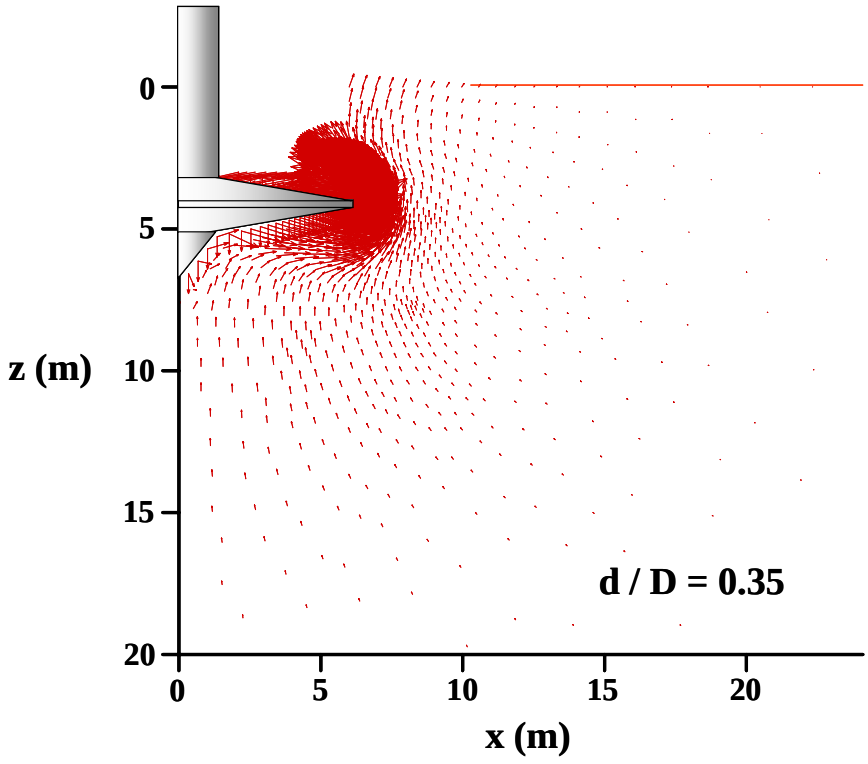

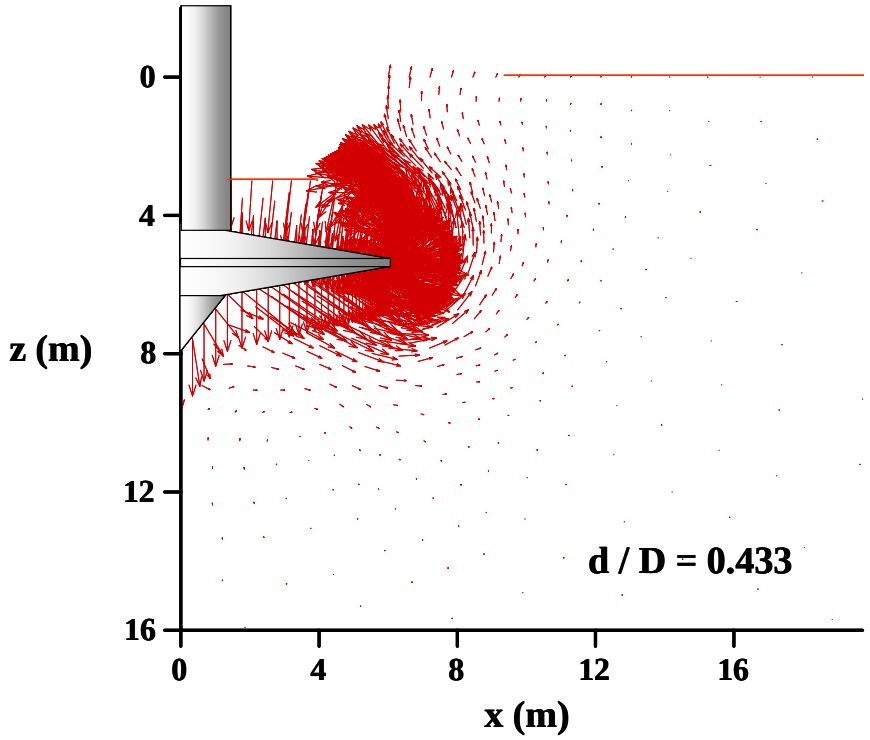
0
4
8
12
16
z (m)
0
4
8
12
16
x (m)
d / D = 0.433

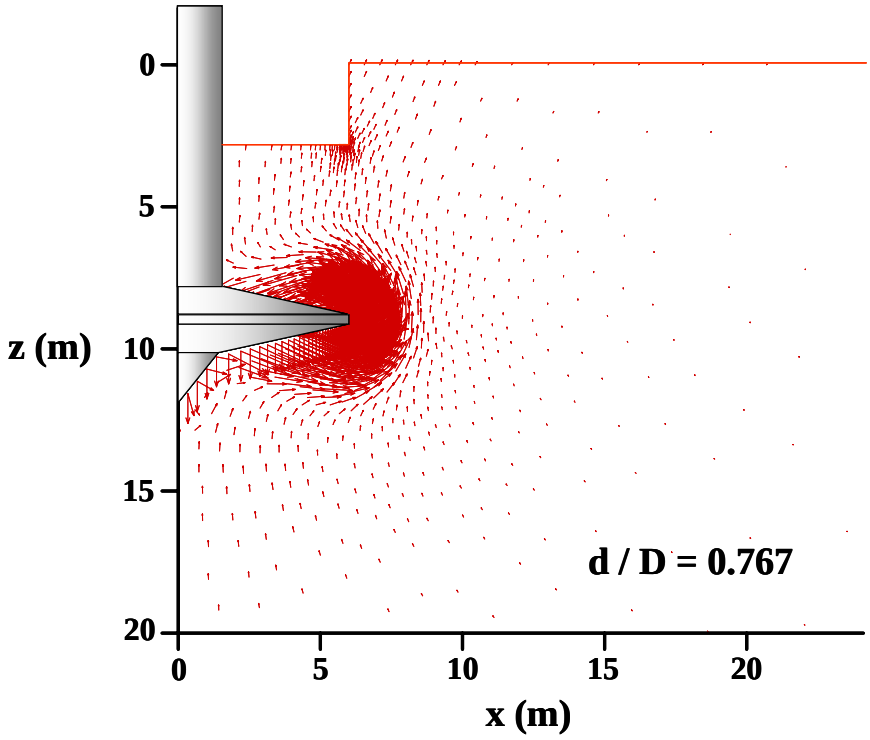
0
5
10
15
20
z (m)
0
5
10
15
20
x (m)
d / D = 0.767

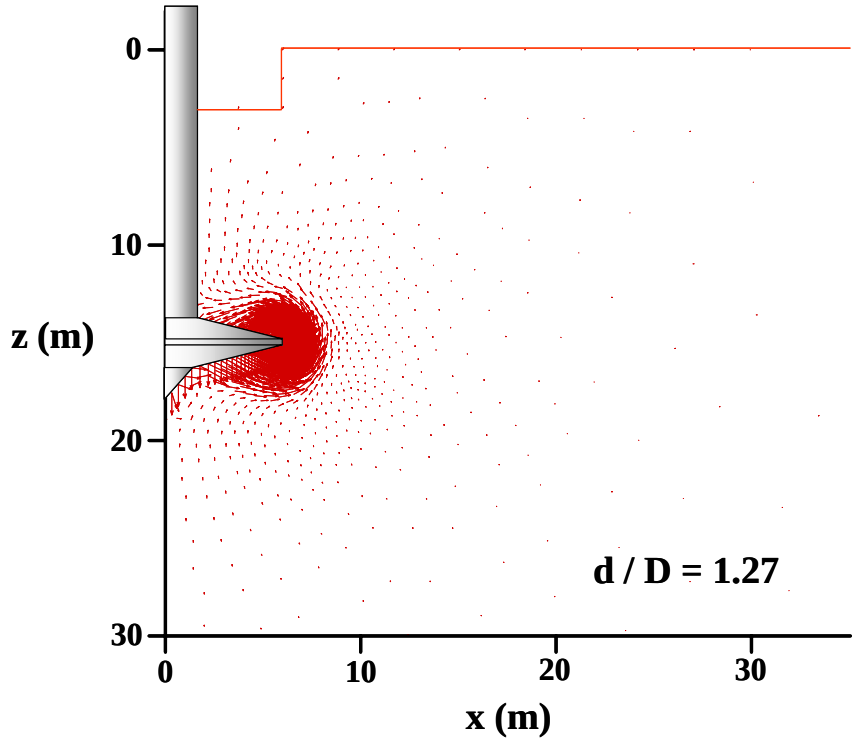

Figure 5.40 Soil failure mechanisms from FE analyses with a Cavity and Partial Backflow (Case III, Table 3.2)

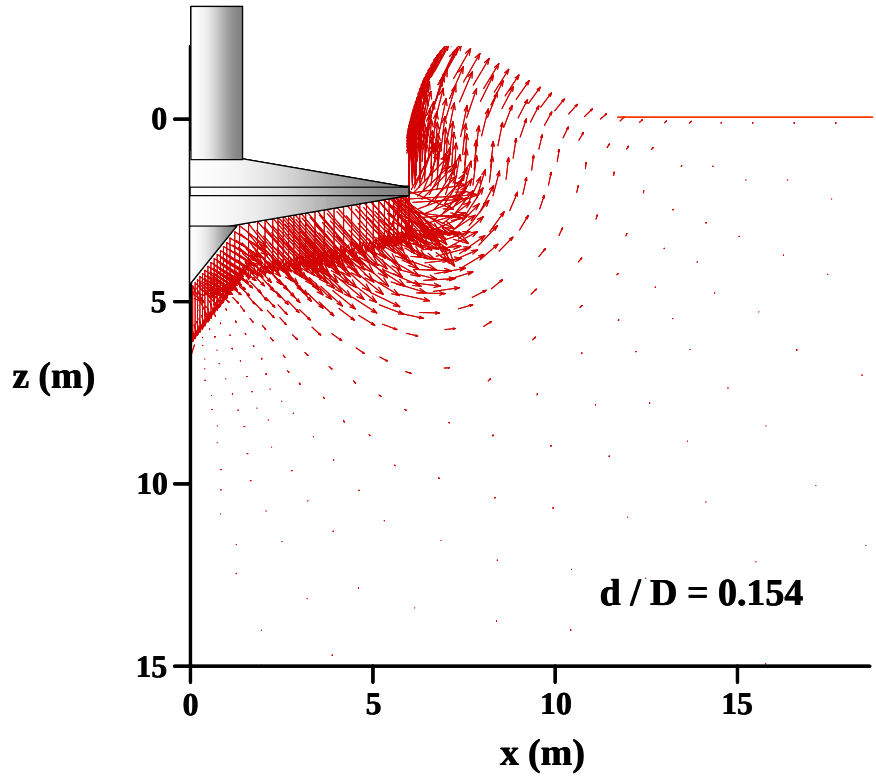

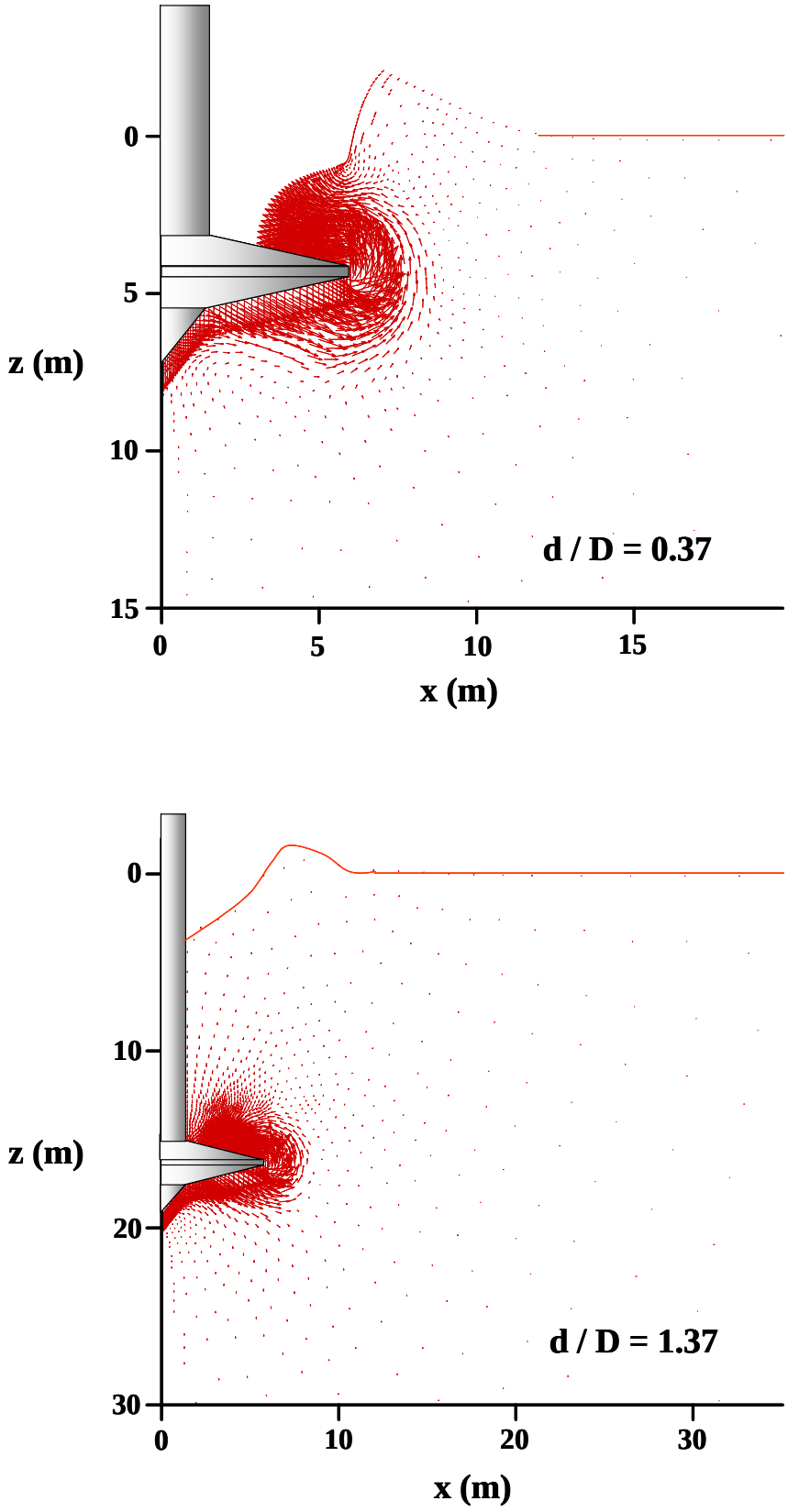

Figure 5.41 Soil failure mechanisms from large deformation FE analyses (Case III, Table 3.2)

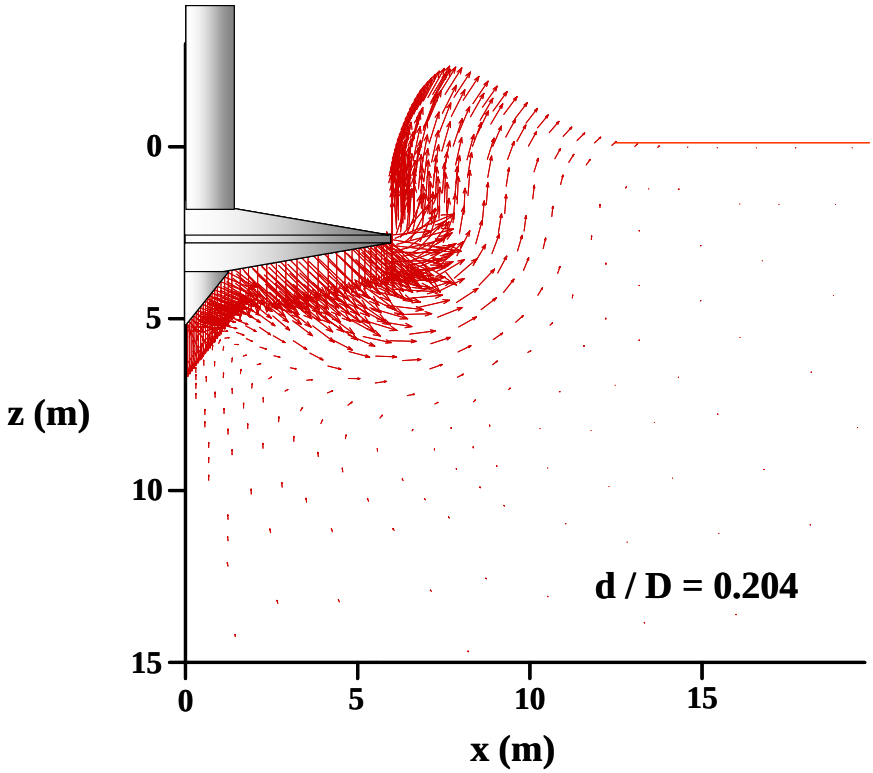
0
5
10
15
z (m)
0
5
10
15
x (m)
d / D = 0.204

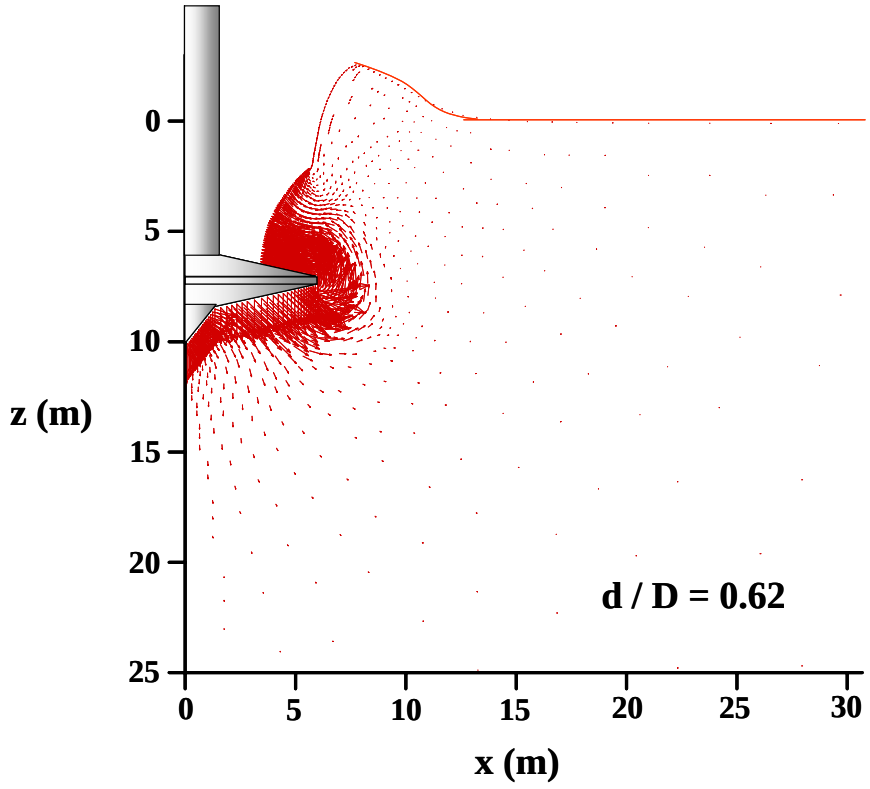
0
5
10
15
20
25
z (m)
0
5
10
15
20
25
30
x (m)
d / D = 0.62

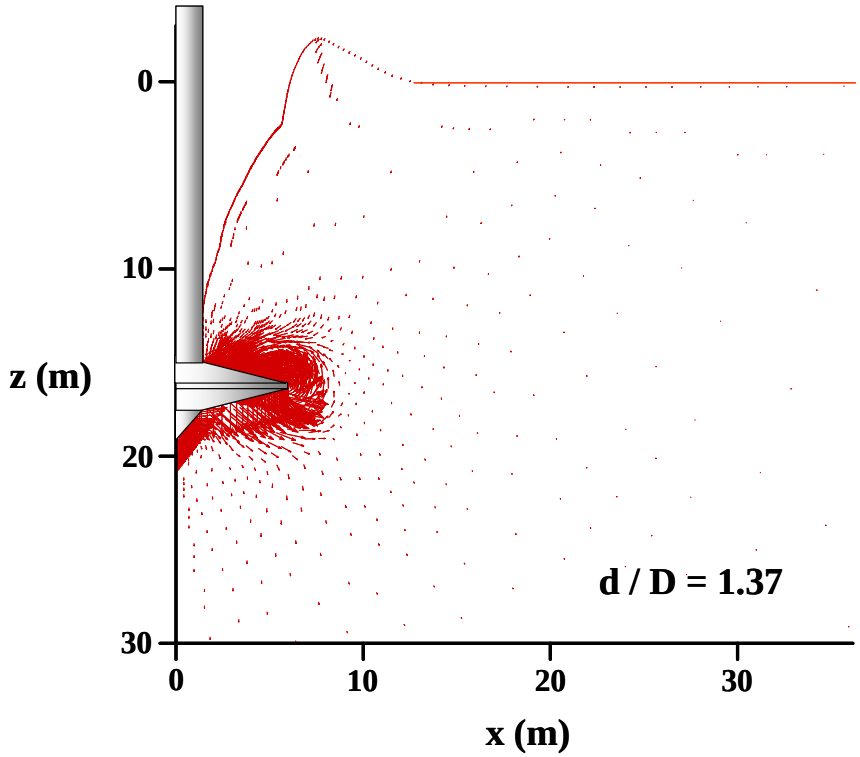

Figure 5.42 Soil failure mechanisms from large deformation FE analyses (Case VI, Table 3.2)

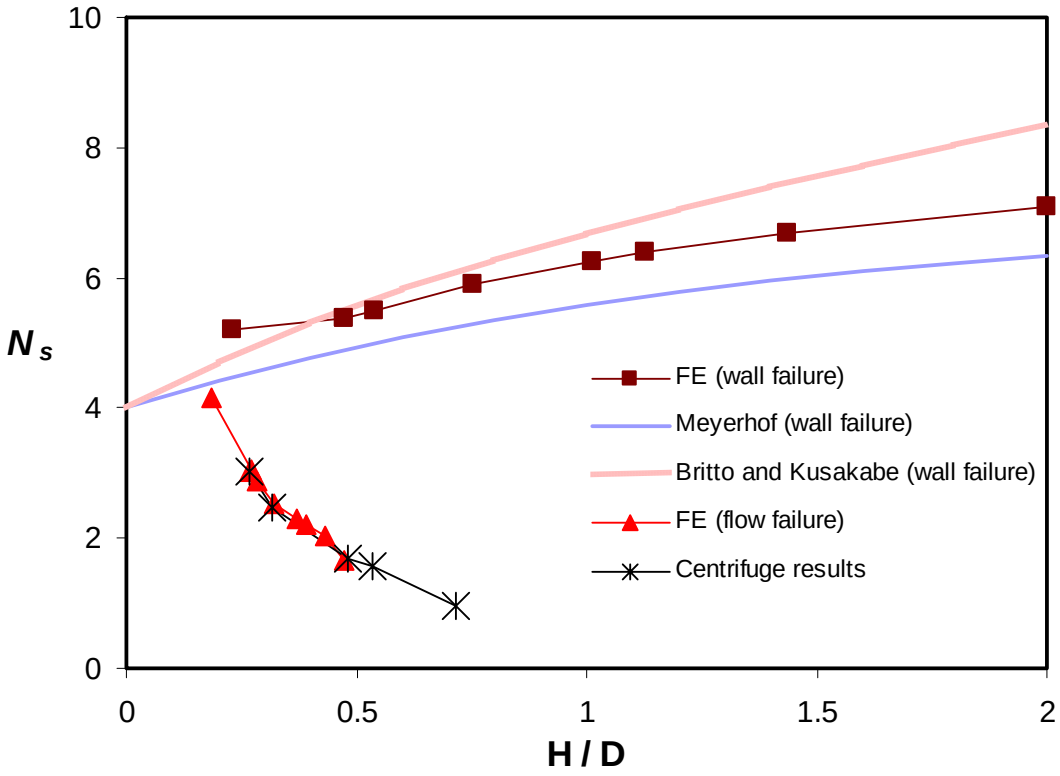

Figure 5.43 Cavity stability from flow failure and wall failure

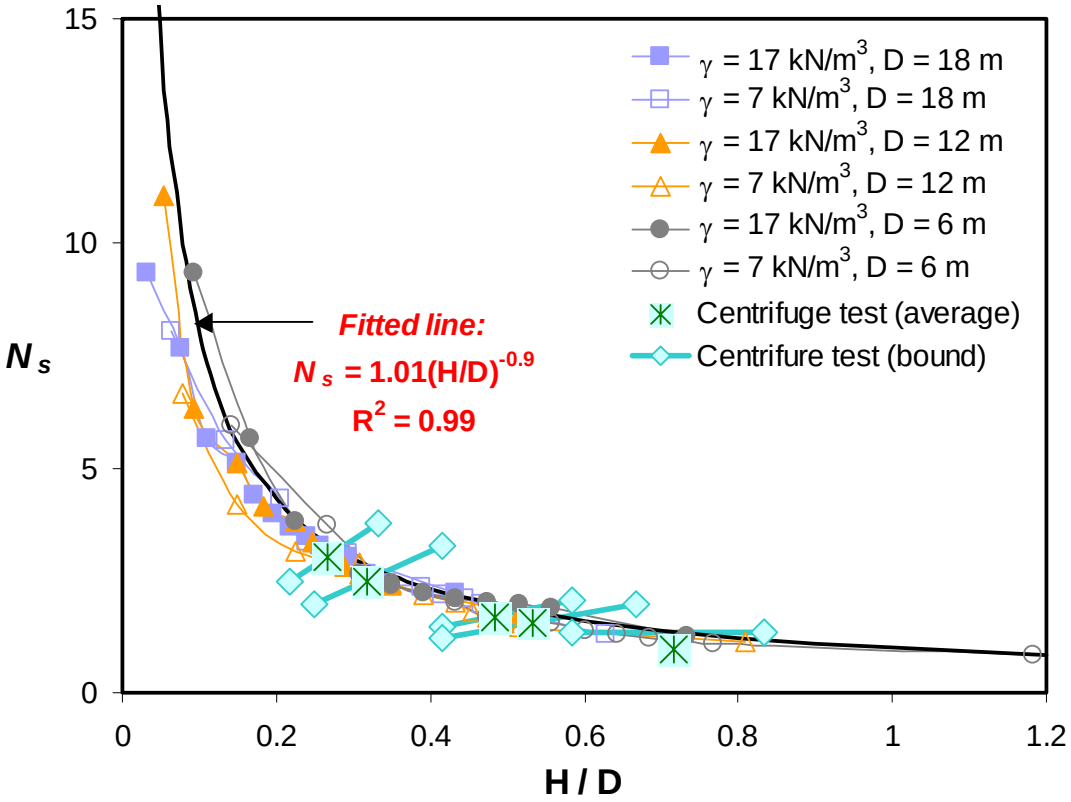

Figure 5.44 Stability chart for flow failure mechanism using stability number, N_s

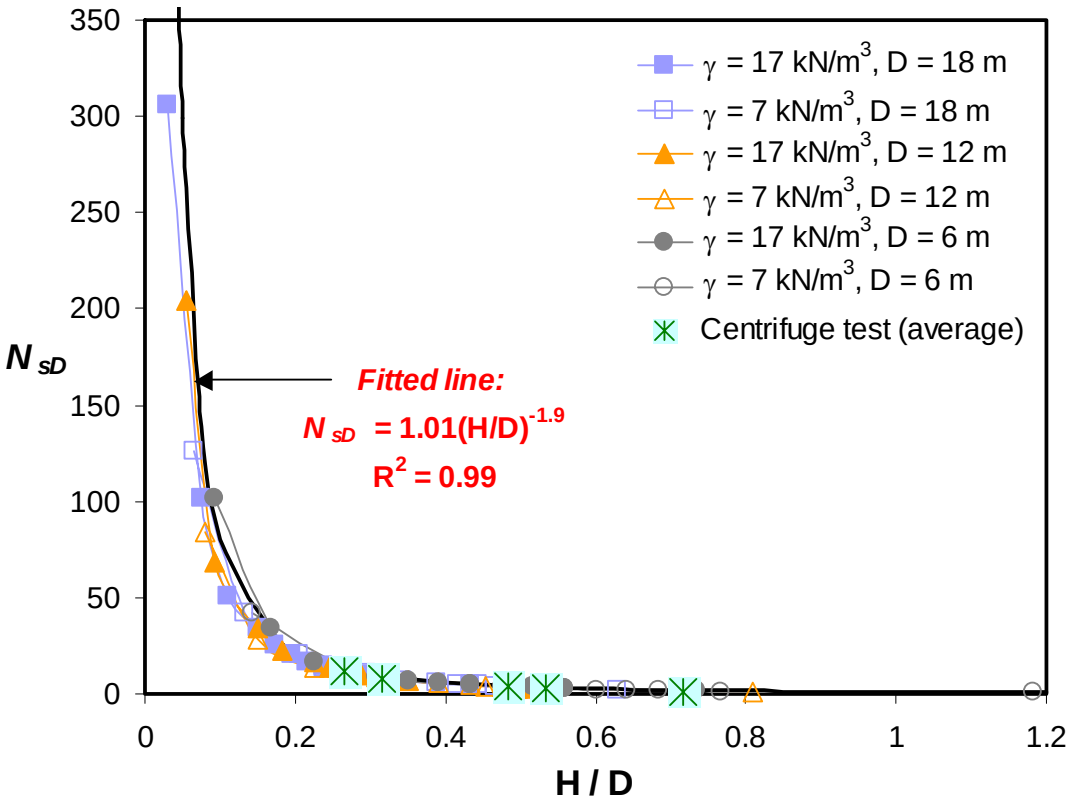

Figure 5.45 Stability chart for flow failure mechanism using stability number, N_{sD}

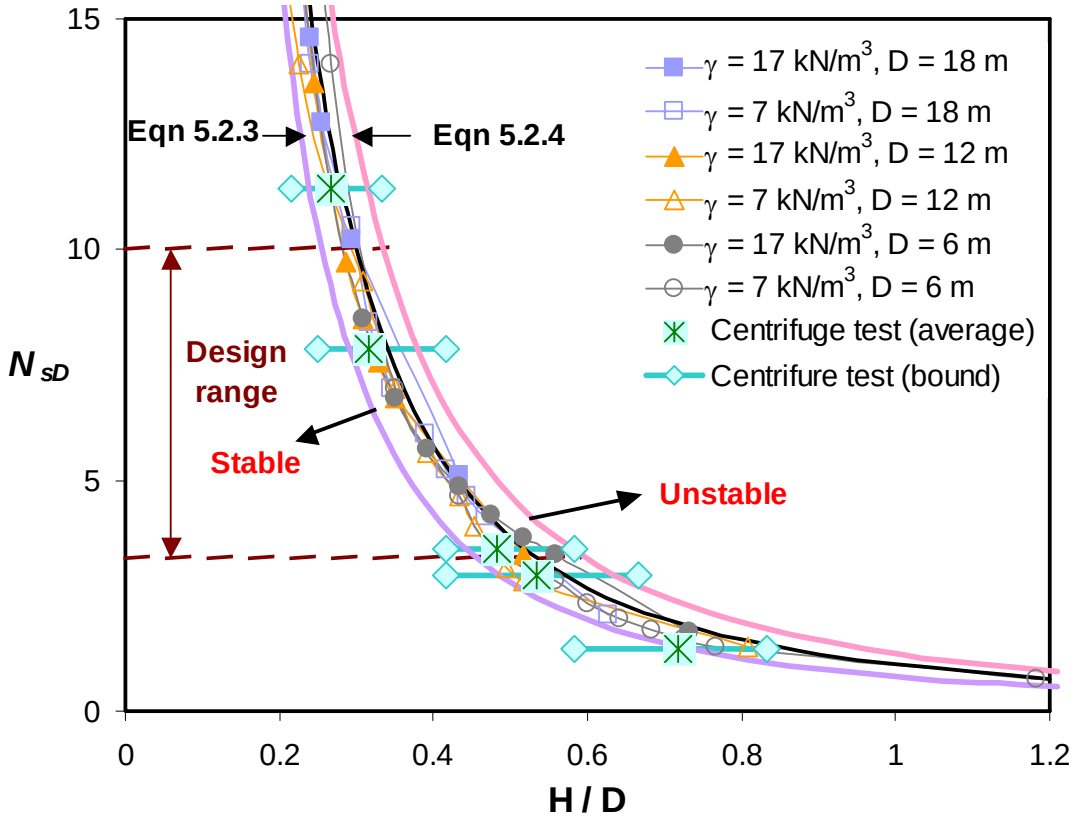

Figure 5.46 Design stability chart for practical using

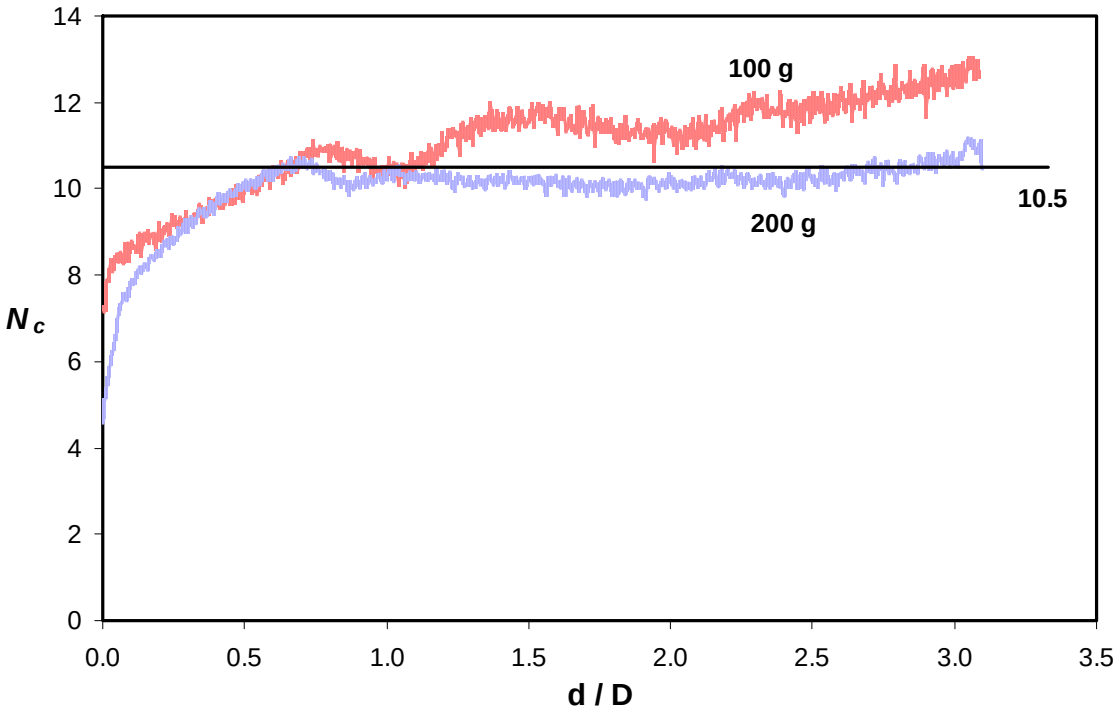

Figure 5.47 Bearing capacity factor, N_c of spudcan in uniform clay (Event 5)

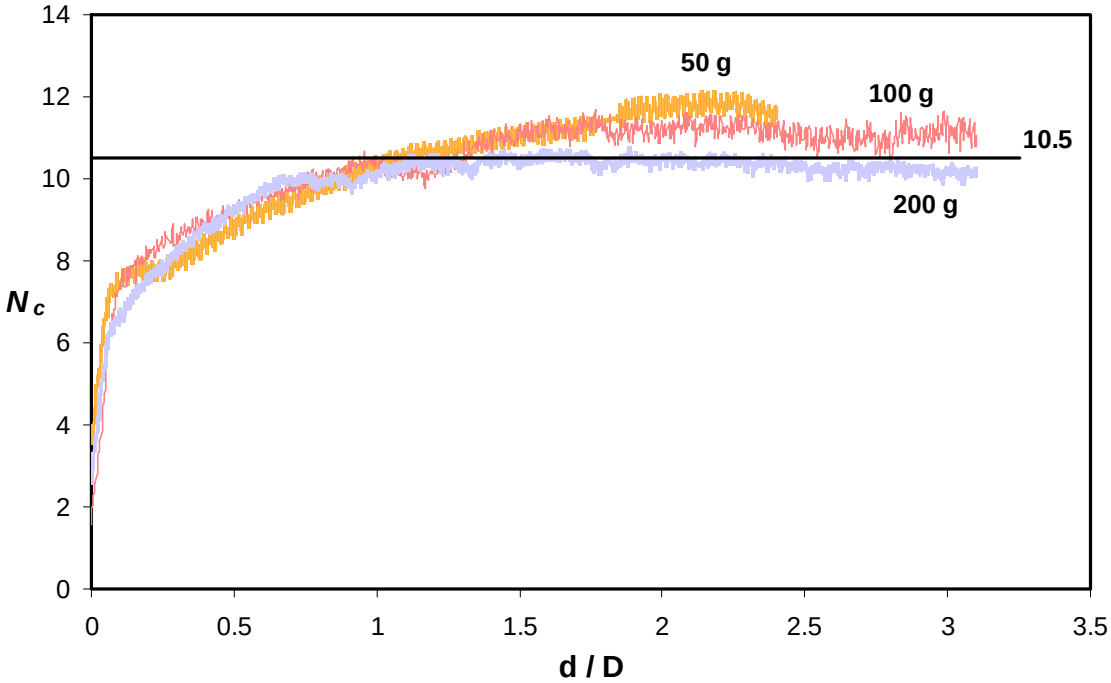

Figure 5.48 Bearing capacity factor, N_c of spudcan in saturated clay (Event 6, without water on top)

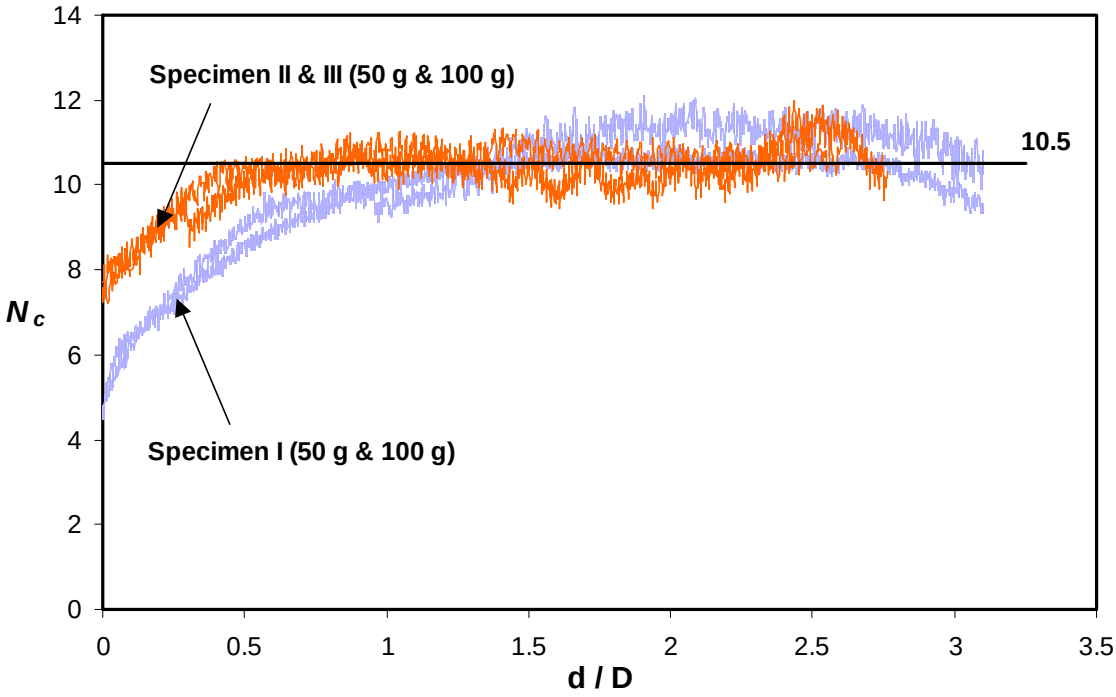

Figure 5.49 Bearing capacity factor, N_c of spudcan in submerged clay (Event 7, with water on top)

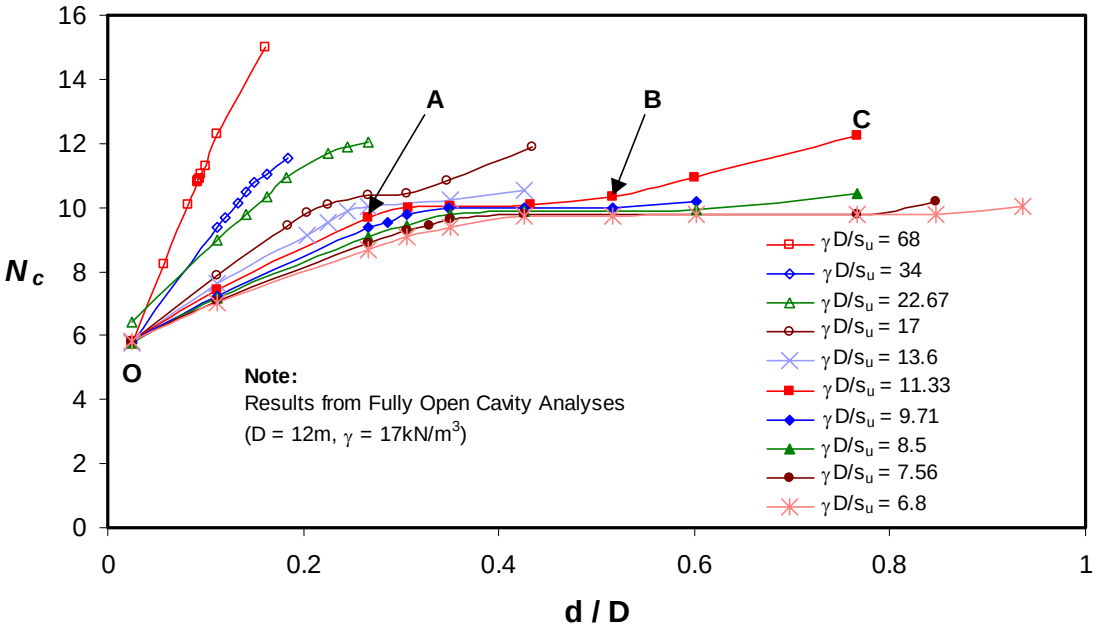

Figure 5.50 Bearing capacity factor, N_c of spudcan with a fully Open Cavity (D = 12m, γ = 17 kN/m^3)

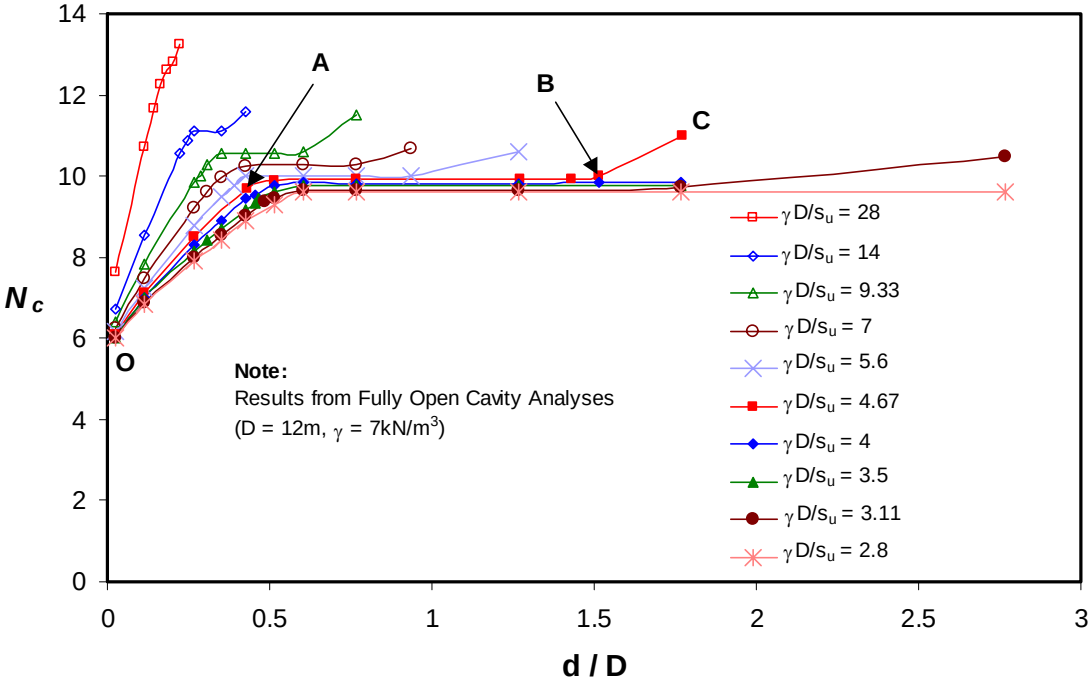

Figure 5.51 Bearing capacity factor, N_c of spudcan with a fully Open Cavity (D = 12 m, γ = 7 kN/m^3)

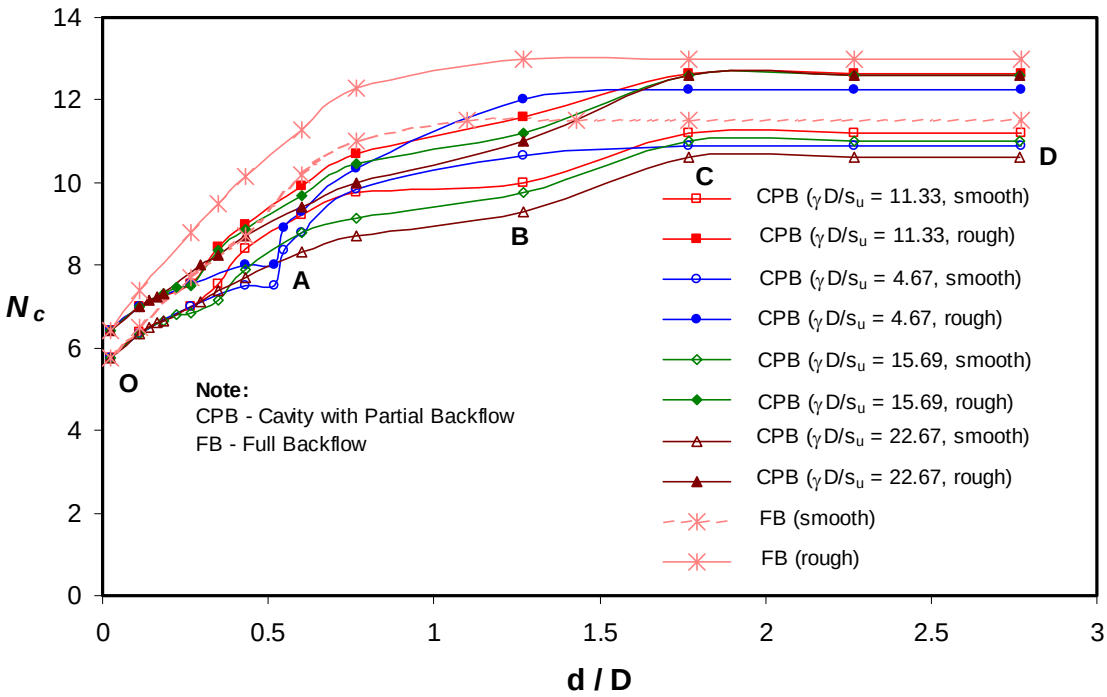

Figure 5.52 Effects of open cavity and soil-spudcan interface on N_c value in Cavity with Partial Backflow and Full Backflow cases (D = 12 m)

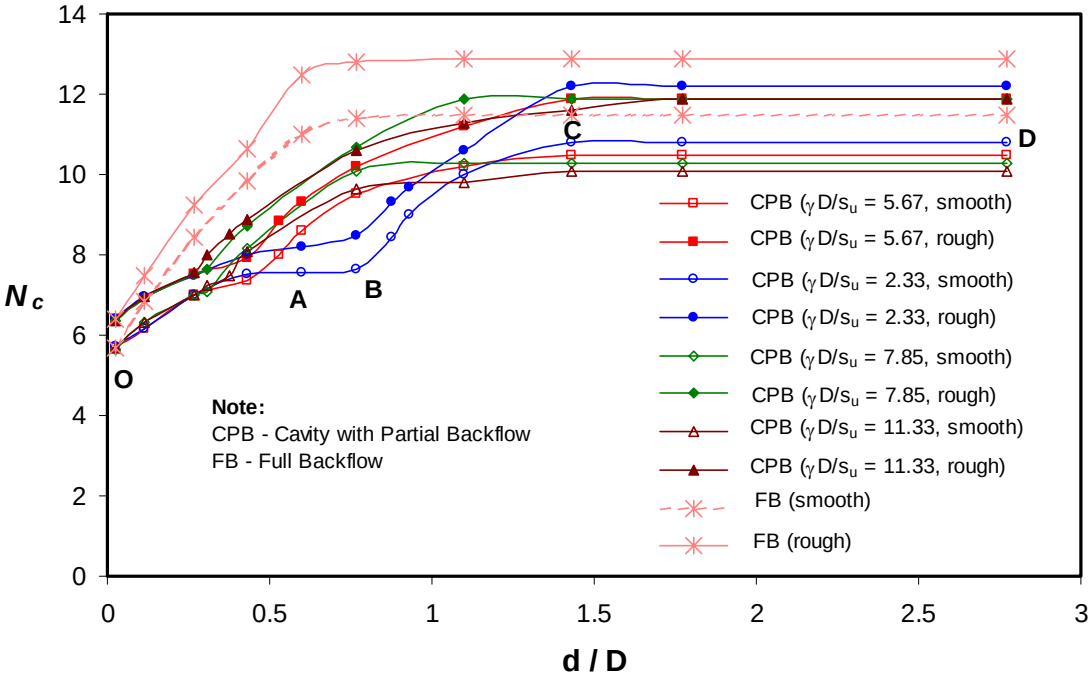

Figure 5.53 Effects of open cavity and soil-spudcan interface on N_c value in Cavity with Partial Backflow and Full Backflow cases (D = 6 m)

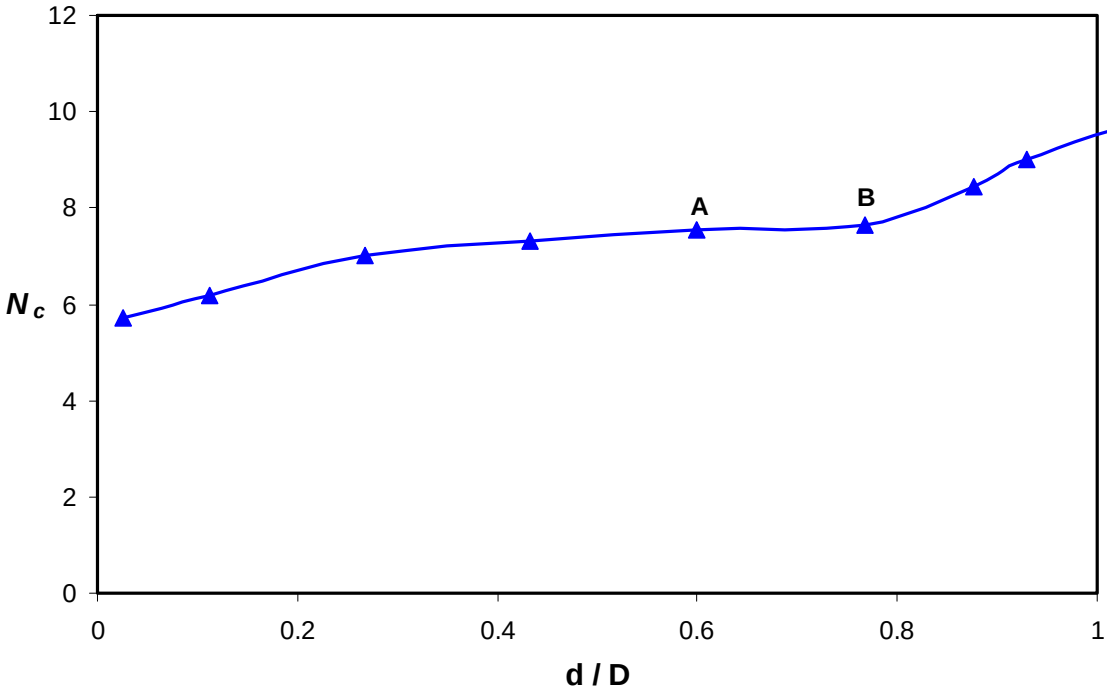

Figure 5.54 Effect of soil backflow on N_c value

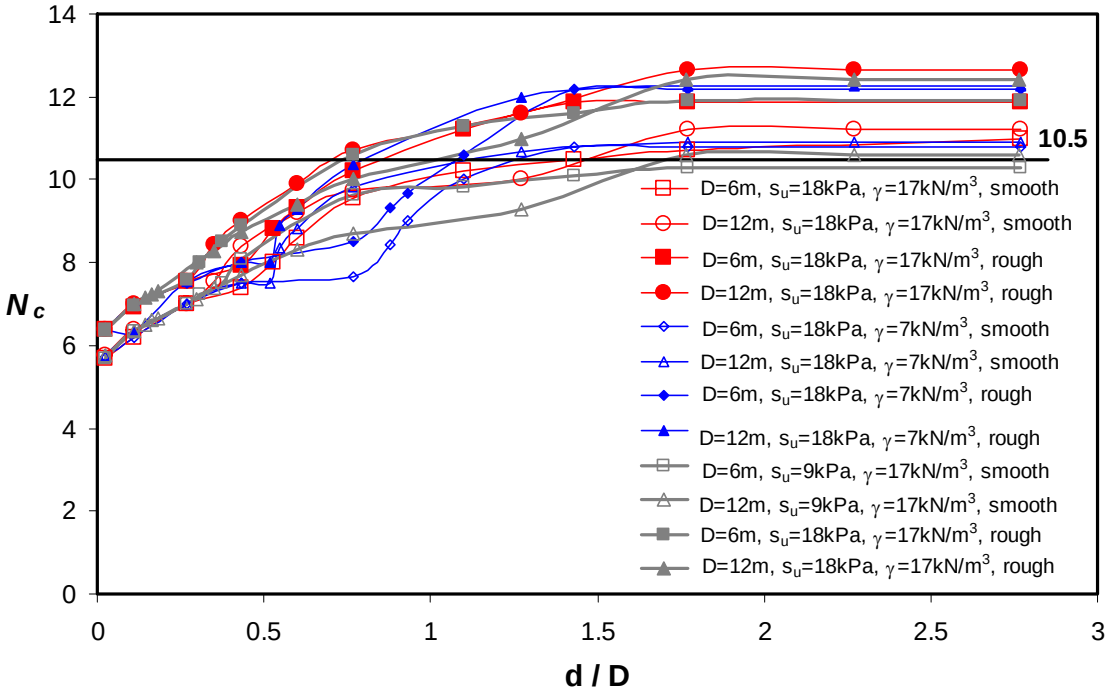

Figure 5.55 Effects of diameter and soil-spudcan interface on N_c value in Cavity with Partial Backflow case

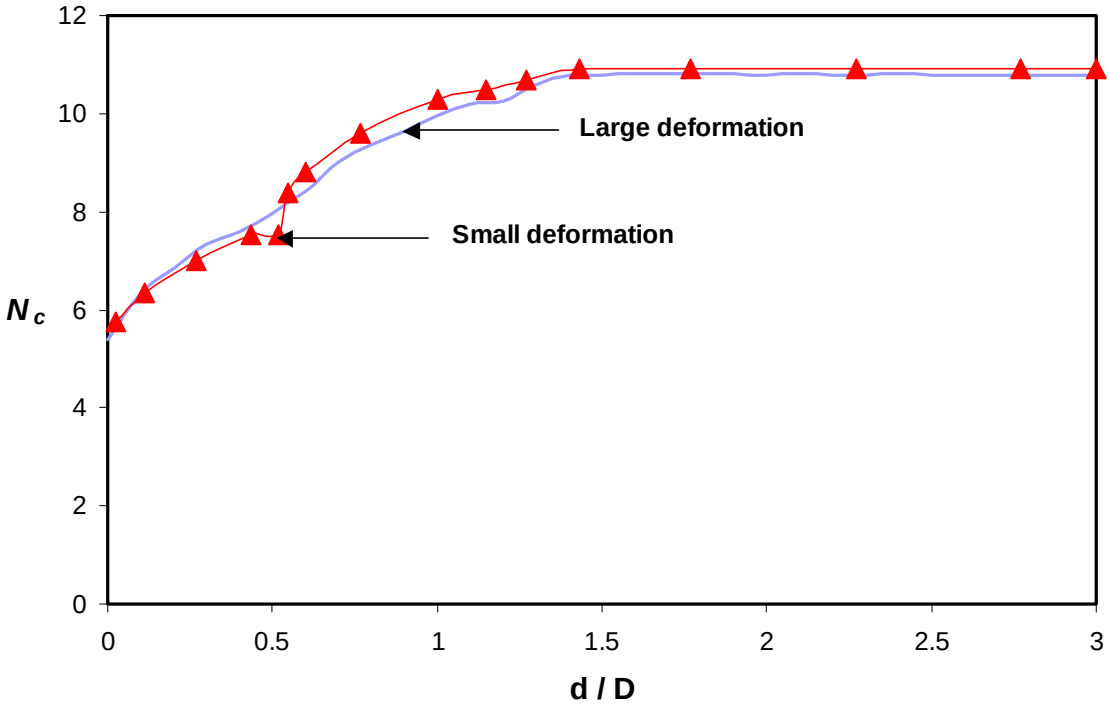

Figure 5.56 Typical bearing capacity profile from small and large deformation FE analysis (D = 12 m, s_u = 18 kPa, γ = 7 kN/m^3)

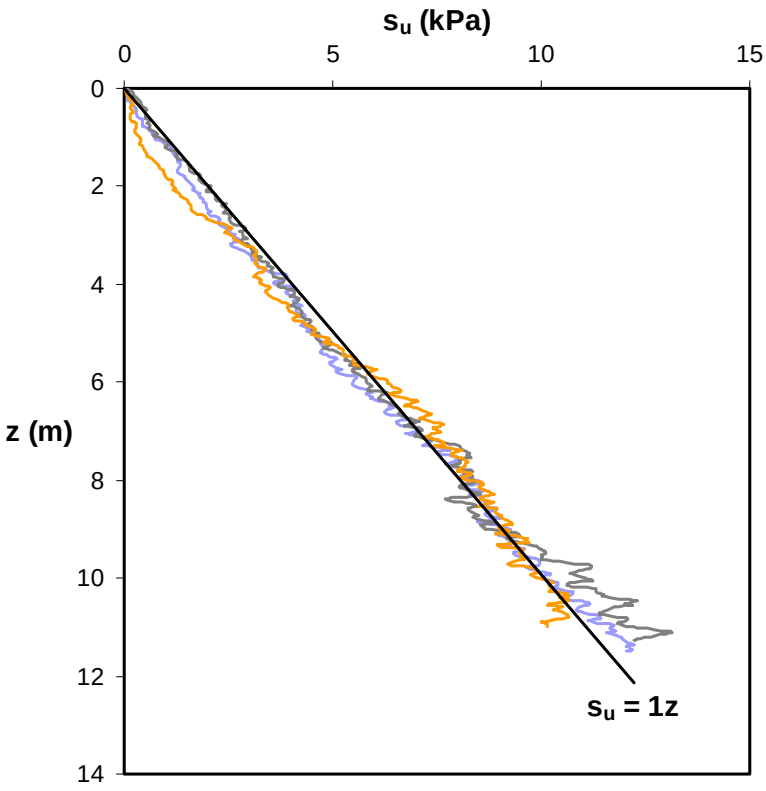

Figure 5.57 Strength profile of NC clay at 100 g

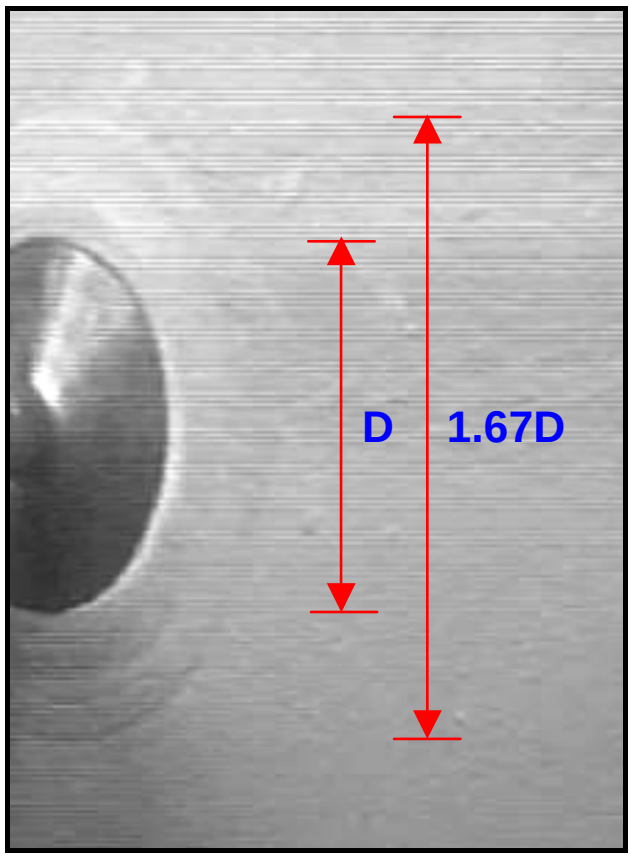

(a) surface foundation

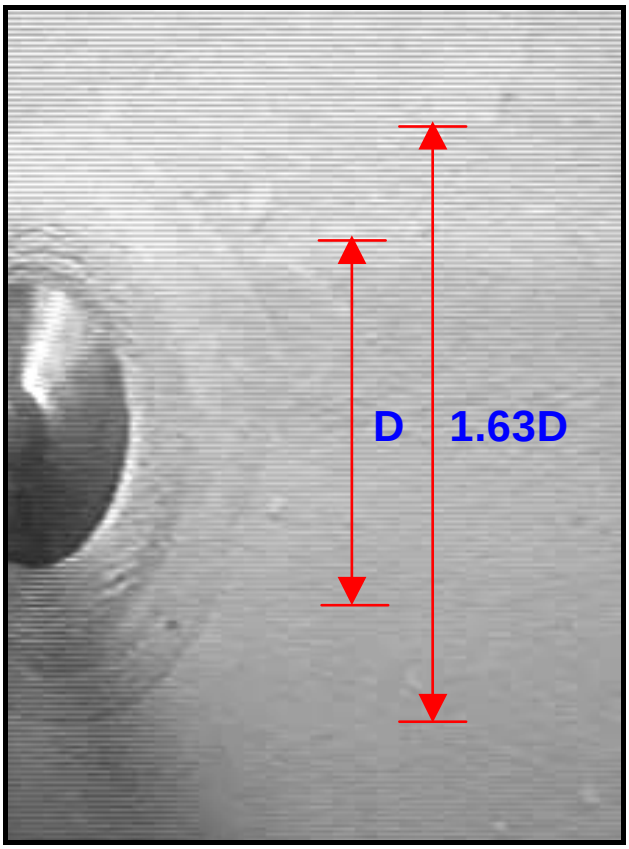

(b) soil backflow

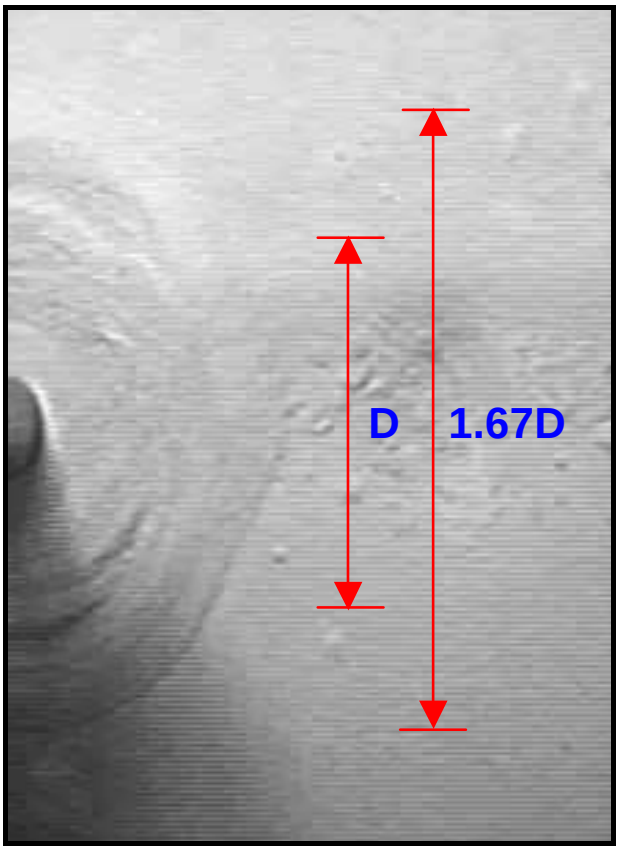

(c) deep foundation

Figure 5.58 Soil flow mechanisms from centrifuge tests in NC clay

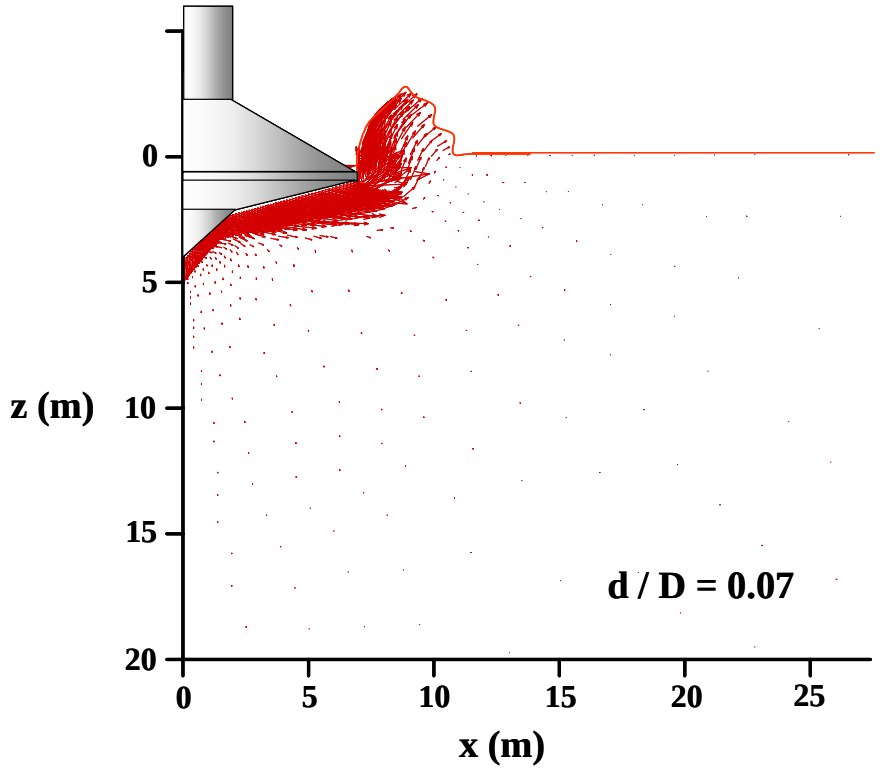

(a) soil heave

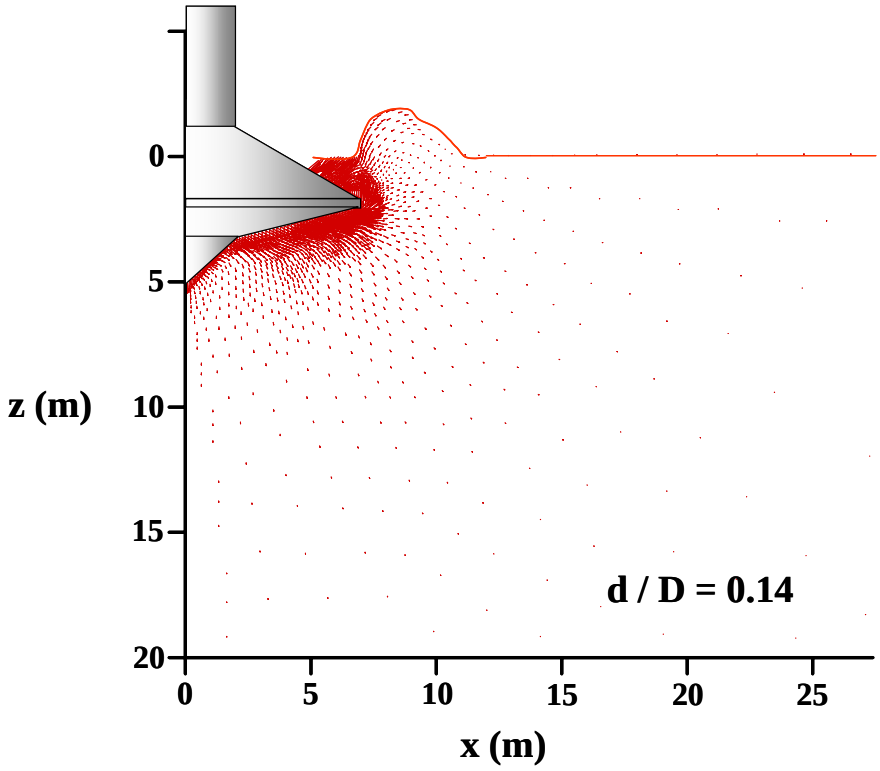

(b) soil back flow

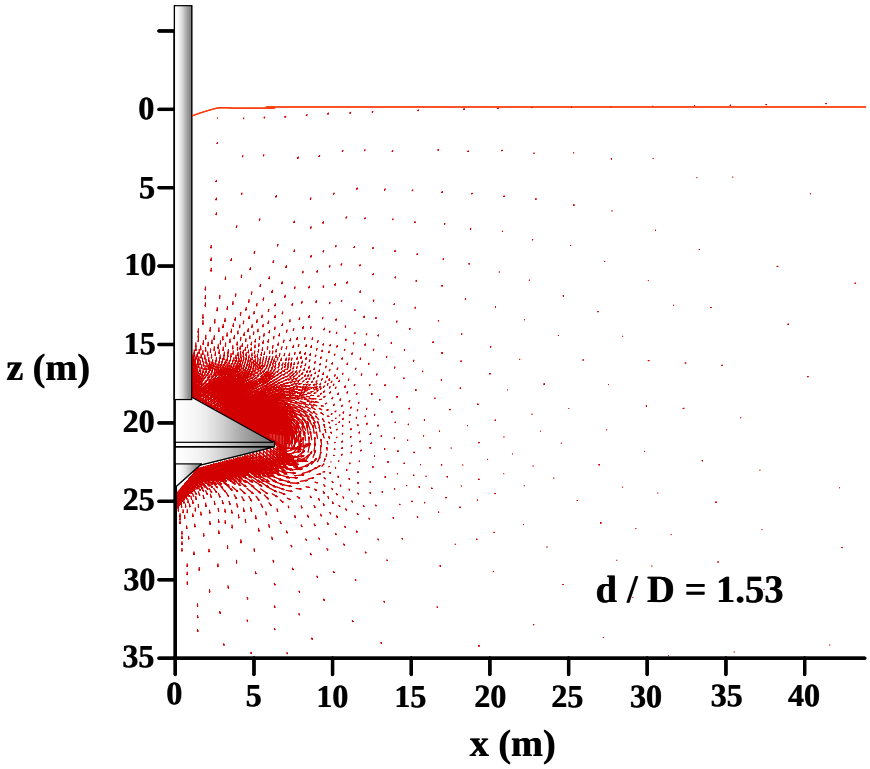

(c) localised flow

Figure 5.59 Soil failure mechanisms from FE analysis in NC clay (s_u = 1z, after Hossain *et al*., 2004)

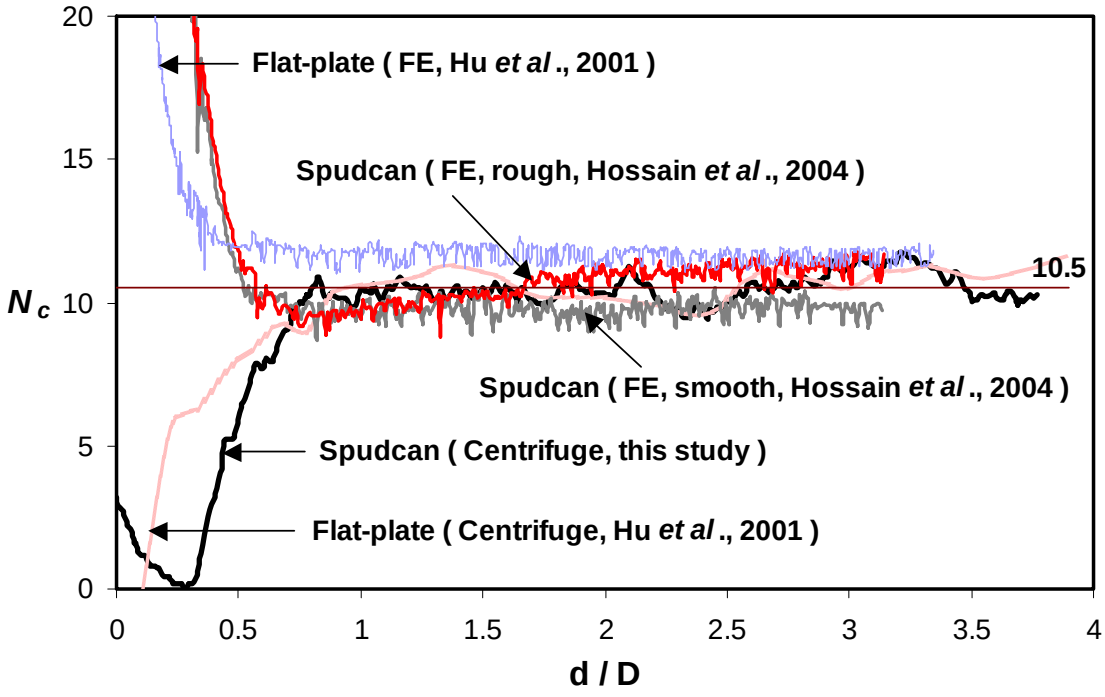

Figure 5.60 Bearing capacity factor, N_c of spudcan in NC clay

CHAPTER 6

CONCLUSIONS AND FUTURE RESEARCH

6.1 Introduction

Drum centrifuge testing and finite element analysis have been conducted to study soil flow mechanisms and bearing capacity response during the preloading of spudcan foundations. Experiments were conducted on a uniform clay bed without and with free water on top. A half-spudcan model, with drawn grids or sprinkled black flock on the soil specimens, was used to film soil deformation during spudcan penetration. The deformation of the drawn grids provided observations on soil deformation. Also the images with black flock were used in subsequent PIV analysis to give soil flow vectors, which showed more accurate measurements of soil deformation than the drawn grids. A full-spudcan model was used to investigate load-penetration response. Small strain and large deformation finite element (FE) analyses were performed using AFENA assuming smooth and rough soil-spudcan interfaces. In small strain FE analysis, an ultimate bearing capacity was explored, where three cavity conditions were simulated: Fully Open Cavity, Cavity with Partial Back Flow and Full Back Flow. A few centrifuge tests were also performed on normally consolidated (NC) clay. The concluding remarks from this study are summarized below.

6.2 Undrained Shear Strength, s_u in Centrifuge

The Kaolin clay samples, which are pre-consolidated at 1 g under pressure from 100 kPa to 200 kPa (σ'_{vp}), show a fairly uniform undrained shear strength after the

consolidation was accomplished. However, under different gravity levels in drum centrifuge such as 50 g, 100 g and 200 g, the soil samples experience swelling and re-consolidation. Thus, a soil strength test - T-bar test needs to be conducted before and after each footing test to obtain actual soil strength during footing penetration.

The swelling and re-consolidation effects depend on the testing gravity level and the corresponding elapsed time in the centrifuge. When the average soil stress level in the soil specimen is lower than the preconsolidation pressure, the soil is subjected to swelling and hence softens. On the contrary, when the soil overburden pressure exceeds the preconsolidation pressure in the specimen, the soil is subjected to reconsolidation and hence stiffens. Apart form the acceleration level, the in-flight elapsed time plays a significant role in these effects (swelling and reconsolidation) and in strength measurements. Therefore, typically for a soil specimen under σ'_{vp} = 150 kPa, a sightly lower strength is obtained at 50 g and 100 g but a higher strength at 200 g test, when comparing with its strength under 1g.

It is also observed that, a slightly higher strength often exists at the upper layer of the soil sample when free water on top was not present. This is due to the desiccation effect by evaporation as it was open to the atmosphere during flight. However, a relatively uniform strength is found in the rest of the soil sample without free water on top.

A softening effect near the surface of soil sample is apparent in the soil sample with free water on top, along with the swelling and reconsolidation effects under various acceleration levels as stated above. The surface softening is due to the water absorption, thus the in-flight elapsed time plays a crucial role here. When the in-flight elapsed time is long enough, an initially uniform soil sample can become a normally consolidated sample with soil strength increasing with depth. Therefore, to conduct a foundation test under a desired soil strength profile, care needs to be taken with the in-flight elapsed time, particularly when soil sample is under free water.

When a soil sample is lightly consolidated under σ_{vp} = 25 kPa pre-consolidation pressure, non-uniform strength profiles are often obtained under centrifuge accelerations, such as 100 g or 200 g. The alarming strength profiles, with higher

strength at the top and bottom layer but lower strength in the middle layer of the soil, is due to the re-consolidation effect near the top and bottom drainage layers. This type of seabed profile opens an opportunity for 'punch-through' failure (major cause of catastrophic failure) of jack-up rig during installation. Therefore, more care needs to be taken when a soil sample is lightly consolidated.

6.3 Soil Flow Mechanisms

In centrifuge testing, in order to visualize the soil failure mechanisms clearly with half-spudcan model, the following techniques eventually are found to work properly:

- 1 mm rubber "O" ring around the spudcan periphery along with a thickened stiffener at the rear side of the leg should be used to ensure that the half-spudcan penetrates tightly against the observing window. This is to stop soil squeezing in between the model spudcan and the window.
- High-resolution digital camera obviously captures better images than video camera.
- Centrifuge sliprings should not be used in transferring images if possible, since they are unreliable.
- The camera should be faced at right angles to the window and focused towards the axis of penetration.
- Black 'flock' powder has provided better images for PIV analysis to give better understanding of soil flow than grids.

In the investigation of soil flow mechanisms during spudcan penetration into uniform clay, half-spudcan centrifuge testing with PIV analysis and FE analysis were performed. There are three stages of soil flow found in this study while the spudcan was penetrating into soil from the surface.

At the initial stage of penetration, as the spudcan foundation penetrates from the soil surface, a fully open cavity is formed above the spudcan foundation. At this stage, a classical feature of soil general bearing capacity failure for shallow footing is observed. It is found that a significant vertical downward movement of soil

underneath the spudcan spigot (up to 1 D deep) forms a soil wedge. The region of this wedge spreads about 0.8 D horizontally. At the same time, the soil around the spudcan shoulders moves with a transition from laterally to upward. Thus soil heave occurs close to the spudcan shoulders at the soil surface. The formation of heave is more marked when a free water layer is present on top of the soil specimen, due to the reduced (effective) unit weight. The lateral deformation zone around the spudcan shoulder extends to 1.5~1.6 D.

At the second stage, soil starts to flow back into the cavity on the exposed top of the spudcan. This backflow causes the spudcan to be embedded. However, the cavity formed at the initial penetration remains open. Note, the depth of soil backflow (or this stable open cavity) depends on the corresponding soil strength (s_u), density (γ without free water, γ' with free water) and footing size (D), i.e. stability number, $N_{sD} = \gamma D/s_u$. Moreover, the stable cavity depth is independent of the spudcan roughness.

At the last stage with deep penetration, the spudcan becomes fully embedded. The soil flow mechanism reaches the deep failure mechanism with fully localised failure zone. The soil wedge moving vertically with the spudcan reduces to about 0.5 D horizontally. The lateral deformation zone also reduces to 1.26~1.32 D.

Different from the observations in the uniform clay, there is no cavity formed when a spudcan penetrates into a NC clay. The spudcan is embedded immediately after it penetrates below the soil surface. The deep failure mechanism is reached at 1.0 D penetration. The lateral distortion zone around the spudcan shoulder is about 1.67 D at surface penetration and reduced to 1.3 D at deep penetration, which agrees well with the result in OC clay.

6.4 Stability Number

Since a cavity is formed at the initial stages of spudcan penetration into a uniform clay, the subsequent mechanism of soil infill into the cavity and remained stable cavity depth (H) were investigated. The finding from this study is compared with the

recommendations in the current offshore design guidelines (SNAME, 1997). The following conclusions can be drawn.

From the centrifuge image analysis and FE numerical analysis, it is found that the soil back flow is due to a *Flow Failure* mechanism, in which the soil flows back into the cavity caused by the spudcan penetration action. However, in the current offshore design guidelines (SNAME, 1997), the stable cavity depth calculation is based on a *Wall Failure* mechanism, when the cavity wall is too high to stand. The FE analysis has revealed that the prediction of stable cavity depth can be 4 times higher by the wall failure mechanism than that by the flow failure mechanism. This fully explains why the wall failure was never observed in the centrifuge tests.

Due to the new findings in determination of the soil back flow mechanism, i.e. *Flow Failure*, a unique new design chart has been developed as N_{sD} vs H/D ($N_{sD} = \gamma D/s_u$, where γ needs to be substituted by γ' for soil under water). It shows that the relative stable cavity depth (H/D) is increasing with decreasing stability number (N_{sD}) parabolically, i.e. with increasing soil strength (s_u) when γ and D are kept the same. This design chart is more convenient for design purpose than the one recommended in the design guidelines, i.e. N_s vs H/D ($N_s = \gamma H/s_u$, where γ needs to be substituted by γ' for soil under water), since in the new chart (N_{sD} vs H/D), the stable cavity depth (H) only appears in one axis (H/D), while in the conventional design chart (N_s vs H/D), H is involved in both axes, thus an iteration is needed to determine the stable cavity depth H. A unique algebraic expression with non-dimensionalised variables has been recommended for any sized spudcan foundations in any uniform soils (Equations 5.3.1 and 5.3.2), which can be used in design in conjunction with the design chart.

6.5 Bearing Capacity

Bearing capacity of spudcan in uniform soil has been investigated in centrifuge with a full spudcan model and in FE analysis. Foundation size, shape, roughness and soil

strength conditions are considered. The bearing capacity factor (N_c) has been a common non-dimensionalised variable in any foundation bearing capacity analysis.

Generally, the bearing capacity – penetration curve follows the three stages of soil flow mechanisms, which are shallow failure mechanism, soil back flow leading the transition from a shallow failure mechanism to a deep failure mechanism and deep failure mechanism. When the spudcan penetrates into soil from the surface, the bearing capacity factor (N_c) increases with penetration, since the fully open cavity generates a surcharge to this surface foundation. At the second stage, soil starts to flow back on to the top of the spudcan due to flow failure. The spudcan bearing capacity increases with penetration due to the transformation of the soil flow mechanism from a shallow foundation to a deep foundation. At the final stage, the spudcan bearing capacity reaches its ultimate value and stays constant, when the soil flow mechanism remains as deep/localised.

When the deep failure mechanism is reached at the last stage of spudcan penetration, the bearing capacity factors are N_c = 10.5 and 12 for smooth and rough spudcan respectively in FE analysis. When free water is absent, the centrifuge test results have shown a close value of N_c = 10.5 or slightly above. This might be due to the well polished spudcan model used in the test. All the test results of soil under water have shown a consistent N_c = 10.5, which may be due to the softened soil formed near the free water layer. Therefore, an ultimate N_c = 10.5 is recommended as a conservative value for spudcan bearing capacity design in uniform clay when the foundation has reached the deep soil failure mechanism.

It is very clear that the cavity formation during the initial penetration of spudcan has a strong effect on the spudcan bearing capacity until the spudcan penetrates deep enough to reach the fully localised deep failure mechanism. The critical penetration depth of the deep failure mechanism ($H_{deep\ failure}$) is found to be 1.0 D after the back flow starts. This is a tentative conclusion. A more accurate one can be obtained when more analyses have been conducted.

The shape effect and roughness effect are also studied. By comparing the result of the spudcan with that of the flat-plate, the bearing capacity of a flat-plate is found to

be 8 % higher than that of a spudcan with the same roughness. By comparing a fully rough spudcan with a full smooth spudcan, a rough spudcan can provide 14 % more bearing capacity than a smooth spudcan. However, the bearing capacity of a smooth spudcan can be used in design safely when the soil-spudcan roughness is not clear.

In NC clay, the bearing capacity factor from the centrifuge test is compared with the results of FE analysis presented elsewhere. The high N_c value in the initial penetration is associated with the very low soil strength near the surface. In FE analysis, the bearing capacity factor stabilised to a constant ultimate value N_c = 10.1 after the spudcan penetration reached 0.75 D for the smooth spudcan. The lower N_c number (compared with N_c = 10.5 in uniform soil) may be due to the soft surface soil trapped underneath the spudcan during penetration. However, the rough spudcan reaches its ultimate value of N_c = 11.1 at a deeper penetration of 1.5 D. This is because that the trapped soil underneath the rough spudcan has a longer and stronger effect on the spudcan bearing capacity. The centrifuge test result shows that the N_c number reaches its ultimate value at 0.75 D penetration, with its value remaining between the ones from the smooth spudcan and the rough spudcan. Although the rough spudcan provides 10 % higher capacity at deeper embedment, for a safe design, N_c = 10.1 should be used in spudcan foundation design when a NC strength profile occurs in the field.

In summary, an ultimate bearing capacity factor for deeply embedded spudcan, N_c = 10.5 is recommended in uniform soil and N_c = 10.1 is suitable for a spudcan in NC soil, for jack-up installation in clayey marine deposits.

6.6 Future Research

6.6.1 Spudcan in NC Clay

Offshore clayey deposits are often found normally consolidated (NC). At UWA, many researchers (for instance Byrne and Cassidy, 2002) have investigated the load-penetration response of spudcan in NC clay. The clay is usually deposited throughout

the drum channel so that a number of tests can be undertaken. However, in these tests the soil flow mechanisms cannot be captured. Thus, the aforementioned technique of black flock, transparent window and PIV analysis might in future be applied by depositing clay within a strongbox, instead of the drum centrifuge channel. To do the test economically, soil can be deposited in two strongboxes at the same time.

6.6.2 Spudcan in Layered Soil

Due to the nature of sediment deposition, offshore deposits are also found in layered profiles. Among all combinations, stiff clay over soft clay and sand layer over soft clay are the major causes for a rapid penetration in a short time that is referred to as a "punch-through" failure. Due to the losses from punch-through failures in the past, it has been a common concern in offshore industry. Craig and Chua (1990, 1991) have tried to reveal the failure mechanisms in layered soil deposits by inserting spaghetti. The shortcomings of these depictions have already been discussed. The aforementioned technique of coloured flock with PIV analysis may be applied to reveal layered soil failure mechanisms not only in the ultimate failure state but also during spudcan continuous penetration.

6.6.3 Spudcan Close to Existing Structures

In offshore industry, it has always been a great challenge to install a jack-up rig close to other in-place structures. However, to comply with the growing demand of current world, it is somewhere essential to be commissioned. A common corresponding example of this type is "spudcan-pile" interaction. Siciliano *et al*. (1990) and Craig (1998) have endeavoured to determine the lateral soil displacement profiles, and to measure the corresponding effect on the behaviour of both placed and placing foundations, surrounding a jack-up rig spudcan penetrating in soil. From their depictions, the progressive soil deformation in this complicated situation was not presented and the reproduced ultimate deformation was not very clear. The technique developed in this study has the potential to reveal the progressive soil deformation and hence to measure corresponding effect on the adjacent structures.

REFERENCES

Ackland, D.F. (1949). "Moving Heaven and Earth, R.G. LeTourneau." *Marshall, Morgan and Scott*, London.

Adrian, R.J. (1991). "Particle imaging techniques for experimental fluid mechanics." *Annual Review of Fluid Mechanics*, Vol. 23, pp. 261-304.

Ahmad, A., and Chandler, J.H. (1999). " Photogrammetric capabilities of the Kodak DC40, DCS420 and DCS460 digital cameras." *Photogrammetric Record*, Vol. 16, No. 94, pp. 601-615.

Al-Tabbaa, A. (1987). "Permeability and stress-strain response of speswhite kaolin." PhD Thesis, University of Cambridge.

Andersen, K.H. (1988). "A review of soft clay under static and cyclic loading." *Invited Lecture, International Conference on Engineering Problems of Regional Soils*, Beijing, China.

API. (1993). "Recommended practice for planning, designing and constructing fixed offshore platforms-load and resistance factor design." *RP 2A-LRFD, ist ed.*, Washington DC: American Petroleum Institute.

Baerheim, M., Manschot, D., and Nortvedt, T. (1997). "Use of the jack-up as a permanent installation for the marginal Siri field." *Proceedings of 6th International Conference Jack-up Platform Design, Construction and Operation*, City University, London.

Baglioni, V.P., Chow, G.S., and Endley, S.N. (1982). "Jack-up foundation stability in stratified soil profiles." *Proceedings 14th Offshore Technology Conference*, Houston, Texas, pp. 363-369, OTC 4409.

Bassett, R.H., Davies, M.C.R., Gunn, M.J., and Parry, R.H.G. (1981). "Centrifuge models to evaluate numerical methods." *Proceedings 10th ICSMFE*, Stockholm, Vol. 1, pp. 557-562.

Bennett, W.T., and Sharples, B.P.M. (1987). "Jack-up legs to stand on?" *Mobile Offshore Structures*, Elsevier, London, pp. 1-32.

Bjerrum, L. (1954). "Geotechnical properties of Norwegian marine clay." *Géotechnique*, Vol. 4, No. 2, pp. 49-69.

Bjerrum, L. (1972). "Embankments on soft ground." *Proceedings ASCE Spec. Conference on Performance of Earth and Earth-Supported Structures*, Perdue, Vol. 2, Pt 1, pp. 1-54.

Bjerrum, L., and Simons, N.E. (1960). "Comparison of shear strength characteristics of normally consolidated clays." *ASCE Research Conference on the Shear Strength of Cohesive Soils*, Boulder, CO, pp. 711-726.

Boon, B., Vrouwenvelder, A., Hengst, S., Boonstra, H., and Daghigh, M. (1997). "System reliability analysis of jack-up structures: possibilities and frustrations." *Proceedings of 6th International Conference on Jack-Up Platform Design, Construction and Operation*, City University, London.

Brinch Hansen, J. (1961). "A general formula for bearing capacity." *Danish Geotechnical Institute Bulletin*, Vol. 11, pp. 38-46.

Brinch Hansen, J. (1970). "A revised and extended formula for bearing capacity." Danish Geotechnical Institute, Copenhagen, pp. 5-11.

Britto, A.M., and Kusakabe, O. (1982). "Stability of unsupported axisymmetric excavations in soft clay." *Géotechnique*, Vol. 32, No. 3, pp. 261-270.

Britto, A.M., and Kusakabe, O. (1983). "Stability of axisymmetric excavations in clays." *Journal of Geotechnical Engineering*, ASCE. Vol. 109, No. 5, pp. 666-681.

Byrne, B.W. (2000). "Investigations of suction caissons in dense sand." D. Phil. Thesis, The University of Oxford.

Byrne, B.W., and Cassidy, M.J. (2002). "Investigating the response of offshore foundations in soft clay soils." *21st International Conference on Offshore Mechanics and Arctic Engineering*, Oslo, Norway.

Carlsen, C.A., Kjeϕy, H., and Eriksson, K. (1986). "Structural behaviour of harsh environment jack-ups." *The Jack-up Drilling Platform Design and Operation*, London: Collins, pp. 90-136.

Carter, J.P., and Balaam, N. (1990). "AFENA User's Manual." Geotechnical Research Centre, The University of Sydney.

Cassidy, M.J. (1999). "Non-linear analyses of jack-up structures subjected to random waves." D. Phil. Thesis, The University of Oxford.

Cassidy, M.J., and Byrne, B.W. (2001). "Drum centrifuge model tests comparing the performance of spudcans and caissons in kaolin clay." *OUEL Report No 2248/01*, Department of Engineering Science, The University of Oxford.

Craig, W.H. (1985). "Modelling pile installation in centrifuge experiments." *Proceedings International Conference on Soil Mechanics and Foundation Engineering*, Vol. 2, pp. 1101-1104.

Craig, W.H., and Chua, K. (1990). "Deep penetration of spudcan foundations on sand and clay." *Géotechnique*, Vol. 40, No. 4, pp. 541-556.

Craig, W.H., and Chua, K. (1991). "Large displacement performance of jack-up spudcans." *Proceedings Conference on Centrifuge '91*, Balkema, Rotterdam.

Craig, W.H. (1998). "Spudcan foundations: installation with deep penetration and subsequent removal." *Proceedings Institution Civil Engineers, Geotechnical Engineering*, Vol. 131, pp. 146-151.

Davis, E.H., and Booker, J.R. (1973). "The effect of increasing stress with depth on the bearing capacity of clays." *Géotechnique*, Vol. 23, No. 4, pp. 551-563.

Davis, E.H., and Christian, J.T. (1971). "Bearing capacity of anisotropic cohesive soils." *Journal of Soil Mechanics and Foundation Engineering Division,* ASCE, Vol. 97, No. 5, pp. 753-769.

de Ruiter, J., and Richards, A.F. (1983). "Marine geotechnical investigations, a mature technology." *Proceedings Geotechnical Practice in Offshore Engineering, American Society of Civil Engineers*, New York.

Dean, E.T.R., James, R.G., Schofield, A.N., and Tsukamoto, Y. (1998). "Drum centrifuge study of three-leg jack-up models on clay." *Géotechnique*, Vol. 48, No. 6, pp. 761-785.

Endley, S.N., Rapoport, V., Thompson, P.J., and Baglioni, V.P. (1981). "Prediction of jack-up rig footing penetration." *Proceedings 13th Offshore Technology Conference*, Houston, OTC 4144.

Ethrog, U. (1994). "Strain measurement by digital image processing." *Proceedings 10th Conference on Recent Advances in Experimental Mechanics*, Balkema: Rotterdam, pp. 411-415.

Fannin, R.J. (1986). "Geogrid reinforcement of granular layers on soft clay - a study at model and full scale." D. Phil. Thesis, The University of Oxford.

Finnie, I.M.S. (1993). "Performance of shallow foundations in calcareous soils." PhD Thesis, The University of Western Australia.

Finnie, I.M.S., and Randolph, M.F. (1994). "Punch-through and liquefaction induced failure of shallow foundations on calcareous sediments." *Proceedings*

International conference on Behaviour of Offshore Structures, BOSS '94, Boston, Vol. 1, pp. 217-230.

Gemeinhardt, J.P., and Focht, J.A. (1970). "Theoretical and observed performance of mobile rig footings on clay." *Proceedings 2nd Offshore Technology Conference*, Houston, OTC 1201.

Gue, S.S. (1984). "Ground heave around driven piles in clay," D. Phil. Thesis, The University of Oxford.

Hambly, E.C., and Nicholson, B.A. (1991). "Jack-up performance and foundation fixity under developing storm conditions." *Proceedings 22nd Offshore Technology Conference*, Houston, pp. 369-380, OTC 6466.

Hampson, K.M., and Power, P.T. (1992). "The influence of recent developments in the use of jack-up units on geotechnical data acquisition practice." *Recent Developments in Jack-up Platforms*, Ed. Boswell, L.F. and D'Mello, C., Pub. Blackwell Scientific Publications.

Henriques, C.C.D., and Petrobras S.A., A.Q.N. (1995). "Utilisation of jack-up platforms for the installation of simplified production platforms." *Proceedings of the 9th International Symposium on Offshore Engineering*, COPPE, Federal University of Rio de Janeiro, Brazil.

Herdy, A.C., and Townsend, F.C. (1983). "Preliminary investigation of the bearing capacity of layered soils by centrifugal modelling." Internal Report, University of Florida.

Higham, M.D. (1984). "Models of jack-up rig foundations." MSc Dissertation, Manchester University.

Heikkila, J., and Silven, O. (1998). "A four step-camera calibration procedure with implicit image correction." *IEEE Computer Society Conference on Computer Vision and Pattern Recognition (CVPR'97)*, San Juan, Puerto Rico.

Hossain, M.S., Mehryar, Z., Hu, Y., and Randolph, M.F. (2004). "Deep penetration of spudcan foundation into NC clay." *Proceedings 23rd International Conference on Offshore Mechanics and Arctic Engineering*, OMAE, Vancouver, Canada.

Houlsby, G.T. (1982). "Theoretical analysis of the fall cone tests." *Géotechnique*, Vol. 32, No. 2, pp. 111-118.

Houlsby, G.T. (1993). "In lecture notes for Reinforced Soil: Mechanics and Design." Short Course at The University of Oxford, 19-21 April.

Houlsby, G.T., and Martin, C.M. (1992). "Modelling of the behaviour of foundations of jack-up units on clay." *Proceedings of the Worth Memorial Symposium, Predictive Soil Mechanics*, Oxford, pp. 339-358.

Houlsby, G.T., and Martin, C.M. (2003). "Undrained bearing capacity factors for conical footings on clay." *Géotechnique*, Vol. 53, No. 5, pp. 513-520.

Houlsby, G.T., and Wroth, C.P. (1982). "Direct solution of plasticity problems in soils by the method of characteristics." *Proceedings of the 4th International Conference on Numerical Methods in Geomechanics*, Edmonton, Vol. 3, pp. 1059-1071.

Houlsby, G.T., and Wroth, C.P. (1983). "Calculation of stresses on shallow penetrometers and footings." *Proceedings of the International Union of Theoretical and applied Mechanics (IUTAM)/International Union of Geodesy and Geophysics (IUGG) Symposium on seabed Mechanics*, Newcastle upon Tyne, pp. 107-112.

House, A.R., Oliveira, J.R.M.S., and Randolph, M.F. (2001). "Evaluating the coefficient of consolidation using penetration tests." *IJPMG-International Journal of Physical Modelling in Geotechnics*, Vol. 3, pp. 17-26.

Hu, Y., and Randolph, M.F. (1998[1]). "A practical approach for large deformation problems in soil." *International Journal of Numerical and Analytical Methods in Geomechanics*, Vol. 22, pp. 327-350.

Hu, Y., and Randolph, M.F. (1998[2]). "H-adaptive FE analysis of elasto-plastic non-homogeneous soil with large deformation." *International Journal of Computer and Geomechanics*, Vol. 23, No. 1/2, pp. 61-84.

Hu, Y., and Randolph, M.F. (1999). "Plate-penetrometer penetration into NC soil using H-adaptive FE method." *Numerical Models in Geomechanics*, Balkema, Rotterdam, pp. 501-506.

Hu, Y., Watson, P.G., and Randolph, M.F. (2001). "Effect of interface on N_c value for plate-penetrometer." *Computer Methods and Advances in Geomechanics*, pp. 931-936.

Jackson, G., and Pennington, D. (2002). "Installation of the hang Tuah ACE platform."

James, R.G., and Shi, Q. (1988). "Centrifuge modelling of the behaviour of surface footings under combined loading." *Proceedings Conference on Centrifuge '88*, Balkema, Rotterdam, pp. 307-311.

James, R.G., and Tanaka, H. (1984). "An investigation of the bearing capacity of footings under eccentric and inclined loading on sand in a geotechnical centrifuge." *Proceedings Symposium on Recent Advance in Geotechnical centrifuge modelling*, University of California, Davis, pp. 88-115.

Jamiolkowski, M., and Garassino, A. (1977). "Soil modulus for laterally loaded piles." *Proceedings 9th International Conference on Soil mechanics and Foundation Engineering*, Spec. Sess. 10, Tokyo, pp. 43-58.

Kee, R., and Ims, B.W. (1984). "Geotechnical hazards associated with leg penetration of jack-up rigs." *Seabed Mechanics*, pp. 169-174.

Kim, S.H. (1994). "Model testing of the interactions between closely spaced tunnels in clay." First Year Report, The University of Oxford.

Knott, T. (1985). "Down amongst the spudcans something is stirring." *Offshore Engineer*, October.

Ko, H.Y. (1988). "Summary of state-of-the-art in centrifuge model testing." *Centrifuge in Soil Mechanics*, pp. 11-18.

Ladd, C.C., Foott, R., Ishihara, K., Schlosser, F., and Poulos, H.G. (1977). "Stress deformation and strength characteristics." *Proceedings of the 9th International Conference on Soil Mechanics and Foundation Engineering*, Tokyo, Vol. 2, pp. 421-494.

Langhaar, H.L. (1951). *Dimensional analysis and theory of models*, John Wiley, New York.

Le Tirant, P. (1979). *Seabed reconnaissance and offshore soil mechanics for the installation of petroleum structures*, Paris.

Le Tirant, P., and Pérol, C. (1993). *Stability and operation of jackups*, Peris: Edition Technip.

Leijten, S.F., and Efthymiou, M. (1989). "A philosophy for the integrity assessment of jack-up units." *Proceedings Society of Petroleum Engineers Conference "Offshore Europe 89"*, Aberdeen, SPE 19236.

Lo, K.Y., and Milligan, V. (1967). "Shear strength properties of two stratified clays." *Journal of the Soil Mechanics and Foundation Engineering Division,* ASCE, Vol. 93, No. 1, No.1-15.

Love, J.P. (1984). "Model testing of geogrids in unpaved roads." D. Phil. Thesis, The University of Cambridge.

Mair, R.J. (1979). "Centrifugal modelling of tunnel construction in soft clay." PhD Thesis, The University of Cambridge.

Martin, C.M. (1994). "Physical and numerical modelling of offshore foundations under combined loads." D. Phil. Thesis, The University of Oxford.

Martin, C.M., and Houlsby, G.T. (1999). "Jack-up units on clay: structural analysis with realistic modelling of spudcan behaviour." *Offshore Technology Conference*, Houston, OTC 10996.

Martin, C.M., and Houlsby, G.T. (2000). "Combined loading of spudcan foundations on clay: laboratory tests." *Géotechnique*, Vol. 50, No. 4, pp. 325-338.

Martin, C.M., and Houlsby, G.T. (2001). "Combined loading of spudcan foundations on clay: Numerical modelling." *Géotechnique*, Vol. 51, No. 8, pp. 687-700.

Martin, C.M., and Randolph, M.F. (2001). "Applications of the lower and upper bound theorems of plasticity to collapse of circular foundations." *Proceedings of the 10th International Conference on Computer Methods and Advance Geomechanics,* Tucson, Vol. 2, pp. 1417-1428.

Martins, J.P. (1983). "Shaft resistance of axially loaded piles in clay." PhD Thesis, Imperial College, The University of London.

McClelland, B., Young, A.G., and Remmes, B.D. (1981). "Avoiding jack-up rig foundation failures." *Proceedings Symposium on Geotechnical Aspects of Coastal and Offshore Structures*, Bangkok, pp. 137-157.

Mehryar, Z., Hu, Y., and Randolph, M.F. (2002). "Penetration analysis of spudcan foundations in NC clay." *12th International Offshore and Polar Engineering Conference, ISOPE*, Kitakyushu, Japan, pp. 679-684.

Mesri, G. (1989). "A re-evaluation of $s_{u(mob)} = 0.22\sigma'_p$ using laboratory shear tests." *Canadian Geotechnical Journal*, Vol. 26, No. 1, pp. 162-164.

Meyerhof, G.G. (1951). "The ultimate bearing capacity of foundations." *Géotechnique*, Vol. 2, No. 4, pp. 301-332.

Meyerhof, G.G. (1953). "The bearing capacity of foundations under eccentric and inclined loads." *Proceedings 3rd International Conference on Soil mechanics and Foundation Engineering*, Zurich, Vol. 1, pp. 440-445.

Meyerhof, G.G. (1961). "The ultimate bearing capacity of wedge-shaped foundations." *Proceedings 5th International Conference on Soil mechanics and Foundation Engineering*, Paris, Vol. 2, pp. 105-109.

Meyerhof, G.G. (1972). "Stability of slurry trench cuts in saturated clay." *Proceedings of the Speciality Conference on Performance of Earth and Earth Supported Structures*, pp. 1451-1466.

National Research Council, Marine Board Committee on Assessment of Safety of OCS Activities, (1981). *Safety and Offshore Oil*, Washington, D.C., National Academy Press.

Newson, T.A., Bransby, M.F., and Watson, P.G. (1999). "Undrained shear strength profiling using a spherical penetrometer." *Canadian Geotechnical Journal*.

Noble Denton Associates (1987). "Foundation fixity of jack-up units: a joint industry study." *Noble Denton & Associates*, London.

Offshore Technology (1999). "Website: http://www.offshore-technology.com/projects/." *Net Resources International Limited*.

Ovesen, N.K. (1979). "The scaling law relationship-panel discussion." *Proceedings 7th European Conference on Soil Mechanics and Foundation Engineering*, Brighton, No. 4, pp. 319-323.

Phillips, R. (1997). "Centrifuge modelling: practical considerations." *Geotechnical Centrifuge Technology*, Ed: Blackie Academic, London, pp. 34-59.

Randolph, M.F., Steenfelt, J.S., and Wroth, C.P. (1979). "The effect of pile type on design parameters for driven piles." *Proceedings 7th European Conference on Soil Mechanics and Foundation Engineering*, Brighton, Vol. 2, pp. 107-114.

Randolph, M.F., and Houlsby, G.T. (1984). "The limiting pressure on a circular pile loaded laterally in cohesive soil." *Géotechnique*, Vol. 34, No. 4, pp. 613-623.

Rapoport, V., and Young, A.G. (1987). "Foundation performance of jack-up drilling units, analysis of case histories." *Proceedings of Jack-up Conference*.

Reardon, M.J. (1986). "Review of the geotechnical aspects of jack-up unit operations." *Ground Engineering*, Vol. 19, No. 7, pp. 21-26.

Rowe, P.W. (1975). "Displacements and failure modes of model offshore gravity platforms founded on clay." *Proceedings of Offshore Europe '75*.

Rowe, P.W., Craig, W.H., and Procter, D.C. (1976). "Model studies of offshore gravity structures founded on clay." *In Behaviour of Offshore Structures,* BOSS, Vol. 76, No. 1, pp. 439-448.

Salencon, J. & Martar, M. (1982). “Capacité portante des foundations superficielles circularies.” *Journal de Mecanique Théorique et Alliquée*, Vol. 1, No. 2, pp. 237-267.

Santa Maria, P.E.L. (1988). "Behaviour of footings for offshore structures under combined loads.” D. Phil. Thesis, The University of Oxford.

Santa Maria, P.E.L., and Houlsby, G.T. (1988). "Model tests for offshore foundations under combined loads." *Proceedings of the Symposium on New Concepts in Laboratory and In Situ Tests in Geotechnical Engineering*, Rio de Janeiro, Vol. 2, pp. 425-438.

Schofield, A.N. (1980). "Cambridge geotechnical centrifuge operations." *Géotechnique*, Vol. 30, No. 3, pp. 227-268.

Semple, R.M., and Johnston, J.W. (1979). "Performance of stingray in soil sampling and in-situ testing." *Proceedings International Conference on Offshore Site Investigation*, Graham and Trotham, London.

Sharples, B.P.M. (1989). "Risk analysis of jack-up rigs." *Second International Conference, The Jack-up Drilling Platform*, London.

Siciliano, R.J., Hamilton, J.M., Murff, J.D., and Phillips, R. (1990). "Effect of jack-up spudcans on piles." *Offshore Technology Conference*, OTC 6467.

Skempton, A.W. (1951). "The bearing capacity of clays." *Proceedings Building Research Congress*, London, pp. 180-189.

Skempton, A.W. (1957). "Discussion on planning and design of the new Hong Kong airport." *Proceedings Instn Civil Engineers*, Vol. 7, pp. 306.

Slama, C.C. (ed.) (1980). *Manual of Photogrammetry, 4rth Edition*, American Society of Photogrammetry.

Smith, M.G. (1993). "A laboratory study of the Marchetti dilatometer." PhD Thesis, University of Oxford.

SNAME (1994). "Guidelines for site specific assessment of mobile jack-up units." *Society of Naval Architects and Marine Engineers, Technical and Research Bulletin 5-5A*, New Jersey.

SNAME (1997). "Guidelines for site specific assessment of mobile jack-up units." *Society of Naval Architects and Marine Engineers*, Technical and Research Bulletin 5-5A, New Jersey.

Springman, S.M. (1989). "Lateral loading of piles due to simulated embankment construction." PhD Thesis, The University of Cambridge.

Springman, S.M. (1993). "Centrifuge modelling in clay marine applications. Keynote address." *4th Canadian Marine Geotechnical Conference*, St Johns, Newfoundland.

Springman, S.M., and Schofield, A.N. (1998). "Monotonic lateral load transfer from a jack-up platform lattice leg to a soft clay deposit." *Proceedings International Conference Centrifuge on Centrifuge 98*, Tokyo, pp. 563-568.

Steenfelt, J.S., Randolph, M.F., and Worth, C.P. (1981). "Instrumented model piles jacked into clay." *Proceedings of 10th International Conference Soil Mechanics and Foundation Engineering,* Stockholm, Vol. 2, pp. 857-864.

Stewart, D.P. (1992). "Lateral loading of pile bridge abutments due to embankment construction." PhD Thesis, The University of Western Australia.

Stewart, D.P., Boyle, R.S., and Randolph, M.F. (1998). "Experience with a new drum centrifuge." *Proceedings International Conference Centrifuge '98*, Tokyo, Japan, Vol. 1, pp. 35-40.

Stewart, D.P., and Randolph, M.F. (1991). "A new site investigation tool for the centrifuge." *Proceedings Conference Centrifuge '91*, Balkema, Rotterdam, pp. 531-538.

Stewart, W.P., White, R.M., Rapoport, V., and Devoy, S.D. (1989). "On-bottom stability of jack-ups." *Offshore Technology Conference*, OTC 6125.

Stiff, J.J., Sharples, B.P.M., and Bowie, R.D. (1997). "Jack-ups: classification past, present, and future." *Proceedings of 6th International Conference Jack-Up Platform Design, Construction and Operation*, City University, London.

Take, W.A. (2002). "The influence seasonal moisture cycles on clay slopes." PhD Dissertation, The University of Cambridge.

Taylor, R.N. (1995). *Geotechnical centrifuge technology*, Blackie Academic and Professional, an imprint of Chapman & Hall, Glasgow.

Taylor, R.N., Grant, R.J., Robson, S., and Hkuwano, J. (1998). "An image analysis system for determining plane and 3-D displacements in soil models." *Proceedings of Centrifuge '98*, Balkema: Rotterdam, pp. 73-78pub.

Terzaghi, K. (1943). *Theoretical soil mechanics*, John Wiley and Sons, New York.

Veldman, H., and Lagers, G. (1997). "50 years offshore." *Foundation for Offshore Studies*, Delft, The Netherlands.

Vesic, A.S. (1975). "Bearing capacity of shallow foundations." *Foundation Engineering Handbook (ed. H. F. Winterkorn & H. Y. Fang)*, New York: Van Nostrand.

Vlahos, G., Martin, C.M., and Cassidy, M.J. (2001). "Experimental investigation of model jack-up unit on clay." *Proceedings of the Eleventh International Offshore and Polar Engineering Conference*, ISOPE, Stavanger, Norway, Vol. 1, pp. 97-105.

Wang, C.X., and Carter, J.P. (2002). "Deep penetration of strip and circular footings into layered clays." *The International Journal of Geomechanics*, Vol. 2**,** No. 2, pp. 205-232.

Watson, P.G. (1999). "Performance of skirted foundations for offshore structures." PhD Thesis, The University of Western Australia.

Watson, P.G., Newson, T.A., and Randolph, M.F. (1998). "Strength profiling in soft offshore soils." *Proceedings 1st International Conference on Site Characterisation -ISC '98*, Atlanta, Vol. 2, pp. 1389-1394.

White, D.J. (2002). "An investigation into the behaviour of pressed-in piles." PhD Thesis, Cambridge University.

White, D.J., and Take, W.A. (2002). "GeoPIV: Particle Image Velocimetry (PIV) software for use in Geotechnical testing." *D-SOILS-TR322*, Cambridge University Engineering Department Technical Report.

White, D.J., Take, W.A., and Bolton, M.D. (2001[1]). "Measuring soil deformation in geotechnical models using digital images and PIV analysis." *Proceedings of the 10th International Conference on Computer Methods and Advances in Geomechanics*, Tucson, Arizona, pp. 997-1002.

White, D.J., Take, W.A., Bolton, M.D., and Munachen, S.E. (2001[2]). "A deformation measuring system for geotechnical testing based on digital imaging, close-range photogrammetry, and PIV image analysis." *Proceedings of the 15th International Conference on soil mechanics and Geotechnical Engineering*, Istanbul, Turkey, pp. 539-542.

White, D.J., Take, W.A., and Bolton, M.D. (2003). "Soil deformation measurement using particle image velocimetry (PIV) and photogrammetry." *Géotechnique*, Vol. 53, No. 7, pp. 619-631.

Wood, D.M. (1980). "Yielding in soft clay at Backebol, Sweden." *Geotechnique*, Vol. 30, No. 1, pp. 49-65.

Wroth, C.P. (1984). "The interpretation of in situ soil tests." *Géotechnique*, Vol. 34, No. 4, pp. 449-489.

Wroth, C.P., and Houlsby, G.T. (1985). "Soil mechanics - property characterisation and analysis procedures." *Proceedings 11th International Conference on Soil mechanics and Foundation Engineering*, San Francisco, Vol. 1, pp. 1-55.

Young, A.G., Remmes, B.D., and Meyer, B.J. (1984). "Foundation performance of offshore jack-up drilling rigs." *Journal of Geotechnical Engineering Division,* ASCE, Vol. 110, No. 7, pp. 841-859.

Zienkiewiecz, O.C., and Zhu, J.Z. (1993). "The superconvergent patch recovery and a posteriori error estimates. Part 1: the recovery technique." *International Journal of Numerical Methods Engineering*, Vol. 33, pp. 1331-1364.

APPENDIX 1

UWA DRUM CENTRIFUGE IMAGE ACQUISITION SYSTEM

Previously, a mini video camera was using to capture soil flow images in the drum centrifuge at UWA. In addition, the captured images were transferred through centrifuge sliprings. As a result, the quality of images was not good. The corresponding drawbacks and possible remedies are discussed below.

A1.1 Drawbacks of Mini Video Camera

1. Low image resolution: 450 × 470 pixels (8 bit digital format after conversion by frame grabber);
2. Low image stability: noise on sliprings, interface on analogue signal, note interlacing bands;

A1.2 Comparison between Digital Photography and Video Capture

Phase	Video Capture	Digital Still Photography
Camera	CCD video camera e.g. Pulnix TM1040 (analogue, 1024 × 1024 pixels, AU$4000); Pulnix TM1320 (digital, 1300 × 1030 pixels, AU$ 6547)	Digital still camera e.g. Olympus C4000 (2278 × 1713 pixels, AU$ 1149); Cannon S40 (2270 × 1704, AU$ 1299)

Camera control	Labview, IMAQ, custom written acquisition software	cam2com PC software (freeware) Cannon remote capture software (free with camera) USB link from control room
Image capture method (frame rate)	Frame grabber card NI 1409 (analogue, AUS$ 3320 + 405 (cable)) NI 1428 (digital, AU$ 4255) Note: maximum frame rate = 50 Hz	cam2com PC software, Cannon remote capture software [http://home.attbi.com/~smenche/Cam2Com/] Note: maximum frame rate = 0.1 Hz
Probable data quality	1024 pixels across 150 mm FOV @ 0.05 pixel PIV resolution = 7.3 microns	2272 pixels across 150 mm FOV @ 0.05 pixel PIV resolution = 3.3 microns
Drawbacks / pitfalls	RS-644 link across sliprings required Relatively low resolution Overall high frame rate for static tests	USB connection across sliprings (or by wireless) required Will camera survive g-level? [UWA camera OK up to 100 g] Lens support required
Total costs of equipment	Approximately AU$ 8000-10000 + RS-644 connection	Approximately AU$ 1200 + USB connection
Time to develop	Arrange RS-644 link, write software to control grabber More	Arrange USB link, manufacture camera lens support Less
Flexibility	Low. Camera plus PC with board	High. Only camera and PC with USB

	required	required. Easily transferable to other experiments

A.1.3 Solutions

Finally it was decided to buy a new digital camera for the UWA drum centrifuge. The Cannon PowerShot S40 camera has been bought. A camera cradle has also been built to fix it within the drum channel. The camera position and direction (focusing angle towards the window) has been corrected. Additionally, the camera has been modified by attaching a small weight to the shutter in order to avoid the transferring of images through sliprings (explained in Section 4.2.4). The camera has been successfully tested up to 100 g (acting perpendicularly to the camera axis) in the drum centrifuge, without loss of functionality. Higher acceleration may be possible, but has not tested yet.

APPENDIX 2

CONSIDERATIONS ON THE RATE OF PROBE PENETRATION

A2.1 Spudcan Installation

Velocity for half-spudcan installation was selected based on three criteria. Firstly, it is necessary to satisfy Finnie's suggestion ($vD/c_v > 30$, where v is the penetration velocity, D is the probe diameter, and c_v is the coefficient of consolidation) to ensure undrained condition. For the kaolin clay used in this investigation (c_v = 2 m^2/year) and spudcan of D = 60 mm, the minimum velocity to satisfy the undrained condition is about 0.03 mm/s.

Secondly, a fast soil particle movement i.e. a high strain gradient of soil between consecutive images is not desirable for tracking the patches on the images properly in PIV analysis. Thus the half-spudcan penetration rate should not be too high. The digital camera (S40) used in this study is capable of capturing images in a maximum rate of 0.4 photos/sec. For this research experimental camera position, the image scale was about 12 pixels/mm (as image width = 193 mm and height = 144 mm and camera resolution 2270 × 1704 pixels). Therefore, a penetration rate of 0.035 mm/sec (≈ 0.4/12) leads 1 pixel of foundation movement per photo.

Thirdly, since a 7.4 V power supply was unavailable on the drum channel, the camera was to be operated from its own battery. In a continuous shooting mode the battery lasts for about 60 minutes or 1440 photos. However, the shooting will end if the memory card of the camera (512 MB) becomes filled: images are typically 400 kB in size, in which case the card fills up after about 1280 photos or 54 minutes of photography. Note, the spudcan was to be penetrated into soil depth of 90-100 mm

and it was decided to film soil flow mechanisms during footing penetration only, not extraction.

By considering all the influential factors stated above, the half-spudcan test was performed (i) at a constant rate of 0.2 mm/s when a mini video camera was used (ii) at a constant rate of 0.04 mm/s when a test was conducted in absence of free water and (iii) at a velocity of 0.05 mm/sec when a test was conducted in presence of free water.

The full-spudcan was penetrated at a constant rate of 0.2 mm/sec. This speed gives a vD/c_v of ~ 95, well above the undrained velocity. However, the total time required, in prototype scale ($T_p = N^2 \times T_m$), for loading up to d/D = 1.67-3.33 is longer than typical preloading time at field practice although well comparable with the penetration rates used by other investigators (Table A2.1).

A2.2 T-Bar Penetration

Velocity for T-bar penetrometer was selected mainly based on the velocity group (vD/c_v) and the previous and on-going research on kaolin clay at UWA. From Finnie's velocity group, in kaolin clay the minimum velocity of T-bar (D = 5 mm) penetration to ensure an undrained condition is about 0.38 mm/s.

At UWA, few researchers launched investigations to find out the rate effect on penetration resistance and subsequently to conclude a suitable rate of penetration. A series of centrifuge tests (at 100 g) in OC kaolin clay were undertaken by Stewart and Randolph (1991) to determine the effects of various penetration rates. The results have been shown on Figure 2.9, indicating a very little difference between penetration rates of 1 and 3 mm/sec.

House *et al*. (2001) also performed a series of T-bar penetration tests (100 g) in NC kaolin clay on a drum centrifuge. Continuous penetration tests were conducted at constant rate, with rate varying from 3 mm/sec down to 0.0059 mm/sec. The lowest profile of resistance was actually achieved for a velocity of v = 0.375 mm/sec (Figure

A2.1). For higher velocities, the resistance was increased due to viscous effects (Craig, 1985). While for lower velocities the resistance was increased due to partial consolidation, and strengthening, of the soil immediately ahead of the probe (Finnie and Randolph, 1994).

Currently, T-bar penetration rate of v = 1 mm/sec is used in almost all the on going centrifuge investigations on drum centrifuge at UWA (like Byrne and Cassidy, 2002 etc.).

Eventually, it was decided to conduct T-bar tests at a constant velocity of 1 mm/sec.

Table A2.1 Rate of spudcan installation

Investigators	Rate of Installation (mm/sec)	Gravity-Level	Notes
Craig and Chua (1990)	7	100 g	Model
Martin (1994)	0.33	1 g	Model
Martin and Houlsby (2000)	0.33	1 g	Model
Vlahos *et al*. (2001)	1.5	1 g	Model
Byrne and Cassidy (2002)	0.1	100 g	Model
This study	0.04-0.2	50-200 g	Model
Commonly used in the jack-up operation (Stewart *et al*., 1989)	7.5	1 g	Field

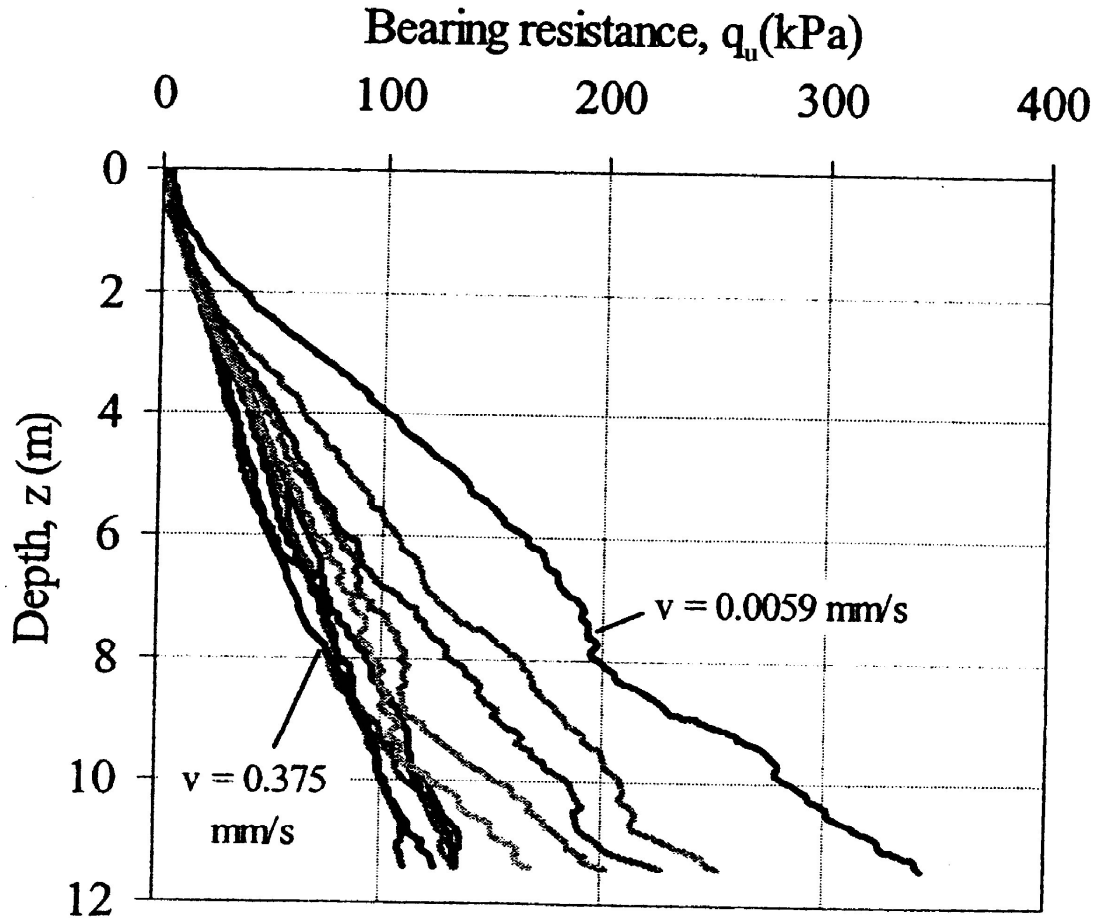

Figure A2.1 Effect of T-bar penetration rate on measured strength (after House *et al.*, 2001)

APPENDIX 3

UNDRAINED SHEAR STRENGTH ESTIMATION: EFFECT OF GRAVITY

Commercially available kaolin was used for the soft clay stratum in the centrifuge models. This study deals with the spudcan penetration into seabed. It was therefore necessary to produce soft clay in several of the centrifuge models, similar to the representative marine uniform clay deposit, and to predict the corresponding undrained shear strength profile with a reasonable degree of accuracy. Several methods of predicting the undrained shear strength of clay deposits are reviewed in this Appendix. And they are used to predict the strength profiles of the centrifuge models presented.

A3.1 Empirical Relationships

The undrained shear strength of saturated normally consolidated clay determined using isotropically consolidated specimens as a function of liquidity index is shown in Figure A3.1. The relationship between undrained strength normalized by the effective overburden stress after isotropic consolidation has been deduced by Worth and Houlsby (1985) using critical state of soil mechanics as

$$\frac{s_u}{\sigma'_v} = 0.129 + 0.00435\ PI \qquad \text{(A3.1)}$$

where s_u is the undrained shear strength, σ'_v is the effective over-burden pressure and PI is the Plasticity Index in percent age (%). For the kaolin used in this study (PI = 34 %), the above expression gives $s_u/\sigma'_v = 0.277$. Alternatively, the following

relationship can be used for normally consolidated to slightly overconsolidated clays with low-to-moderate plasticity (Jamiolkowski *et al*., 1985)

$$\frac{s_u}{\sigma'_{vp}} = 0.23 \pm 0.04 \qquad \text{(A3.2)}$$

where σ'_{vp} is the preconsolidation stress, and s_u is the strength from direct simple shear. Similar empirical expression for the estimation of undrained shear strength in a normally consolidated clay has been proposed by Skempton (1957):

$$\frac{s_u}{\sigma'_v} = 0.11 + 0.0037\ PI \qquad \text{(A3.3)}$$

This expression compares favourably with field data from a number of sites in Figure A3.2, after Bjerrum (1954) and Skempton (1957). For the kaolin used in this study (PI = 34 %), the above expression gives $s_u/\sigma'_v = 0.24$.

For overconsolidated soil deposits it is necessary to take into account the previous stress history when estimating the shear strength. Relationships of the following form are often used:

$$\frac{s_u}{\sigma'_v} = a\ OCR^{\,b} \qquad \text{(A3.4)}$$

where a and b are constants. On the basis of a limited series of vane shear tests performed in the laboratory, values of a = 0.17 and b = 0.86 were derived by Stewart (1992). These values are well comparable to values determined for the kaolin used at Cambridge University as a = 0.19 to 0.22 and b = 0.62 to 0.71 (Springman, 1989) and a = 0.253 and b = 0.754 (Martin, 1994). According to Houlsby (1993), the typical values of a and b are 0.25 and 0.8 respectively, which are both close to the values quoted above. Worth (1984) and Ladd *et al*. (1977) presented theoretical and experimental evidence to suggest that b = 0.8 is an appropriate estimate for most soils. The ratio for the laboratory clay would be expected to be slightly lower than

that normally found in field deposits, since the influence of long term chemical effects and secondary compression (which will lead to higher strengths – Bjerrum, 1972) are not present. On the other hand, the value of the ratio (s_u/σ'_v) determined in the laboratory from a triaxial consolidated-undrained test on undisturbed samples is generally greater than the actual value because of the anisotropic consolidation in the field. However, since the clay is a reconstituted kaolin, the degree of anisotropy in consolidation characteristics is likely to be minimal.

The influence of overconsolidation on the undrained shear strength of clays is shown by Figures A3.3 and A3.4. In Figure A3.3, the undrained strength is normalized by the initial effective overburden pressure. In Figure A3.4, the normalized strength of the overconsolidated clay is further normalized to the normalized strength of the normally consolidated clay.

Mesri (1989) conducted a review of field and laboratory strength test data and concluded that $s_u = 0.22\ \sigma'_{vp}$ (where σ'_{vp} is the preconsolidation stress) provided the best method of strength prediction for stability analysis, when vane shear test data are not available. This expression can be reduced to:

$$s_u = 0.22\ OCR \qquad (A3.5)$$

for comparison with Equation A3.4. All of these empirical relations to evaluate undrained shear strength of kaolin clay have been summarised in Table A3.1.

A3.2 Shear Strength Prediction

In this study, all experimental work has been performed through physical centrifuge modelling, not laboratory floor testing. Reconstituted Speswhite kaolin clay, with the key properties presented in Table 4.2, was preconsolidated in a consolidation frame, prior to final consolidation or reconsolidation in the centrifuge to prepare uniform clay bed. Most of the tests were conducted without water on top while only a few tests were performed with water on top. In the case of tests without water on top, the

saturated unit weight of clay and total stress analysis are considered. And, in the case of tests with water on top, the submerged unit weight of clay and effective stress analysis are assumed.

It would be reasonable to expect an expression in the form of Equation A3.4 to provide a good fit to the observed variation of undrained strength with depth. Consider a soil element at a depth h below the surface of a typical clay sample with saturated unit weight (γ). During the consolidation procedure described above, this element is subjected to a maximum vertical stress of

$$\sigma_{vo} = \sigma_{vp} + \gamma h \qquad \text{(A3.6)}$$

However, as the sample was sliced after consolidation in this study to prepare the test specimen (except box consolidation, as explained in Section 4.3.4), it was very difficult to calculate additional contribution of γh in Equation A3.6. In addition, on laboratory floor the contribution by γh to vertical stress is very low relative to σ_{vp}, hence it is neglected here. Upon total removal of the compressive load, and after pore suctions have dissipated, the vertical stress is simple $\sigma_v = \gamma h$ (self weight). The OCR at depth h on laboratory floor or at 1 g is therefore

$$OCR = \frac{\sigma_{vp}}{\gamma h} \qquad \text{(A3.7)}$$

But at elevated gravity i.e. at N g, the vertical stress will be $\sigma_v = \gamma d$. where d is the prototype depth (=N h), and hence the OCR at depth d at N g is therefore

$$OCR = \frac{\sigma_{vp}}{\gamma d} \qquad \text{(A3.8)}$$

Then clay strength can be calculated, in the form of Equation A3.4, as

$$s_u = a\, \sigma_v\, OCR^b \qquad \text{(A3.9)}$$

where $\sigma_v = \gamma d$ and OCR as defined by Equation A3.8. When test is conducted with water on top, clay buoyant unit weight (γ') is necessarily be considered. In this case, clay strength is therefore

$$s_u = a\, \sigma'_v\, OCR^b \qquad \text{(A3.10)}$$

where $\sigma'_v = \gamma' d$ and OCR can be defined by

$$OCR = \frac{\sigma_{vp}}{\gamma' d} \qquad \text{(A3.11)}$$

Expressions of this form can be drawn providing excellent fits to the measured strength from centrifuge tests over the depth range considered for strength prediction. However, the values of regression coefficients a and b are need to be varied with g level and corresponding in-flight elapsed time and also with the specimen condition, whether submerged or saturated, rather than a fixed values, like other investigators. Table A3.2 shows these values in comparison with the to values from Stewart (1992), who performed centrifuge tests on the same kaolin clay (UWA).

In the case of tests on specimens without water on top i.e. on saturated clay, a constant value of b = 0.95 is obtained. However, the values of a are slightly varied from 0.09-0.13 as soil is swelling and reconsolidating at elevated gravity although a constant value is resulted at 200 g of 0.13. In the case of test on specimen with water on top i.e. on submerged clay, only a few tests were conducted and a widely varied value of a = 0.125-0.38 and b = 0.5-0.7 can be picked. This variation is due to in-flight elapsed time effect in presence of free water (as discussed in Section 5.3). Furthermore, these values are far away from Stewart's values from centrifuge tests. The reason could be partly that Stewart did the tests without water on top of the soil specimen, and partly might be due to the testing system, after consolidation samples sliced, were put into the strongbox and then tested at drum centrifuge rather than samples tested directly after consolidation in beam centrifuge. To draw an excellent conclusion, further investigations are mandatory.

Table A3.1 Empirical relationships to evaluate shear strength (s_u) of kaolin clay

Investigators	Clay	Shear strength
Skempton (1957)	Normally Consolidated	$s_u = 0.24\ \sigma'_v$
Worth and Houlsby (1985)	Normally Consolidated	$s_u = 0.277\ \sigma'_v$
Jamiolkowski *et al*. (1985)	Normally Consolidated to slightly Overconsolidated	$s_u = 0.23 \pm \sigma'_{vp}$
Mesri (1989)	Overconsolidated	$s_u = 0.22\ \sigma'_{vp}$
Springman (1989)	Overconsolidated	$s_u = 0.19\sim0.22\ OCR^{0.62\sim0.71}\ \sigma'_v$
Stewart (1992)	Overconsolidated	$s_u = 0.17\ OCR^{0.86}\ \sigma'_v$
Houlsby (1993)	Overconsolidated	$s_u = 0.25\ OCR^{0.8}\ \sigma'_v$
Martin (1994)	Overconsolidated	$s_u = 0.253\ OCR^{0.754}\ \sigma'_v$

Table A3.2 Values of regression coefficients a and b from centrifuge tests

Test Condition	G-Level →	1 g		50 g		100 g		200 g		110 g (Stewart, 1992)	
	σ_{vp} (kPa) ↓	a	b	a	b	a	b	a	b	a	b
Without Water on top	100	**	**	**	**	**	**	0.13	0.95	**	**
	150	**	**	**	**	0.093	0.95	0.13	0.95	**	**
		0.162	0.95	0.123	0.94	0.112	0.95	0.13	0.95	**	**
	200	**	**	**	**	0.092	0.95	0.12	0.95	**	**
With water on top	150	**	**	0.38	0.5	0.125	0.7	**	**	**	**
	100	**	**	**	**	**	**	**	**	0.185	0.85

** No data available

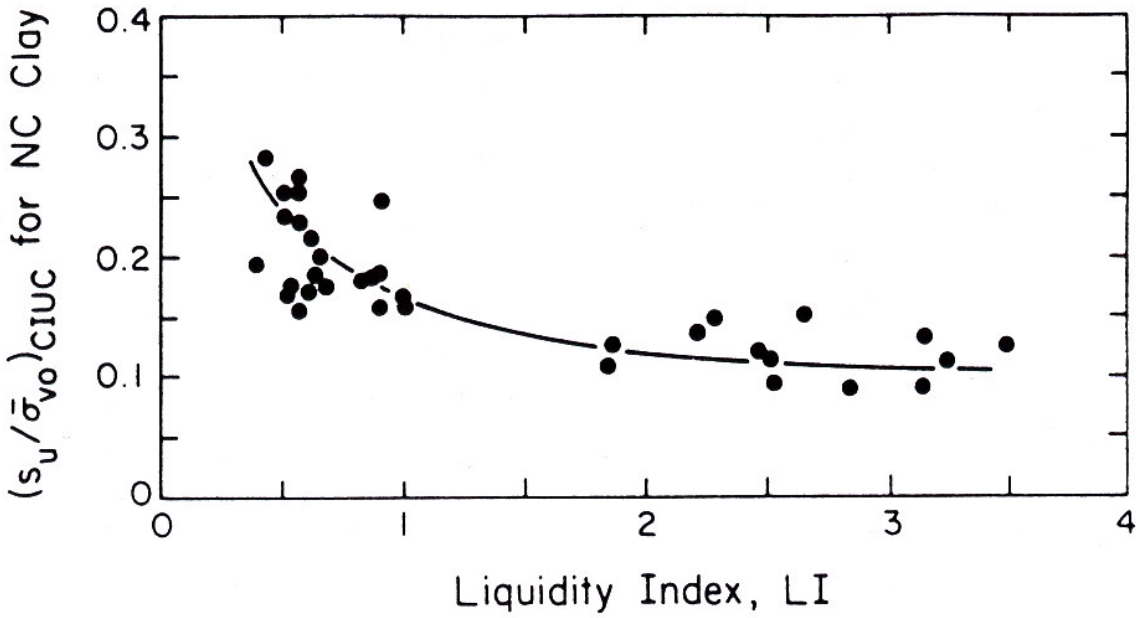

Figure A3.1 Normalized undrained shear strength of normally consolidated clay as a function of liquidity Index (after Bjerrum and Simons, 1960)

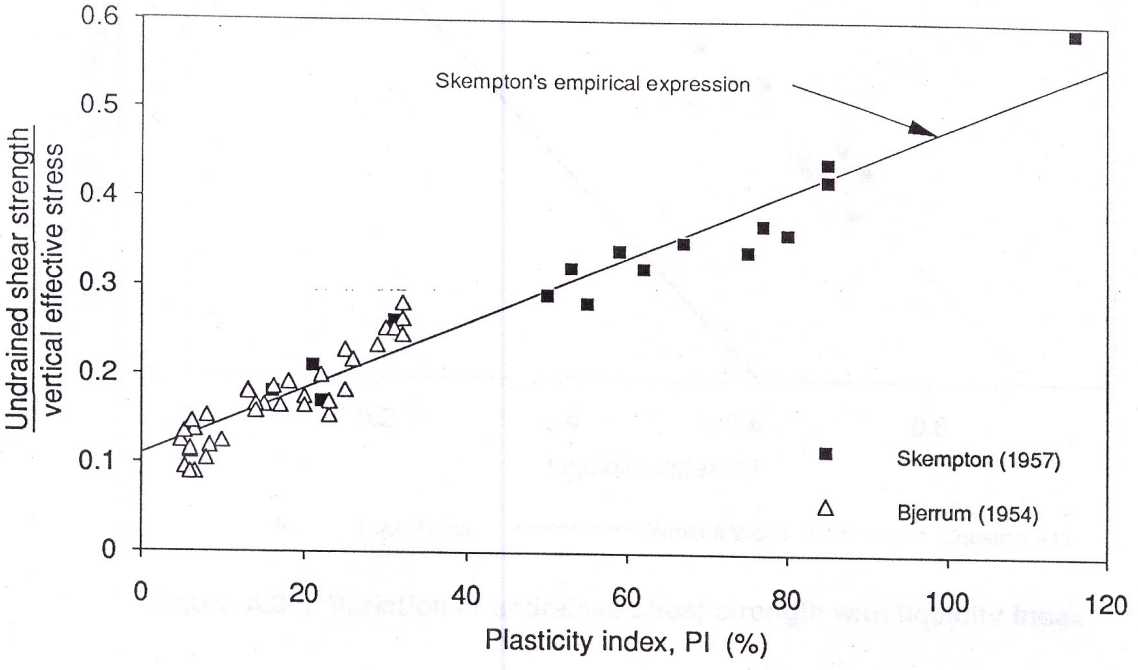

Figure A3.2 Undrained shear strength of normally consolidated clays (after Stewart, 1992)

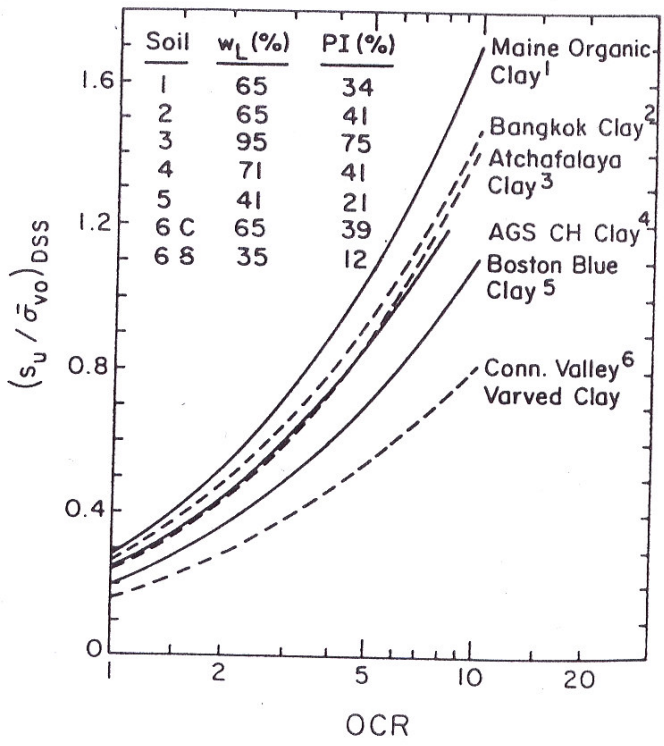

Figure A3.3 Effect of overconsolidation on the normalized undrained shear strength of several clays (after Ladd *et al*., 1977)

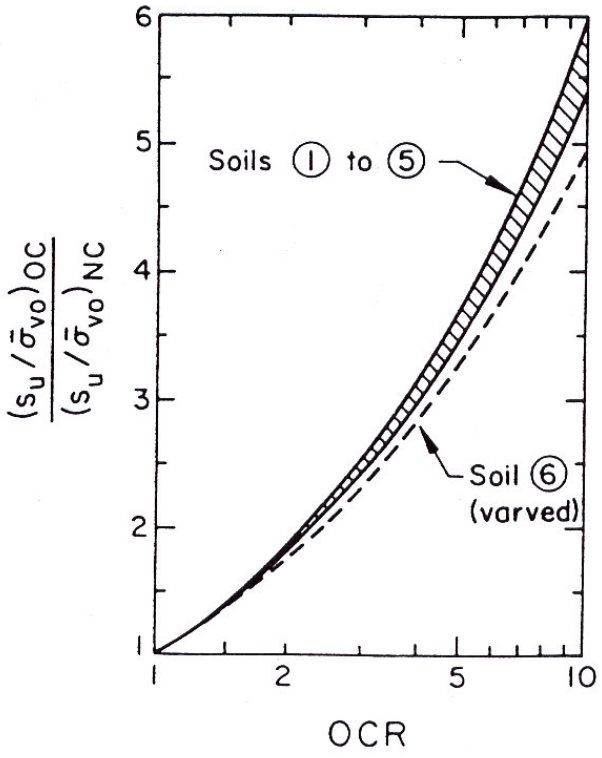

Figure A3.4 Normalized undrained shear strength ratio as a function of overconsolidation ratio (after Ladd *et al*., 1977)

APPENDIX 4

TYPICAL CLAYEY SEABED IN SITU

Clayey seabed is scattered all over the world. Types vary from normally consolidated to overconsolidated, with uniform strength or strength increasing with depth, or combined. Additionally, in some places thin stiff crust formed close to the mudline, underlaid by an overconsolidated clay. This study concentrated only on overconsolidated clay, some relevant typical field examples are stated below.

- **Gulf of Mexico, offshore Texas and Western Louisiana (after Young *et al*., 1984):** A thin surficial layer of recent clay underlaid by a desiccated, overconsolidated clay. Below this clay crust, the shear strength dropped off to a fairly constant value of s_u = 48 kPa.
- **Gulf of Mexico (after Endley *et al*., 1981):** Uniform clay of strength s_u = 20-27 kPa.
- **Louisiana cost line (after Gemeinhardt and Focht, 1970):** Recent clays of the Louisiana coast have strengths of normally increasing with depth.
- **Mississippi River delta (after Gemeinhardt and Focht, 1970):** Very soft clay extends to substantial depths.
- **South Timbalier (after Gemeinhardt and Focht, 1970):** The soil strength at this location s_u = 1.92 + 1z kPa, where z is soil depth.

In Australia, a uniform clay bed is widely investigated, as stated below, by Stewart (1992), Stewart and Randolph (1994), Newson *et al*. (1999) and Watson (1999). Of course, it is a riverbed, not seabed.

- **Burswood Peninsular in Perth, Western Australia (after Watson, 1999):** The site comprises a relatively homogeneous soft clay deposit about 18 m thick, this clay layer is overlain by several meters of partly cemented fill,

which mainly comprises fly ash. The soil has been gradually deposited in the Swan River's flood plain, and is an organic silty clay containing numerous shell fragments. Strength profile has been shown in Figure A4.1.

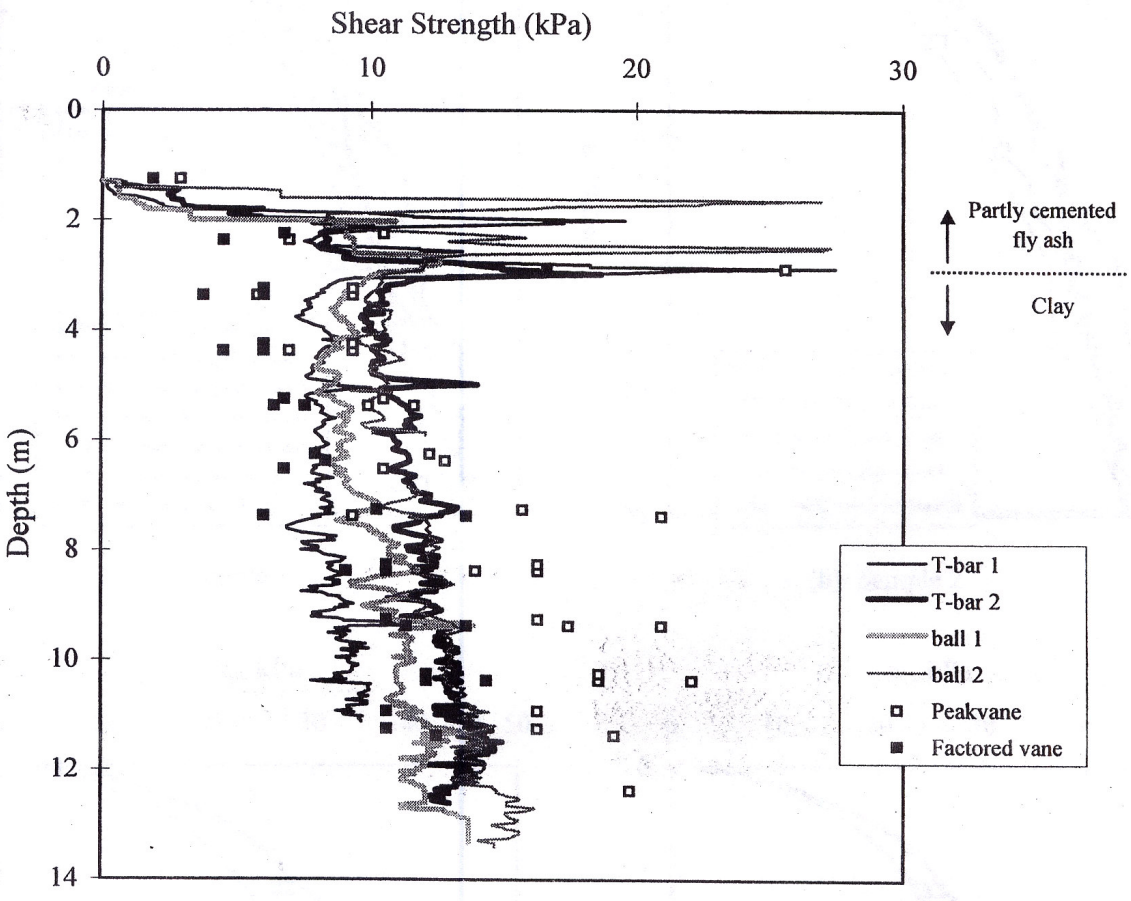

A4.1 Swan Riverbed profile (Burswood Peninsular, Western Australia) (after Watson, 1999)